

# Optical and MR Molecular Imaging Probes and Peptide-based Cellular Delivery for RNA Detection in Living Cells

A Thesis  
Presented to  
The Academic Faculty  
by  
Nitin Nitin

In Partial Fulfillment  
of the Requirements for the Degree  
Doctor of Philosophy in the  
Department of Biomedical Engineering

Georgia Institute of Technology  
December, 2005

# Optical and MR Molecular Imaging Probes and Peptide-based Cellular Delivery for RNA Detection in Living Cells

Approved by:

Dr Gang Bao, Advisor  
Department of Biomedical Engineering  
Georgia Institute of Technology

Dr Alfred Merrill  
School of Biology  
Georgia Institute of Technology

Dr Nicholas V. Hud  
School of Chemistry and Biochemistry  
Georgia Institute of Technology

Dr Niren Murthy  
Department of Biomedical Engineering  
Georgia Institute of Technology

Dr Xiaoping Hu  
Department of Biomedical Engineering  
Georgia Institute of Technology

Approval Date: 21, July, 2005

## ACKNOWLEDGEMENTS

I will like to express my gratitude to all those you have helped me complete this dissertation.

First of all I will to thank my family for their constant love, encouragement and support, which enabled me to complete this work. Special thanks to my parents for their selfless love and support throughout my life. Thanks to Manu and Sameer for being wonderful brothers and friends for my life. Thanks to my wife, Madhu for her love, encouragement, support and lots of patience with everything in life.

I will like to thank my academic family, Dr Bao, present and ex-Bao lab members for their academic support in this research. I will to convey my special thanks to Dr Bao for being supportive of various research ideas, providing academic freedom to learn and also for his advice and support with future career. I will also like to convey my special thanks to Dr Xiaoping Hu and Dr Shuming Nie for their key advice on various aspects of this dissertation. I will like to thank Dr Leslie LaConte for being a key partner in the magnetic nanoparticle work and also for her key support and valuable discussions on various research issues. Thanks to Dr Philip Santangelo, for his support, valuable discussions and advice on various aspects of molecular beacon research. Thanks to Dr Xu (Jason) for his friendship, support and help in learning various laboratory techniques. Thanks to Dr Andrew Tsourkas for his friendship, and help with initial stages of research. Thanks to Charles Glaus for his friendship, encouraging discussions and help with certain experiments. Thanks to Brent Nix for his help with PCR and support with certain experiments. Thanks to Allison Dennis and Cindy Glick for various research and social aspects of Baolab. I will like to thank all the undergraduate research assistants for their help with this dissertation and general research in Baolab. Special thanks to Tashan Mistree for her valuable help with PCR, chemical assays and, organizational support in

Baolab. Thanks to Colin for his help with RBC studies and Simone for molecular beacon studies. Thanks to all Baolab members for making lab an interesting and supportive place for research.

I will like to thank my friends in US especially in Atlanta for all their friendship and support. Special thanks to my room-mates and friends Babu and Ramanan for being a family here in Atlanta. Special thanks to Babu for all his support, care and patiently listening to all problems, complaints and various discussions in past four years. Thanks to Harvinder Gill, for his friendship and for discussions on various course assignments, project teams and research projects. Thanks to Nitin Jain, Lalithya Yeramilli, Sushma Pavan and Radhika for their friendship and encouragement.

# TABLE OF CONTENTS

ACKNOWLEDGEMENTS .....	ii
LIST OF TABLES .....	xi
LIST OF FIGURES.....	xii
SUMMARY .....	xvi
CHAPTER 1: Introduction .....	1
Molecular Beacons (hairpin probes) .....	2
RNA Secondary Structure .....	11
Modified Oligonucleotide Chemistry.....	13
Modified Oligonucleotide Chemistry.....	14
Intracellular RNA Targets .....	16
Cytoplasmic and nuclear RNA.....	17
Cellular delivery of probes.....	29
Cell permeable Peptides .....	32
Challenges in Imaging of mRNA using Molecular Beacons.....	36
Organization of the Thesis .....	38
References.....	40
CHAPTER 2: Peptide linked molecular beacons for imaging of endogenous RNAs in living cells.....	53
Introduction .....	53
Materials and Methods.....	55
Design of peptide-linked molecular beacons .....	55
Peptide conjugation.....	59
Solution assays of hybridization kinetics and signal-to-background ratio .....	61

Cellular delivery of peptide-linked molecular beacons .....	62
Fluorescence in-situ hybridization .....	62
Delivery of molecular beacons using commercial transfection reagents.....	63
Results and Discussion .....	63
Hybridization kinetics of peptide-linked molecular beacons .....	63
Detection of GAPDH mRNA using peptide-linked molecular beacons.....	65
Comparison with in-situ hybridization.....	69
Detection of survivin mRNA .....	71
Comparison with conventional transfection methods.....	73
Discussion .....	75
References .....	78
CHAPTER 3: Subcellular localization and co-localization of mRNAs in the cytoplasm of living cells.....	81
Introduction .....	81
Material and Methods.....	82
Design of Molecular Beacons .....	82
Cell culture .....	83
Molecular beacon delivery via cell permeable peptide.....	85
Nocodazole treatment .....	85
Fluorescence <i>in-situ</i> hybridization .....	85
Fluorescence microscopy imaging .....	86
Organelle labeling and fluorescence imaging .....	86
Results and Discussion.....	87
Control studies for mRNA localization.....	93
Summary.....	101
References .....	102

CHAPTER 4: Imaging the effects of mTOR and PI-3 Kinase mediated inhibition of translation on the organization of mRNA in living cells using MB probes .....	104
Introduction .....	104
Material and Methods.....	109
Chemicals .....	109
Molecular Beacons.....	109
Cell Culture .....	109
Imaging .....	109
Cellular Studies with Molecular Beacons .....	110
Fixed cell studies.....	111
Studies with 2' o methyl MB probes .....	111
RNA Isolation, RT-PCR, and qt-PCR.....	112
Results and Discussions .....	113
Effect of Rapamycin and Wortamannin treatment on the MB-based detection of mRNAs in living cells.....	113
Sub cellular fate of mRNAs after treatment with rapamycin and wortamannin .....	121
Effect of MB probe chemistry on the stability of MB-RNA structure with the repression of translational processes .....	130
Summary.....	133
CHAPTER 5: Measurement of intracytoplasmic mobility of endogenous messenger RNAs using MB probes in living cells.....	140
Introduction .....	140
Material and Methods.....	145
Chemicals .....	146
Design of Molecular Beacons .....	146
Cell culture .....	146

FRAP Assay.....	146
Molecular beacon delivery via cell permeable peptide.....	147
Microtubule perturbations.....	148
ATP depletion.....	148
Fluorescence <i>in-situ</i> hybridization.....	148
Results and Discussion.....	149
Design of MB probes.....	149
Mobility of GAPDH mRNAs at 37 °C.....	150
Mobility of GAPDH mRNAs in fixed sample.....	153
Effect of Temperature on the mobility of mRNAs in the cytoplasm.....	156
Effect of ATP depletion on the mobility of GAPDH mRNAs in the cytoplasm.....	159
Effect of Microtubule network on the mobility of GAPDH mRNAs.....	163
Mobility of 28-s rRNA in the cytoplasm of living cells.....	170
Calculation of apparent diffusion coefficients.....	174
Summary.....	177
References.....	178
CHAPTER 6: Peptide linked MBs for imaging of endogenous RNAs in nuclei of living cells.....	181
Introduction.....	181
Material and Methods.....	184
Peptides.....	184
Cell Line.....	185
Chemicals.....	185
Peptide Conjugation.....	185
Solution assay to measure the signal-to-background ratio of modified and unmodified Molecular Beacons.....	186

Cellular delivery of peptide-linked Molecular Beacons.....	186
Fixed cell studies.....	187
Results and Discussion.....	188
Design of peptide linked MB .....	188
Signal-to-Noise ratio of peptide-linked molecular beacons .....	191
Imaging of U3 snoRNP, U1 and U2 snRNPs in the nucleus of living cells using multifunctional probes .....	191
In-situ <i>hybridization in fixed cells</i> .....	195
Control Studies in living cells .....	202
Summary.....	204
References.....	205
CHAPTER 7: Development of magnetic nanoparticles based MR contrast agents .....	208
Introduction .....	208
Specific Aims.....	209
Materials and Methods.....	211
Coating of Magnetic Nanoparticles .....	211
Size Determination.....	212
Bioconjugation and Functionalization.....	213
Iron Concentration Determination .....	213
Cell Culture .....	214
Fluorescent Imaging.....	214
Magnetic Contrast Measurements .....	215
Results and Discussion.....	215
Summary.....	225
References.....	226

CHAPTER 8: Effect of coating thickness on magnetic relaxation characteristics of iron-oxide nanoparticles .....	229
Introduction .....	229
Material and Methods.....	234
Coating of Magnetic Nanoparticles .....	234
Size Determination.....	235
Iron Concentration Determination .....	235
Magnetic Contrast Measurements .....	236
Results and Discussion.....	237
Summary.....	246
References.....	247
CHAPTER 9: Summary and Future Work.....	251
Summary.....	251
Future Work .....	255
Future work in technology development .....	255
Development of design rules for MBs to target various RNAs .....	255
Detection of point mutations .....	256
Delivery in tissue samples .....	256
Development of biophysical tools to understand probe and RNA dynamics .....	257
Future Work in areas of fundamental biological studies.....	257
Interactions of RNA with RNA-binding proteins in living cells.....	257

## LIST OF TABLES

<b>Table1.1</b> Summary of proteins bound to pre-mRNA.....	21
<b>Table2.1</b> Design of peptide-linked molecular beacons.....	56
<b>Table3.1</b> Design of molecular beacons.....	85
<b>Table5.1</b> Design of molecular beacons.....	150
<b>Table5.2</b> Apparent diffusivity of GAPDH mRNAs.....	177
<b>Table6.1</b> The design of NLS peptide-linked molecular beacons.....	190
<b>Table8.1</b> Properties and applications of some SPIO agents.....	233
<b>Table8.2</b> Variation of diameter of coated mMIONS with changes in coating size.....	239

## LIST OF FIGURES

<b>Figure1.1</b> Illustrations of molecular beacons.....	5
<b>Figure1.2</b> Three thermodynamic phases of molecular beacons in presence of target.....	7
<b>Figure1.3</b> Thermal denaturation profiles of solutions containing molecular beacons.....	8
<b>Figure1.4</b> Structure-function relations of molecular beacons.....	9
<b>Figure1.5</b> Schematic representation of Molecular Beacon based detection and imaging of mRNA in live cell.....	13
<b>Figure1.6</b> HnRNP proteins and mRNP proteins along the pathway of mRNA biogenesis.....	19
<b>Figure1.7</b> Representation of cytoskeletal elements (microtubule and microfilaments) involved in localization and transport of mRNA .....	25
<b>Figure1.8</b> Illustration of the Tat mediated delivery of various cargos across the plasma membrane of living cells.....	35
<b>Figure2.1</b> A schematic illustration of three different conjugation schemes for linking the delivery peptide to molecular beacons.....	58
<b>Figure2.2</b> Probe-target hybridization kinetics of unmodified and peptide-linked molecular beacons.....	65
<b>Figure2.3</b> Detection of GAPDH mRNA in HDF cells using 0.5 $\mu$ M of peptide-linked molecular beacons.....	68
<b>Figure2.4</b> Control studies using fluorescence in situ hybridization (FISH).....	70
<b>Figure2.5</b> Detection of Survivin mRNA in live HDF and MiaPaca-2 cells.....	72
<b>Figure2.6</b> Cellular delivery using conventional transfection methods.....	75
<b>Figure3.1</b> Co-localization of GAPDH m RNA with Mitochondria.....	90
<b>Figure3.2</b> Human dermal fibroblast images: A,D) mitochondrial stain, MitoFluor™ Green (green), B,E) ER-Tracker™ (red), and C,F) merge of A and B, and merge of D and E...91	91

<b>Figure3.3</b> A)-GAPDH mRNA in HDF cells (Filamentous structure). (B)-Effect of nocodazole treatment on localization of GAPDH mRNA (Treatment for 30 minutes with 30 $\mu$ m Nocodazole).....	93
<b>Figure3.4</b> Control studies of mRNA localization.....	96
<b>Figure3.5</b> Fluorescence <i>in situ</i> hybridization studies.....	98
<b>Figure3.6</b> A control study for the localization of the molecular beacons in live cells....	101
<b>Figure4.1</b> Effect of the Rapamycin and the Wortmannin treatment (repression of translation) on MB-based detection of the GAPDH and K-Ras mRNAs in living cells.....	116
<b>Figure4.2</b> Colocalization of GAPDH mRNAs with Mitochondria in untreated and treated (translationally repressed) cells.....	120
<b>Figure4.3</b> Colocalization of K-Ras mRNAs with Mitochondria in untreated and treated cells (repression of translation).....	121
<b>Figure4.4</b> PCR results for the GAPDH and the K-Ras mRNAs in treated (Rapamycin or Wortmannin treatment for repression of translation) and untreated cells.....	125
<b>Figure4.5</b> Fluorescent in-situ hybridization (FISH) based detection of GAPDH and K-Ras mRNAs in treated (Rapamycin or Wortmannin treatment for repression of translation) and untreated cells.....	127
<b>Figure4.6</b> (A): Distribution of 28-s Ribosomal RNA in living cells.....	130
<b>Figure4.7</b> (A)-(B):Detection of K-Ras mRNAs using 2' O Methyl MB probes in untreated and Rapamycin treated cells respectively.....	133
<b>Figure5.1</b> Schematic representation of a FRAP experiment in a cytoplasm of a cell...	146
<b>Figure5.2</b> FRAP analysis of the mobility of GAPDH mRNAs at 37°C using MB probes.....	152
<b>Figure5.3</b> FRAP analysis of the mobility of GAPDH mRNAs in a fixed cell samples using MB probes to estimate the contribution of the off-rate of MB probes in recovery of bleached areas.....	156
<b>Figure5.4</b> FRAP analysis of the mobility of GAPDH mRNAs at 25 °C using MB probes.....	159

<b>Figure5.5</b> FRAP analysis of the mobility of GAPDH mRNAs at 37 °C with depletion of ATP by treatment with 2-de-oxyglucose and Na Azide at 5 mM concentration for 15 minutes.....	162
<b>Figure5.6</b> FRAP analysis of the mobility of GAPDH mRNAs at 37 °C with perturbation of microtubule network by treatment with 2 μM concentration of Nocodazole for 30 minutes.....	166
<b>Figure5.7</b> FRAP analysis of the mobility of GAPDH mRNAs at 37 °C with perturbation of microtubule network by treatment with 10 μM concentration of Taxol for 30 minutes.....	169
<b>Figure5.8</b> FRAP analysis of the mobility of 28-s rRNA at 37°C and 25 °C using MB probes.....	173
<b>Figure6.1</b> Shows a schematic design of a peptide linked Molecular beacon and its delivery into the nucleus of living cells.....	191
<b>Figure6.2</b> Signal to noise ratio of the NLS linked Molecular Beacons and the unmodified molecular beacons.....	193
<b>Figure6.3</b> Imaging of U3 snoRNA, U1 and U2 snRNAs in the nucleus of living cells using NLS linked MB probes respectively.....	194
<b>Figure6.4</b> Fluorescent In-situ hybridization (FISH) to image the U3 snoRNA, U1 and U2 snRNAs in the nucleus of fixed cells.....	198
<b>Figure6.5</b> Imaging of Co-localized U1 and U2 snRNAs in the nucleoplasm of living cells using peptide linked Molecular Beacons.....	200
<b>Figure6.6:</b> Fluorescent in situ hybridization to validate the co-localization of U1 and U2 snRNAs in fixed cells.....	202
<b>Figure6.7</b> Negative Controls to validate the measurements made in this study.....	204
<b>Figure7.1</b> The scheme for the development of micelle-encapsulated superparamagnetic iron oxide magnetic nanoparticles (mMIONS).....	218
<b>Figure7.2</b> The size of mMIONS.....	219
<b>Figure7.3</b> Steps for conjugating Tat peptide and fluorescent label (TxRed) to mMIONS for cellular delivery and imaging (microscopy, MRI).....	221
<b>Figure7.4</b> Fluorescent images of Tat-linked, TxRd-labeled mMIONS in living cells.....	224
<b>Figure7.5</b> The effect of mMIONS on water relaxation inside living cells.....	225
<b>Figure8.1</b> (A) SPIO crystal in the absence of an external magnetic field ( $B_o$ ); the orientation of the magnetic domains is random. (B) Application of an external magnetic field aligns the magnetic domains with $B_o$ .....	231

**Figure8.2** Variation of  $R_2$  for mMIONs coated with micelle coating of various sized phospholipid-PEG chains (DSPE-PEG 550, 750,1000,2000 and 5000).....241

**Figure8.3** Variation of  $R_1$  for mMIONs coated with micelle coating of various sized phospholipid-PEG chains (DSPE-PEG 550, 750,1000,2000 and 5000).....243

**Figure8.4** (A) Schematic picture of the exclusion volume concept used for monte-carlo simulation for calculation of relaxivity values for coated magnetic nanoparticles. (B) Predicted variation of  $R_2$  values as a function coating thickness obtained from numerical simulation.....246

## SUMMARY

Detection, imaging and quantification of gene expression in living cells can provide essential information on basic biological issues and disease processes. To establish this technology, we need to develop molecular probes and cellular delivery methods to detect specific RNAs in live cells with potential for in vivo applications. In this thesis work, the major focus is placed on the development of molecular beacons and biochemical approaches (peptides etc.) to deliver such probes to different cellular compartments. These approaches are then employed to study the expression and localization of mRNAs, co-localization of mRNAs with cytoplasmic organelles and cytoskeleton, and co-localization of RNA molecules in the nuclei of living cells.

Further along this direction, we were interested in developing a better understanding of the functional states of mRNAs and the fluorescent signal observed in optical imaging experiments. To achieve this goal, we altered the translational process and studied its effect on the detection of mRNAs in living cells. The results of these studies indicate that the translational state of mRNAs favors the hybridization of molecular beacon with its target sequence. This study has also provided the evidence that molecular beacons are reversibly bound to target mRNAs and the repression of the translational process can prevent molecular beacon from binding to its target mRNA. Further, using these approaches in combination with FRAP based biophysical analysis, the dynamics of endogenous RNA in living cells are studied. These studies revealed the possible subcellular organization of RNA molecules and their dynamics in living cells. The results also demonstrated the role of cytoskeleton and ATP in the mobility of specific mRNAs in the cytoplasm.

In addition to optical probes, studies have been carried out to develop an MRI contrast agent using iron-oxide nanoparticles for deep tissue molecular imaging. Specifically, we have functionalized magnetic nanoparticles that are water-soluble, mono-dispersed, biocompatible, and easily adaptable for multifunctional bioconjugation of probes and ligands. We have successfully delivered magnetic nanoparticle bioconjugates into live cells and demonstrated their effect on relaxivity. We have further studied the role of coating thickness for optimization of contrast and further enhance the fundamental understanding of contrast mechanisms.

# CHAPTER 1

## Introduction

### Introduction

Various technologies and methodologies have been developed to study intracellular RNA biology by creating tagged full length RNAs or using RNA targeting probes. In most cases these tags are fluorescent, chemical (such as digoxigenin), or radioactive. For example, tagged full length RNA has been introduced into living cells using microinjection ([3]; [4]; [5]) to monitor the localization of a specific mRNA or nuclear RNA.

Labeled linear oligonucleotide (ODN) probes of 20-50 bases have been used to study intracellular mRNA (e.g. [6]; [7]; [8]; [9]) via *in situ* hybridization (ISH) in which cells are fixed and permeabilized to increase the probe delivery efficiency and unbound probes are removed by washing, therefore reducing background and achieving specificity. To enhance the signal level, multiple probes targeting the same mRNA can be used (e.g. [10]). However, fixation agents and other supporting chemicals can have a considerable effect on signal ([11]) and possibly on the integrity of certain organelles such as mitochondria. Therefore, fixation of cells, by either cross-linking or denaturing agents, combined with the use of proteases in ISH may not provide an accurate description of intracellular mRNA localization. Labeled linear ODN probes are not very useful in detecting mRNA in live cells since it is impossible to remove unbound probes by washing and thus difficult to distinguish between signal and background.

In addition to oligonucleotide probes, tagged RNA-binding proteins such as those with GFP tags have been used to detect mRNA in live cells ([12]). One limitation is that it requires the identification of a unique protein, which only binds to the specific mRNA of interest. To address this issue, recently a transgene with a binding site for the phage

MS2 protein was synthesized ([13]). Generation of a GFP tagged phage MS2 protein in *Drosophila* eggs allowed the specific targeting of the nanos mRNA in a living egg system. However, there is still a significant challenge in generating transgenes with the same functionality as endogenous mRNA.

To detect endogenous gene expression in living cells, we need to develop a probe, which can be delivered specifically to cytoplasm of living cells and on binding its target mRNA it can provide a signal different from its unbound state. One such design of probe, which has been mainly developed, for PCR applications are molecular beacons. These molecular beacons are hairpin probes. In the following section, we discuss in more details the design of hairpin probes for gene detection in living cells.

### **Molecular Beacons (hairpin probes)**

The detection and quantification of specific mRNAs require probes to have high sensitivity and specificity, especially for low abundance genes and with a small number of diseased cells in clinical samples. Further, for detecting genetic alterations such as mutations and deletions, the ability to recognize single nucleotide polymorphisms (SNPs) is essential. When designed properly, hairpin nucleic acid probes have the potential to be highly sensitive and specific, with fast probe-target hybridization kinetics. As shown in Figure 1a, one class of such probes is known as molecular beacons, which are dual-labeled oligonucleotide probes with a fluorophore at one end and a quencher at the other end ([14]). They are designed to form a stem-loop structure in the absence of a complementary target so that fluorescence of the fluorophore is quenched. Hybridization with target nucleic acid in solution or in a living cell opens the hairpin and physically separates the fluorophore from quencher, allowing a fluorescence signal to be emitted upon excitation. Thus, molecular beacons enable a homogenous assay format where background is low, without the need to wash away unbound probes. The design

of the hairpin structure provides an independently adjustable energy penalty for hairpin opening which improves probe specificity ([15]; [16]). The ability to transduce target recognition *directly* into a fluorescence signal with high signal-to-background ratio, coupled with an improved specificity has allowed molecular beacons to enjoy a wide range of biological and biomedical applications.

There are three major design issues of nanostructured molecular probes for gene detection in living cells: specificity, melting temperature, and secondary structure of target mRNA. First, to ensure specificity, for each gene to target, one can use BLAST or a similar software to select 16-20 base target sequences that are unique for the target mRNA. Secondly, since the melting temperature of molecular beacons affects both the signal-to-background ratio and detection specificity, especially for mutation detection, one has to systematically adjust the G-C content of the target sequence, the loop and stem lengths and the stem sequence of the molecular beacon to realize the optimal melting temperature. In particular, it is necessary to understand the effect of molecular beacon design on melting temperature so that, at 37°C, single-base mismatch in target mRNAs can be differentiated. Finally, since mRNA molecules often have secondary (folded) structures, it is important to avoid targeting sequences that are buried (i.e., where double stranded RNA was formed). One difficulty in the molecular beacon design is that, although predictions of mRNA secondary structure can be made using software such as *mfold*, they may not be accurate due to limitations of the biophysical models used. Therefore, for each gene to target, it is often necessary to select multiple target sequences, and have corresponding molecular beacons designed, synthesized and tested in living cells ([17]).

A conventional molecular beacon has four essential components: loop, stem, fluorophore and quencher, as illustrated in **Figure 1.1 A**. The loop usually consists of 15-

25 nucleotides and is selected based on target sequence, melting temperature, and the secondary structure of the target mRNA. The stem, formed by two complementary short-arm sequences, is typically 4-6 bases long and is usually chosen to be independent of the target sequence (**Figure 1.1 B**). Molecular beacons, however, can also be designed such that one arm of the stem participates in both stem formation and target hybridization (shared-stem molecular beacons), as illustrated schematically in **Figures 1.1 C**. Although a molecular beacon can be labeled with any desired reporter-quencher pair, proper selection of the reporter and quencher could improve the signal-to-background ratio and multiplexing capabilities.

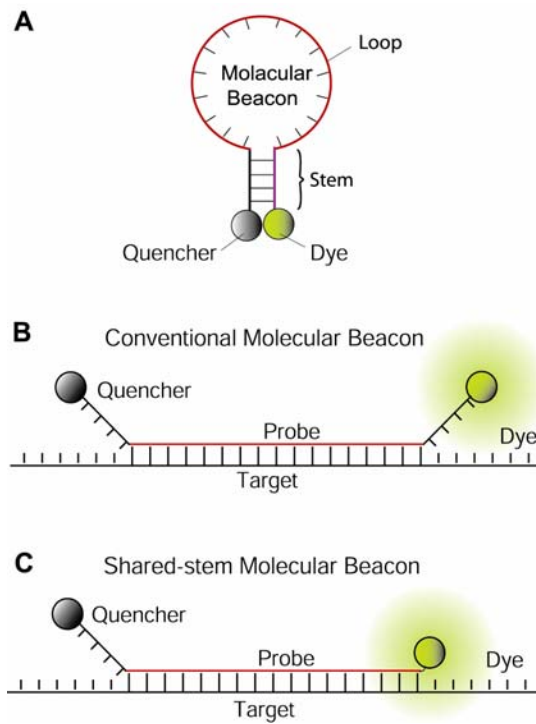


**Figure 1.1:** Illustrations of molecular beacons. (A) Molecular beacons are stem-loop hairpin oligonucleotide probes labeled with a reporter fluorophore at one end and a quencher molecule at the other end. (B) Conventional molecular beacons are designed such that the short complementary arms of the stem are independent of the target sequence. (C) Shared-stem molecular beacons are designed such that one arm of the stem participates in both stem formation and target hybridization.

The loop, stem lengths and sequences are the critical design parameters for molecular beacons, since at any given temperature they largely control the fraction of molecular beacons in each of three different conformational states: bound-to-target, stem-loop, and random-coil ([15]). The adapted representation of three states of molecular beacons is shown in **Figure 1.2**. In many applications, the choices of the probe sequence are limited by target-specific considerations, such as the sequence surrounding a single nucleotide polymorphism (SNP) of interest. **Figure 1.3** represents the melting curve analysis of molecular beacons in presence of perfect complementary and single base mismatched targets. This study indicates the selection of SNP's vs. perfect complementary sequences in a homogeneous assay. However, the probe and stem lengths, and stem sequence, can be adjusted to optimize the performance (i.e. specificity, hybridization rate and signal-to-background ratio) of a molecular beacon for a specific application ([18];[16]). **Figure 1.4** illustrates the role of length of stem in controlling the melting point of molecular beacons. It is interesting to note, however, that stem-less molecular beacons, which lack the short complementary arms and rely solely on the random-coiled nature and interactions between the dye and quencher to maintain a dark state, are still able to differentiate between bound and unbound states ([19]).

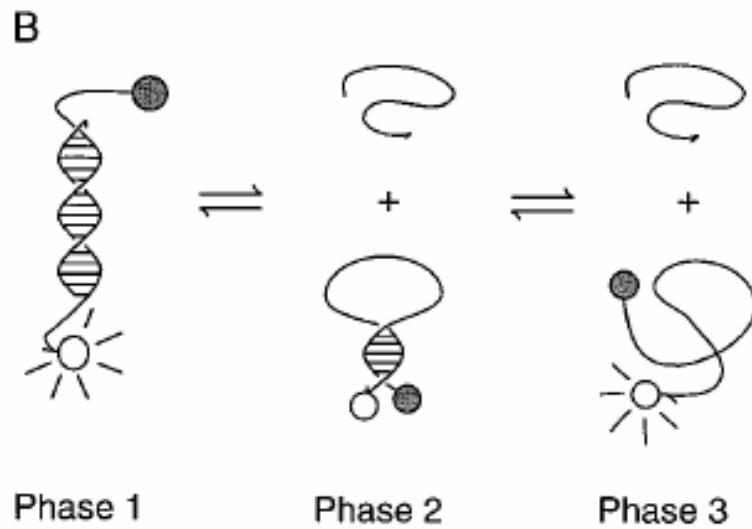


**Figure 1.2:** Three thermodynamic phases of molecular beacons in presence of target

Phase (1) - Target hybridized with molecular beacon which provides signal due to opening of hairpin.

Phase (2) - Molecular beacon in hairpin shape (unhybridized to target)

Phase (3) - Randomly opened beacon which will contribute to background signal

(Adapted Ref (13) )

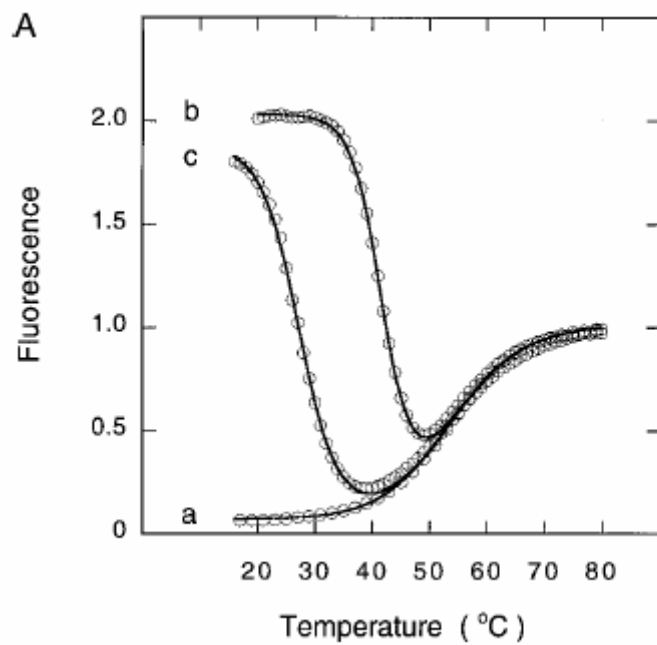


**Figure 1.3:** Thermal denaturation profiles of solutions containing molecular beacons.

Curve a: Absence of targets;

Curve b: Presence of a 6-fold excess of perfectly complementary targets

Curve c: Presence of a 6-fold excess of single-base mismatched targets

Adapted from Ref. 13

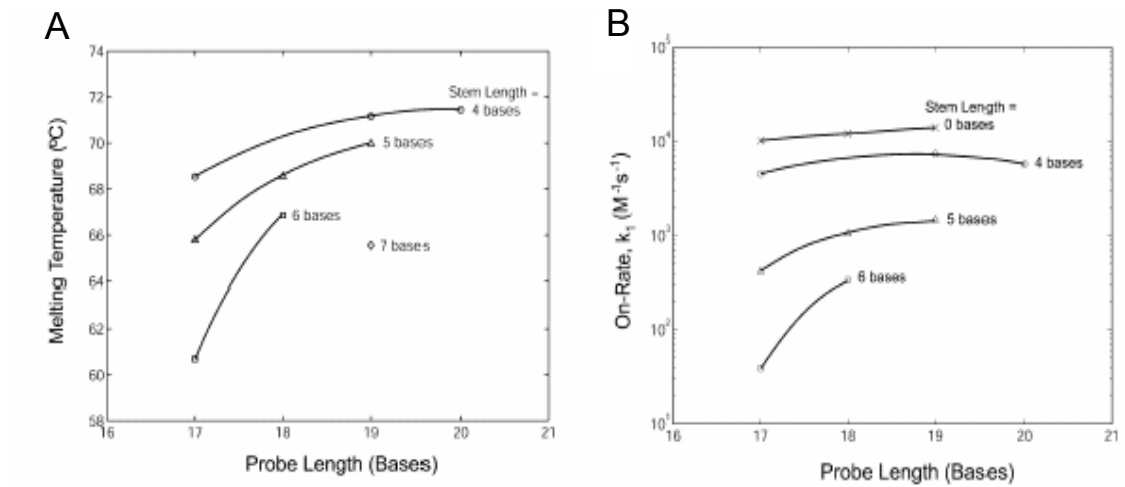


**Figure 1.4:** Structure-function relations of molecular beacons  
 (a) Melting temperatures for molecular beacons with different structures in the presence of target.  
 (b) The rate constant of hybridization  $k_1$  (on-rate constant) for molecular beacons with various probe and stem lengths hybridized to their complementary targets (Adapted from Ref. 16)

In the previous section, we have discussed the design of molecular beacons to detect mRNA. All the discussions regarding design of molecular beacons/hairpin probes is based on homogeneous assays such as solution studies with short oligonucleotides or PCR with mRNA /c-DNA strands but at elevated temperatures. This implies that there is no significant constraint of secondary structure of mRNA, or RNA-protein complex during detection. This constraint of both secondary/tertiary mRNA structure and RNA-protein complexes becomes a major challenge in designing probes for detection of mRNA in living cells.

When *in situ* hybridization (ISH) techniques are applied for detection of mRNA in fixed cells, the challenge of mRNA secondary structure is overcome by using fixative agents (precipitation of proteins/removal of agents) in combination with permeablizing agents, proteases to cleave proteins, and high temperature for hybridization. The specificity of ISH assays is realized by extensive washing. None of these can be realized for live cell assays. Although the use of longer linear probes can provide some signal even with partial hybridization, it can also lead to false-positive signals. Therefore, there are many challenges in living cell mRNA detection both due to the possible difficulties in target accessibility and the lack of predictive models, as discussed in the next section.

## **RNA Secondary Structure**

RNA secondary and tertiary structures play an important role in the accessibility of nanostructured probes in living cell gene detection. This structural aspect provides a significant challenge in designing nanostructured probes as secondary structure of RNA can inhibit binding of the hairpin oligonucleotide probe to complementary sequences on the target. However, no existing model or software can give accurate prediction of mRNA secondary or tertiary structure in living cells is mainly due to the limited understanding of RNA-protein interactions and RNA intra-sequence interactions. Thus, most investigators have relied on empirical approaches where multiple targeting sequences are selected by “walking” along the length of the target RNA and the optimal binding sites are predicted based on the RNase H assay or gel shift assays.

A number of computational programs have been developed to predict the secondary structure of mRNA based on the sequence of mRNA and salt concentration but without considering RNA-protein interactions. The existing algorithms can be classified into two groups: (1) predictions based on minimizing free energy (e.g. Mfold, RNAsoft, Vienna RNA package); (2) probabilistic or stochastic prediction based on the alignment and phylogenetic trees of the sequences and the evolutionary conservation of critical structural components of mRNA (e.g. Pfold). For example, the algorithms initially developed by [20] based on minimizing free energy and later modified by [21] to include base pairing probabilities (Vienna RNA Secondary Structure Prediction) have been widely used as a structural prediction tool in the nucleic acids research community. One of the major limitations of the minimum-energy based models (e.g., Mfold) is the inability to predict pseudoknots in the secondary structure of mRNA. Although a significant progress has been made in predicting the secondary structure of a naked mRNA, it is still far from making accurate predictions of mRNA structure taking into account the

interactions between proteins and target mRNA in an intracellular environment. This is very problematic in the design of nanostructure oligonucleotide probes for living cell mRNA detection.

Understanding the structural changes in target mRNA upon binding of probes ([22]) is also important, since alterations in native structure of a target mRNA due to the binding of short oligonucleotides may drastically change its functionality. It has been suggested that the binding of DNA probes may prevent translation by either blocking the process or by RNase H activation. To study probe/RNA interactions, tools such as OligoWalk ([23]) and PairFold ([24]) have been developed. For example, OligoWalk predicts the interaction of oligonucleotide probes (both DNA/RNA) with target RNA structure based on equilibrium affinity at 37°C, and allows the user to study the effects of probe length, concentration, and to some extent backbone chemistry (RNA or DNA) on the local and global structure of target RNA.

After a probe is designed based on BLAST searches for unique target sequences and secondary structure prediction using mFold, we typically perform solution studies to measure the signal-to-background ratio of the molecular beacons synthesized. Here the probe synthesis also plays a crucial role, since a well designed probe could have a low signal-to-background ratio if a large fraction of beacons do not have a quencher attached to it. The ultimate test is to deliver the molecular beacons to living cells with high efficiency and measure the signal level. It is also necessary to use negative control beacons to measure the background signal. **Figure 1.5** is a schematic representation of molecular beacon based detection of cellular mRNA in cells.

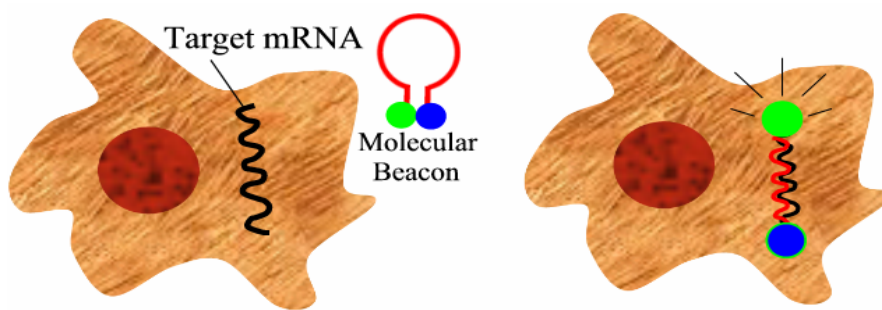


**Figure 1.5:** Schematic representation of Molecular Beacon based detection and imaging of mRNA in live cell

## Modified Oligonucleotide Chemistry

How does the oligonucleotide backbone chemistry affect a hairpin probe's behavior within the cellular environment? The backbone chemistry of a hairpin probe has profound implications for the behavior of the probe within the environment of a cell. Modified oligonucleotide backbones affect probe affinity, melting temperatures, and nuclease resistance. The antisense field of research has put considerable effort into backbone modification to confer nuclease resistance while maintaining RNase H-mediated mRNA degradation, so much learned from this research can be applied to the design of hairpin probes.

The most commonly used modification in the antisense field uses a phosphorothioate bond instead of the phosphodiester bond within the oligonucleotide. In phosphorothioate oligonucleotides (PS-ONs), a sulfur atom replaces one of the non-bridging oxygen atoms in the phosphate backbone. This modification has been shown to have greater resistance to nuclease degradation than phosphodiester oligonucleotides while maintaining RNase H-mediated mRNA degradation ([25]). The melting temperature of the PS-ON-target RNA duplex is slightly lower than the comparable phosphodiester oligonucleotide duplex and PS-ONs have lower affinities than the natural DNA oligonucleotides for the RNA target ([25]). A major drawback to this backbone modification, as described by ([25]) is its polyanionic backbone, which can lead to elevated protein binding and immune problems. Excess protein binding would certainly negatively impact the ability of a hairpin probe to bind to its target mRNA. It also activates RNase H activity, which is desirable for antisense therapy, but not when the goal is a minimally invasive probe of cellular activity.

Modification of the sugar portion of oligonucleotides forms the basis for another class of modified oligonucleotides. A number of modifications have been made at the 2'

position of the sugar ring ([26]). Adding a 2'-O-methyl group at this position significantly increases binding affinity and confers nuclease resistance. An increase in melting temperature in the sequence has been shown to be on the order of 1°C per modified oligonucleotide ([27]). This modification is not ideal for antisense work because it is RNase H-resistant (the duplex looks more like an RNA:RNA duplex than a DNA:RNA duplex that RNase H recognizes); however, when designing a hairpin probe, it is desirable to avoid inducing RNase H-mediated RNA degradation.

Another nucleic acid analog in which the sugar ring has been modified has been described as “locked nucleic acid” (LNA) ([28]). In this backbone modification, the 2'O and 4'C are linked by a methylene linker. This “locks” the sugar into the conformation (C3'-endo sugar) that is supposedly ideal for recognition of RNA. This modification gives significant increases in melting temperatures (ranging from 1° to 8° C against DNA) and has higher selectivity than native DNA oligonucleotides. LNAs have higher affinity for targets primarily due to slower dissociation, as shown by stopped-flow kinetics experiments ([28]). LNAs have also been shown to be stable in the presence of a number of nucleases ([29]).

Peptide nucleic acids (PNAs) are nucleotide analogs that also offer advantages for the design of hairpin probes. PNA is a DNA mimic where the phosphodiester-linked backbone has been replaced with an N-(2-aminoethyl)glycine backbone ([30],[31]) and behaves according to traditional Watson-Crick base-pairing rules. PNAs have very high binding affinity for single-stranded DNA and RNA; the melting temperature is increased by 1.45° per monomeric PNA unit ([32]). The rate of hybridization is at least as fast as DNA:DNA duplex formation. PNA:RNA duplexes are also more stable at lower salt concentrations due to the neutral character of the PNA backbone. PNA oligonucleotides exhibit both high affinity and high specificity ([33]). PNA oligonucleotides are completely

nuclease-resistant. Also, they have the unique ability to “invade” a DNA duplex, although this strand displacement occurs only at salt concentrations much lower than physiologically relevant ([32]). A careful study of the ability of PNA probes to bind to structured targets (i.e. those with hairpin structural motifs) showed that the higher affinity conferred by the PNA backbone enhances probe binding over a natural DNA probe ([31]), suggesting that PNA hairpin probes will have a distinct advantage when targeting a sequence suspected of significant secondary and tertiary structure.

Optimization of probe design will require much empirical determination, as there are innumerable variations to be examined. The antisense field has shown that partial backbone modifications (modifying only a few of the oligonucleotide units) often confers desired properties while minimizing undesirable ones. Some combination of any of the above described modifications may lead to the ideal probe for a given situation; each target sequence, however, may offer unique challenges. One target sequence, for example, may exhibit significant secondary structure, while another may be occluded by a number of bound proteins. Hybridization to either of these sequences may require a specific set of backbone modifications. In this study, we have used regular DNA chemistry, Phosphothiorate chemistry and 2' o methyl chemistry in design of our probes.

### **Intracellular RNA Targets**

One of the most exciting and promising applications of nanostructured molecular probes such as molecular beacons is their potential use for real-time visualization of RNA expression *in vivo* (i.e., in living cells and tissues). For example, the ability to monitor the level of mRNA expression *in vivo* will provide important information concerning the temporal and spatial processing, localization, and transport of specific mRNA under various conditions. Further, detecting pathogenic markers will provide a

means of locating and identifying diseased cells, allowing rapid diagnosis and prognosis of a disease.

To have sensitive detection and quantification of mRNA in live cells, it is extremely important to understand the form, distribution, dynamics and lifetime of target mRNA *in vivo* in order to optimize the probe design and measurement. Further, it is important to understand the impact of the probe on the cell, including its delivery, chemistry, possible toxicity, and non-specific interactions. In the following sections, we describe the basic features of mRNA in living cells, aiming to set a stage for understanding the challenges for intracellular mRNA detection and quantification.

### Cytoplasmic and nuclear RNA

In a living cell, the functional forms of pre-mRNA/mRNA exist as ribonucleoprotein complexes (RNPs) in which numerous heterogeneous nuclear ribonucleoproteins (hnRNPs) bind to the transcript ([34]). The association of these proteins begins during transcription, and there is evidence to show that some of these proteins remain bound to the mRNA all the way to the ribosome. The distribution of these proteins along the transcript, as well as the dynamic nature of the protein/RNA association, has a significant impact on the accessibility of pre-mRNA/mRNA to hairpin probes.

*Transcription and polyadenylation* mRNA is transcribed by a protein transcription complex containing RNA polymerase II which, especially the carboxy-terminal domain, couples transcription with mRNA processing ([35]). All pre-mRNA processing is a co-transcriptional event, including addition of the poly(A) tail and splicing. Even as the nascent transcript (20-25 nucleotides in length) is emerging from the transcription complex, a capping enzyme binds the 5' end, attaching the 5'-7-methylguanosine cap ([36]). This cap is then methylated in order to stabilize the transcript against 5' exonucleolytic attack ([36]). The methylated end is also a signal for nuclear cap binding

proteins that facilitate the interaction between the 5' splice site of a pre-mRNA containing introns and a protein complex called the spliceosome. Depending upon a functional poly(A) signal and the terminal splice acceptor site of the terminal intron ([37]), the termination of transcription occurs far downstream of the poly(A). **Figure 1.6** illustrates the overview of the protein-RNA interactions involved in the export of mRNAs from the nucleus to the cytoplasm of cells.

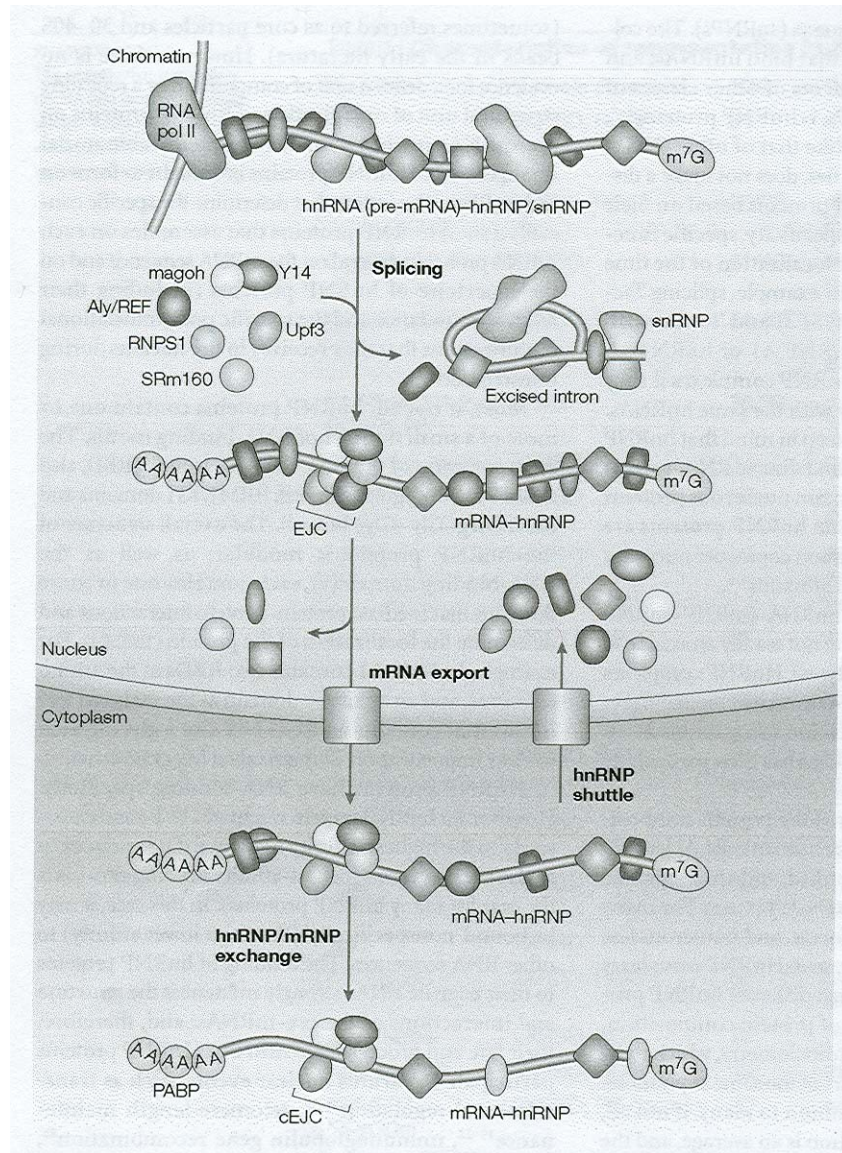


**Figure 1.6:** HnRNP proteins and mRNP proteins along the pathway of mRNA biogenesis. Overview of the interaction and dynamics of the myriad of RNA-binding proteins with pre-mRNA and mRNA. EJC, exon-exon junction complex; NMD, nonsense-mediated mRNA decay; RNA pol II, RNA polymerase II; hnRNP, heterogeneous nuclear ribonucleoprotein; nRNP, small nuclear ribonucleoprotein; mRNP, mRNA-protein complex; PABP, poly(A)-binding protein; m<sup>7</sup>G, methylguanosine cap. Adapted from Ref. ([34])

site ([35]), either before or at the same time as poly(A) is cleaved due to cleavage factors ([38]). The addition of the 3' poly(A) tail of a pre-mRNA requires more than a dozen polypeptides to be present ([36]). The pre-mRNA first undergoes endonucleolytic cleavage by an endonuclease at the poly(A) synthesis initiation site, followed by processive poly(A) synthesis by a poly(A) polymerase. The poly(A) tail (ranging in length from 20 to 250 nucleotides) is then bound by poly(A) binding proteins ([34]).

*Splicing.* During pre-mRNA processing, introns are removed from pre-mRNA by a ribonucleoprotein (RNP) machine (spliceosome) that contains at least 50 proteins and 5 small nuclear RNAs ([39]). This spliceosome is assembled at each intron, excising the intron and then releasing it in a branched “lariat” form along with the spliced pre-mRNA. Many of the splicing proteins remain bound to mRNA after splicing ([40]; [41]), generating a specific nucleoprotein complex that facilitates mRNA export ([42]). Specifically, some of the bound proteins are members of the SR (serine-arginine) protein family of splicing factors ([42]), a number of which have been shown to shuttle between the nucleus and cytoplasm ([40]). Proteins within this complex (such as Y14 and Mago) can target an mRNA for nonsense-mediated mRNA decay or recruit proteins such as TAP/p15 to assist in nuclear export.

*Nuclear export and localization.* Trans-acting factors (proteins that bind to *cis* elements or “zipcode” sequences within RNA) for mRNA localization are often present in granules (ribonuclear protein–RNP–complexes) that contain all components necessary for RNA processing, transport, localization, anchoring, and translation ([43]). In other words, mRNA localization is a process initiated in the nucleus, based on the proteins that are bound during processing and accompany the mature mRNA from the nucleus to the cytoplasm. The hnRNP (heterogeneous nuclear ribonuclear protein) A/B family is one group of proteins that play a significant role in mRNA localization. Both hnRNP A1 and

A2 leave the nucleus with mRNAs and then dissociate from the mRNA in the cytoplasm. Specifically, hnRNP A2 has been shown to help localize myelin basic protein (MBP) mRNA in oligodendrocytes ([43]). In addition, it has roles in splicing, nuclear export, translational regulation, and RNA stabilization. hnRNP A2 binds to a 21-nucleotide element in the 3' untranslated region (UTR) of mRNA ([44] ; [45]). A second example of a nuclear-bound trans-acting factor is zipcode-binding protein 2 (ZBP2), which binds to the 3' UTR of  $\beta$ -actin mRNA ([46]).

Tap protein is another protein that plays a significant role in nuclear RNA export ([47]). This protein contains an RNA binding domain, a nuclear export signal, and a binding domain for nucleoporins (proteins that make up the nuclear pore) ([48]). The recruitment of this protein to spliced mRNA has been proposed to be the final step required before nuclear pore binding ([48]).

**Table 1.1:** Summary of proteins bound to pre-mRNA

Type of Protein	Comments
RNA polymerase II	
Capping enzyme	
Cap binding proteins	May stay attached all the way through export from nucleus ([36])
Polyadenylation machinery	At least 12 proteins including an as-of-yet unidentified endonuclease and Poly(A) polymerase, along with many other required protein factors.

Poly(A) binding proteins	
Spliceosome	A ribonucleoprotein (RNP) machine that contains at least 50 proteins and 5 small nuclear RNAs. Some of these proteins remain bound after splicing and are required for nuclear export ([49]).
Exon-exon junction complex	Multi-protein complex 20-24 nucleotides upstream of an exon-exon junction ([50]; [34]). This complex binds to as little as eight nucleotides
hnRNP proteins	An assortment of at least 20 proteins that associate with nascent pre-mRNA; has roles in localization, processing and nuclear transport. The binding sites of some of these proteins has been identified as being in the 3' UTR of mRNAs. Others (of the hnRNP C family) associate preferentially with introns.

*Distribution of RNA between nucleus and cytoplasm.* An important issue pertaining to the measurement of mRNA levels using hairpin probes is the relative levels of RNA in the nucleus and cytoplasm. It has been reported that a large fraction of RNA (>95%) synthesized by RNA polymerase II never leaves the nucleus as mature mRNA ([51]). Further, over 1/3 of the RNAs never reaches the cytoplasm due to mRNA processing events (removal of introns, transcription termination). There is also a population of

primary transcripts that are not polyadenylated or transported from the nucleus (termed “nonproductive hnRNAs”), and therefore never destined to produce mRNA ([51]). It is therefore possible for probes to bind to mRNAs in the nucleus that may never be translated.

*Transport and localization of mRNP.* Following export from the nucleus, an mRNP is often transported to specific regions within cells. It is believed that the specific localization of mRNPs has a key role in the compartmentalization of protein synthesis in the cytoplasm ([52];[53]; [54]). Key questions remain open in this area include: (1) Are mRNPs localized in cells? If so, is there a general cell structure where most of the mRNPs are localized? (2) What is the intracellular system along which they are being transported to their destination? (3) What factors decide specific localization of mRNPs? (4) What is the biological significance of mRNP localization in cells?

Most mRNPs are believed to be associated with the cytoskeleton, which may be used to transport and localize the mRNP to specific sites within a cell. Although the details of this process remain elusive, there is growing evidence suggesting the importance of the cytoskeleton in mRNA localization. The key evidence is that there exists a close association of polyribosomes (also referred to as polysomes) with the cytoskeleton ([10]; [54]; [55]; [2]). In addition, studies have shown that microtubules are involved in the assembly of membrane-bound polyribosomes ([56];[57]). Using drug treatment to depolymerize microtubules, membrane-bound ribosomes were prevented from initiating protein synthesis and showed a decreased level of total poly(A) mRNP and fibronectin mRNP. Although these studies did not identify the nature of the interaction between membrane (ER) bound polysomes and microtubules, they did show a close relationship between the cytoskeleton, ER bound polysomes, mRNP transport and protein synthesis. Further, using both *in vitro* reconstitution and biochemical

fractionation provided EM evidence that a fraction of polyribosomes/mRNPs was bound to microtubules ([57, 58]). **Figure 1.7** illustrates the proposed models for transport of mRNAs in the cytoplasm of cells.

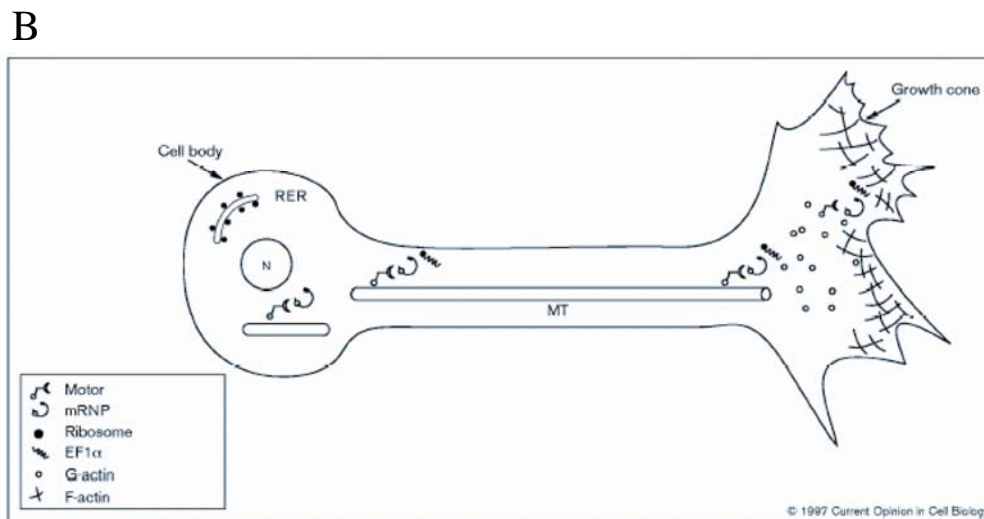
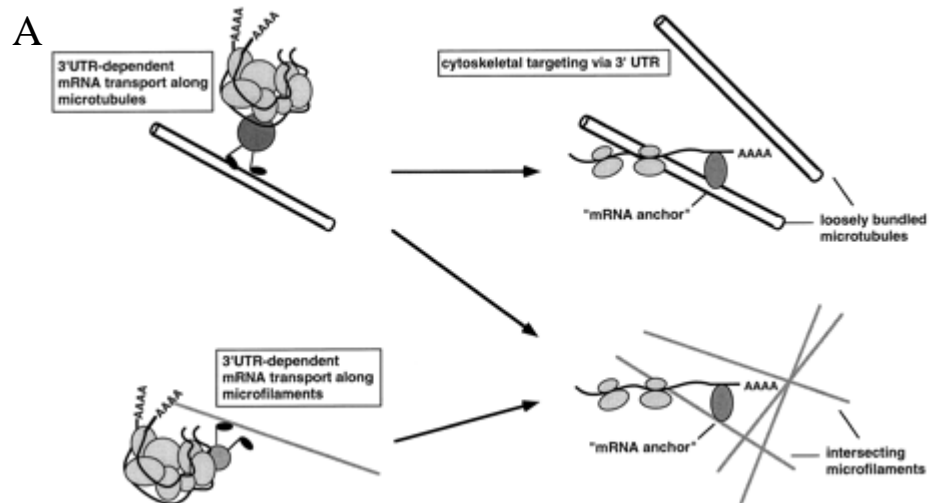


**Figure 1.7:** A: Representation of cytoskeletal elements (microtubule and microfilaments) involved in localization and transport of mRNA (Adopted from Ref. ([1])

B: Transport of specific mRNA along microtubule in an axon of a neuron (Adopted from Ref ([2]).

*Localization of mRNPs and mRNAs.* At present, there is no clear consensus as to what fraction of mRNPs are localized with the cytoskeleton. Biochemical evidence provided by ([59]) suggests that 70-80% of mRNPs in a cell are co-localized with the cytoskeleton. Due to the lack of fluorescent or chemical tags, the verification of the biochemical results in intact cells has been limited to one or two specific mRNPs. For example, using *in situ* hybridization and biochemical fractionation, [60, 61] and [62] have demonstrated co-localization of mRNPs of the myosin heavy chain with cytoskeletal elements. The studies by [2, 6, 63] have shown the association of actin and poly(A) mRNAs with cytoskeletal elements, especially microtubules. Using a similar *in situ* approach, a study by ([55]) have implicated cytoskeletal localization of metallothionein I. There is a clear need to better understand the localization of mRNPs, their association with specific elements in a cell and the biological significance of co-localization.

It has been shown ([9, 64]) that the 3' UTR plays a significant role in specific localization of certain mRNA's in cells. Specifically, using genetic engineering to perturb mRNA in the 3' UTR region, it has been shown that the 3' UTR regions of heavy chain myosin, actin, c-myc, metallothionein-I are critical for the localization of these specific mRNPs. Although the localization signal in the mRNA sequence has been identified, the structural basis of the 3' UTR, the associated binding proteins and, perhaps more importantly, the processes involved in specific localization and transport are still poorly understood. To date, proteins responsible for the specific localization of mRNA have been identified only for oskar and nanos mRNA in *Drosophila* oocytes ([65]; [13]) and for actin mRNA in chicken fibroblasts ([66, 67]). In both cases, cytoskeletal elements have been shown to be involved in transport and localization of the mRNAs.

As mentioned earlier, it is mRNP rather than mRNA alone that provides the functional unit for localized protein synthesis. In order to understand the intracellular

transport and localization of mRNA, extensive studies need to be performed to track the movement of mRNP complexes. Possible approaches for doing so include labeling proteins with GFP ([12]), generating transgenes with high affinity binding sites for a GFP tagged proteins ([13]), site-specific protein labeling using FLAsH ([68]), and targeting mRNAs using molecular beacons ([69]). These approaches in combination with high-resolution microscopy ([70]) or EM may reveal the detailed structural organization of mRNP transport and localization in living cells.

*Degradation of mRNA.* One of major pathways of regulating posttranscriptional gene expression is the degradation of mRNA. Considerable focus has been placed on understanding the transcriptional controls of mRNA synthesis, but there is very limited understanding of the mechanisms responsible for controlling the rate of mRNA degradation, which affects the intracellular mRNA level. It has been suggested that a variety of physiological signals such as hormones ([70-72]), iron binding proteins and cell cycle regulators ([73]) may have significant effects on the decay rates of specific mRNAs, and the half-life of different mRNA's is closely related to its biological role. It has been found that specific cis acting elements rich in AU sequences, designated as the AU rich element (ARE) in the 3' UTR determine the stability of mRNA. Sequence analysis of various mRNAs with short half-lives has confirmed the presence of consensus ARE sequences. Further comparisons across species (*C. elegans* and humans) have indicated the evolutionary conservation of ARE domains ([74]). ARE sequences are homologous across different mRNAs but their copy number and their clustering pattern (groups of pentamers etc.) is different. This may account for differences in mRNA lifetimes.

Association of ARE binding proteins with ARE rich domains have been proposed as the key regulatory step in controlling the turnover of RNA. Currently, we do not have

a rigorous understanding of this class of proteins. Do regulatory protein-complexes such as exosomes directly bind to ARE regions? What are the structural requirements for such recognition and what is the key recognition domain? Is it structural such as hairpin loops or a combination of structural and sequence dependence? Answering these questions requires fundamental understanding of the structural features of protein-RNA complexes, as well as the dynamics of protein-RNA interactions in the cytoplasm.

The hypothesis of ARE binding protein mediated regulation is based on remodeling of local RNA structure, which leads to recruitment of additional *trans* acting elements such as ribonucleases or helicases to degrade and unfold RNP complexes. mRNA molecules may be stabilized by the binding of signaling proteins or competing proteins, which may disrupt or interfere with the proteins involved in mRNA degradation. This model has been proposed for the self-stabilization of Bcl-2 mRNA since the Bcl-2 protein binds to the ARE rich domain of its own mRNA.

In addition to the above ARE model of mRNA degradation, several theories have been proposed to explain the decay pathways of mRNA using a yeast-based model system. For example, ([75]) has proposed a relationship between mRNA stability and the length of mRNA. However, studies by [76] using microarray analysis of mRNA stability in yeast have failed to correlate stability with the length of mRNA. Their data suggest that mRNA decay is closely related to specific functions of a given mRNA and is controlled by interactions of mRNA with specific signaling proteins. In addition, a nonsense-mediated decay pathway both in the nucleus and the cytoplasm but independent of the 3' UTR region has been described as a control mechanism for mRNA degradation ([77]; [78]).

Much remains to be elucidated regarding the processes of mRNA production, transport, localization and degradation. It is obvious, however, that at each step, from

transcription to nuclear export of a mature mRNA, to mRNA decay, *proteins are always associated with pre-mRNA and mRNA*. These associations are dynamic in nature with regard to both protein type and binding sites. An mRNA molecule that gets exported to the cytoplasm is more precisely an mRNP (ribonucleoprotein complex) ([34]). The proteins bound to the mRNA not only play a crucial role in the processing of pre-mRNA but also are ([79]; [49]; [80]) involved in the export, transport, localization, and stability of mRNA in the cytoplasm. Although we are still in the early stages of identifying proteins that are associated with mRNPs, some specific protein–RNA associations have been uncovered using both biochemical and genetic methods (e.g. [81], [41]; [82]). Specifically, proteins have been shown to be associated at exon-exon junctions, the 3'UTR region, and the 5' cap regions of mRNA. This is a critical issue in mRNA detection in that probes cannot hybridize to the target regions occupied by RNA-binding proteins. It is necessary to identify the mechanisms for mRNA transport and degradation as controlled by the RNA/protein interactions. As the steps of mRNA production, transport and localization are further clarified, it will become easier to design nanostructured hairpin probes to target regions of pre-mRNA that are least likely to be occluded by bound proteins. Probe design should therefore take into account what is already known about proteins bound to pre-mRNA; specifically, probes should not be designed to target the 3' UTR, the exon-exon junction, or introns due to the proven presence of protein complexes in this region.

### **Cellular delivery of probes**

One of the most critical aspects of measuring the intracellular level of mRNA using synthetic probes is the ability to deliver these probes into cells through the plasma membrane. In what follows we discuss the existing methods for delivering hairpin probes

into live cells and the possible effects of delivery on intracellular distribution, dynamics, binding and lifetime of the probes.

The plasma membrane is quite lipophilic and restricts the transport of large and charged molecules. Therefore, it is a very robust barrier to polyanionic molecules such as hairpin oligonucleotides. Further, even if the probes enter the cells successfully, the efficiency of this process must be defined not by how many probes can enter the cell or how many cells have probes internalized, but how many probes remain functional inside cells and hybridize to their targets with high specificity. This is very different from both antisense and gene delivery applications where the level of protein expression or reduction is the final metric used to define efficiency or success. It is also important to examine how the delivery technique might impact the fate of the probes inside a cell. Since a significant amount of RNA molecules (including mRNA and rRNA) are in the cytoplasm, any delivery method aimed at measuring intracellular RNA should result in a large amount of probes in the cytoplasm.

Existing cellular delivery techniques can be divided into two categories: endocytic and non-endocytic methods. Endocytic delivery typically employs cationic and polycationic molecules such as liposomes and dendrimers, while non-endocytic methods include microinjection, and the use of cell-penetrating peptides (CPP) or streptolysin O (SLO). Here we focus on the applications of these methods to delivering oligonucleotide (ODN) probes into live cells and how delivery would impact the functionality of the probes.

Endocytic Methods. ODN probes can be transported into live cells by simply incubating them in solution with cells for ~ 2 h. The delivery is mediated by the endocytic pathway is by specific membrane surface receptors and studies have shown the existence of at least 5 major cell surface receptors that bind specifically to ODNs ([83]). Fluorescently

labeled ODN probes usually exhibit a punctate fluorescence pattern indicating endocytosis. Electrostatic complexes of anionic ODNs with cationic liposomes or polymeric dendrimers (such as polyamidoamine or polyethyleneimine) have been shown to enhance ODN uptake; they are designed to provide some level of nuclease protection and have in many cases incorporated pH sensitive molecules that enhance their ability to escape from endosomes. However, even with all these, the efficiency of cytoplasmic delivery of functional probes was estimated to be only 0.01-10 percent ([83]) due to the fact that once internalized via endocytosis, the ODN probes are predominately trapped inside endosomes and often lysosomes, and being degraded there.

During endocytosis, the receptors on the cell surface are activated by the ODN probes, which are then being enclosed in a small portion of the plasma membrane that pinches off to form an endocytic vesicle called early endosomes. The environment within early endosomes is fairly acidic, with a pH of approximately 6. As they proceed to become late endosomes, the pH continues to decrease and the newly synthesized acid hydrolases are accumulated within them. Unless escaped from the endosomes, the ODN probes will be trapped in lysosomes, which are membrane-enclosed vesicles filled with hydrolytic enzymes for intracellular digestion. Most of the active cytoplasmic nucleases are in the lysosomes, not in the cytosol itself. Clearly, inside a lysosome the environment is extremely bad for ODN probes and therefore it is imperative that the ODN probes are released from the early endosomes as soon as possible. For example, viruses, both enveloped and non-enveloped, have specific mechanisms to enable their genetic material to escape from the endosomes/lysosomes and be efficiently delivered to the cytosol.

To overcome this difficulty, polyamidoamine dendrimers were designed to escape from endosomes by polymer swelling and osmotic-induced swelling, as theorized by ([84]). At neutral pH, electrostatic repulsion between protonated primary

amines causes the fractured dendrimer to be fully extended which, after binding electrostatically with DNA, collapse into a more compact form. Once the pH decreases within the endosome, tertiary amines become protonated and the excess polymer is released from the complex, resulting in endosomal swelling and subsequent rupture. A large excess of dendrimer is usually required to promote high delivery efficiency, possibly because the excess non-complexed dendrimers swell and help burst the endosomes.

Even with this mechanism for endosomal exit of probes, it is still unclear how nucleic acids are released from cationic molecules. For liposomes it has been suggested ([85]) that once inside a vesicle, anionic lipids from the cytoplasmic-facing monolayer diffuse into the complex, fusing with the cationic liposome and therefore releasing the oligonucleotide. Dissociation of nucleic acids from cationic molecules may occur in endosomes, cytosol or the nucleus, but in most cases the mechanisms are unknown.

Many issues remain to be addressed in endocytic delivery of ODN probes, for example, how to protect ODN probes from nucleases in the endosomes, and why endocytic delivery often results in internalization of nucleic acids into the nucleus. Various studies have shown that, when internalized through the endocytic pathway, a large portion of ODN probes are trapped within intracellular vesicles such as endosomes and lysosomes, degraded by nucleases, and prevented from reaching their target ([83]).

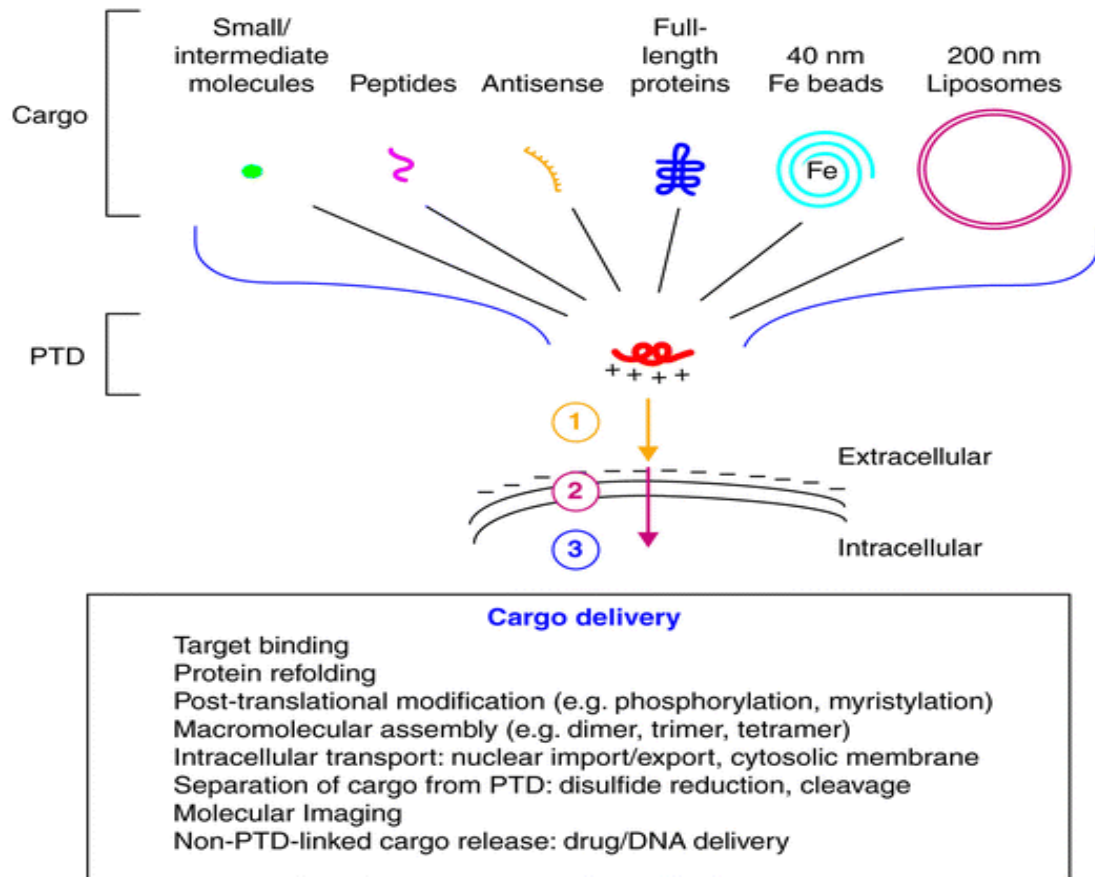
### Cell permeable Peptides

As mentioned above, intracellular delivery can be very challenging as the plasma membrane forms a formidable barrier for biomolecules. The discovery of cell permeable peptides has made it possible to transduce a broad range of agents into living cells ([86], [87]). These peptides have been used to deliver range of biomolecules such a proteins

[88], peptides (including phosphopeptides [89]), PNA [90], liposomes [91] into live cells. **Figure 1.8** outlines some of the potential application of CPP mediated delivery of macromolecules. Even though at present there is very limited understanding of transduction mechanism, this technology is emerging as a useful tool for targeting heterologous cargos in living cells. Among the host of peptides with membrane translocating activity are antennapedia, HSV-1 VP22, and the HIV-1 tat peptide (Tat<sub>48-60</sub>). The HIV-1 tat peptide and its derivatives have received the most attention because they are short and very efficient in delivery (can deliver huge macromolecules across cell membrane in less than 30 mins). The Tat protein from HIV-1 is an 86 amino acid transactivation protein that is involved in promoting transcription of the HIV-1 virus. The Tat peptide is rich in cationic amino acids and especially arginines (Amino acids 49-60 of the Tat protein). Arginines are very common in many of the cell permeable peptides (CPP), yet there seems to be little homology among them. The exact mechanism for membrane translocation is currently unknown. It has been shown to be very effective method to deliver proteins etc in living cells as well as for *in-vivo* applications ([92]; [87]). This makes this peptide based delivery an interesting candidate for our study, as we are interested in developing probes for live cells measurement using optical detection as well as MR contrast agents for *in-vivo* applications. Thus we can extend our learning from development of peptide- MB constructs to deliver probes in living cells to *in-vivo* applications. With this motivation, we have decided to pursue peptide-based delivery in living cells as a first step towards achieving our long-term research goals for *in-vivo* imaging.

In addition, CPP's are of interest to wide range of researchers due to their efficient translocation of macromolecules across cell membrane. This poses an interesting question regarding mechanism of translocation across cell membrane. Answer to this question, may help us develop better drug delivery strategies and also

understand the basic cellular physiology involved in translocation of CPP's across cell membrane. Although, in present research our major focus is to develop approaches for imaging of cellular process using molecular probes, we plan to use some of the imaging tools to address the possible nature of interaction of CPP's to the cell surface. In this study, we have selected to use HIV-1 Tat peptide (49-60 amino acids) and poly Arg peptide (11 mer).



Current Opinion in Biotechnology

**Figure 1.8:** Illustration of the Tat mediated delivery of various cargoes across the plasma membrane of living cells

## **Challenges in Imaging of mRNA using Molecular Beacons**

Based on our discussion in previous sections, it is clear that the major challenges in measuring endogenous gene expression in living cells and tissue is the design of highly sensitive and selective reporter probes with a wide dynamic range. For oligonucleotide-based probes, in addition to challenges of delivery and maintaining integrity of probe in cell cytoplasm, the biggest challenge is to find a segment of mRNA, which can be targeted by the probe. This segment of mRNA has to be unique, such that it does not have significant sequence homology with other RNA sequences and also it should not have a structural constraint that may prevent hybridization of the probe. As discussed in previous sections, proteins play a significant role in controlling the tertiary structure of mRNP's. Although at present the theoretical prediction of the tertiary structure of RNPs is not feasible, yet using secondary structure predictions of RNAs may provide a first order approximation towards rational design of MB probes.

Further in cellular imaging, a significant challenge is the sensitivity of our detection system. In this study, we have used confocal microscopy for most of the studies. We have also validated our confocal measurements using epifluorescence microscopy. Both these methods of imaging have their relative advantages and disadvantages. Confocal microscopy uses a narrow source of light (laser of fixed wavelength) to excite the sample, further the detection system (confocal pin hole) is designed with a pinhole to allow for detection of light only from a focus area using PMT (Photomultiplier Tube). This system allows us to take thin slices in a living cell sample, without significant background and out of focus fluorescence. The ability to optically section the cells can be extremely useful in understanding the distribution of the mRNAs in living samples. Further PMTs are highly sensitive in detection of the fluorescent signal as the signal is amplified within the PMT detector. The limitation of using PMT can be the higher level of noise in the detector especially if the PMT's is not cooled. Further

challenge in using PMT as a detector is the non-uniform response of the PMT to the wavelength range of interest. PMTs have a peak in their detection efficiency around 540-570 nm, but a detection efficiency decays rapidly for near-IR wavelength range (680 nm or higher wavelength range). Some of these challenges can be overcome by using APD's as they have much flat response in their detection efficiency over a wide range of wavelengths. The other major advantage of confocal imaging is the ability to simultaneously detect multi-color labeling which can be extremely useful for co-localization experiments.

The epi-fluorescence microscopy has a distinct advantage of providing a comprehensive intensity over a thick slice in a cell, which can be useful especially if the signal intensity is particularly low. The epi-fluorescence microscopy can be further improved by combining de-convolution of the fluorescence images to remove out of focus blur, which is a major limitation of this imaging method. Further using automated stage we can improve the ability to optically section living cells and also take z slices similar to a confocal imaging set up.

Further the challenge in sensitivity also comes from the lack of ability to detect single molecules or few molecules of fluorescent dyes. This limitation is inherent in this study, as neither of our set-ups have the ability to detect signal with this sensitivity. This implies if mRNAs are not localized in the cells, our imaging system may not be able to detect them. Thus with our system, our results in imaging are biased towards areas with high intensity of fluorescent signal. This is the inherent limitation of most of the imaging methods. Thus localized RNAs can lead to significant enhancement of our signal to noise ratio in the cells, in addition to inherent signal to noise of a molecular beacons.

## Organization of the Thesis

With this background information, the part-1 of this study is focused on developing a probe -based approach to image RNAs in living cells. In this area, my focus is in developing MB probes as a potential probe for imaging of RNAs in living cells. In the early part of this study, my objective was to develop a delivery approach, which can allow for effectively delivery of MB probes in living cells. Further we wanted to develop a method, which is not only limited to cell culture but also has a potential for in-vivo imaging in a small animal models. With this focus, I have chosen to adapt a cell permeable peptide as a carrier for MB probes (**Chapter 2**). Using this approach we have demonstrated effective delivery of MB probes to the cytoplasm of living cells and spepcific detection of mRNAs in living cells. In nest stage, I have studied the co-localization of specific mRNAs with the sub cellular structures using previously developed peptide linked MB probes in living cells (**Chapter 3**). This part provides us insight into specific organization of mRNAs in living cells. This addresses a key biological question, regarding sub-cellular localization and co-localization of specific mRNAs in the cytoplasm of living cells.

In a next step in this direction, my research has been aimed at understanding at what stage our probes hybridize with mRNAs (**Chapter 4**). This is a central question, which address the issues related to understanding if the probes have a preferred accessibility to hybridize to mRNAs during a specific stage in its life cycle in the cytoplasm. This also provides us insight into issues related to RNA secondary structure and sub-cellular localization. This understanding is also critical for relating the fluorescence intensity from the MB probe signal with gene expression. For this study we have combined chemical perturbations with the MB probes to study this question. I have also explored the role of backbone chemistry in this direction.

Further in next part of this study, I have combined a FRAP (Fluorescence recovery after photo bleaching) based biophysical imaging approach with the MB probes to understand the dynamics of the target mRNAs (**Chapter 5**). This part has focused on understanding the role of various cellular structures and biochemical activities which regulate the transport/ dynamics of the target mRNAs. This study has provided further insight into the structure- function relationship in sub-cellular organization of mRNAs.

To expand the potential of MB probes for study of mRNA biology, we have extended the previously developed peptide based delivery approach to target MBs to the nucleus of living cell. This approach in combination with the earlier developed method for imaging of RNA in the cytoplasm can allow us to image the integrated distribution of mRNAs from the nucleus to the cytoplasm. In this direction I have focused on detection and imaging of small nuclear RNAs in nuclei of living cells (**Chapter 6**).

In second part of this thesis, I have focused on development of magnetic nanoparticles based probes for MR based imaging. In this area, the first study was focused on development of biocompatible functionalized particles with a very narrow size distribution (**Chapter 7**). In (**Chapter 8**), I have extending this research towards further development and optimization of contrast of these magnetic nanoparticles. In this study, we have evaluated the role of coatings thickness in optimization of MR contrast. The major motivation for this effort has been to develop a magnetic nanoparticles based probes, which can allow for deep tissue imaging. This initial study has identified and in certain cases addressed various challenges in adapting inorganic nanoscale particles to biological samples.

## References

- [1] R. P. Jansen, RNA-cytoskeletal associations, *Faseb J* 13 (1999) 455-466.
- [2] G. Bassell, and R. H. Singer, mRNA and cytoskeletal filaments, *Curr Opin Cell Biol* 9 (1997) 109-115.
- [3] J. B. Glotzer, R. Saffrich, M. Glotzer, and A. Ephrussi, Cytoplasmic flows localize injected oskar RNA in *Drosophila* oocytes, *Curr Biol* 7 (1997) 326-337.
- [4] Q. Huang, and T. Pederson, A human U2 RNA mutant stalled in 3' end processing is impaired in nuclear import, *Nucleic Acids Res* 27 (1999) 1025-1031.
- [5] M. R. Jacobson, and T. Pederson, Localization of signal recognition particle RNA in the nucleolus of mammalian cells, *Proc Natl Acad Sci U S A* 95 (1998) 7981-7986.
- [6] G. J. Bassell, C. M. Powers, K. L. Taneja, and R. H. Singer, Single mRNAs visualized by ultrastructural in situ hybridization are principally localized at actin filament intersections in fibroblasts, *J Cell Biol* 126 (1994) 863-876.
- [7] M. Somasundaran, M. L. Zapp, L. K. Beattie, L. Pang, K. S. Byron, G. J. Bassell, J. L. Sullivan, and R. H. Singer, Localization of HIV RNA in mitochondria of infected cells: potential role in cytopathogenicity, *J Cell Biol* 126 (1994) 1353-1360.
- [8] J. L. Veyrone, G. P. Campbell, J. Wiseman, J. M. Blanchard, and J. E. Hesketh, A localisation signal in the 3' untranslated region of c-myc mRNA targets c-myc mRNA and beta-globin reporter sequences to the perinuclear cytoplasm and cytoskeletal-bound polysomes, *J Cell Sci* 109 (Pt 6) (1996) 1185-1194.
- [9] P. Mahon, K. Partridge, J. H. Beattie, L. A. Glover, and J. E. Hesketh, The 3' untranslated region plays a role in the targeting of metallothionein-I mRNA to the perinuclear cytoplasm and cytoskeletal-bound polysomes, *Biochim Biophys Acta* 1358 (1997) 153-162.
- [10] G. J. Bassell, R. H. Singer, and K. S. Kosik, Association of poly(A) mRNA with microtubules in cultured neurons, *Neuron* 12 (1994) 571-582.

- [11] S. Behrens, B. M. Fuchs, F. Mueller, and R. Amann, Is the in situ accessibility of the 16S rRNA of *Escherichia coli* for Cy3-labeled oligonucleotide probes predicted by a three-dimensional structure model of the 30S ribosomal subunit? *Appl Environ Microbiol* 69 (2003) 4935-4941.
- [12] A. S. Brodsky, and P. A. Silver, Identifying proteins that affect mRNA localization in living cells, *Methods* 26 (2002) 151-155.
- [13] K. M. Forrest, and E. R. Gavis, Live imaging of endogenous RNA reveals a diffusion and entrapment mechanism for nanos mRNA localization in *Drosophila*, *Curr Biol* 13 (2003) 1159-1168.
- [14] S. Tyagi, and F. R. Kramer, Molecular beacons: probes that fluoresce upon hybridization, *Nat Biotechnol* 14 (1996) 303-308.
- [15] G. Bonnet, S. Tyagi, A. Libchaber, and F. R. Kramer, Thermodynamic basis of the enhanced specificity of structured DNA probes, *Proc Natl Acad Sci U S A* 96 (1999) 6171-6176.
- [16] A. Tsourkas, M. A. Behlke, S. D. Rose, and G. Bao, Hybridization kinetics and thermodynamics of molecular beacons, *Nucleic Acids Res* 31 (2003) 1319-1330.
- [17] A. Tsuji, H. Koshimoto, Y. Sato, M. Hirano, Y. Sei-lida, S. Kondo, and K. Ishibashi, Direct observation of specific messenger RNA in a single living cell under a fluorescence microscope, *Biophys J* 78 (2000) 3260-3274.
- [18] A. Tsourkas, M. A. Behlke, Y. Xu, and G. Bao, Spectroscopic features of dual fluorescence/luminescence resonance energy-transfer molecular beacons, *Anal Chem* 75 (2003) 3697-3703.
- [19] H. Kuhn, V. V. Demidov, J. M. Coull, M. J. Fiandaca, B. D. Gildea, and M. D. Frank-Kamenetskii, Hybridization of DNA and PNA molecular beacons to single-stranded and double-stranded DNA targets, *J Am Chem Soc* 124 (2002) 1097-1103.
- [20] M. Zuker, and P. Stiegler, Optimal computer folding of large RNA sequences using thermodynamics and auxiliary information, *Nucleic Acids Res* 9 (1981) 133-148.
- [21] J. S. McCaskill, The equilibrium partition function and base pair binding probabilities for RNA secondary structure, *Biopolymers* 29 (1990) 1105-1119.

[22] D. J. Ecker, T. A. Vickers, T. W. Bruice, S. M. Freier, R. D. Jenison, M. Manoharan, and M. Zounes, Pseudo-half-knot formation with RNA, *Science* 257 (1992) 958-961.

[23] D. H. Mathews, M. E. Burkard, S. M. Freier, J. R. Wyatt, and D. H. Turner, Predicting oligonucleotide affinity to nucleic acid targets, *Rna* 5 (1999) 1458-1469.

[24] M. Andronescu, R. Aguirre-Hernandez, A. Condon, and H. H. Hoos, RNAsoft: A suite of RNA secondary structure prediction and design software tools, *Nucleic Acids Res* 31 (2003) 3416-3422.

[25] S. Agrawal, Importance of nucleotide sequence and chemical modifications of antisense oligonucleotides, *Biochim Biophys Acta* 1489 (1999) 53-68.

[26] M. Manoharan, 2'-carbohydrate modifications in antisense oligonucleotide therapy: importance of conformation, configuration and conjugation, *Biochim Biophys Acta* 1489 (1999) 117-130.

[27] E. A. Lesnik, C. J. Guinosso, A. M. Kawasaki, H. Sasmor, M. Zounes, L. L. Cummins, D. J. Ecker, P. D. Cook, and S. M. Freier, Oligodeoxynucleotides containing 2'-O-modified adenosine: synthesis and effects on stability of DNA:RNA duplexes, *Biochemistry* 32 (1993) 7832-7838.

[28] M. Petersen, and J. Wengel, LNA: a versatile tool for therapeutics and genomics, *Trends Biotechnol* 21 (2003) 74-81.

[29] M. Frieden, H. F. Hansen, and T. Koch, Nuclease stability of LNA oligonucleotides and LNA-DNA chimeras, *Nucleosides Nucleotides Nucleic Acids* 22 (2003) 1041-1043.

[30] M. Egholm, O. Buchardt, L. Christensen, C. Behrens, S. M. Freier, D. A. Driver, R. H. Berg, S. K. Kim, B. Norden, and P. E. Nielsen, PNA hybridizes to complementary oligonucleotides obeying the Watson-Crick hydrogen-bonding rules, *Nature* 365 (1993) 566-568.

[31] S. A. Kushon, J. P. Jordan, J. L. Seifert, H. Nielsen, P. E. Nielsen, and B. A. Armitage, Effect of secondary structure on the thermodynamics and kinetics of PNA hybridization to DNA hairpins, *J Am Chem Soc* 123 (2001) 10805-10813.

[32] A. De Mesmaeker, K. H. Altmann, A. Waldner, and S. Wendeborn, Backbone modifications in oligonucleotides and peptide nucleic acid systems, *Curr Opin Struct Biol* 5 (1995) 343-355.

- [33] T. Ratilainen, A. Holmen, E. Tuite, P. E. Nielsen, and B. Norden, Thermodynamics of sequence-specific binding of PNA to DNA, *Biochemistry* 39 (2000) 7781-7791.
- [34] G. Dreyfuss, V. N. Kim, and N. Kataoka, Messenger-RNA-binding proteins and the messages they carry, *Nat Rev Mol Cell Biol* 3 (2002) 195-205.
- [35] S. McCracken, N. Fong, K. Yankulov, S. Ballantyne, G. Pan, J. Greenblatt, S. D. Patterson, M. Wickens, and D. L. Bentley, The C-terminal domain of RNA polymerase II couples mRNA processing to transcription, *Nature* 385 (1997) 357-361.
- [36] A. J. Shatkin, and J. L. Manley, The ends of the affair: capping and polyadenylation, *Nat Struct Biol* 7 (2000) 838-842.
- [37] M. J. Dye, and N. J. Proudfoot, Terminal exon definition occurs cotranscriptionally and promotes termination of RNA polymerase II, *Mol Cell* 3 (1999) 371-378.
- [38] C. E. Birse, L. Minvielle-Sebastia, B. A. Lee, W. Keller, and N. J. Proudfoot, Coupling termination of transcription to messenger RNA maturation in yeast, *Science* 280 (1998) 298-301.
- [39] C. A. Collins, and C. Guthrie, The question remains: is the spliceosome a ribozyme? *Nat Struct Biol* 7 (2000) 850-854.
- [40] J. F. Caceres, G. R. Screaton, and A. R. Krainer, A specific subset of SR proteins shuttles continuously between the nucleus and the cytoplasm, *Genes Dev* 12 (1998) 55-66.
- [41] H. Le Hir, M. J. Moore, and L. E. Maquat, Pre-mRNA splicing alters mRNP composition: evidence for stable association of proteins at exon-exon junctions, *Genes Dev* 14 (2000) 1098-1108.
- [42] M. L. Luo, Z. Zhou, K. Magni, C. Christoforides, J. Rappsilber, M. Mann, and R. Reed, Pre-mRNA splicing and mRNA export linked by direct interactions between UAP56 and Aly, *Nature* 413 (2001) 644-647.
- [43] K. L. Farina, and R. H. Singer, The nuclear connection in RNA transport and localization, *Trends Cell Biol* 12 (2002) 466-472.
- [44] K. Ainger, D. Avossa, A. S. Diana, C. Barry, E. Barbarese, and J. H. Carson, Transport and localization elements in myelin basic protein mRNA, *J Cell Biol* 138 (1997) 1077-1087.

- [45] K. S. Hoek, G. J. Kidd, J. H. Carson, and R. Smith, hnRNP A2 selectively binds the cytoplasmic transport sequence of myelin basic protein mRNA, *Biochemistry* 37 (1998) 7021-7029.
- [46] W. Gu, F. Pan, H. Zhang, G. J. Bassell, and R. H. Singer, A predominantly nuclear protein affecting cytoplasmic localization of beta-actin mRNA in fibroblasts and neurons, *J Cell Biol* 156 (2002) 41-51.
- [47] B. R. Cullen, Nuclear RNA export, *J Cell Sci* 116 (2003) 587-597.
- [48] B. R. Cullen, Connections between the processing and nuclear export of mRNA: evidence for an export license? *Proc Natl Acad Sci U S A* 97 (2000) 4-6.
- [49] M. J. Luo, and R. Reed, Splicing is required for rapid and efficient mRNA export in metazoans, *Proc Natl Acad Sci U S A* 96 (1999) 14937-14942.
- [50] I. M. Palacios, RNA processing: splicing and the cytoplasmic localisation of mRNA, *Curr Biol* 12 (2002) R50-52.
- [51] D. A. Jackson, A. Pombo, and F. Iborra, The balance sheet for transcription: an analysis of nuclear RNA metabolism in mammalian cells, *Faseb J* 14 (2000) 242-254.
- [52] G. Aakalu, W. B. Smith, N. Nguyen, C. Jiang, and E. M. Schuman, Dynamic visualization of local protein synthesis in hippocampal neurons, *Neuron* 30 (2001) 489-502.
- [53] E. A. Shestakova, R. H. Singer, and J. Condeelis, The physiological significance of beta -actin mRNA localization in determining cell polarity and directional motility, *Proc Natl Acad Sci U S A* 98 (2001) 7045-7050.
- [54] J. E. Hesketh, Sorting of messenger RNAs in the cytoplasm: mRNA localization and the cytoskeleton, *Exp Cell Res* 225 (1996) 219-236.
- [55] P. Mahon, J. Beattie, L. A. Glover, and J. Hesketh, Localisation of metallothionein isoform mRNAs in rat hepatoma (H4) cells, *FEBS Lett* 373 (1995) 76-80.
- [56] P. R. Walker, and J. F. Whitfield, Cytoplasmic microtubules are essential for the formation of membrane-bound polyribosomes, *J Biol Chem* 260 (1985) 765-770.

- [57] B. Zhou, and M. Rabinovitch, Microtubule involvement in translational regulation of fibronectin expression by light chain 3 of microtubule-associated protein 1 in vascular smooth muscle cells, *Circ Res* 83 (1998) 481-489.
- [58] D. Hamill, J. Davis, J. Drawbridge, and K. A. Suprenant, Polyribosome targeting to microtubules: enrichment of specific mRNAs in a reconstituted microtubule preparation from sea urchin embryos, *J Cell Biol* 127 (1994) 973-984.
- [59] S. K. Pramanik, R. W. Walsh, and J. Bag, Association of messenger RNA with the cytoskeletal framework in rat L6 myogenic cells, *Eur J Biochem* 160 (1986) 221-230.
- [60] J. W. Wiseman, L. A. Glover, and J. E. Hesketh, Localisation of beta-globin reporter sequences to the perinuclear cytoplasm by myosin heavy chain and vimentin 3'untranslated regions, *Biochem Soc Trans* 24 (1996) 188S.
- [61] J. W. Wiseman, L. A. Glover, and J. E. Hesketh, Evidence for a localization signal in the 3'untranslated region of myosin heavy chain messenger RNA, *Cell Biol Int* 21 (1997) 243-248.
- [62] B. Russell, and D. J. Dix, Mechanisms for intracellular distribution of mRNA: in situ hybridization studies in muscle, *Am J Physiol* 262 (1992) C1-8.
- [63] G. J. Bassell, Y. Oleynikov, and R. H. Singer, The travels of mRNAs through all cells large and small, *Faseb J* 13 (1999) 447-454.
- [64] E. H. Kislauskis, Z. Li, R. H. Singer, and K. L. Taneja, Isoform-specific 3'-untranslated sequences sort alpha-cardiac and beta-cytoplasmic actin messenger RNAs to different cytoplasmic compartments, *J Cell Biol* 123 (1993) 165-172.
- [65] D. Ferrandon, L. Elphick, C. Nusslein-Volhard, and D. St Johnston, Staufen protein associates with the 3'UTR of bicoid mRNA to form particles that move in a microtubule-dependent manner, *Cell* 79 (1994) 1221-1232.
- [66] E. H. Kislauskis, X. Zhu, and R. H. Singer, beta-Actin messenger RNA localization and protein synthesis augment cell motility, *J Cell Biol* 136 (1997) 1263-1270.
- [67] V. M. Latham, Jr., E. H. Kislauskis, R. H. Singer, and A. F. Ross, Beta-actin mRNA localization is regulated by signal transduction mechanisms, *J Cell Biol* 126 (1994) 1211-1219.

- [68] B. A. Griffin, S. R. Adams, J. Jones, and R. Y. Tsien, Fluorescent labeling of recombinant proteins in living cells with FIAsh, *Methods Enzymol* 327 (2000) 565-578.
- [69] N. Nitin, P. J. Santangelo, G. Kim, S. Nie, and G. Bao, Peptide-linked molecular beacons for efficient delivery and rapid mRNA detection in living cells, *Nucleic Acids Res* 32 (2004) e58.
- [70] S. W. Hell, Toward fluorescence nanoscopy, *Nat Biotechnol* 21 (2003) 1347-1355.
- [71] J. Ross, mRNA stability in mammalian cells, *Microbiol Rev* 59 (1995) 423-450.
- [72] J. Ross, Control of messenger RNA stability in higher eukaryotes, *Trends Genet* 12 (1996) 171-175.
- [73] N. Heintz, H. L. Sive, and R. G. Roeder, Regulation of human histone gene expression: kinetics of accumulation and changes in the rate of synthesis and in the half-lives of individual histone mRNAs during the HeLa cell cycle, *Mol Cell Biol* 3 (1983) 539-550.
- [74] A. Bevilacqua, M. C. Ceriani, S. Capaccioli, and A. Nicolini, Post-transcriptional regulation of gene expression by degradation of messenger RNAs, *J Cell Physiol* 195 (2003) 356-372.
- [75] T. C. Santiago, I. J. Purvis, A. J. Bettany, and A. J. Brown, The relationship between mRNA stability and length in *Saccharomyces cerevisiae*, *Nucleic Acids Res* 14 (1986) 8347-8360.
- [76] Y. Wang, C. L. Liu, J. D. Storey, R. J. Tibshirani, D. Herschlag, and P. O. Brown, Precision and functional specificity in mRNA decay, *Proc Natl Acad Sci U S A* 99 (2002) 5860-5865.
- [77] D. Muhrad, and R. Parker, Premature translational termination triggers mRNA decapping, *Nature* 370 (1994) 578-581.
- [78] A. B. Maderazo, J. P. Belk, F. He, and A. Jacobson, Nonsense-containing mRNAs that accumulate in the absence of a functional nonsense-mediated mRNA decay pathway are destabilized rapidly upon its restitution, *Mol Cell Biol* 23 (2003) 842-851.
- [79] S. Pinol-Roma, and G. Dreyfuss, Shuttling of pre-mRNA binding proteins between nucleus and cytoplasm, *Nature* 355 (1992) 730-732.

- [80] I. E. Gallouzi, and J. A. Steitz, Delineation of mRNA export pathways by the use of cell-permeable peptides, *Science* 294 (2001) 1895-1901.
- [81] C. G. Burd, and G. Dreyfuss, Conserved structures and diversity of functions of RNA-binding proteins, *Science* 265 (1994) 615-621.
- [82] F. Stutz, A. Bachi, T. Doerks, I. C. Braun, B. Seraphin, M. Wilm, P. Bork, and E. Izaurralde, REF, an evolutionary conserved family of hnRNP-like proteins, interacts with TAP/Mex67p and participates in mRNA nuclear export, *Rna* 6 (2000) 638-650.
- [83] S. Dokka, and Y. Rojanasakul, Novel non-endocytic delivery of antisense oligonucleotides, *Adv Drug Deliv Rev* 44 (2000) 35-49.
- [84] M. X. Tang, C. T. Redemann, and F. C. Szoka, Jr., In vitro gene delivery by degraded polyamidoamine dendrimers, *Bioconjug Chem* 7 (1996) 703-714.
- [85] O. Zelphati, and F. C. Szoka, Jr., Mechanism of oligonucleotide release from cationic liposomes, *Proc Natl Acad Sci U S A* 93 (1996) 11493-11498.
- [86] A. D. Frankel, and C. O. Pabo, Cellular uptake of the tat protein from human immunodeficiency virus, *Cell* 55 (1988) 1189-1193.
- [87] A. Joliot, C. Pernelle, H. Deagostini-Bazin, and A. Prochiantz, Antennapedia homeobox peptide regulates neural morphogenesis, *Proc Natl Acad Sci U S A* 88 (1991) 1864-1868.
- [88] M. Pooga, M. Hallbrink, M. Zorko, and U. Langel, Cell penetration by transportan, *Faseb J* 12 (1998) 67-77.
- [89] H. Hall, E. J. Williams, S. E. Moore, F. S. Walsh, A. Prochiantz, and P. Doherty, Inhibition of FGF-stimulated phosphatidylinositol hydrolysis and neurite outgrowth by a cell-membrane permeable phosphopeptide, *Curr Biol* 6 (1996) 580-587.
- [90] M. Pooga, U. Soomets, M. Hallbrink, A. Valkna, K. Saar, K. Rezaei, U. Kahl, J. X. Hao, X. J. Xu, Z. Wiesenfeld-Hallin, T. Hokfelt, T. Bartfai, and U. Langel, Cell penetrating PNA constructs regulate galanin receptor levels and modify pain transmission in vivo, *Nat Biotechnol* 16 (1998) 857-861.
- [91] V. P. Torchilin, R. Rammohan, V. Weissig, and T. S. Levchenko, TAT peptide on the surface of liposomes affords their efficient intracellular delivery even at low temperature

and in the presence of metabolic inhibitors, *Proc Natl Acad Sci U S A* 98 (2001) 8786-8791.

[92] S. J. Bolton, D. N. Jones, J. G. Darker, D. S. Eggleston, A. J. Hunter, and F. S. Walsh, Cellular uptake and spread of the cell-permeable peptide penetratin in adult rat brain, *Eur J Neurosci* 12 (2000) 2847-2855.

[93] M. Kloc, N. R. Zearfoss, and L. D. Etkin, Mechanisms of subcellular mRNA localization, *Cell* 108 (2002) 533-544.

[94] M. Kloc, and S. M. Bilinski, RNA localization and its role in the spatially restricted protein synthesis, *Folia Histochem Cytobiol* 41 (2003) 3-11.

[95] J. Hesketh, D. Jodar, A. Johannessen, K. Partridge, I. Pryme, and A. Tauler, Enrichment of specific mRNAs in cytoskeletal-bound and membrane-bound polysomes in Chinese hamster ovary cells, *Biochem Soc Trans* 24 (1996) 187S.

[96] R. Rizzuto, P. Pinton, W. Carrington, F. S. Fay, K. E. Fogarty, L. M. Lifshitz, R. A. Tuft, and T. Pozzan, Close contacts with the endoplasmic reticulum as determinants of mitochondrial Ca<sup>2+</sup> responses, *Science* 280 (1998) 1763-1766.

[97] R. Ishitani, M. Tanaka, K. Sunaga, N. Katsube, and D. M. Chuang, Nuclear localization of overexpressed glyceraldehyde-3-phosphate dehydrogenase in cultured cerebellar neurons undergoing apoptosis, *Mol Pharmacol* 53 (1998) 701-707.

[98] V. P. Skulachev, Mitochondrial filaments and clusters as intracellular power-transmitting cables, *Trends Biochem Sci* 26 (2001) 23-29.

[99] N. Nitin, Santangelo, P.J., Kim, G., Nie, S, Bao, G., Peptide-linked molecular beacons for efficient delivery and rapid mRNA detection in living cells, *Nucleic Acids Res* 32 (2004) e58.

[100] P. J. Santangelo, Nix, B., Tsourkas, A., and Bao, G., Dual FRET molecular beacons for mRNA detection in living cells, *Nucleic Acids Res* 32 (2004) e57.

[101] L. Berrueta, S. K. Kraeft, J. S. Tirnauer, S. C. Schuyler, L. B. Chen, D. E. Hill, D. Pellman, and B. E. Bierer, The adenomatous polyposis coli-binding protein EB1 is associated with cytoplasmic and spindle microtubules, *Proc Natl Acad Sci U S A* 95 (1998) 10596-10601.

- [102] F. Gergely, C. Karlsson, I. Still, J. Cowell, J. Kilmartin, and J. W. Raff, The TACC domain identifies a family of centrosomal proteins that can interact with microtubules, *Proc Natl Acad Sci U S A* 97 (2000) 14352-14357.
- [103] C. Molenaar, S. A. Marras, J. C. Slats, J. C. Truffert, M. Lemaitre, A. K. Raap, R. W. Dirks, and H. J. Tanke, Linear 2' O-Methyl RNA probes for the visualization of RNA in living cells, *Nucleic Acids Res* 29 (2001) E89-89.
- [104] P. B. Moore, and T. A. Steitz, The structural basis of large ribosomal subunit function, *Annu Rev Biochem* 72 (2003) 813-850.
- [105] S. Paillason, M. Van De Corput, R. W. Dirks, H. J. Tanke, M. Robert-Nicoud, and X. Ronot, In situ hybridization in living cells: detection of RNA molecules, *Exp Cell Res* 231 (1997) 226-233.
- [106] M. F. Liaud, C. Lichtle, K. Apt, W. Martin, and R. Cerff, Compartment-specific isoforms of TPI and GAPDH are imported into diatom mitochondria as a fusion protein: evidence in favor of a mitochondrial origin of the eukaryotic glycolytic pathway, *Mol Biol Evol* 17 (2000) 213-223.
- [107] P. J. Santangelo, B. Nix, A. Tsourkas, and G. Bao, Dual FRET molecular beacons for mRNA detection in living cells, *Nucleic Acids Res* 32 (2004) e57.
- [108] S. Takyar, R. P. Hickerson, and H. F. Noller, mRNA helicase activity of the ribosome, *Cell* 120 (2005) 49-58.
- [109] X. Chen, S. T. Cheung, S. So, S. T. Fan, C. Barry, J. Higgins, K. M. Lai, J. Ji, S. Dudoit, I. O. Ng, M. Van De Rijn, D. Botstein, and P. O. Brown, Gene expression patterns in human liver cancers, *Mol Biol Cell* 13 (2002) 1929-1939.
- [110] S. E. DePrimo, M. Diehn, J. B. Nelson, R. E. Reiter, J. Matese, M. Fero, R. Tibshirani, P. O. Brown, and J. D. Brooks, Transcriptional programs activated by exposure of human prostate cancer cells to androgen, *Genome Biol* 3 (2002) RESEARCH0032.
- [111] M. B. Eisen, and P. O. Brown, DNA arrays for analysis of gene expression, *Methods Enzymol* 303 (1999) 179-205.
- [112] J. M. Levsky, and R. H. Singer, Fluorescence in situ hybridization: past, present and future, *J Cell Sci* 116 (2003) 2833-2838.

- [113] A. M. Femino, K. Fogarty, L. M. Lifshitz, W. Carrington, and R. H. Singer, Visualization of single molecules of mRNA in situ, *Methods Enzymol* 361 (2003) 245-304.
- [114] A. M. Femino, F. S. Fay, K. Fogarty, and R. H. Singer, Visualization of single RNA transcripts in situ, *Science* 280 (1998) 585-590.
- [115] Y. Shav-Tal, X. Darzacq, S. M. Shenoy, D. Fusco, S. M. Janicki, D. L. Spector, and R. H. Singer, Dynamics of single mRNPs in nuclei of living cells, *Science* 304 (2004) 1797-1800.
- [116] D. L. Sokol, X. Zhang, P. Lu, and A. M. Gewirtz, Real time detection of DNA:RNA hybridization in living cells, *Proc Natl Acad Sci U S A* 95 (1998) 11538-11543.
- [117] S. Tyagi, and O. Alsmadi, Imaging native beta-actin mRNA in motile fibroblasts, *Biophys J* 87 (2004) 4153-4162.
- [118] J. Perlette, and W. Tan, Real-time monitoring of intracellular mRNA hybridization inside single living cells, *Anal Chem* 73 (2001) 5544-5550.
- [119] G. Dreyfuss, Y. D. Choi, and S. A. Adam, The ribonucleoprotein structures along the pathway of mRNA formation, *Endocr Res* 15 (1989) 441-474.
- [120] Y. Oleynikov, and R. H. Singer, RNA localization: different zipcodes, same postman? *Trends Cell Biol* 8 (1998) 381-383.
- [121] U. Sheth, and R. Parker, Decapping and decay of messenger RNA occur in cytoplasmic processing bodies, *Science* 300 (2003) 805-808.
- [122] E. Yang, E. van Nimwegen, M. Zavolan, N. Rajewsky, M. Schroeder, M. Magnasco, and J. E. Darnell, Jr., Decay rates of human mRNAs: correlation with functional characteristics and sequence attributes, *Genome Res* 13 (2003) 1863-1872.
- [123] A. Grolleau, J. Bowman, B. Pradet-Balade, E. Puravs, S. Hanash, J. A. Garcia-Sanz, and L. Beretta, Global and specific translational control by rapamycin in T cells uncovered by microarrays and proteomics, *J Biol Chem* 277 (2002) 22175-22184.
- [124] V. K. Rajasekhar, A. Viale, N. D. Socci, M. Wiedmann, X. Hu, and E. C. Holland, Oncogenic Ras and Akt signaling contribute to glioblastoma formation by differential recruitment of existing mRNAs to polysomes, *Mol Cell* 12 (2003) 889-901.

- [125] V. K. Rajasekhar, and E. C. Holland, Postgenomic global analysis of translational control induced by oncogenic signaling, *Oncogene* 23 (2004) 3248-3264.
- [126] C. G. Proud, Ras, PI3-kinase and mTOR signaling in cardiac hypertrophy, *Cardiovasc Res* 63 (2004) 403-413.
- [127] A. C. Gingras, B. Raught, and N. Sonenberg, mTOR signaling to translation, *Curr Top Microbiol Immunol* 279 (2004) 169-197.
- [128] A. C. Gingras, B. Raught, and N. Sonenberg, Regulation of translation initiation by FRAP/mTOR, *Genes Dev* 15 (2001) 807-826.
- [129] K. Hara, Y. Maruki, X. Long, K. Yoshino, N. Oshiro, S. Hidayat, C. Tokunaga, J. Avruch, and K. Yonezawa, Raptor, a binding partner of target of rapamycin (TOR), mediates TOR action, *Cell* 110 (2002) 177-189.
- [130] D. H. Kim, D. D. Sarbassov, S. M. Ali, J. E. King, R. R. Latek, H. Erdjument-Bromage, P. Tempst, and D. M. Sabatini, mTOR interacts with raptor to form a nutrient-sensitive complex that signals to the cell growth machinery, *Cell* 110 (2002) 163-175.
- [131] C. G. Proud, Role of mTOR signalling in the control of translation initiation and elongation by nutrients, *Curr Top Microbiol Immunol* 279 (2004) 215-244.
- [132] C. G. Proud, mTOR-mediated regulation of translation factors by amino acids, *Biochem Biophys Res Commun* 313 (2004) 429-436.
- [133] D. D. Sarbassov, D. A. Guertin, S. M. Ali, and D. M. Sabatini, Phosphorylation and regulation of Akt/PKB by the rictor-mTOR complex, *Science* 307 (2005) 1098-1101.
- [134] A. Sekulic, C. C. Hudson, J. L. Homme, P. Yin, D. M. Otterness, L. M. Karnitz, and R. T. Abraham, A direct linkage between the phosphoinositide 3-kinase-AKT signaling pathway and the mammalian target of rapamycin in mitogen-stimulated and transformed cells, *Cancer Res* 60 (2000) 3504-3513.
- [135] M. Miron, P. Lasko, and N. Sonenberg, Signaling from Akt to FRAP/TOR targets both 4E-BP and S6K in *Drosophila melanogaster*, *Mol Cell Biol* 23 (2003) 9117-9126.
- [136] B. K. Bhandari, D. Feliers, S. Duraisamy, J. L. Stewart, A. C. Gingras, H. E. Abboud, G. G. Choudhury, N. Sonenberg, and B. S. Kasinath, Insulin regulation of protein translation repressor 4E-BP1, an eIF4E-binding protein, in renal epithelial cells, *Kidney Int* 59 (2001) 866-875.

- [137] T. Preiss, J. Baron-Benhamou, W. Ansorge, and M. W. Hentze, Homodirectional changes in transcriptome composition and mRNA translation induced by rapamycin and heat shock, *Nat Struct Biol* 10 (2003) 1039-1047.
- [138] M. Miron, J. Verdu, P. E. Lachance, M. J. Birnbaum, P. F. Lasko, and N. Sonenberg, The translational inhibitor 4E-BP is an effector of PI(3)K/Akt signalling and cell growth in *Drosophila*, *Nat Cell Biol* 3 (2001) 596-601.
- [139] M. Ridderstrale, and H. Tornqvist, PI-3-kinase inhibitor Wortmannin blocks the insulin-like effects of growth hormone in isolated rat adipocytes, *Biochem Biophys Res Commun* 203 (1994) 306-310.
- [140] S. A. Barker, K. K. Caldwell, A. Hall, A. M. Martinez, J. R. Pfeiffer, J. M. Oliver, and B. S. Wilson, Wortmannin blocks lipid and protein kinase activities associated with PI 3-kinase and inhibits a subset of responses induced by Fc epsilon R1 cross-linking, *Mol Biol Cell* 6 (1995) 1145-1158.
- [141] F. Rozen, I. Edery, K. Meerovitch, T. E. Dever, W. C. Merrick, and N. Sonenberg, Bidirectional RNA helicase activity of eucaryotic translation initiation factors 4A and 4F, *Mol Cell Biol* 10 (1990) 1134-1144.
- [142] F. Gebauer, and M. W. Hentze, Molecular mechanisms of translational control, *Nat Rev Mol Cell Biol* 5 (2004) 827-835.
- [143] P. De Rijk, E. Robbrecht, S. de Hoog, A. Caers, Y. Van de Peer, and R. De Wachter, Database on the structure of large subunit ribosomal RNA, *Nucleic Acids Res* 27 (1999) 174-178.
- [144] W. H. Kalle, M. V. Macville, M. P. van de Corput, B. G. de Grooth, H. J. Tanke, and A. K. Raap, Imaging of RNA in situ hybridization by atomic force microscopy, *J Microsc* 182 (Pt 3) (1996) 192-199.
- [145] J. C. Politz, R. A. Tuft, and T. Pederson, Diffusion-based transport of nascent ribosomes in the nucleus, *Mol Biol Cell* 14 (2003) 4805-4812.
- [146] A. Tsourkas, M. A. Behlke, and G. Bao, Hybridization of 2'-O-methyl and 2'-deoxy molecular beacons to RNA and DNA targets, *Nucleic Acids Res* 30 (2003) 5168-5174.

## CHAPTER 2

### Peptide linked molecular beacons for imaging of endogenous RNAs in living cells

#### Introduction

Quantitative methods to measure gene expression *in vitro*, such as real-time PCR and microarray analysis, have revolutionized molecular biology and drug development ([1]-[4]). These approaches, however, are generally used with purified DNA or RNA from cell lysates. The ability to detect and quantify the expression of specific endogenous mRNA in living cells and tissues in real time will offer tremendous opportunities for biological and disease studies, and will significantly impact drug discovery and medical diagnostics. However, currently available technologies for gene detection in intact cells such as in-situ hybridization (ISH) cannot be used *in vivo*, since ISH studies rely on washing away unbound probes to reduce background signal ([5],[6]). To perform gene detection in living cells, the probes must be able to recognize the target with high specificity, convert target recognition *directly* into a measurable signal with high signal-to-background ratio, and allow for differentiation between true and false-positive events ([7]). Probes must also be delivered into living cells with high efficiencies.

Among the technologies currently under development for living cell gene detection and quantification, the most promising one is perhaps molecular beacons. Molecular beacons are dual-labeled antisense oligonucleotide (ODN) probes with a fluorophore at one end and a quencher at the other end ([8],[9]). In contrast to fluorescently labeled linear ODN probes, molecular beacons are designed to form a stem-loop (hairpin) structure in the absence of complementary target so that fluorescence of the fluorophore

is quenched. Hybridization with target mRNA opens the hairpin and physically separates the reporter from quencher, allowing a fluorescence signal to be emitted upon excitation. Thus, molecular beacons enable a homogenous assay format where background is low without the need to wash away free probes. However, to detect mRNA *in vivo*, one needs to deliver molecular beacons into living cells with high efficiencies and fast kinetics. Conventional delivery approaches are based on DNA transfection techniques, such as those employing liposomes or dendrimers. These approaches are inefficient (<80%) ([10]), slow (delivery times ~4 h), and can potentially trap molecular beacons in the endosomes and degrade them in the lysosomes, significantly increasing the background signal ([11]). The long delivery time also gives rise to significant degradation of cytoplasmic molecular beacons by nuclease, further increasing false positive detection ([12]). Although the reversible membrane permeabilization method using streptolysin O (SLO) is faster (~ 2 h) and not based on endocytosis ([13]), it can only be used in *ex-vivo* cellular assays. Other delivery methods, such as microinjection ([14]) and electroporation ([15]) are invasive and may cause severe damage to cells. Further, microinjection is labor-intensive and only practical for studying a small number of cells.

To overcome these difficulties, we have developed novel peptide-linked molecular beacons that can quickly and efficiently enter living cells without the need of any other delivery reagent. Recent research has identified several small regions (9-16 amino acids) of proteins called protein transduction domains (PTDs) or cell penetrating peptides (CPPs) that confer the ability to traverse biological membranes efficiently ([16]-[18]). Here we show that conjugating one such peptide (TAT-1) to molecular beacons yields a multifunctional probe that can enter into living cells with nearly 100% efficiencies, fast (~30 min) delivery kinetics, and the ability to localize in cell cytoplasm. Further, these peptide-linked molecular beacons function well for mRNA detection in

living cells as compared with the results of *in situ* hybridization. This novel molecular beacon design can thus provide a powerful means for rapid detection of gene expression in living cells and tissues in real time, with high specificity and sensitivity.

## **Materials and Methods**

### **Design of peptide-linked molecular beacons**

We designed and synthesized peptide-linked molecular beacons targeting the human GAPDH (glyceraldehyde 3-phosphate dehydrogenase) and survivin mRNAs, as well as molecular beacons with a 'random' probe sequence. The specific design of these molecular beacons, and the sequence of the 11 amino-acid TAT-1 peptide used in the study are shown in **Table 2.1**. GAPDH is a glycolytic protein that has a diverse range of activities in mammalian cells including membrane fusion, microtubule bundling, nuclear RNA export, DNA replication and repair ([20]). These activities suggest that GAPDH is involved in apoptosis, age-related neurodegenerative disease, prostate cancer and viral pathogenesis. Survivin is a member of the inhibitor of apoptosis protein (IAP) family and also regulates cell division ([21]). The GAPDH beacon is comprised of a 19-base probe domain targeting the Exon 6 region of GAPDH gene flanked by complementary 5-base sequences that hybridize to form the stem. The survivin beacon has a 16-base target sequence with a similar design of the stem.

The 'random' beacon was designed as a negative control, with a 17-base probe sequence that does not have any match in the entire human genome. To ensure good target accessibility, we typically design and test molecular beacons complementary to different segments of the same mRNA molecule to avoid targeting sequences that are occupied by RNA-binding proteins or where double stranded RNA is formed.

**Table 2.1:** Design of peptide-linked molecular beacons

	<b>Peptide</b>
TAT	(N terminus) TyrGlyArgLysLysArgArgGlnArgArgArg (C terminus)
	<b>Molecular Beacon</b>
GAPDH	5'-Cy3- <u>CGACGGAGTCCTTCCACGATACCACG</u> /thiol-dT/ <u>CG-BHQ2</u> -3'
Survivin	5'-Cy3- <u>CGACGGAGAAAGGGCTGCCACG</u> /thiol-dT/ <u>CG-BHQ2</u> -3'
Random	5'-Cy3- <u>CGACGCGACAAGCGCACCGATACG</u> /thiol-dT/ <u>CG-BHQ2</u> -3'

Three conjugation strategies were developed in attaching the delivery peptide to molecular beacons, as illustrated in **Figure 2.1**. In the first approach (**Figure 2.1 A**), peptides were linked to a molecular beacon through a streptavidin-biotin bridge by introducing a modified oligonucleotide, biotin-dT, to the quencher arm of the stem through a carbon-12 spacer. The peptide-linked molecular beacon consisted the biotin-modified molecular beacon, a streptavidin molecule, and biotin-modified TAT-1 peptides. Since each streptavidin molecule has four biotin-binding sites, we were able to link biotin-modified molecular beacons and delivery peptides on the same streptavidin molecule. The stoichiometry was controlled so that the probability of having more than one molecular beacons linked to the same streptavidin is small. In the second design (Fig. 1b), we placed a thiol group to the quencher-arm of the molecular beacon stem through a carbon linker; the thiol group then reacted with a maleimide group added to the C terminus of the peptide to form a thiol-maleimide linkage (**Figure 2.1 B**). Both the streptavidin-biotin bridge and the thiol-maleimide linkage are stable in the cell cytoplasm.

We and others have demonstrated that, for certain cell types, CPPs including TAT-1 peptide tend to carry cargos into cell nucleus ([18],[22]). While this may be useful in detecting nuclear RNA targets such as polyadenylated nuclear RNA (PAN), in most applications however, the target mRNAs are in the cytoplasm, so should be the molecular beacons.

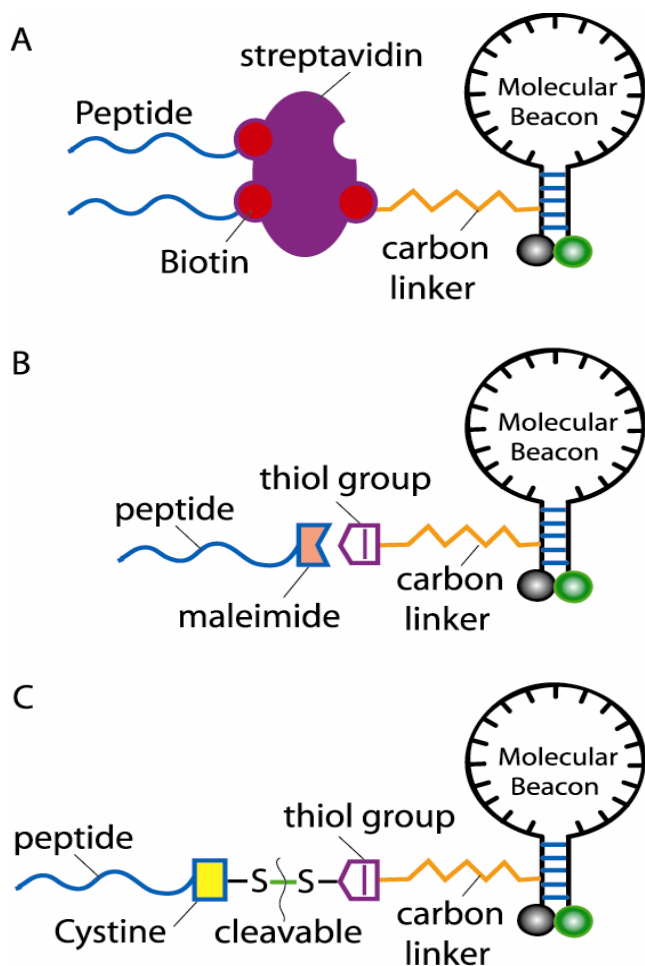


**Figure 2.1:** A schematic illustration of three different conjugation schemes for linking the delivery peptide to molecular beacons

- (A) The streptavidin-biotin linkage in which a molecular beacon is modified by introducing a biotin-dT to the quencher arm of the stem through a carbon-12 spacer.
- (B) The thiol-maleimide linkage in which the quencher-arm of the molecular beacon stem is modified by adding a thiol group which can react with a maleimide group placed to the C terminus of the peptide to form a direct, stable linkage.
- (C) The cleavable disulfide bridge in which the peptide is modified by adding a cysteine residue at the C terminus which forms a disulfide bridge with the thiol-modified molecular beacon.

Thus, as the third approach, we functionalized the TAT-1 peptide by adding a cysteine residue at the C terminus which forms a disulfide bridge with the thiol-modified molecular beacon as shown in **Figure 2.1 C**. This cleavable design was based on the rationale that the reducing environment of the cytoplasm will cleave the disulfide bond once the construct enters the cell, thereby separating peptide from probe. This has been demonstrated by Hallbrink et al using a TAT-peptide linked cargo-quencher construct ([23]). Specifically, a peptide-conjugated, fluorescently-labeled cargo was linked to a fluorescence quencher through a disulfide bond, resulting in a reduction-sensitive construct. Upon internalization into Bowes human melanoma cells, the disulfide bond was quickly reduced, as indicated by the increased fluorescence intensity. Since fast cleavage of disulfide bridge inside living cells is well documented ([24]), we believe that, once the cleavable, peptide-linked molecular beacons (**Figure 2.1 C**) are inside the cell, the disulfide bridge will be reduced, leaving the molecular beacons in the cytoplasm.

Further the affinity of the MB probes for mRNA target in the cytoplasm may limit their delivery only to the cytoplasm of living cells. The delivery to the nuclei has been observed for cases when the cargo molecules/ beads etc. did not have any target in the cytoplasm. This is significantly different in this case, where we have a target mRNAs in the cytoplasm.

### **Peptide conjugation**

In the design shown in **Figure 2.1 A**, streptavidin was chosen as a linker molecule because of its high affinity for biotin and availability of multiple biotin-binding sites. The modified nucleotide (dT) at the third base from the 3' end on the quencher-arm of the stem was linked to biotin through a 12-carbon spacer, and the biotin-modified peptides

were conjugated to the biotin-modified molecular beacon through binding between biotin and streptavidin. The peptide-linked molecular beacon complex was dialyzed with PBS (1X) overnight using a Slide-A-Lyzer Dialysis Unit, 10K MWCO (Pierce Biotech Inc., Rockford, IL) to exchange the buffer and to remove the unconjugated peptide. The modified molecular beacons were synthesized at Integrated DNA Technologies, Inc (Coralville, IA) and MWG Biotech, Inc (High Point, NC), and the modified peptides were synthesized by Invitrogen Inc (Carlsbad, CA) and Synpep Corporation (Dublin, CA).

In the direct linkage approaches shown in **Figures 2.1 B and 2.1 C**, the same position on the quencher-arm of the stem bore a modified nucleotide dT-amine group with a 6-carbon spacer. To generate a direct, stable linkage between the peptide and molecular beacon, the peptide was modified with a maleimide group at its C terminus. Amine-modified molecular beacons were reacted in PBS buffer with a twofold molar excess of the heterobifunctional crosslinker SPDP, N-Succinimidyl 3-(2-pyridyldithio)propionate (Sigma-Aldrich) for 2 h, followed by reduction with a twentyfold molar excess of TCEP, 3,3',3''-Phosphinidyne-triisopropionic acid hydrochloride (Sigma-Aldrich), to create a free thiol (-SH) functional group. This thiolated beacon was then reacted with maleimide-modified peptide to form a stable chemical bridge between the beacon and the peptide. The peptide-linked molecular beacon complex was dialyzed overnight using Slide-A-Lyzer Dialysis Unit, 10K MWCO (Pierce Biotech Inc., Rockford, IL) to remove the unconjugated peptide. A similar approach was used in forming a cleavable disulfide bridge between the cysteine-modified peptide and the amine-modified molecular beacon. To reduce the probability of forming beacon-beacon conjugates, a higher (1.5x) concentration of peptides was used compared with that of beacons. Further, the positive charge of peptides helped prevent homodimerization of peptides.

### **Solution assays of hybridization kinetics and signal-to-background ratio**

Measurement of hybridization kinetics and signal-to-background ratio of peptide linked molecular beacons was carried out using a SAFIRE microplate monochromator reader (TECAN, Austria). For kinetic studies, 200 nM peptide-linked molecular beacons were mixed with 1  $\mu$ M complementary oligonucleotide target at 37°C and the fluorescence intensity was recorded as a function of time for conventional molecular beacons, direct linked (stable and cleavable) peptide-molecular beacon complexes, and streptavidin-linked peptide-molecular beacon complex. To determine the signal-to-background ratios, 200 nM conventional and peptide-linked molecular beacons were mixed with 200 nM of complementary target respectively in the microplate reader, and the fluorescence intensity at equilibrium was recorded. The fluorescence signal of each molecular beacon type (conventional and peptide-linked) in the absence of target was recorded as the background signal. All solution assays were performed in 1x PBS buffer.

### **Cellular delivery of peptide-linked molecular beacons**

Primary human dermal fibroblast (HDF) cells (Cambrex, NJ) and a pancreatic cancer cell line MiaPaca-2 (ATCC, VA) were used for this study. These cells were cultured in an 8-well Nalge Nunc culture plate with a glass coverslip bottom in their respective cell culture media for 24 h prior to experiments. Delivery assays were performed by incubating cells at 37°C with the media containing peptide-linked molecular beacons. For molecular beacons targeting GAPDH, peptide-linked molecular beacons with three different concentrations (0.25  $\mu$ M, 0.5  $\mu$ M and 1.0  $\mu$ M) were incubated with HDF cells for 30, 60 and 90 min. For molecular beacons targeting survivin, 0.5  $\mu$ M of peptide-linked molecular beacons were incubated with HDF and MiaPaca-2 cells for 30 min. For all assays, the cells were washed twice with PBS to remove the incubation medium and placed in fresh medium for fluorescence imaging, which was carried out using a confocal microscope (Axiovert LSM-100, Zeiss).

### **Fluorescence in-situ hybridization**

Normal human dermal fibroblast cells were cultured in 8-well chambered coverslips for 24 hours in normal growth medium (FGM-2 Cambrex Co.) and then washing with 1x PBS (without Ca or Mg). The slide was fixed in 100% methanol at -20 °C for 10 minutes. After removing the methanol, the slides were allowed to air dry and stored overnight at -80 °C. In-situ hybridization assays were then performed by first washing the slides for 5 minutes in 1x PBS and hybridizing them overnight at 37 °C in 1x PBS (no Ca or Mg) containing 200 nM of unmodified GAPDH-targeting molecular beacons. After removing the hybridization solution with washing and adding 1x PBS, the cells were imaged using an Axiovert 100 epi-fluorescent microscope.

### **Delivery of molecular beacons using commercial transfection reagents**

To compare the efficiency and functionality of different delivery methods, we used three commercially available transfection reagents: Effectine (Qiagen), Superfect (Qiagen), and Oligofectimine (Invitrogen). Transfection assays were carried out according to the procedure recommended by respective suppliers; both primary HDF cells and MiaPaca-2 pancreatic cancer cells were incubated with conventional (unmodified) molecular beacons for 0.5, 2 and 3.5 h.

## **Results and Discussion**

### **Hybridization kinetics of peptide-linked molecular beacons**

To determine the effect of peptide conjugation on molecular beacon function, in-solution hybridization assays were carried out for the binding kinetics of peptide-linked molecular beacons with different conjugation methods. One concern was that, when the positively charged TAT-1 peptide is conjugated to a molecular beacon, it might interact with the negatively charged hairpin oligonucleotide, thus interfering with proper probe-target binding. Shown in **Figure 2.2 A** are normalized fluorescence intensity verses time curves as a result of probe-target hybridization for unmodified GAPDH-targeting molecular beacons and peptide-linked molecular beacons with the streptavidin-biotin linkage, the stable thiol-maleimide linkage, and the cleavable disulfide bridge. Peptide-linked molecular beacons with the thiol-maleimide linkage had almost exactly the same probe-target hybridization kinetics as unmodified molecular beacons (black and green curves respectively in **Figure 2.2 A**), indicating that the conjugation of peptide using the thiol-maleimide linkage has essentially no effect on the functionality of molecular

beacons. Molecular beacons with the cleavable disulfide bridge also behaved similarly to the unmodified ones. With streptavidin-biotin linkage, the hybridization kinetics of peptide-linked molecular beacons was slightly slower, but it did not affect the signal level, as can be seen from **Figure 2.2 A**. It is possible that the streptavidin molecule, whose size is comparable to that of the molecule beacon, may have sterically hindered binding between the target and the hairpin probe, leading to a slightly reduced hybridization kinetic rate. The effect of different conjugation methods on signal-to-background ratio (S/B) is relatively small (**Figure 2.2 B**), although the S/B for peptide-linked molecular beacons was slightly lower than that of the unmodified ones. Taken together, the results shown in **Figure 2.2** clearly indicate that conjugation of peptide to molecular beacons did not impair their normal function.

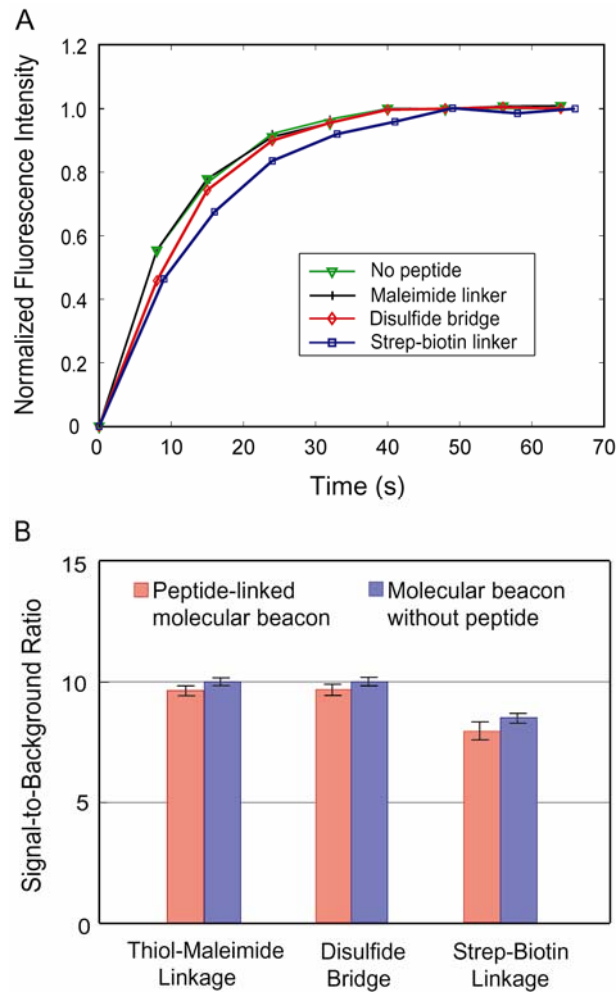


**Figure 2.2:** Probe-target hybridization kinetics of unmodified and peptide-linked molecular beacons

(A) Normalized fluorescence intensity as a function of time for unmodified molecular beacons, and for the three types of peptide-linked molecular beacons. Note that the probe-target hybridization kinetic curves of peptide-linked molecular beacons with the thiol-maleimide linkage (black curve) and unmodified molecular beacons (green curve) are almost identical.

(B) Signal-to-background ratios (red) of probe-target hybridization for peptide-linked molecular beacons with different conjugation methods. The signal-to-background ratios for thiol-modified and biotin-modified molecular beacons (blue) without peptide are also shown for comparison.

## Detection of GAPDH mRNA using peptide-linked molecular beacons

To demonstrate the delivery and mRNA targeting functions of peptide-linked molecular beacons, we first detected mRNA of a housekeeping gene human GAPDH in normal human dermal fibroblast (HDF) cells. After just 30 min of incubation with TAT-peptide conjugated GAPDH-targeting molecular beacons, we observed clear and localized fluorescence signal in HDF cells as a result of molecular beacon-target mRNA hybridization for all three conjugation schemes, i.e., thiol-maleimide (**Figure 2.3 A**), disulfide bridge (**Figure 2.3 B**) and streptavidin-biotin (**Figure 2.3 C**). In contrast, peptide-linked random-sequence molecular beacons with streptavidin-biotin conjugation gave essentially no signal 30 min after delivery (**Figure 2.3 D**). Similar results were obtained using random-sequence molecular beacons with thiol-maleimide and disulfide linkages for peptide (data not shown). This demonstrates that peptide-linked molecular beacons remained highly specific in living cells after internalization. Further, we found that GAPDH mRNAs displayed a very intriguing filament-like localization pattern in HDF cells, with a clear tendency of surrounding the cell nucleus and following the cell morphology. Interestingly, molecular beacons with the cleavable (thiol-cysteine disulfide bridge) design seemed to give better localization patterns than those with the thiol-maleimide linkage, and the latter seemed to perform better than molecular beacons with the streptavidin-biotin linkage. Cleavage of the delivery peptide from the construct may have provided molecular beacons a better access to target mRNA molecules, although more studies of this phenomenon are required to validate this assumption. It is likely that a molecular beacon with a relatively bulky streptavidin molecule is less able to penetrate into the secondary structure of the GAPDH mRNA, thus reducing its ability to seek out its targets. Almost all the HDF cells exposed to GAPDH peptide-linked

molecular beacons showed strong fluorescence signal, implying a near 100% delivery efficiency (data not shown).

Similar results were obtained after 60 min of incubation (**Figure 2.3 E-H**). About the same level of fluorescence was observed for GAPDH-targeting molecular beacons with different linkages for peptide, whereas the random-sequence molecular beacons did not give much signal. Even after 90 min, there was essentially no increase in the signal level (data not shown), indicating that most of the peptide-linked molecular beacons entered the HDF cells within the first 30 min. Further, fluorescence signal levels and mRNA localization patterns in HDF cells were similar for experiments at three different nominal molecular beacon concentrations (0.25  $\mu$ M, 0.5  $\mu$ M and 1.0  $\mu$ M). Due to the peptide conjugation process, it was estimated that, with 0.25  $\mu$ M nominal molecular beacon concentration, the actual concentration of peptide-linked molecular beacons used in the assay was about 150–200 nM.

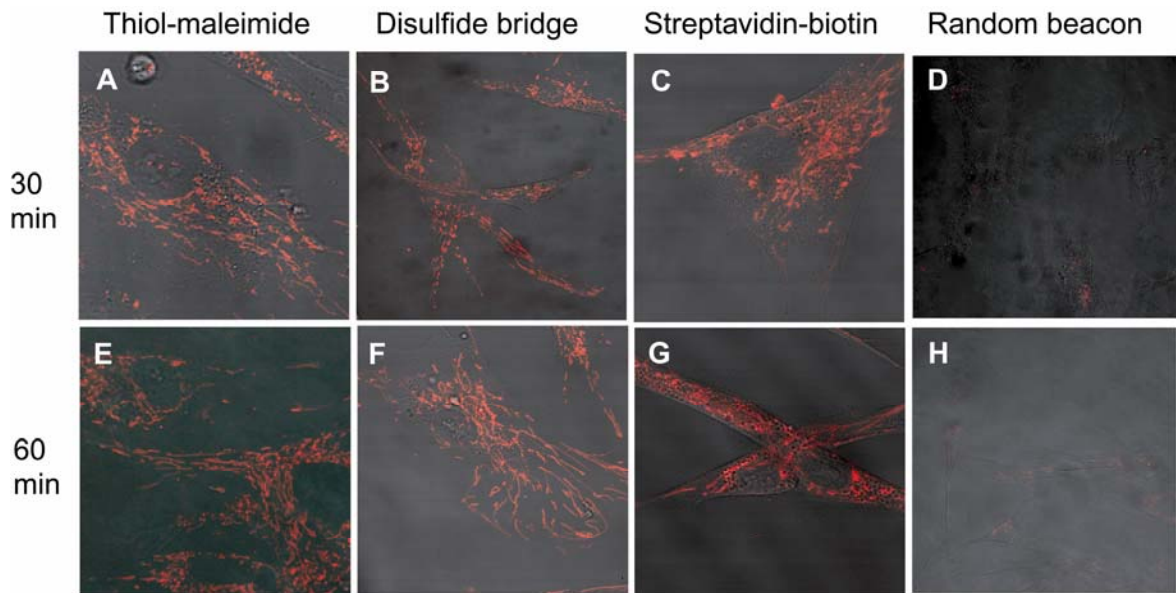


**Figure 2.3:** Detection of GAPDH mRNA in HDF cells using 0.5  $\mu$ M of peptide-linked molecular beacons

(A-C), fluorescence images of HDF cells after 30 min of incubation with TAT-peptide conjugated, GAPDH-targeting molecular beacons, with (A) thiol-maleimide, (B) disulfide bridge and (C) streptavidin-biotin linkages. (D) With peptide-linked random-sequence molecular beacons, essentially no detectable signal 30 min after delivery.

(E-G) fluorescence images of HDF cells after 60 min of incubation of the peptide-linked, GAPDH-targeting molecular beacons with (E) thiol-maleimide, (F) disulfide bridge and (G) streptavidin-biotin linkages. The signal level of peptide-linked random-sequence molecular beacons after 60 min is shown in (H). Clearly, the fluorescence signal level did not increase when incubation time was doubled, indicating that most of the molecular beacons internalized within the first 30 min. Note the intriguing GAPDH mRNA localization patterns shown in (A-C) and (E-G).

### **Comparison with in-situ hybridization**

To correlate the results of present method with a traditional method, we performed fluorescence *in situ* hybridization (FISH) assays targeting GAPDH mRNA in fixed HDF cells. The probes used in the FISH assays were fluorescently labeled linear probes (5'-Cy5-GAGTCCTTCCACGATACCA-3') that have the same probe sequence as the GAPDH-targeting molecular beacon. As demonstrated in **Figure 2.4 A**, the fluorescence image obtained in FISH assays of GAPDH mRNA in HDF cells gave a filamentous localization pattern similar to that shown in **Figure 2.3**, confirming that the mRNA localization revealed in this study is not an artifact. However, the fluorescence signal as a result of FISH was not as sharp as that in living cell assays. Since the probes entered into both the cell cytoplasm and nucleus during FISH, a diffused fluorescence signal appeared in the fixed HDF cell nuclei (**Figure 2.4 A**). This is in contrast to the living cell images shown in Fig. 3 where very low signal can be observed in cell nucleus. We believe that this diffused signal may reflect the high abundance as well as a rather uniform distribution of GAPDH mRNA in cell nucleus. As a negative control, we performed a FISH assay with fluorescently labeled linear Poly-A probes (5'-Cy5-AAAAAAAAAAAAAAAAAAAA-3') and the resulting background signal was very low, as can be seen from **Figure 2.4 B**. This further confirmed that the fluorescence signal observed in our live cell and fixed cell studies of specific mRNA detection was truly due to probe/target hybridization.

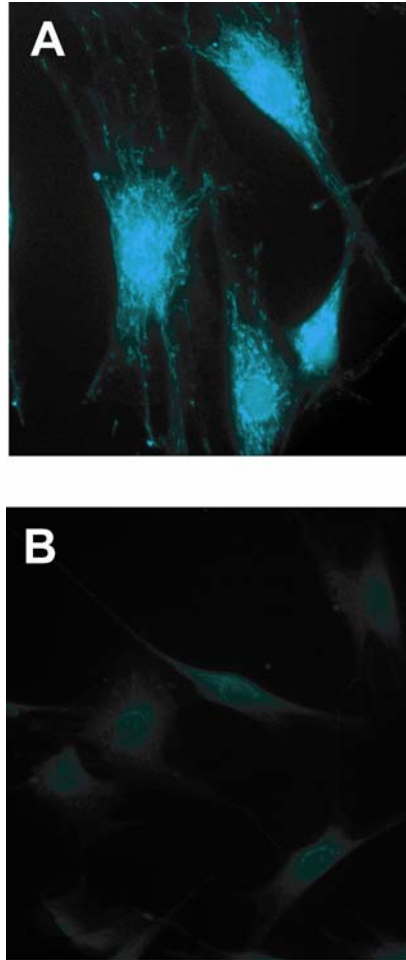


**Figure 2.4:** Control studies using fluorescence in situ hybridization (FISH).

(A) Detection of GAPDH mRNA in Fixed HDF cells. The filamentous localization pattern of GAPDH mRNA was similar to that revealed in living cell assays, although the signal was not as sharp. Note the diffused fluorescence signal in cell nuclei.

(B) A negative control study of the FISH assay using fluorescently labeled linear Poly-A probes resulted in very low background.

## Detection of survivin mRNA

After successful study of the delivery of the MB linked probes to the cells and detection of the specific mRNAs in the cytoplasm of living cells, our next goal was to demonstrate the feasibility to detect differential levels of mRNA in living cells. The ability to detect differential levels of the mRNA holds a key opportunity for this method to be useful for the disease detection studies. To demonstrate this using the MB probes, we decided to study Survivin mRNA as a candidate gene of interest.

We and others have demonstrated that the Survivin expression level is very low in HDF cells, whereas in MiaPaCa-2 cells the level is relatively high. After 60 min of incubation with peptide-linked molecular beacons, the fluorescence signal in MiaPaca-2 cells was quite high, as shown in **Figure 2.5 A**, but in HDF cells, only very low fluorescence signal can be observed (**Figure 2.5 C**). In addition, Survivin mRNAs shown an intriguing localization pattern, i.e., the Survivin mRNA molecules in MiaPaCa-2 cells seemed to be concentrated near one side of the cell nucleus (**Figure 2.5 B**). Although with very low expression level, Survivin mRNA localized in HDF in a similar fashion (**Figure 2.5 C**). Previous research suggested that the expression level and localization of Survivin may be an important indicator for cancer progression or prognosis ([25]).

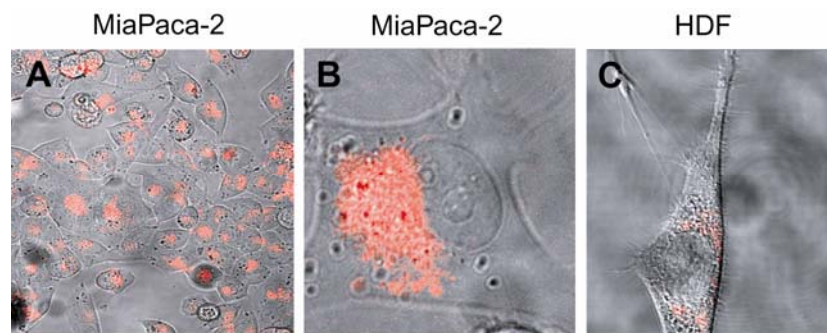


**Figure 2.5:** Detection of Survivin mRNA in live HDF and MiaPaca-2 cells.

(A) Strong fluorescence signal was observed in MiaPaca-2 cells after 60 min of incubation with peptide-linked molecular beacons. Note that essentially all cells shown fluorescence.

(B) Survivin mRNA molecules in MiaPaca-2 cells seemed to be concentrated near one side of the cell nucleus HDF cells. (C) Only very low fluorescence signal can be observed in HDF cells, but with a survivin mRNA localization pattern.

### **Comparison with conventional transfection methods**

As mentioned above, cellular delivery of molecular beacons using conventional transfection methods, either liposome based or dendrimer based, typically requires 3-4 hours of incubation during which a high level of background signal is generated. To compare the efficiency of delivery and the stability of molecular beacons during internalization, we performed delivery studies of unmodified GAPDH-targeting molecular beacons with three commercially available transfection reagents: Superfect (dendrimer-based), Oligofectamine (liposome-based), and Effectene (liposome based), and followed all the manufacturers' instructions. When fluorescence in HDF cells was observed after 30 min of GAPDH beacon delivery using Superfect, Oligofectamine or Effectene, there was essentially no signal (data not shown). We found that, after 3.5 h of transfection with Superfect, the molecular beacons gave strong signal in HDF cells. However, the fluorescence image had different characteristics from that of peptide-linked molecular beacons. Specifically, the fluorescence signals were concentrated in random 'bright spots' in both cytoplasm and nucleus (**Figure 2.6 A**), suggesting that molecular beacons were trapped and degraded by endosomes, lysosomes and nucleus. Even more disturbing is that the random-sequence molecular beacons showed similar fluorescence signal levels and 'bright spots' in HDF cells (**Figure 2.6 D**), indicating that the signals in both cases were largely due to molecular beacon degradation. With Oligofectamine transfection, the results after 3.5 h incubation were even worse: only highly concentrated bright spots were present in the HDF cells, with a similar signal level generated by GAPDH-targeting and random-sequence molecular beacons (**Figure 2.6 B and E**). Using Effectene for molecular beacon delivery gave fluorescence images (GAPDH-targeting and random-sequence molecular beacons, respectively) that resembled the corresponding images shown in **Figures 2.6 A and 2.6 E**. Clearly, caution must be

taken in using these transfection methods in delivering molecular beacons for living cell gene detection assays.

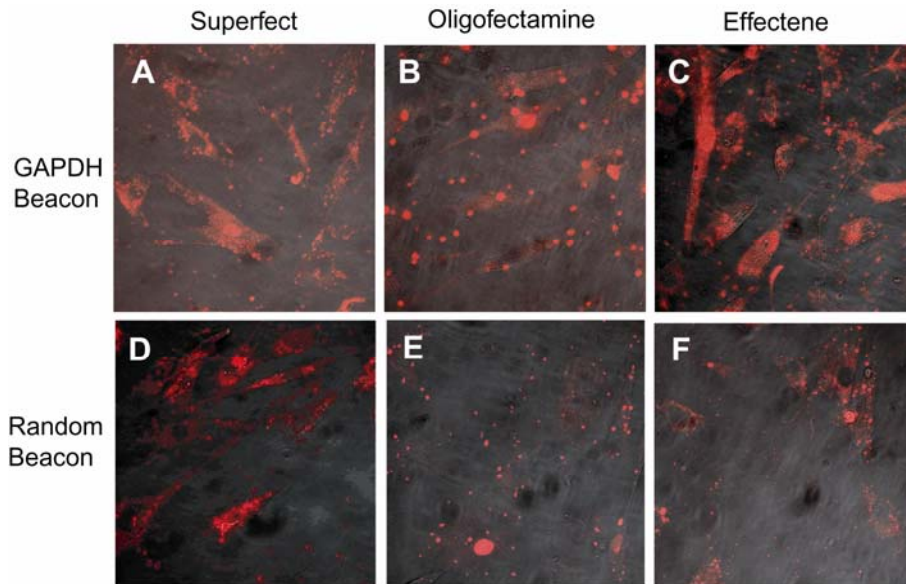


**Figure 2.6:** Cellular delivery using conventional transfection methods

(A-C) Fluorescence signal in HDF cells after 3.5 h transfection of unmodified GAPDH-targeting molecular beacons with (A) Superfect, (B) Oligofectamine and (C) Effectene. Note the concentrated 'bright spots' in both cytoplasm and nucleus.

(D-F) Similar fluorescence signal level was observed after 3.5 h delivery of random-sequence molecular beacons with (D) Superfect, (E) Oligofectamine and (F) Effectene. The resulting 'bright spots' in HDF cells indicate that the fluorescence signals in (A-F) were largely due to molecular beacon degradation.

## Discussion

We have clearly demonstrated that cellular delivery of molecular beacons using the peptide-based approach has far better performance compared with conventional transfection methods. This opens new opportunities that become possible only with peptide-linked molecular beacons. For example, the fast delivery kinetics (~30 min) and high efficiency in probe internalization, combined with the high specificity and signal-to-background ratio of molecular beacon makes the peptide-linked molecular beacon probes a unique and novel system for studying gene expression in living cells in real time. We and other have shown that when delivered through the endocytic pathway (e.g., liposome-based transfection), antisense oligonucleotide probes tend to be trapped inside endocytic vesicles and degraded in the endosomes and lysosomes by nucleases ([26]). Peptide-based internalization has the potential to avoid the endocytic pathway, therefore reducing false-positive signals due to nuclease degradation. Consequently, ODN backbone modifications of the probe such as the use of 2'-O-methyl modified molecular beacons may not be necessary. As demonstrated in our study, combining fast probe delivery with prompt optical imaging, a high signal-to-background can be realized in live cell mRNA detection. The peptide-linked molecular beacons approach, is a faster (~30 min) and simpler, which may be more suitable for certain applications, including basic biological studies of mRNA expression level in living cells in response to drug molecules, toxin and external stimuli, the knock-down effect of RNAi, and disease detection and diagnosis. Using NIR fluorophores as the reporter, peptide-linked molecular beacons have the potential to become a powerful tool for shallow tissue molecular imaging with high sensitivity and spatial resolution.

Although our results demonstrated the high efficiency of peptide-based probe delivery, the underlying mechanism of cell membrane penetration remains largely unknown. Some studies suggest that cell entry is independent of the endosomal

pathway ([28]) with the notion that the internalization is much faster than known endocytotic processes ([29]), whereas others suggest that the CPP-induced cargo internalization is due to classical endocytosis ([30],[31]). One possibility is that the initial interaction between the peptide and cell surface is due to electrostatic forces, but subsequent cell membrane penetration is mediated by glycosaminoglycans ([32]). However, many questions still remain open. For example, for certain cell lines the TAT-1 and other peptides have the ability to deliver cargos into cell nuclei, suggesting a directed motion in the cytoplasm. It is still unclear whether different CPPs follow a common mechanism or have different pathways. More biochemical and biophysical studies of the CPP-based delivery mechanism are clearly warranted.

There are many challenges in quantifying mRNA expression in living cells, including the need to create an internal control for fluorescence intensity of the reporter fluorophore in the intracellular environment, and determine the fraction of mRNA molecules hybridized with probes. The detection sensitivity is also affected by the properties of fluorophore, fluorescence detection method, the optical imaging instrumentation used and background signal. It has been suggested that the molecular beacon based approach could detect as low as 10 mRNA molecules in a single cell ([14]). Alternatively, the average mRNA expression over a large number of cells can be obtained using FACS (Fluorescence Activated Cell Sorter) to yield more reproducible and statistically more significant results.

## References

- [1] Karge, W.H. 3rd, Schaefer, E.J., Ordovas, J.M. (1998) Quantification of mRNA by polymerase chain reaction (PCR) using an internal standard and a nonradioactive detection method. *Methods Mol. Biol.* **110**, 43-61.
- [2] Jung, R., Soondrum, K., Neumaier, M. (2000) Quantitative PCR. *Clin. Chem. Lab. Med.* **38**, 833-836.
- [3] Brown, P.O., Botstein, D. (1999) Exploring the new world of the genome with DNA microarrays. *Nat. Genet.* **21**, 33-37.
- [4] DeRisi, J.L., Iyer, V.R. (1999) Genomics and array technology. *Curr. Opin. Oncol.* **11**, 76-79.
- [5] Femino, A.M, Fay, F.S., Fogarty, K. & Singer, R.H. (1998) Visualization of single RNA transcripts *in situ*. *Science* **280**, 585-590.
- [6] Levisky, J.M., Shenoy, S.M., Pezo, R.C., Singer, R.H. (2002) Single-cell gene expression profiling. *Science* **297**, 836-840.
- [7] Molenaar, C., Marras, S.A., Slats, J.C., Truffert, J.C., Lemaitre, M., Raap, A.K., Dirks, R.W., Tanke, H.J. (2001) Linear 2' O-Methyl RNA probes for the visualization of RNA in living cells. *Nucleic Acids Res.* **29**, E89-9.
- [8] Tyagi, S., Kramer, F.R. (1996) Molecular beacons: probes that fluoresce upon hybridization. *Nat. Biotechnol.* **14**, 303-308.
- [9] Tyagi, S., Bratu, S.P., Kramer, F.R. (1998) Multicolor molecular beacons for allele discrimination. *Nat. Biotechnol.* **16**, 49-53.
- [10] Barton, G.M., Medzhitov, R. (2002) Retroviral delivery of small interfering RNA into primary cells. *Proc. Natl. Acad. Sci. U.S.A.* **99**, 14943-14945.
- [11] Cheung, C.Y., Murthy, N., Stayton, P.S., Hoffman, A.S. (2001) . A pH-sensitive polymer that enhances cationic lipid-mediated gene transfer. *Bioconjug. Chem.* **12**, 906-910.

- [12] Mitchell, P. (2001) Turning the spotlight on cellular imaging. *Nat. Biotechnol.* **19**, 1013-1017.
- [13] Faria, M., Spiller, D.G., Dubertret, C., Nelson, J.S., White, M.R., Scherman, D., Helene, C., Giovannangeli, C. (2001) Phosphoramidate oligonucleotides as potent antisense molecules in cells and in vivo. *Nat. Biotechnol.* **19**, 40-44.
- [14] Sokol, D.L., Zhang, X., Lu, P., Gewirtz, A.M. (1998) Real time detection of DNA:RNA hybridization in living cells. *Proc. Natl. Acad. Sci. U.S.A.* **95**, 11538-11543.
- [15] Yin, D., Tang, J.G. (2001) Gene therapy for streptozotocin-induced diabetic mice by electroporational transfer of naked human insulin precursor DNA into skeletal muscle in vivo. *FEBS Lett.* **495**, 16-20.
- [16] Wadia, J.S., Dowdy, S.F. (2002) Protein transduction technology. *Curr. Opin. Biotechnol.* **13**, 52-56.
- [17] Becker-Hapak, M., McAllister, S.S., Dowdy, S.F. (2001) TAT-mediated protein transduction into mammalian cells. *Methods* **24**, 247-256.
- [18] Snyder, E.L. and Dowdy, S.F. (2001) Protein/peptide transduction domains: potential to deliver large DNA molecules into cells. *Curr. Opin. Mol. Ther.* **3**, 147-152.
- [19] Tsourkas, A., Behlke, M.A., Xu, Y. & Bao, G. (2003) Spectroscopic features of dual fluorescence/luminescence resonance energy transfer molecular beacons. *Analytic. Chemistry* **75**, 3697-3703.
- [20] Sirover, M.A. (1999) New insights into an old protein: the functional diversity of mammalian glyceraldehyde-3-phosphate dehydrogenase. *Biochim. Biophys. Acta* **1432**, 159-84.
- [21] Chiou, S.K., Jones, M.K., Tarnawski, A.S. (2003) Survivin - an anti-apoptosis protein: its biological roles and implications for cancer and beyond. *Med. Sci. Monit.* **9**, PI25-29.
- [22] Nori, A., Jensen, K.D., Tijerina, M., Kopeckova, P., Kopecek, J. (2003) Tat-conjugated synthetic macromolecules facilitate cytoplasmic drug delivery to human ovarian carcinoma cells. *Bioconjug. Chem.* **14**, 44-50.

- [23] Hallbrink, M., Floren, A., Elmquist, A., Pooga, M., Bartfai, T., Langel, U. (2001) Cargo delivery kinetics of cell-penetrating peptides. *Biochim. Biophys. Acta* **1515**, 101-109.
- [24] Feener, E.P., Shen, W.C., Ryser, H.J. (1990) Cleavage of disulfide bonds in endocytosed macromolecules. A processing not associated with lysosomes or endosomes. *J. Biol. Chem.* **265**, 18780-18785.
- [25] Okada, E., Murai, Y., Matsui, K., Isizawa, S., Cheng, C., Masuda, M., Takano, Y. (2001) Survivin expression in tumor cell nuclei is predictive of a favorable prognosis in gastric cancer patients. *Cancer Lett.* **163**, 109-116.
- [26] Dokka, S., Rojanasakul, Y. (2000) Novel non-endocytic delivery of antisense oligonucleotides. *Adv. Drug Deliv. Rev.* **44**, 35-49.
- [27] Santangelo, P. J., Nix, B., Tsourkas, A. and Bao, G. (2004) Dual FRET molecular beacons for mRNA detection in living cells. *Nucleic Acids Res.*, in press.
- [28] Simeoni, F., Morris, M.C., Heitz, F., and Divita, G. (2003) Insight into the mechanism of the peptide-based gene delivery system MPG: implications for the delivery of siRNA into mammalian cells. *Nucleic Acids Res.* **31**, 2717-2724.
- [29] Vives, E., Richard, J.P., Rispoli, C. and Lebleu, B. (2003) TAT peptide internalization: seeking the mechanism of entry. *Curr. Protein Pept. Sci.* **4**, 125-132.
- [30] Lundberg, M., Wikstrom, S. and Johansson, M. (2001) Cell surface adherence and endocytosis of protein transduction domain. *Mol. Ther.* **8**, 143-150.
- [31] Console, S., Marty, C., Garcia-Echeverria, C., Schwendener, R., Ballmer-Hofer, K. (2003) Antennapedia and HIV transactivator of transcription (TAT) "protein transduction domains" promote endocytosis of high molecular weight cargo upon binding to cell surface glycosaminoglycans. *J. Bio. Chem.* **278**, 35109-35114.
- [32] Ziegler, A., Blatter, X.L., Seelig, A. and Seelig J. (2003) Protein transduction domains of HIV-1 and SIV TAT interact with charged lipid vesicles. Binding mechanism and thermodynamic analysis. *Biochemistry* **42**, 9185-9194.

## CHAPTER 3

### Subcellular localization and Co-localization of mRNAs in the cytoplasm of living cells

#### Introduction

mRNA localization is a widespread post-transcriptional mechanism for targeting protein synthesis to specific subcellular locations ([1]). It is believed that the specific localization of mRNAs plays a key role in the compartmentalization of protein synthesis in the cytoplasm, and facilitates protein-protein interactions ([2]). Clearly, mRNA localization requires the formation of mRNA ribonucleoprotein particles (mRNPs) that can be targeted to specific regions of a cell ([3]), where polyribosomes (also referred to as polysomes) are assembled. It has also been shown that both mRNP transport and polyribosome formation involves cytoskeletal structures ([4-6]). However, many important questions remain open concerning mRNA localization. For example, little is known about subcellular localization and organelle association of mRNAs. Although it was suggested that 70-80% of mRNPs in a cell are co-localized with the cytoskeleton, such a co-localization has been confirmed for only a very small number of mRNAs ([4-8]).

Based on the review of literature (**Chapter 1**), there is very limited understanding of localization of mRNA in cells. The few studies conducted using insitu hybridization, have shown localization of mRNA with cytoskeleton structure. There is very limited specification to which of the cytoskeleton elements are crucial for localization, the roles of each cytoskeleton elements (Microtubule, Actin and Intermediate Filaments). In addition, there is no discussion on role of cytoplasmic organelles e.g. ER, Mitochondria etc. for any possible involvement in translation of cytoplasmic soluble proteins. The

isolated view of cytoskeleton as the only system involved in mRNA localization is far from complete as it has been shown in various other studies that many of these organelles- especially mitochondria/ ER are closely associated with cytoskeleton ([9]).

In this study, we have made our first attempt to understand the organization of endogenous mRNAs in the cytoplasm of living cells. In this chapter, we present the study on direct visualization of sub cellular localization of GAPDH mRNAs using molecular beacons, and reveal their co-localization with mitochondria ([10]). The motivation for this study has come from our earlier results (**Chapter 2**) of localized distribution of GAPDH mRNAs in the cytoplasm of living cells. Based on our earlier experiments, we discovered a particular filamentous localization of GAPDH mRNAs in the cytoplasm of living cells, with a clear tendency of surrounding the nucleus and following cell morphology. To address the question of mRNA localization and organization in the cytoplasm, we designed experiments to address following key questions:

- 1) What intracellular organelles are involved in localization of GAPDH mRNA?
- 2) What are the key cytoskeletal elements involved in localization of GAPDH mRNA?

## **Material and Methods**

### **Design of Molecular Beacons**

In this study we have used the same MB probe design for targeting GAPDH mRNA as used in **Chapter (2)**. Further in this study, we have designed multiple controls to validate the localization of GAPDH mRNA observed using MB probes is specific and independent of Tat based delivery approach. For one of the positive control experiment

we designed a sequence targeting 28-s ribosomal RNA. Ribosomal RNA was chosen as a target RNA as its localization has been well studied ([18-19]). Further we have used random control beacon design to detect the background signal due to non specific interactions in living cells. The sequences of MBs are shown in **Table 3.1**. In addition to these control MBs we also designed a fluoescently labeled poly A (24 mer) linear oligonucleotide to detect the signal after delivery of Tat-Poly A oligonucleotide complex in living cells.

### **Cell culture**

Normal human dermal fibroblasts (Cambrex, NJ) were grown in Clonetics fibroblast growth medium supplemented with 2% fetal bovine serum (Cambrex, NJ), insulin, fibroblast growth factor, Gentamicin Sulfate and Amphotericin-B.

**Table 3.1:** Design of molecular beacons

---

*GAPDH molecular beacon*

5'-Cy3-CGACGGAGTCCTTCCACGATACCACG/thiol-dT/CG-BHQ2-3'

---

*28S rRNA molecular beacon*

---

5'-Cy3-CGACTACCACCAAGATCTGCAGTCG/HQ-2/-3'

---

*'Random' sequence molecular beacons*

MB: 5'-/Cy3/CACGTCGACAAGCGCACCGATACGTG/BHQ-2/-3'

---

### **Molecular beacon delivery via cell permeable peptide**

The molecular beacon targeted to GAPDH (see Table 3.1) was linked via a disulfide bridge to the Tat peptide ((N terminus) TyrGlyArgLysLysArgArgGlnArgArgArg (C terminus)-Cys) (as discussed in **Chapter 2**). For delivery of molecular beacon, the peptide-linked molecular beacons were mixed with the regular media and incubated with the specific cells at 37°C for 30 minutes. When labeling mitochondria, cells were incubated with MitoFluor™ Green dye for half an hour in regular culture medium. After labeling, cells were washed and incubated with Tat linked GAPDH targeting beacon in a regular culture medium for 30 minutes. The cells were then washed twice with PBS to remove the incubation medium and placed in fresh medium for fluorescence imaging, which was carried out using a Zeiss Axiovert LSM-1000 confocal microscope.

### **Nocodazole treatment**

For these experiments, cells were grown normally and plated in 4 well, Lab-tek II chambered coverslips. Twenty-four hours after plating the MB probes were delivered to them. After 30 minutes of delivery, the cells were treated with 30µM concentration of nocodazole. The cells were imaged after 60 minutes after incubation with nocodazole.

### **Fluorescence *in-situ* hybridization**

Normal human dermal fibroblasts were cultured in 8-well chambered coverslips for 24 hours in normal growth medium (FGM-2 Cambrex Co.) and then washed with 1x PBS (without Ca or Mg). The slide was fixed in 100% methanol at -20°C for 10 minutes. After removing methanol, the slides were allowed to air dry and stored overnight at -80°C. In-situ hybridization assays were then performed by first washing the slides for 5 minutes in 1x PBS and hybridizing them overnight at 37°C in 1x PBS (no Ca or Mg)

containing 400 nM of fluorescently labeled linear probes targeting GAPDH. The cells were imaged, after removing the hybridization solution with washing and final incubation of cells in 1 x PBS.

### **Fluorescence microscopy imaging**

Fluorescence imaging of live cells was performed using a Zeiss Axiovert LSM-100 confocal microscope. For assays using the single beacon approach delivered via the Tat peptide, the Cy3 dye on the GAPDH targeted beacon was excited with 543 nm laser and detected using 565-625 nm filter. For viewing MitoFluor™ Green on the confocal, excitation was achieved using the 488 nm emission from an Argon ion laser with detection using a band pass filter from 510-530 nm.

### **Organelle labeling and fluorescence imaging**

MitoFluor Green was used to label mitochondria as directed by Molecular Probes. Fluorescence imaging of live and fixed HDF cells was performed using a Zeiss Axiovert LSM-100 confocal microscope. Imaging assays with peptide-linked, GAPDH-targeting molecular beacons were performed using a Zeiss confocal microscope with a 565-625 nm filter for emission detection under excitation at 543 nm. The fluorescence signal of MitoFluor Green was detected using a bandpass filter of 510-530 nm under the excitation wavelength of 488 nm.

## Results and Discussion

To address the first question regarding the role of intracellular organelles in localization of GAPDH mRNA, we decided to simultaneously label certain key organelles- mitochondria and ER in addition to detecting GAPDH MB signal. Since the pattern of fluorescent signal from MB probes targeting GAPDH mRNA was similar with the mitochondrial staining in HDF cells as reported by ([11], Molecular Probes website), so in our first experiment we decided to co-label mitochondria in addition to detecting MB signal.

In this study, we decided to label mitochondria with a dye (MitoFlour green). Mitochondria in living cells are stained with 200 nanomolar concentrations of MitoFlour Green FM dye which exhibits bright green, fluorescein-like fluorescence. MitoFlour Green FM dye has an added advantage that it is essentially non fluorescent in aqueous solutions, only becoming fluorescent once it accumulates in the lipid environment of mitochondria. Hence, background fluorescence is negligible, enabling clear visualization of mitochondria in live cells immediately following addition of the stain. In addition this stain is more photostable as compared to conventional dye such as Rhodamine 123. The other reason we selected MitoFlour Green was to avoid any spectral overlap with Cy3 emission spectrum. This allowed us to simultaneously image the fluorescence signal from mitochondrial staining and MB probes using a standard confocal set up. The results of the co-localization of GAPDH and mitochondria are shown in **Figure 3.1**. **Figure 3.1(A)** detection of mitochondrial staining using mitofluor green dye, **Figure 3.1(B)** shows the fluorescent signal from MB probes hybridized to GAPDH mRNAs. The overlay of the two channels to determine the co-localization is shown in **Figure 3.1(C)**. The results show a high degree of co-localization of GAPDH mRNAs with the mitochondria. The extent of co-localization improved with increase in

distance from the nucleus. In the peri-nuclear regions, we could also detect some GAPDH mRNA signal not highly co-localized with the mitochondria.

The other organelle, we decided to label in this study was ER. The reason we selected ER as it has been indicated in literature that ER is closely associated with mitochondria, and ER is also a site of translation for various proteins, which are exported from cells or present on various membranes of cells. ER and mitochondria association is required for lipid transfer from ER to mitochondria and also for homeostasis of  $\text{Ca}^{2+}$  ions in cells. In this study, we decided to co-label mitochondria and ER using MitoFlour, ER Tracker respectively. This approach allowed us to simultaneously label both the organelles and validate the close relationship between mitochondria and ER. This approach will address our hypothesis of involvement of Mitochondria/ER in subcellular localization of GAPDH mRNA. The results of co-localizations of ER and the mitochondria are shown in **Figure 3.2**. The results show that mitochondria do overlap with the segments of ER, while ER extends through most of the cytoplasm. This result taken together with the result described in **Figure 3.1**, suggests that GAPDH mRNA could be co-localized with both ER and mitochondria, although its pattern of distribution in the cytoplasm is better correlated with mitochondrial distribution as compared with ER distribution. In this study, we could not directly label ER and detect signal from MB probes due to spectral overlap of the ER stain with Cy3 emission spectra.

A

B

C

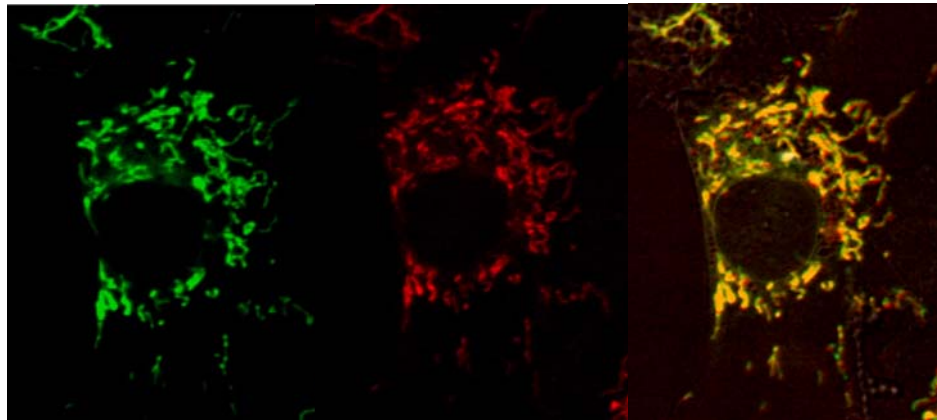


**Figure 3.1:** Co-localization of GAPDH m RNA with Mitochondria  
(A) Mitochondria staining using Mitofluor green (Green color)  
(B) GAPDH m RNA detection using molecular beacons (Red Color)  
(C) Overlap of MB signal with Mitostain green (Yellow color- Resulting from overlap)

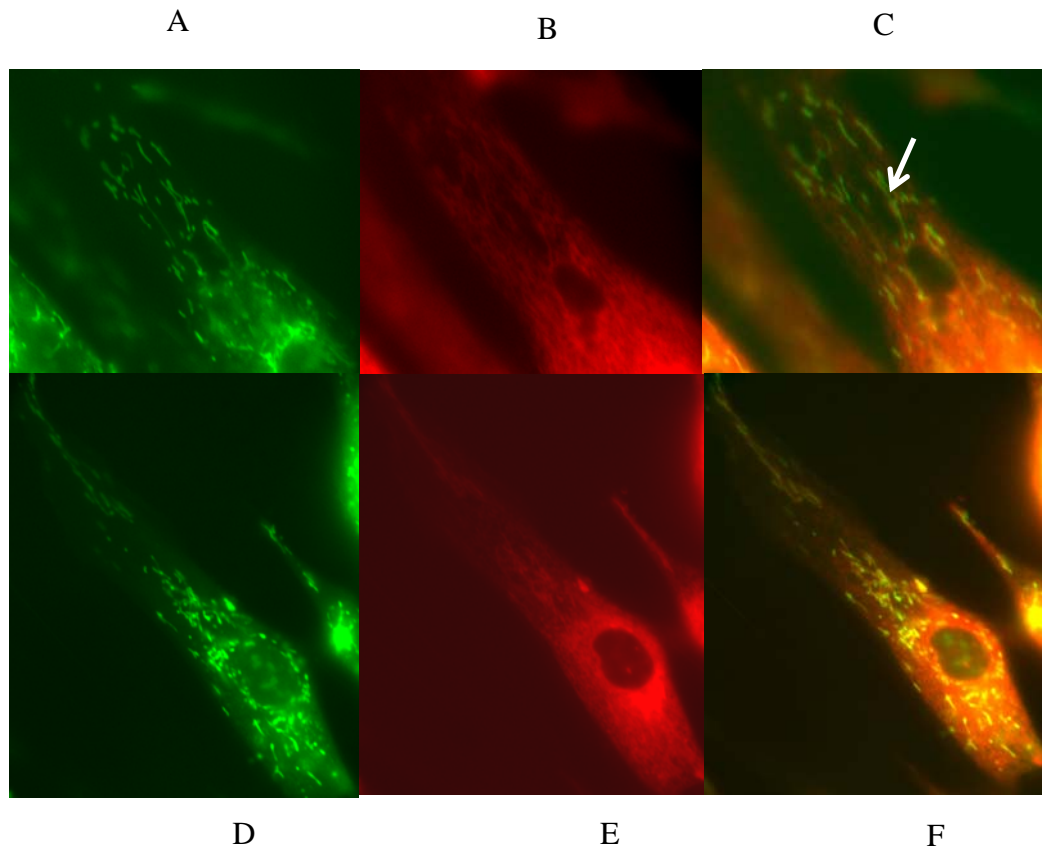
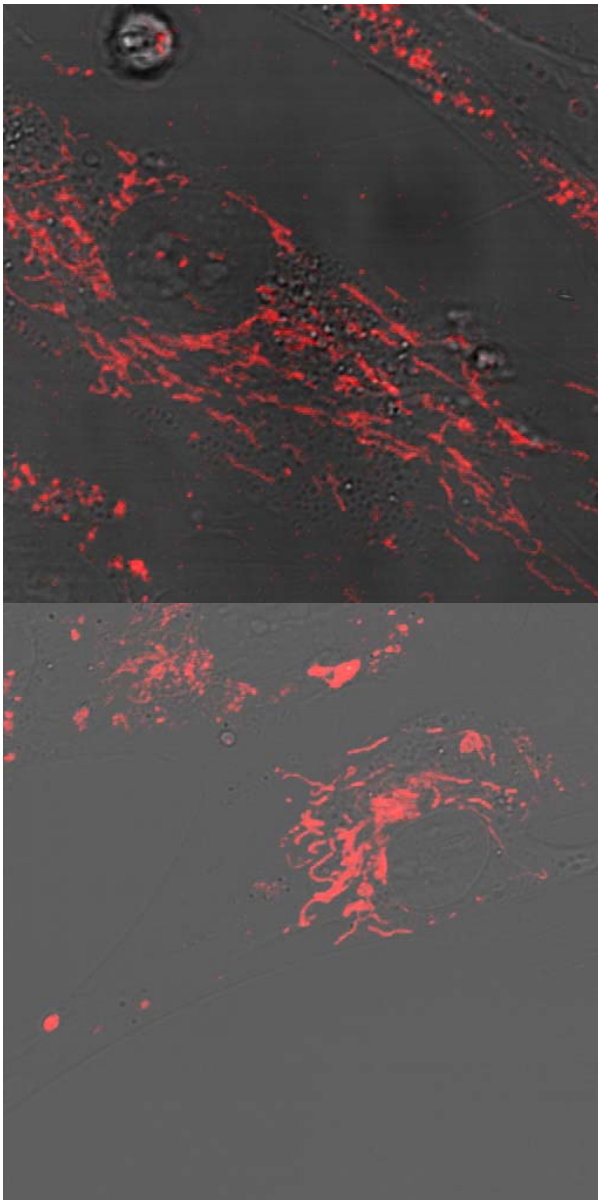


**Figure 3.2:** Human dermal fibroblast images: A,D) mitochondrial stain, MitoFluor™ Green (green), B,E) ER-Tracker™ (red), and C,F) merge of A and B, and merge of D and E.

To address the next question, regarding the role of cytoskeletal structures in localization of GAPDH mRNA in living cells, we have studied the effect of microtubule depolymerization on the distribution of GAPDH MB probe signal in the cytoplasm. The major reason for selection of microtubules was their close association with mitochondria and ER. For microtubule depolymerization, we have used nocodazole, which is an anti-neoplastic agent and exerts its effect by de-polymerization of microtubules.

The result of nocodazole treatment and its effect on the localization of GAPDH mRNAs is shown in **Figure 3.3**. **Figure 3.3 (A)** shows the distribution of GAPDH mRNAs in the cytoplasm of control cells. **Figure 3.3 (B)** shows the distribution of GAPDH mRNAs signal after nocodazole treatment as described in the Material and Methods section. The result clearly shows significant changes in the distribution of GAPDH mRNAs signal in the cytoplasm. This result clearly highlights the association of GAPDH mRNAs with microtubule network. This result in combination with previous results of co-localization with mitochondria and ER clearly indicates the close relationship of various organelles and the cytoskeleton in mediating the localization of mRNAs. Studies in **Chapter 5** will further address the role of microtubules in mediating the transport of GAPDH mRNAs in the cytoplasm of living cells.



A

B

**Figure 3.3:** (A)-GAPDH m RNA in HDF cells (Filamentous structure)  
(B)-Effect of nocodazole treatment on localization of GAPDH mRNA  
(Treatment for 30 minutes with 30  $\mu$ m Nocodazole)

### **Control studies for mRNA localization**

To confirm that mRNA localization and co-localization patterns shown in **Figure 3.1** was a result of specific probe-target hybridization, control studies were performed by delivering negatively charged Cy3 or Cy5 dyes into HDF via SLO and detecting the corresponding fluorescence signal. As shown in **Figure 3.4 A and 3.4 B**, although the signals of Cy3 and Cy5 shows some degree of localization due to non-specific binding to certain cellular structures, they did not give the filamentous localization pattern of mitochondria. This suggested that the Cy3 and Cy5 reporter dyes were not attracted specifically to mitochondria, whose surfaces are also negatively charged. Therefore, the fluorescence signal of Cy3- and Cy5-labeled molecular beacons in live HDF cells shown in **Figure 3.1** was due to their specific hybridization to the mRNA targets, not an artifact of the reporter dyes.

In our previous study (**Chapter 2**) we delivered, 'random'-sequence molecular beacons using peptide-linked 'random'-sequence molecular beacons into HDF cells, and detected the resulting fluorescence signal. This provide a negative control in that, if the images in **Figure 3.1** showing co-localization of the GAPDH mRNAs with mitochondria were resulted from non-specific opening of molecular beacons near mitochondria, the same would occur with 'random' beacons. However, using the same excitation and emission detection optics, the 'random' beacons gave very low background signal as compared with the true signal ([12, 13]), indicating that the fluorescence signal from the GAPDH beacons was indeed a result of specific mRNA detection. As a further control, we delivered into HDF cells Cy3-labeled linear 24-mer poly-A oligonucleotide conjugated with Tat-1 peptide through a stable chemical linkage ([12, 13]). As shown in **Figure 3.4 C**, 30 min after delivery, this fluorescent oligonucleotide construct accumulated in the perinuclear region of the cell due to the very low affinity for a target in the cytoplasm. The signal level in the cytoplasm due to unquenched Poly A oligonucleotide was fairly

low as compared with MB signal due to hybridization with GAPDH mRNAs. To detect this signal we have to increase the pinhole and voltage gain on photo multiplier tube during confocal imaging. This highlights an interesting aspect that if fluorophores are dispersed in the cytoplasm, the effective signal is much lower than the case of localized signal with same concentration of fluorophores. This control experiment clearly demonstrates that, with Tat-1 peptide as the delivery vehicle, labeled oligonucleotide probes may localize differently depending on the target, further confirming that the filament-like localization GAPDH mRNAs shown in **Figure 3.1** was a result of specific targeting of molecular beacons. In addition to peptide-based delivery, we internalized GAPDH-targeting molecular beacons into HDF cells using Streptolysin O and imaged the resulting fluorescence using a confocal microscopy. As can be seen from **Figure 3.4 D**, GAPDH mRNAs shown a clear filamentous pattern, similar to the results obtained using peptide-linked, GAPDH-targeting molecular beacons. The detection of GAPDH mRNAs using two different delivery methods (both peptide-based and SLO) served as a crosscheck of the results shown in **Figure 3.1**.

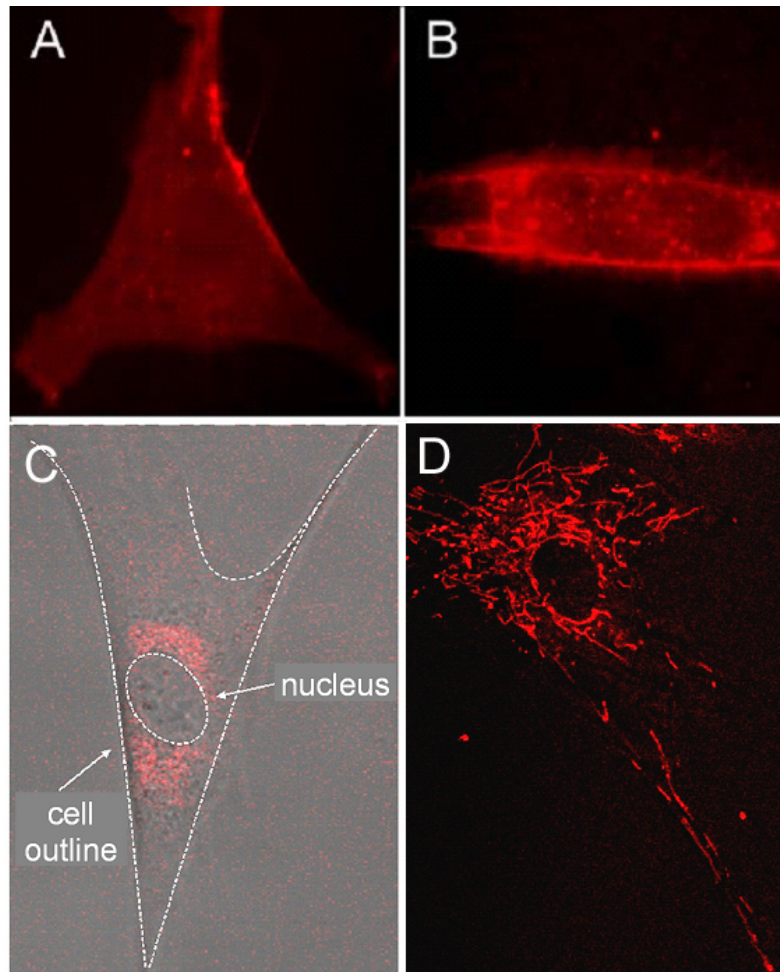


**Figure 3.4:** Control studies of mRNA localization.

In A) and B), the fluorescence of Cy3 and Cy5 dyes alone inside HDF cells is shown respectively, indicating that free Cy3 and Cy5 dyes inside a living cell did not result in a filamentous mRNA localization pattern shown in Figure. 1C

In C), the overlap of white-light image of an HDF cell and the fluorescence signal of Cy3-labeled, Tat-peptide conjugated 24-mer poly-A oligonucleotides in an HDF cell is shown. Note that most of the labeled oligonucleotides accumulated in the perinuclear region due to the very low affinity of the probe for any target in the cytoplasm.

In D), a confocal fluorescence image of the localization of GAPDH mRNA is shown as the result of SLO based delivery. Clearly, SLO-based and peptide-based delivery gave very similar filamentous patterns of GAPDH mRNA localization.

As a positive control, we performed fluorescence *in situ* hybridization (FISH) assays to see if the filamentous pattern of mRNA localization could be observed in fixed cells. The epifluorescence images of GAPDH mRNA detection using FISH are displayed in **Figure 3.5 A**, indicating that their localization patterns in the cytoplasm are similar to that in living cells as shown in **Figure 3.1 B**. In the FISH assays, methanol was employed for fixation which is often used to maintain the subcellular structure and retain molecules associated with microtubule ([14, 15]) together, these positive and negative control studies suggest that the mRNA localization patterns shown in **Figure 3.1 C** are true. We also performed fluorescence *in situ* hybridization (FISH) using 28S rRNA-targeting molecular beacons in methanol fixed cells. As can be seen from the FISH image displayed in **Figure 3.5 B**, the fluorescence intensity is quite high in the rough ER (the “waffle-like” pattern in the cytoplasm), which is different from the localization pattern of the GAPDH mRNAs shown in **Figure 3.1** and **3.5 A**.

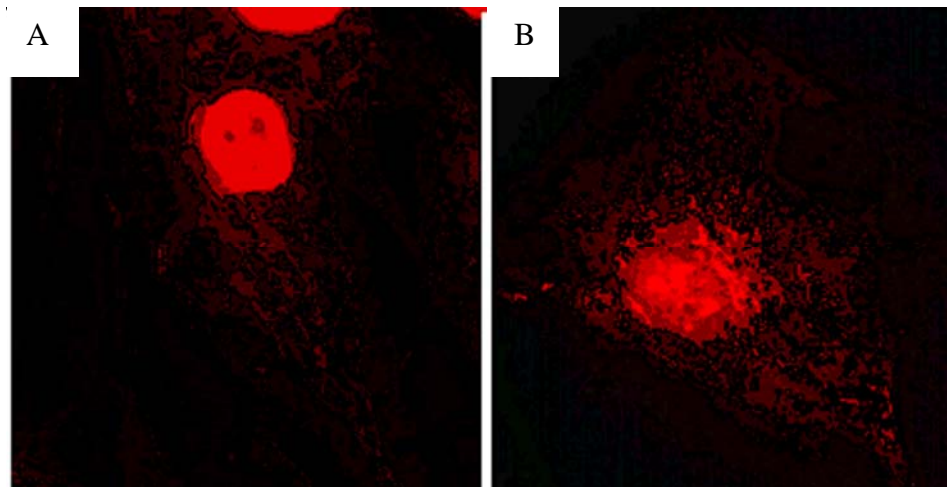


**Figure 3.5:** Fluorescence *in situ* hybridization studies

In A), the FISH results of GAPDH mRNA detection are shown respectively as positive controls, further confirming the filamentous mRNA localization pattern displayed in Figure 3.1 (A).

In B), the FISH image of the 28S rRNA beacon displaying significant localization with ER.

### **Localization of 28S rRNA and its co-localization with rough ER**

It has been shown that 28s ribosomal RNA molecules accumulate to rough endoplasmic reticulum (ER), not co-localize with mitochondria nor have a filament-like localization patterns ([16-18]). To demonstrate a different RNA localization pattern using molecular beacons, we designed a molecular beacon to target the human 28s ribosomal RNA (rRNA) with the same hybridization domain as used by ([18]) and ([16]) where living cell detection of 28s rRNA was performed and the accessibility of target sequence was demonstrated. Detection of 28s rRNA provides an excellent control for subcellular RNA localization because most of the 28s rRNA molecules in the cytoplasm are known to be either localized to the rough ER or bound to free ribosomes ([17]).

We delivered molecular beacons targeting 28s rRNA into live HDF cells using SLO ([13]) and performed fluorescence imaging of the resulting signal using a confocal microscope. As shown in **Figure 3.6 A**, most of the fluorescence signal as a result of beacon-rRNA hybridization was near the cell nucleus. Imaging the cell with white light (**Figure 3.6 B**) and then overlapping the two images demonstrates that the beacon-induced signal in the cytoplasm was localized with the rough ER, as shown in **Figure 3.6 C**. This pattern of 28S rRNA co-localization with the rough ER is *significantly different* from those displayed in **Figure 3.1** where the filamentous localization of GAPDH mRNAs seems to coincide with mitochondria. We also performed a negative control study to deliver single 'random'-sequence molecular beacons into HDF cells using SLO; the resulting fluorescence signal is shown in **Figure 3.6 D**, along with the white-light image of the same cells shown in **Figure 3.6 E**; the overlap of the images in **Figure 3.6 D** and **6 E** is given in **Figure 3.6 F**. The very low background signal displayed in **Figure 3.6** after 1 h of incubation confirms that the image shown in **Figure 3.6 A** was indeed due to specific detection of 28S rRNA by molecular beacon.

Our results shown in **Figure 3.6 A-C** are consistent with what reported by Molenaar et al. ([18]) using a FISH (fluorescence *in situ* hybridization) assay to image 28S rRNA. Specifically, most of the signal in the cell cytoplasm was concentrated near the cell nucleus, suggesting a co-localization of 28S rRNA with rough ER. However, in the same study, the live-cell imaging of 28S rRNA using microinjection failed to detect 28S rRNA in the cytoplasm, largely due to the delivery method (microinjection) that has been shown to concentrate oligonucleotides rapidly into cell nucleus ([20]). Positive detection of 28S rRNA in the cytoplasm of live HeLa cells has also been reported ([17]), although issues such as the signal-to-background ratio and the concentration of the linear probes render the direct comparison difficult.

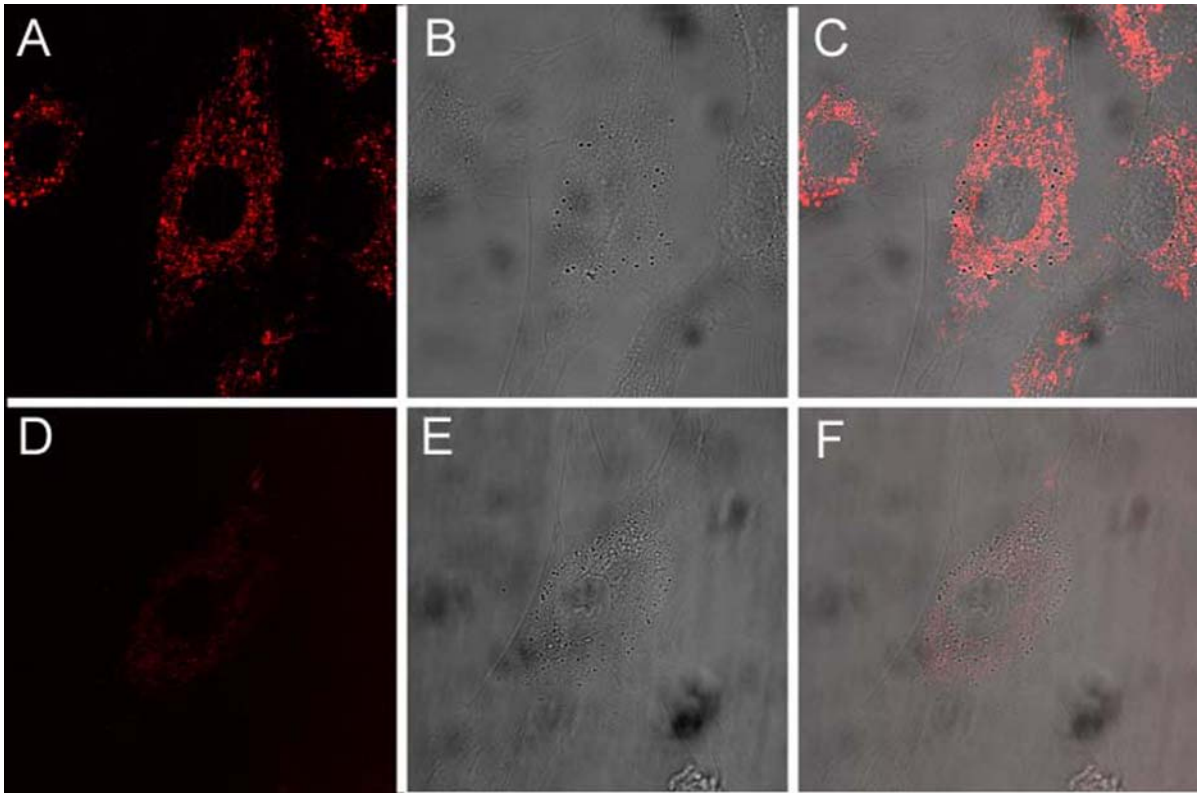


**Figure 3.6:** A control study for the localization of the molecular beacons in live cells. The fluorescence signal from 28S rRNA-targeting single molecular beacons in HDF cells. B) A white light image of the same cell using a confocal microscope. C) The overlap of the images in A) and B) indicating 28S rRNA co-localization with the rough ER. The results of a negative control assay using Cy3-labeled “random” beacon are given in D), E) and F) showing respectively the fluorescence signal of “random” beacons, the white light image of the same cell and their overlap. The very low background signal of “random” beacons confirms the specificity of 28S rRNA detection using molecular beacons.

## Summary

Taken together, our observations strongly suggest that GAPDH mRNA molecules are co-localized with mitochondria, which in turn are associated with ER and microtubules. GAPDH proteins, which are essential to glycolysis and the production of pyruvate, have been shown to be associated with mitochondria ([19], [10]). Therefore, co-localization of GAPDH transcripts with mitochondria may facilitate the localization of their corresponding proteins to mitochondria. Although the physical basis of the association of GAPDH mRNAs with the ER, mitochondria and microtubules needs to be further explored, our unexpected finding may stimulate further studies of the transport, localization and organelle association of mRNA. For example, it will be important to study the localization of mRNAs corresponding to different classes of proteins, and to reveal the biological significance of mRNA-mitochondria association.

Molecular beacon based RNA detection in living cells may provide a novel approach for studying the dynamics of subcellular localization of specific RNAs and revealing their biological functions. Unlike FISH studies in which cells need to be fixed, living cell RNA detection using molecular beacons enables real-time dynamic measurements of RNA localization, including mRNA trafficking and transport to and from mitochondria as well as changes in mRNA localization patterns in response to drug molecules and external stimuli such as growth factors and applied shear stress. For example, the structural dynamics of localized mRNA can be studied using molecular beacons in conjunction with FRAP (fluorescence recovery after photobleaching, **Chapter 5**). It should also be possible to visualize alterations in mRNA localization as a result of the deletion of specific sequences (e.g., 'zipcode') on a target mRNA, which may help uncover the molecular mechanisms underlying mRNA localization.

## References

- [1] M. Kloc, N. R. Zearfoss, and L. D. Etkin, Mechanisms of subcellular mRNA localization, *Cell* 108 (2002) 533-544.
- [2] M. Kloc, and S. M. Bilinski, RNA localization and its role in the spatially restricted protein synthesis, *Folia Histochem Cytobiol* 41 (2003) 3-11.
- [3] R. P. Jansen, RNA-cytoskeletal associations, *Faseb J* 13 (1999) 455-466.
- [4] G. J. Bassell, R. H. Singer, and K. S. Kosik, Association of poly(A) mRNA with microtubules in cultured neurons, *Neuron* 12 (1994) 571-582.
- [5] J. Hesketh, D. Jodar, A. Johannessen, K. Partridge, I. Pryme, and A. Tauler, Enrichment of specific mRNAs in cytoskeletal-bound and membrane-bound polysomes in Chinese hamster ovary cells, *Biochem Soc Trans* 24 (1996) 187S.
- [6] P. Mahon, J. Beattie, L. A. Glover, and J. Hesketh, Localisation of metallothionein isoform mRNAs in rat hepatoma (H4) cells, *FEBS Lett* 373 (1995) 76-80.
- [7] B. Russell, and D. J. Dix, Mechanisms for intracellular distribution of mRNA: in situ hybridization studies in muscle, *Am J Physiol* 262 (1992) C1-8.
- [8] J. W. Wiseman, L. A. Glover, and J. E. Hesketh, Evidence for a localization signal in the 3'untranslated region of myosin heavy chain messenger RNA, *Cell Biol Int* 21 (1997) 243-248.
- [9] R. Rizzuto, P. Pinton, W. Carrington, F. S. Fay, K. E. Fogarty, L. M. Lifshitz, R. A. Tuft, and T. Pozzan, Close contacts with the endoplasmic reticulum as determinants of mitochondrial Ca<sup>2+</sup> responses, *Science* 280 (1998) 1763-1766.
- [10] R. Ishitani, M. Tanaka, K. Sunaga, N. Katsube, and D. M. Chuang, Nuclear localization of overexpressed glyceraldehyde-3-phosphate dehydrogenase in cultured cerebellar neurons undergoing apoptosis, *Mol Pharmacol* 53 (1998) 701-707.
- [11] V. P. Skulachev, Mitochondrial filaments and clusters as intracellular power-transmitting cables, *Trends Biochem Sci* 26 (2001) 23-29.

- [12] N. Nitin, Santangelo, P.J., Kim, G., Nie, S, Bao, G., Peptide-linked molecular beacons for efficient delivery and rapid mRNA detection in living cells, *Nucleic Acids Res* 32 (2004) e58.
- [13] P. J. Santangelo, Nix, B., Tsourkas, A., and Bao, G., Dual FRET molecular beacons for mRNA detection in living cells, *Nucleic Acids Res* 32 (2004) e57.
- [14] L. Berrueta, S. K. Kraeft, J. S. Tirnauer, S. C. Schuyler, L. B. Chen, D. E. Hill, D. Pellman, and B. E. Bierer, The adenomatous polyposis coli-binding protein EB1 is associated with cytoplasmic and spindle microtubules, *Proc Natl Acad Sci U S A* 95 (1998) 10596-10601.
- [15] F. Gergely, C. Karlsson, I. Still, J. Cowell, J. Kilmartin, and J. W. Raff, The TACC domain identifies a family of centrosomal proteins that can interact with microtubules, *Proc Natl Acad Sci U S A* 97 (2000) 14352-14357.
- [16] C. Molenaar, S. A. Marras, J. C. Slat, J. C. Truffert, M. Lemaitre, A. K. Raap, R. W. Dirks, and H. J. Tanke, Linear 2' O-Methyl RNA probes for the visualization of RNA in living cells, *Nucleic Acids Res* 29 (2001) E89-89.
- [17] P. B. Moore, and T. A. Steitz, The structural basis of large ribosomal subunit function, *Annu Rev Biochem* 72 (2003) 813-850.
- [18] S. Paillason, M. Van De Corput, R. W. Dirks, H. J. Tanke, M. Robert-Nicoud, and X. Ronot, In situ hybridization in living cells: detection of RNA molecules, *Exp Cell Res* 231 (1997) 226-233.
- [19] M. F. Liaud, C. Lichtle, K. Apt, W. Martin, and R. Cerff, Compartment-specific isoforms of TPI and GAPDH are imported into diatom mitochondria as a fusion protein: evidence in favor of a mitochondrial origin of the eukaryotic glycolytic pathway, *Mol Biol Evol* 17 (2000) 213-223.

## CHAPTER 4

### Imaging the effects of mTOR and PI-3 Kinase mediated inhibition of translation on the organization of mRNA in living cells using MB probes

#### Introduction

Imaging of RNA in living cells or tissue is important for various applications including diagnostics, drug development and for fundamental understanding of RNA cell biology. In this direction, we are interested in developing an exogenous oligonucleotide probe based approach to image RNA in living cells and potentially in-vivo. To achieve this aim, we have developed few methods in our previous studies ([1, 2], **Chapters 2 and 3**) to image endogenous mRNAs in living cells with high specificity and sensitivity. Combining the delivery approaches (Tat-peptide and Streptolysin O- (SLO) based) with molecular beacons, we have studied the intracellular distribution of endogenous RNAs in living cells ([1, 2]). In our previous studies, we have observed that both GAPDH and K-Ras mRNAs were highly localized in the cytoplasm and co-localized with a mitochondrial structure (Santangelo et. al, JBO Accepted). Further, we are interested in evaluating the characteristics of MB probes in living cells, evaluating the state of mRNAs (high accessibility) when these MB probes hybridize with a target sequence. This will help develop a better understanding of the relationship between fluorescent signal from MB probes and gene expression profile in cells.

Having successfully imaged specific mRNAs in living cells, we are interested in further exploring the critical question regarding what population of RNP's we are able to detect using a hybridization-based detection in living cells? Can we control the probe design, including its chemistry, to control or extend the fractions of RNPs it can hybridize with? These questions have significance in both diagnostic and fundamental RNA cell

biology applications. From a diagnostic prospective, if we are to relate the signal from the hybridized MB probes in living cells to the relative levels of gene expression in those samples, we need to establish what population of RNAs and what functional state of those RNAs we are able to hybridize with? From a fundamental biological prospective, MB probes can provide information regarding the sub-cellular localization of RNAs in the cytoplasm. The fundamental question we can address in this direction is, “how localization and co-localization of RNA is effected by different stages of RNA life?” The answers to these questions can enhance our understanding of MB probes, provide us with a knowledge base, which can allow us to tailor MB probe design including chemistry to target various RNAs in living cells and also address key biological questions in above areas.

In this study, we have made our first attempt to address these challenges by understanding the effect of translational inhibition on hybridization of MB probes and organization of specific RNA targets in living cells. The rationale for selection of this approach is based on a fundamental understanding that active translational state of mRNAs is related to functional gene expression in living cells. As it is during this stage of mRNA life, the ribonucleotide sequence information is translated into polypeptides. Further we wanted to extend our understanding of the relationship between a specific organization of RNAs observed in our previous studies ([1, 2], (**Chapter 2, 3**) and the functional state of these RNAs. Furthermore, the repression of translation is an important approach for various therapeutic interventions ([20, 21]) especially in cancer treatment ([22]). Thus, understanding the ability of MB probes to measure such effects can be a valuable tool for diagnostic applications. In addition there are defined and established approaches to inhibit translation processes in living cells within the time scale of our studies ([23-31]). The approaches selected for this study are based on a signaling mediated repression of translational states. This approach also allows understanding of

the role of intra-cellular signaling processes in the organization of RNPs. At present there is a very limited understanding of the role of signaling in sub-cellular organization of RNAs, although extensive knowledgebase has been developed to understand the changes in translation as well as transcriptional profiles with various signaling events in cells using array based approaches ([6, 21, 22]). Thus this study will complement the present understanding of global trends in levels of transcripts and polypeptides with specific sub cellular changes in mRNA distribution with signaling processes.

In this direction, we have designed a study where we have perturbed the translation processes in living cells using small molecule based approaches. Using this approach we have studied the response of MB probes and target RNAs to the repression of translation process in living cells. To achieve this aim, translation process is disrupted by targeting the mTOR pathway, which plays a central role in translation and cell growth ([24]) and also by indirect signaling through inhibition of PI-3 Kinase, which is a key signaling protein upstream of mTOR pathway ([31]). PI-3 Kinase is a critical signaling protein which links the extra- cellular events, including the serum response and the growth factor stimuli, with intracellular signaling in cells ([31, 32]). Ability to link extra- cellular events with RNA biology in cytoplasm can provide new information regarding the regulation of RNA in the cytoplasm of living cells. In addition to these facts, deregulation of PI-3 Kinase mediated signaling due to mutations in *PTEN* gene have been established in various cancer models including prostate and glioblastoma ([31]). If the PI-3 Kinase signaling events are deregulated in those cancer models, it is likely that the mTOR signaling and its control on the translation events are also deregulated in such scenarios ([21, 31]). The ability to understand the molecular changes in RNA life cycles under such conditions can not only enhance our understanding of the pathological process but also provide a key insight into regulation of RNA. This study

provides a first example of our attempts to link MB based imaging of specific RNAs with functional cellular assays using small molecule based inhibition approaches.

mTOR pathway is a central pathway responsible for sensing nutrient and cellular energy levels and it exercises control over cell growth and translational machinery in response to variety of these stimuli ([29, 33, 34]). It exerts its control over translation processes by direct signaling to multiple downstream effectors including ribosomal S6 kinase 1(S6K1) and eukaryotic translational initiation factor 4E binding protein 1 (4E-BP1) ([2, 24, 32]). It controls these effector molecules by inducing phosphorylation at multiple sites. Rapamycin (inhibitor of the mTOR pathway) is known to cause a rapid dephosphorylation of the 4E-BP1 and in turn inhibit the cap-dependent mRNA translation ([28, 31, 33]). This inhibition is caused by binding of dephosphorylated 4E-BP1 with mRNA cap binding protein. (Eukaryotic initiation factor 4E (eIF4E)). This process is mediated by binding of Rapamycin with a widely expressed intracellular protein FKBP12 (FRAP), which then forms an active complex. This active complex then binds with mTOR protein with high affinity ([20]).

PI-3 kinase pathway is a central regulator of mitogenic stimuli and growth factor based signaling events in cells ([31]). It has been demonstrated that PI-3 kinase directly signals to the mTOR pathway through downstream activation of AKT. ([32]). Both mTOR and PI-3 kinase pathways converges on downstream effectors of the translation initiation machinery, i.e., 4E-BP-1 and the Ribosomal S6 kinase ([35]). In this study Wortamannin (at 1  $\mu\text{M}$  concentration) was used to inhibit the activity of PI-3 kinase. Wortamannin has been shown to be a potent inhibitor of PI-3 kinase-based signaling events in various cellular studies ([36, 37]).

Here we have inhibited the translational processes in living cells by using rapamycin-based (10  $\mu\text{M}$ ) direct inhibition of mTOR pathway and Wortamannin-based inhibition of PI-3 kinase (1  $\mu\text{M}$ ). Disruption of the mTOR pathway, which directly

influences the translation process in living cells, provides us a method to directly disrupt this process and study its influence on specific mRNA targets and the MB probes bound to those targets. Wortmannin-based (1  $\mu\text{m}$ ) inhibition of PI-3 kinase allows us to model the effects of extra-cellular conditions, specifically on the role of PI-3 kinase activation/inhibition, on organization of mRNA targets, and the corresponding MB probes hybridized with these targets.

## **Material and Methods**

### **Chemicals**

Wortmannin, Phosphate buffered saline, DMSO, TCEP, Streptolysin O (SLO) were purchased from Sigma Aldrich, St. Louis, MO. Rapamycin was purchased from Calbiochem Corp, CA. Mitoflour green dye for live cell staining of mitochondria was obtained from Molecular probes.

### **Molecular Beacons**

Molecular beacon probes as shown in **Table 4.1** (same as used in our earlier studies (**Chapter 2 and 3**)) were synthesized by MWG Biotech, NC and Biosource Corp, CA. The Molecular beacon probes were designed with regular DNA chemistry (De-oxy ribonucleotide backbone) for each of the target RNA. In addition, MB probes for K-Ras mRNA studies were also designed with the same sequence but with 2' o methyl chemistry. The probes were purified using double HPLC. MB probes were designed with Cy3 fluorophore and BHQ-II quencher pair. In all cases quencher end was the 3' end, while dye was conjugated to the 5'- end.

### **Cell Culture**

All experiments in this study were carried out using primary human dermal fibroblast cells. These primary cells were obtained from Cambrex Corp., NJ. These were the same cell type as used in our previous studies (**Chapter 2 and 3**). HDF cells were cultured using standard media formulation provided by Cambrex Corp., NJ. A batch of HDF cells were cultured only for about 10 splitting cycles. For imaging experiments, cells were plated on 4 well or 8 well Nalgene-Nunc chamber cover slides 24 hours prior to the experiment.

### **Imaging**

All imaging experiments for detection of MB signal in living cells were carried out using a confocal microscope (Zeiss Axiovert LSM-100) with an optical pin hole of 2.4 airy units with excitation @ 543 nm and detection using a band pass filter from 560-615 nm. These settings were chosen to provide a thick slice in a confocal image and in turn provide integration of the fluorescent signal over a significant depth. This was helpful in establishing that the signal from MB probes decreases throughout the cell with inhibition of translation process rather than a single thin slice. For simultaneous imaging of mitochondria and MB signal, we have used laser excitations @ 488 nm and 543 nm. The detection was carried out using band-pass filter 510-530 nm and 560-615 nm.

### **Cellular Studies with Molecular Beacons**

For cellular delivery of MB probes, experiments were carried out using HDF cells. For delivery, cells were treated with activated streptolysin O (SLO) for a period of 10 minutes as described in (**Chapter 3**) with a slight modification in the experimental procedure. Specifically the incubation with SLO+ MB probes was carried out in a regular serum rich medium as we have observed no noticeable difference in the efficiency of MB delivery in a regular media as compared with a serum free media used in previous study (3). This allowed us to maintain same extra-cellular conditions throughout the experiment. After this incubation period of 10 minutes, the regular medium with SLO was changed to regular serum rich media. The cells were incubated for a period of 30 minutes following this change of media. Following this period, we imaged the signal obtained by hybridization of MB probes. This was carried out to confirm the binding of MB probes in all samples of interest. The results of this study are similar to the ones reported in our previous study (**Chapter 2 and 3**). Following this, we added small molecules (Rapamycin or Wortmannin) of interest to the regular media for 40 minutes to perturb the translation process. For targeting mTOR pathway we have used rapamycin at a concentration level of 10  $\mu$ m and for PI-3 mediated changes we have

used Wortmannin at 1  $\mu\text{M}$  concentration. After drug treatment, the cells were imaged live using the confocal microscopy set up as described above.

### **Fixed cell studies**

Normal human dermal fibroblasts were cultured in 8-well chambered coverslides for 24 hours in normal growth medium (FGM-2 Cambrex Co.) and then washed with 1x PBS (without Ca or Mg). The slide was fixed in 100% methanol at  $-20^{\circ}\text{C}$  for 10 minutes. After removing the methanol, the slides were allowed to air dry and stored overnight at  $-80^{\circ}\text{C}$ . In-situ hybridization assays were then performed by first washing the slides for 5 minutes in 1x PBS and hybridizing them overnight at  $37^{\circ}\text{C}$  in 1x PBS (no Ca or Mg) containing 100 nM of MB probes targeting GAPDH and K-Ras. After removing the hybridization solution with washing and adding 1x PBS, the cells were imaged. The in-situ hybridization for wortmannin and rapamycin treated cells was carried under same conditions as the untreated cells. The experiments were repeated three times and images were taken from multiple cells (typically 20 cells per well).

### **Studies with 2' o methyl MB probes**

To understand the role of chemistry of MB probe, we designed the probes with 2' o methyl chemistry in addition to regular DNA chemistry. These 2' o methyl probes have the same sequence as regular MB probes, but have modified backbone chemistry that enhances the affinity of these probes and also increases the melting point of a hybridized structure. These probes were introduced in living cells using SLO as with unmodified MB probes. These probes were incubated for about 4 hours after removal of excess SLO. This time period was required to get sufficient hybridization with intracellular RNA target. This was primarily due to a higher melting point of these modified MB probes (approximately  $80^{\circ}\text{C}$ ), much higher than the regular MB probes with melting temperature (around  $55^{\circ}\text{C}$ ). Further these probes have a 2' o methyl

backbone chemistry, which renders them resistant to nuclease activity, thus longer incubation periods were not considered a significant disadvantage in this study.

### **RNA Isolation, RT-PCR, and qt-PCR**

RNA from treated and untreated cells was isolated using Qiagen's RNeasy isolation kit. An absorbance reading was taken at 280nm and RT reactions were set-up with equal concentrations of total RNA from each sample. The RT reaction was performed with random hexamer primers. For the PCR reaction 2µl of RT product was used for each sample. For regular PCR the cycle parameters for GAPDH were 95 for 45s, 60 for 45s, 72 for 1min 30s for 30 cycles and for K-ras 95 for 30s, 52 for 1min, 72 for 1min for 40 cycles. The qt-PCR reactions were run on a Bio-Rad iCycler using Bio-Rad's iQ SYBR Green Supermix. It was a two-step reaction with 95 for 10s followed by the corresponding annealing temperature listed above for 45s and 40 cycles. The starting concentrations were determined with Bio-Rad's MyiQ software. The primer sequences used are as follows; GAPDH forward (CGA CCC ATG GCA AAT TCC ATG GCA), GAPDH reverse (TCT AGA CGG CAG GTC AGG TCC ACC), K-ras forward (GAT TCC TAC AGG AAG CAA GT), and K-ras reverse (TAA TGG TGA ATA TCT TC).

## **Results and Discussions**

In this study our hypothesis was that the translation state of mRNAs favors the hybridization of MB probes with its target mRNAs. This hypothesis was based on current understanding that multiple ribosomes loaded on mRNAs during translation process favors the opening of local secondary structure ([3, 38]) and also favors the removal of bound proteins to allow for an effective read out of the mRNA sequence for translation into polypeptide. Further it has been shown that major structural changes take place at a global scale of mRNA secondary structure during the translation process ([39]). These changes involve the formation of a lariat structure, which brings together the 3' and the 5' ends of a mRNA through an association of eIF4G complex with a polyA binding proteins and eIF4E ([39]). Additionally, the EM data of RNA molecules with multiple ribosomes loaded across its length suggests a high degree of accessibility (Wells et al, 1998) for a short oligonucleotide probe (~ 18 bp) for hybridization with its target. With this understanding we have designed this study to address the above discussed questions related to MB probes, RNA organization and translational process.

### **Effect of Rapamycin and Wortmannin treatment on the MB-based detection of mRNAs in living cells**

The aim of this first experiment was to understand the effect of translation repression on MB-based detection of mRNAs. We chose to study GAPDH and K-Ras mRNAs as we have demonstrated in our previous studies ([1, 2]) the specific and sensitive detection of these mRNAs using MB probes. Using the same design of MB probes as in our previous studies and the methods as described in the methods section here, the probes were introduced into living cells. Following an initial incubation of cells with MB probes for specific mRNA targets for 30 minutes, the cells were treated with either Rapamycin (10  $\mu\text{M}$  conc.) or Wortmannin (1  $\mu\text{M}$  conc.) for 40 minutes along with

an untreated control sample. The initial incubation was carried out to allow for the hybridization of MB probes with target mRNAs in unperturbed conditions. Following this initial incubation of MBs, the incubated cells were briefly imaged to detect the signal from the hybridized MB probes (data not shown). The results of these studies for both the GAPDH and the K-Ras are shown in **Figure 4.1**. **Figure 4.1 A** shows a localized signal of the GAPDH mRNA in living cells in agreement with our previous studies ([1, 2]). **Figure 4.1 B** shows the effect of rapamycin treatment on the distribution of GAPDH mRNAs. Prior to rapamycin or wortmannin treatment, the samples incubated with MBs had the same distribution as untreated cells shown in **Figure 4.1 A**. After 40 minutes of treatment, we observed a significant decrease in the MB fluorescence signal in the cytoplasm. The results suggests that MB probes, which were hybridized with the target mRNA before treatment, have come off the target mRNA after incubation of cells with rapamycin and formed a closed, nonfluorescent hairpin structure. In **Figure 4.1 B** we could only detect some signal in the peri-nuclear region of cytoplasm. This signal is an integrated signal for a thick optical slice of 2.5 airy units on a confocal system. This pinhole thickness was chosen to avoid the limitations of a smaller thickness of a typical confocal slice in the detection of a reduced fluorescence signal in this case.

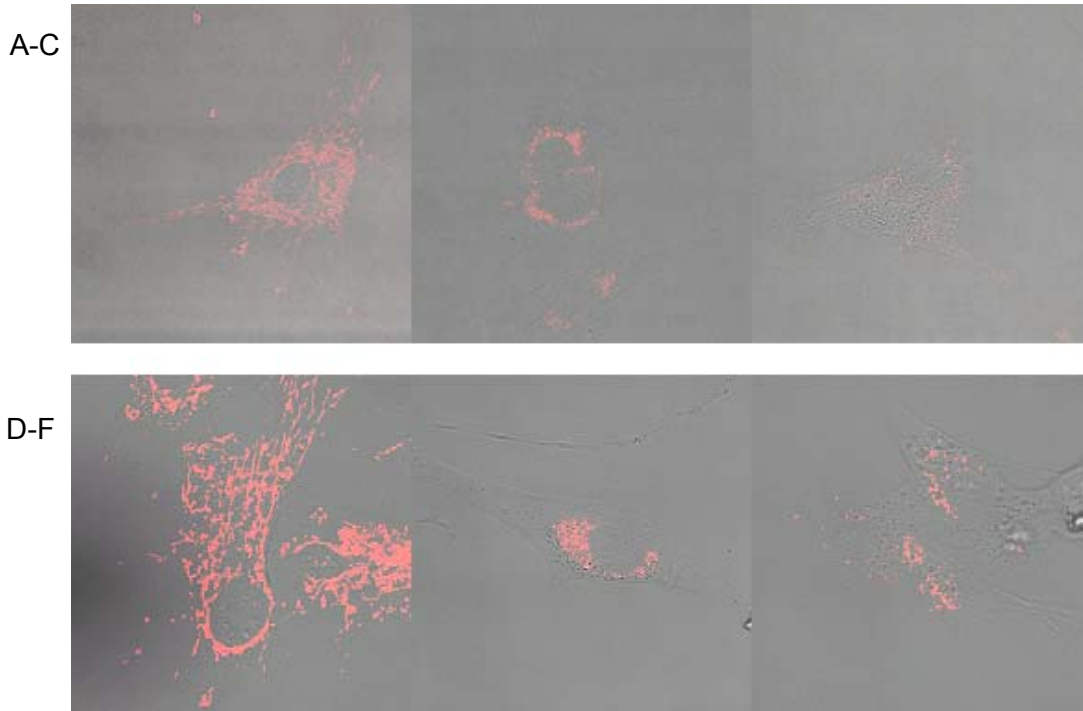


**Figure 4.1:** Effect of the Rapamycin and the Wortmannin treatment (repression of translation) on MB-based detection of the GAPDH and K-Ras mRNAs in living cells.

(A) Image of the distribution of GAPDH mRNAs in living cells using MBs in untreated cells. (B)-(C) Images of the GAPDH distribution in living cells using MBs treated with Rapamycin (10  $\mu$ M for 40 minutes) and Wortmannin (1  $\mu$ M for 40 minutes) respectively. The MBs were hybridized for 30 minutes similar to the untreated cells, after 30 minutes of MB incubation cells were treated with Rapamycin and Wortmannin. The results show a reduction in signal intensity in the cytoplasm and also the residual signal intensity was observed in the peri-nuclear region only. These cells had similar signal intensity and distribution of GAPDH mRNAs as untreated cells shown in Figure 1(A) before treatment with Rapamycin and Wortmannin.

(D) Image of the distribution of K-Ras mRNAs in living cells using MBs in untreated cells.

(E)-(F) Images of the K-Ras distribution in living cells using MBs treated with Rapamycin (10  $\mu$ M for 40 minutes) and Wortmannin (1  $\mu$ M for 40 minutes) respectively. The MBs were hybridized for 30 minutes similar to the untreated cells, after 30 minutes of MB incubation cells were treated with Rapamycin and Wortmannin. The results show a reduction in signal intensity in the cytoplasm and also the residual signal intensity was observed in the peri-nuclear region only.

**Figure 4.1 C** shows the result of wortamannin treatment using the same GAPDH MB probe and the same incubation time as in **Figure 4.1 B**. The result shows a similar decrease in the fluorescent signal from a MB probe in the cytoplasm as observed in case of **Figure 4.1 B**. The result of wortamannin treatment also shows some signal in the peri-nuclear region of the cytoplasm. The images of **Figure 4.1 A-C** were taken under the same imaging conditions including the optical pinhole, the voltage gain on PMT etc. The combined results of **Figure 4.1 A-C** clearly indicate that the MB probes are reversibly bound, i.e., the MB probes bound to mRNA target can come off the target with the repression of a translational process. Furthermore, this observation indicates that the MB probes can even fold back into a hairpin MB structure, which will bring the fluorophore in close approximation to the quencher and quench the resultant fluorescent signal, upon removal from the target mRNA. With this decrease in the fluorescent signal from MB probes, we still could not clearly deduce the fate of mRNA with this perturbation. Further we cannot establish if this trend is more generic for the various other MB probes targeted to different mRNAs or is it specific to the GAPDH target with this particular MB probe

To answer this question, we carried out a study with a MB probe, which targets K-Ras mRNA in living cells. We have validated this probe in our previous studies ([1, 2]). The results of this study, shown in **Figure 4.1 D-F**, indicate a similar trend as observed for the GAPDH mRNAs with and without the repression of translation. **Figure 4.1 D** shows a similar localization of K-Ras mRNA in living cells as observed in our previous studies ([1, 2]). Upon treatment with rapamycin and wortamannin we observed a similar decrease in the MB fluorescent signal in the cytoplasm, and also detected some signal in the peri-nuclear region of cytoplasm similar to the case of GAPDH MB study (**Figure 4.1 (A-C)**). Imaging of the K-Ras based MB detection was carried out using a same optical pinhole as in case of the GAPDH detection in **Figure 4.1** but at a higher PMT

gain voltage. This was done because the fluorescent signal intensity obtained from hybridization of K-Ras MB probe was lower than the intensity obtained from hybridization of GAPDH MB probe at a same PMT gain value. This can be attributed to the lower level of K-Ras mRNAs as compared with GAPDH mRNAs.

The combined result of these studies clearly indicates that MB probes can come off the bound target and fold back to the hairpin state when translation processes are repressed in cells. Since we have observed these changes with two different mRNAs, targeted with two different MB probes, this trend appears to be more generic than the case of a specific MB probe and a specific mRNA. Further this study highlights that the translational states of mRNAs in the cells can have a direct effect on the hybridization of MB probes. Due to decrease in signal from MB probes, we could not establish information regarding the fate of these mRNAs or the subcellular organization of these mRNAs with other cellular structures with this experiment.

#### **Effect on the subcellular organization and MB based detection of mRNAs upon treatment with Wortmannin and Rapamycin**

In our previous study (**Chapter 3**), we have demonstrated the co-localization of GAPDH and K-Ras mRNAs with mitochondrial structure in living cells. The aim of this part of the study was to understand if the co-localization of mRNAs (based on our MB probes) with mitochondrial structure is affected by the repression of translational process. Although this part of the study will only provide us a relationship between the fluorescent signal from MB based probes and the intracellular organization of mitochondrial and may not represents the actual behavior of mRNAs, it will still help us understand the sub-cellular structural changes with the repression of translation. In combination with the next part of this study including FISH, PCR and other controls, this will help us complete this understanding.

**Figure 4.2** and **Figure 4.3** shows the data for MB probes targeting GAPDH and K-Ras mRNAs respectively in living cells with co-staining of mitochondria. **Figure 4.2 A** shows the co-localization of GAPDH mRNAs with mitochondrial staining in living cells. This result is in agreement with our previous study (**Chapter 3**). **Figure 4.2 B** and **4.2 C** show the effect of rapamycin and wortmannin treatment on the co-localization of GAPDH MB fluorescent signal with mitochondria.

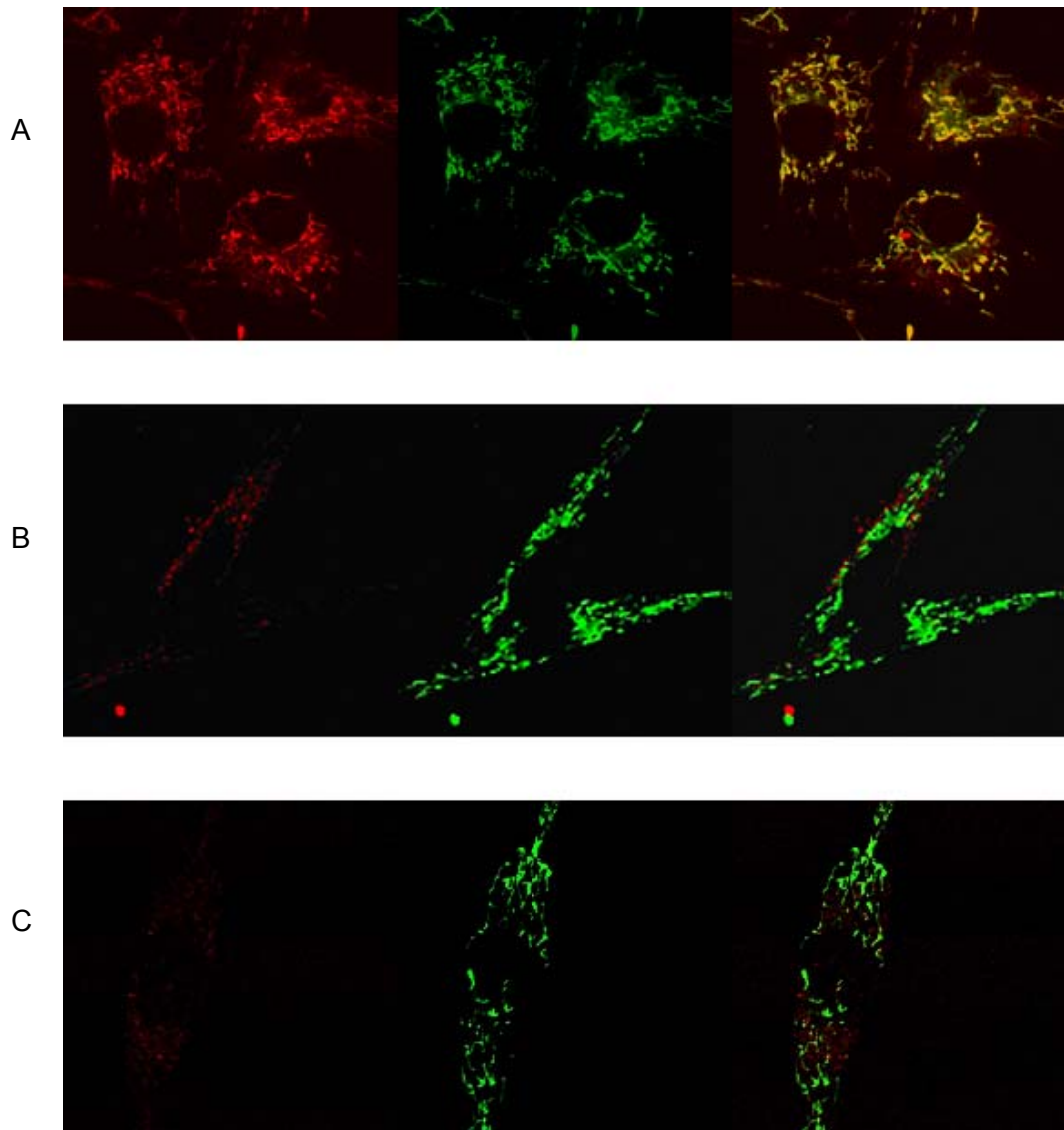


**Figure 4.2:** Colocalization of GAPDH mRNAs with Mitochondria in untreated and treated (translationally repressed) cells.

(A) - Images show the distribution of Mitofluor green and the MB signal for GAPDH mRNAs in two confocal channels and their overlap to indicate the co-localization of GAPDH mRNAs with the mitochondria in untreated cells. Yellow color in the overlaid image indicates the high degree of co-localization of mRNAs with the mitochondria.

(B)-(C)- Images show the distribution of Mitofluor green and the MB signal for the GAPDH mRNAs in two confocal channels and their overlap to indicate the co-localization of GAPDH mRNAs with the mitochondria in Rapamycin (10  $\mu\text{M}$  for 40 minutes) and Wortmannin (1  $\mu\text{M}$  for 40 minutes) treated cells respectively.

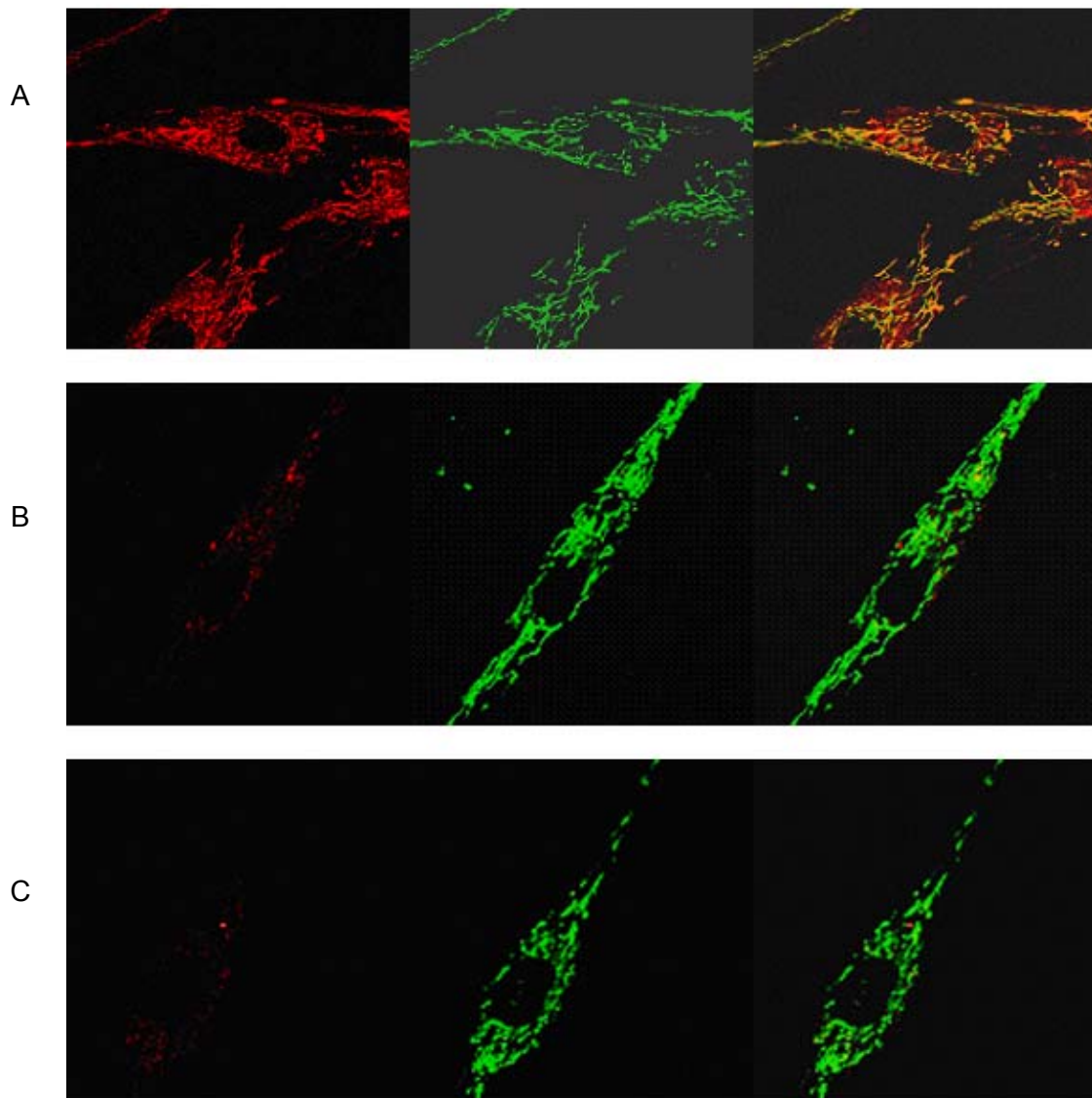


**Figure 4.3:** Colocalization of K-Ras mRNAs with Mitochondria in untreated and treated cells (repression of translation).

(A)- Images show the distribution of Mitofluor green and the MB signal for the K-Ras mRNAs in two confocal channels and their overlap to indicate the co-localization of K-Ras mRNAs with the mitochondria in untreated cells.

(B)-(C)- Images show the distribution of Mitofluor green and the MB signal for the K-Ras mRNAs in two confocal channels and their overlap to indicate the co-localization of K-Ras mRNAs with the mitochondria in Rapamycin (10  $\mu$ M for 40 minutes) and Wortmannin (1  $\mu$ M for 40 minutes) treated cells respectively.

**Figure 4.2 B and C** clearly indicates a lack of any significant co-localization of MB fluorescence signal with mitochondrial staining. The MB signal does not follow the pattern of mitochondrial staining in the cytoplasm of these cells including the peri-nuclear region after treatment with rapamycin and wortamannin. Mitochondrial staining after treatment has a similar extended filamentous distribution as in case of untreated control sample.

Similar results were obtained for K-Ras mRNAs in living cells. **Figure 4.3 A** shows the co-localization of K-Ras mRNAs with mitochondria in an untreated control case. The results show a high degree of co-localized K-Ras mRNAs, especially away from the peri-nuclear region in the cytoplasm (indicated by yellow- overlap of green- Mitostain and red colors-MB signal) in agreement with our previous study (**Chapter 3**). Upon treatment with rapamycin and wortamannin, we observed no co-localization of fluorescent MB signal with mitochondrial staining (**Figure 4.3(B) and 4.3(C)**). This trend is similar with the result obtained for GAPDH MB fluorescent signal after treatment with rapamycin or wortamannin (**Figure 4.2 B-C**).

This study shows that the translational repression by incubation of samples with rapamycin or wortamannin does not significantly change the distribution and organization of mitochondria in cells. Further a reduced peri-nuclear signal from MB probes does not co-localize with mitochondria after the treatment. This raises an interesting aspect that the translation state favors the co-localization of MB signal and in effect the mRNAs (GAPDH and K-Ras) with mitochondrial structure in cells. At present we cannot resolve the fate of these mRNAs but the signal from MB probes does not show co-localization with mitochondria after treatment.

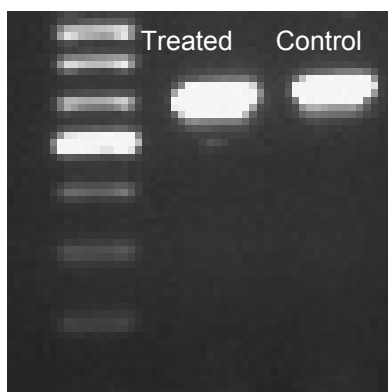
#### **Sub cellular fate of mRNAs after treatment with rapamycin and wortamannin**

Until this stage in our study, we have only looked indirectly at specific mRNAs using the fluorescent signal from MB probes. With the decrease in the fluorescent signal

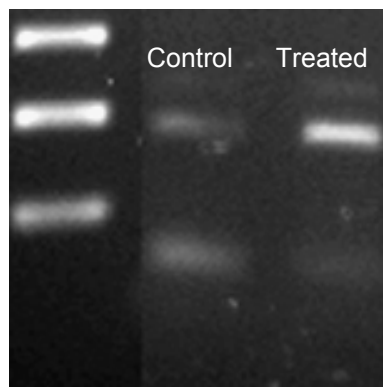
from MB probes upon repression of translational process, we could not clearly deduce the fate of mRNAs. At this stage of our study we had three plausible hypotheses that could explain the significant decrease in the signal from MB probes with the repression of translation machinery:

1. Decay of mRNAs
2. Secondary structure changes or RNA binding proteins etc –Significant changes in the secondary structure/ RNA binding protein complexes may be able to compete- off MB probes from its target mRNAs. Such changes may be induced when translation state of cells is repressed. If this observation is true, it will support our hypothesis that the hybridization of these specific MB probes is favored by active translational state.
3. Dispersal of mRNAs in the cytoplasm- Dispersal of RNAs in the cytoplasm can reduce the resultant fluorescent intensity from hybridization of MB probes as compared to a highly localized distribution in the cytoplasm. This can be potentially overcome by using imaging set-up with single molecule detection in living cells.

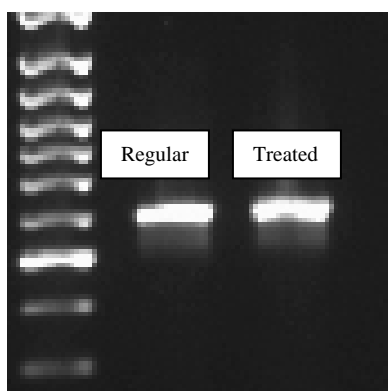
To assess which of this plausible hypothesis truly represent the behavior of mRNAs upon treatment with rapamycin or wortamannin, we did the following studies. First, RT-PCR was performed to determine the levels of K-RAS and GAPDH mRNAs pre- and post-treatment. The PCR results clearly show that with rapamycin treatment, we only observed about 10-20 % increases in the levels of K-Ras and GAPDH mRNAs as compared with untreated control samples (**Figure 4.4 A-B**). Upon treatment with wortamannin, we did not observe any significant changes in the levels of K-Ras and GAPDH mRNAs as compared with control samples (**Figure 4.4 C-D**). These results clearly suggest that mRNA level for GAPDH and K-Ras has not decreased upon treatment with either rapamycin or wortamannin.



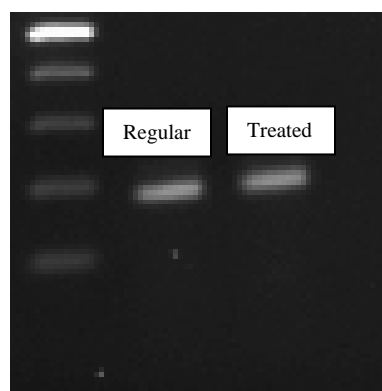
(A) RT-PCR GAPDH  
Rapamycin and Control



(B) RT-PCR K-Ras  
Control and Rapamycin



(C) RT-PCR GAPDH-  
Control and Wortamannin



(D) RT-PCR K-Ras  
Control and Wortamannin

**Figure 4.4:** PCR results for the GAPDH and the K-Ras mRNAs in treated (Rapamycin or Wortamannin treatment for repression of translation) and untreated cells

(A)- (B): Comparison of the GAPDH and the K-Ras mRNAs in Rapamycin treated (10  $\mu$ M for 40 minutes) and untreated cells respectively. The result shows relative increase in the GAPDH and the K-Ras mRNA levels in Rapamycin treated cells.

(C)- (D): Comparison of the GAPDH and the K -Ras mRNAs in Wortamannin treated (1  $\mu$ M for 40 minutes) and untreated cells. The result shows relative increase in the GAPDH and the K-Ras mRNA levels in Wortamannin treated cells.

With this we have two other plausible explanations to understand the changes in MB signal, as they no longer correspond to the changes in mRNA levels. To resolve which of these processes is responsible for the changes in the fluorescent MB signal and what is the fate of the mRNAs with the repression of translation, we performed in-situ hybridization. We realize that using our imaging methods it is not possible to probe the secondary structure of RNA in living cells/ fixed cells. Still in-situ hybridization in certain cases can increase the accessibility of the target for its probe due to the effect of fixative agents (Methanol/Acetone), some of which tends to disrupt RNA-protein complexes (precipitation of proteins etc.) and also dissolve some of the lipid components. Further we chose this as it will also help us to directly access the possibility related to dispersal of mRNAs in the cytoplasm. Thus, this assay would help us understand the changes and address both the plausible hypothesis.

The results of in-situ hybridization to detect GAPDH mRNAs in an untreated control sample and treated samples with rapamycin or wortamannin are shown in **Figure 4.5 A-C** respectively. The results in **Figure 4.5 A** shows a similar distribution of the GAPDH mRNA in fixed cells (control case) as obtained with untreated live cells (**Figure 4.1 A**). **Figure 4.5 B and C** show the distribution of GAPDH mRNAs in rapamycin and wortamannin treated fixed cells respectively. The results show a distinct change in the distribution of mRNAs in treated cells as compared with an untreated sample. The localization of GAPDH mRNAs does not have extended filamentous structure in the cytoplasm but instead, it has an aggregated distribution in the cytoplasm. The relative intensity levels in the translationally repressed cells are not significantly different than those obtained with an untreated fixed sample.

Similar results were obtained when HDF cells were fixed for detection of K-Ras mRNAs in an untreated and treated sample. In untreated control cells (**Figure 4.5 D**) we can observe the extended cytoplasmic localization of K-Ras mRNAs, which agrees with

our live cells studies in the present and previous studies ([1, 2]). On treatment with rapamycin and wortmannin (**Figure 4.5 D-E**), we observe that the K-Ras mRNAs also have an aggregated peri-nuclear distribution in the cytoplasm. This distribution is similar to the one obtained for GAPDH mRNAs in a treated sample. (**Figure 4.5 B-C**)

Based on these results, we have obtained an understanding that mRNAs upon treatment with rapamycin or wortmannin are distributed significantly differently than the untreated regular cells. It is clear that although the MB probes are not able to follow the changes in the RNA localization with translational repression, the same probes during in-situ hybridization assay could hybridize with a target RNA. This clearly suggests that we have been able to increase the accessibility for MB probes using methanol as a fixative. These results suggest that the changes in structure of mRNA molecules with the repression of translation process are responsible for the removal of MB probes from its target.

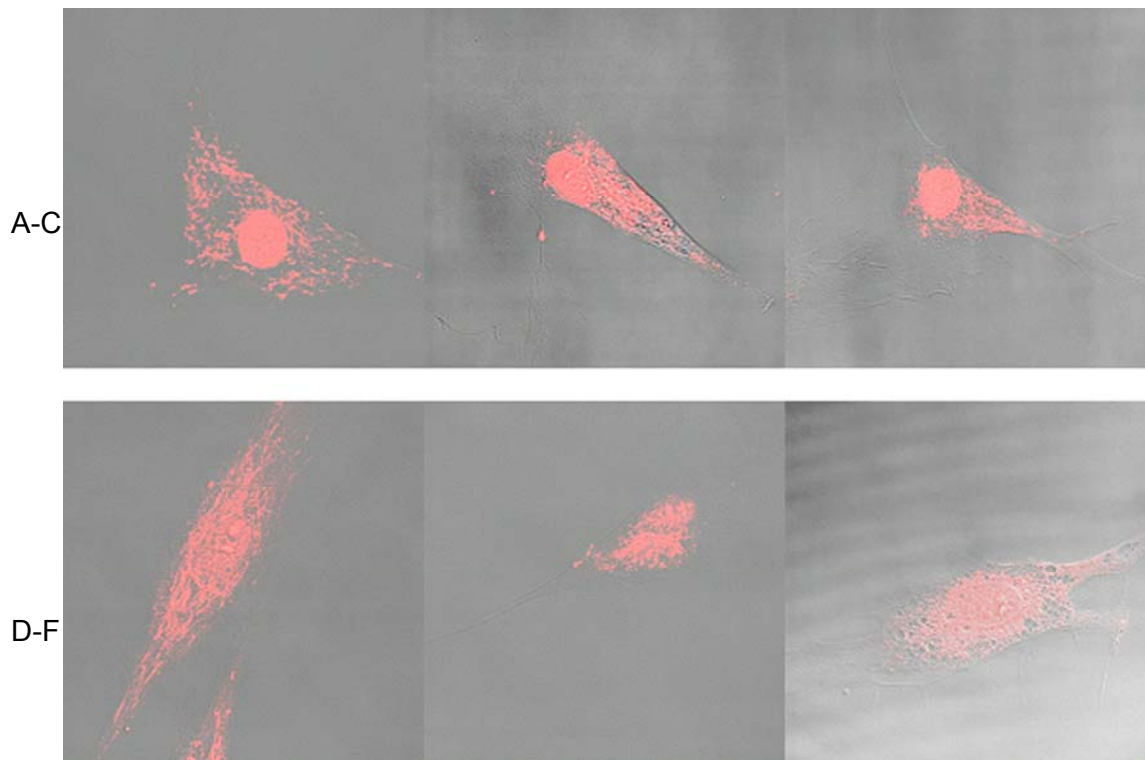


**Figure 4.5:** Fluorescent in-situ hybridization (FISH) based detection of GAPDH and K-Ras mRNAs in treated (Rapamycin or Wortamannin treatment for repression of translation) and untreated cells.

(A) and (D) FISH based detection of GAPDH and K-Ras mRNAs in untreated cells. Cells were fixed in methanol (-20 C for 5 minutes) and hybridized overnight in 1X PBS with 100 nM MBs targeting the GAPDH and K-Ras mRNAs respectively. The result shows very similar filamentous distribution of the GAPDH and K-Ras mRNAs in the cytoplasm as observed for living cells.

(B)-(C) and (E)-(F) FISH based detection of GAPDH and K-Ras mRNAs in treated (Rapamycin or Wortamannin) cells respectively. The same fixation protocol was used as in Figure (A) and (D). Cells were treated for 40 minutes and with the same concentration of drugs as in live cell assays before fixation. The results show a distinctly different pattern of localization of both mRNAs in the treated cells as compared with untreated cells. In treated cells, most of the signal is observed in the peri-nuclear sites with mRNAs showing an aggregated distribution. No significant reduction in the intensity of the MB signal was observed with treatment as compared with the regular cells.

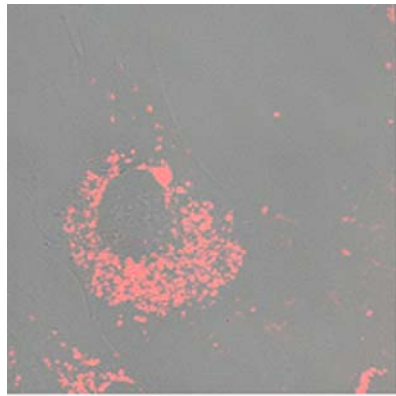
In our previous study (**Chapter 3**) and in this study, we have shown that the distribution of GAPDH and K-Ras mRNAs co-localizes with mitochondria in living cells. Similar distribution of these mRNAs was observed in fixed cell samples of untreated control cells (**Figure 4.5 A and D**). Upon treatment with rapamycin or wortamannin, neither mRNAs in fixed cells nor MB probes in living cells are co-localized with mitochondrial structure. This evidence taken together clearly highlights that upon repression of translation there is no significant co-localization of these mRNAs with mitochondria. Thus the translational state not only favors the binding of our probe to the target mRNAs but also favors the co-localization of mRNAs with mitochondria. This result highlights the functional information regarding the state of the mRNA and its localization with mitochondria. This extends our previous study, where we have earlier reported this observation with these two mRNAs.

Further the results of in-situ hybridization study also disproves the third plausible explanation, in which a signal from the MB probe is reduced due to the dispersal of mRNAs upon treatment with rapamycin or wortamannin. With this we believe that the changes in the secondary structure of mRNAs upon treatment cause MB probes to come off a bound target. Although the direct evidence of such structural changes in a cell is not possible with current method, the evidence obtained from this study strongly suggest this as a well founded hypothesis for the changes observed in the MB fluorescent signal in living cells and localization in fixed cells.

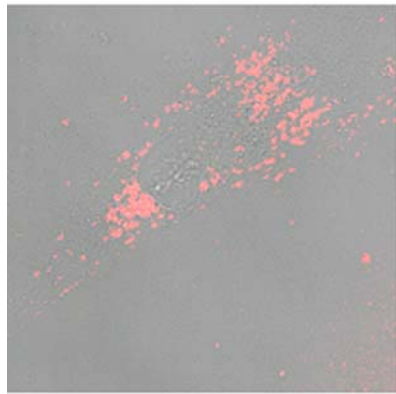
To further prove that the above changes in a MB signal are co-related with the inhibition of translation of mRNAs, we decided to study the effect of wortamannin or rapamycin treatment on MB probes hybridized with a non-translated RNA in the cytoplasm of living cells. If our hypothesis is true, this study will serve as a positive control to prove that the MB probes targeted to non-translated RNAs are not affected by

treatment with either rapamycin or wortamannin. For this study, we chose 28-s rRNA as a candidate non-translated RNA in the cytoplasm of living cells. This RNA is a part of ribosomal complex and we have successfully targeted this RNA in our previous study (**Chapter 3**). The results of this experiment are shown in **Figure 4.6**. **Figure 4.6 A** shows the distribution of the 28-s rRNAs in untreated control cells. This distribution is similar to the results obtained in our previous study. Most of the fluorescence signal is distributed in a peri-nuclear section of the cytoplasm. Upon treatment with rapamycin (**Figure 4.6 B**), we did not observe any significant decrease in the fluorescent signal intensity of MB probes targeted to 28-s rRNA, further there are no significant changes in the localization of fluorescent signal with treatment. Similar results are obtained upon treatment of cells with wortamannin (**Figure 4.6 C**).

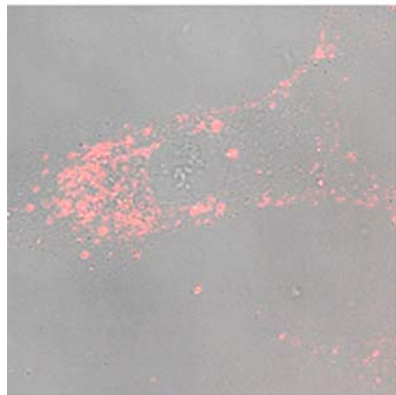
These results provide us an understanding that MB probes targeted to non-translated RNAs (non-mRNA) are not affected upon treatment with rapamycin or wortamannin. This clearly illustrates that the translation state of GAPDH and K-Ras mRNAs was responsible for the changes in MB signal upon treatment. These findings also suggest that it is possible to target a translationally inactive RNA only if the secondary structure has been well established and extensive studies have been performed to experimentally evaluate its structure and accessibility for a target probe.



A



B



C

**Figure 4.6:** (A): Distribution of 28-s Ribosomal RNA in living cells without any treatment using MB probes. MB probes designed to target 28-s rRNA were delivered to the cells using same protocol for delivery of MBs targeting GAPDH and K-Ras mRNAs. The image shows distribution of 28-s rRNA in the cytoplasm, which is distinctly different from the distribution of K-Ras and GAPDH mRNAs.

(B)- (C): Distribution of 28-s Ribosomal RNA in Rapamycin (10  $\mu$ M for 40 minutes) and Wortmannin (1  $\mu$ M for 40 minutes) treated cells respectively. The treatment of Rapamycin or Wortmannin does not affect the signal intensity as well as the distribution of 28-s rRNA. This observation validates that the MB probes does not change their conformation non -specifically upon treatment.

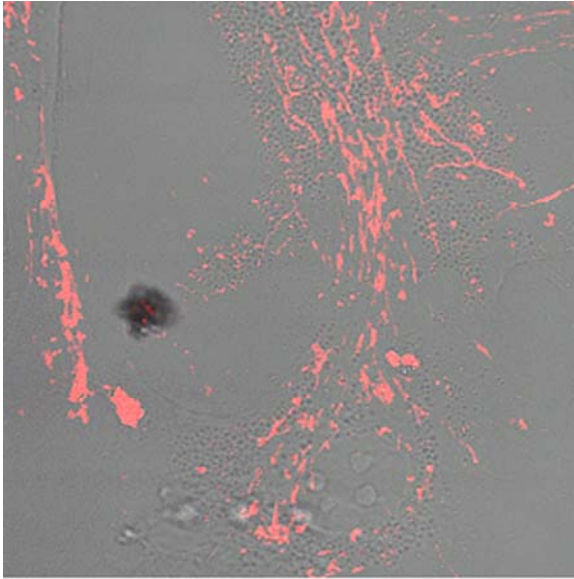
In this case, the accessibility of this particular MB probe sequence for targeting 28-s rRNA has been well established using both FISH and live cell studies ([40-42]). For the case of mRNAs this is a harder problem, as their structure is highly dynamic and thus prediction of local static structure is difficult ([14]). Thus designing MB probes for a local static secondary structure of an RNA target, which has global changes in its conformations during its life in a cytoplasm, may not be possible without extensive studies. Nevertheless, the increased accessibility of mRNA during active translation processes may provide an alternative to such a challenge and may allow for an easy design of MB probe for specific targeting of mRNAs, although such designs may not be able to detect different states of target mRNA.

#### **Effect of MB probe chemistry on the stability of MB-RNA structure with the repression of translational processes**

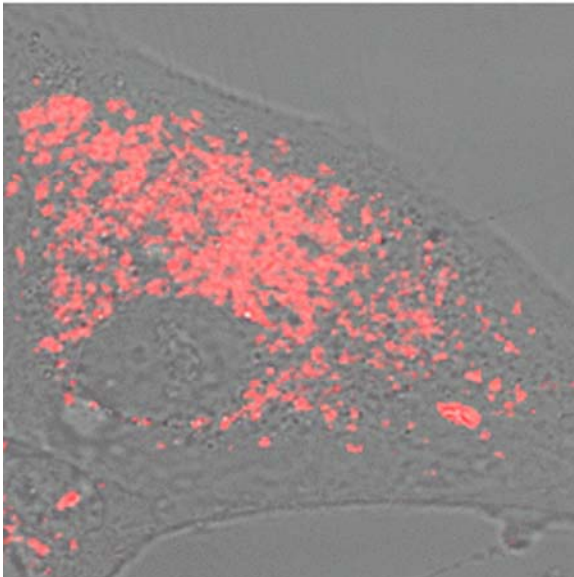
In this study till this stage we have used regular deoxynucleotide chemistry in the design of MB probes. Using this probe chemistry we have established that the MB probes designed to target GAPDH and K-Ras mRNAs come off the hybridized target upon treatment with rapamycin or wortamannin. In this direction, we were interested in exploring if high affinity probe chemistries such as 2' O methyl chemistry will show a similar trend as observed with regular DNA chemistry probes. With this motivation, we designed MB probe with 2'O methyl chemistry to target K-Ras mRNAs in living cells. With this chemistry we maintained the same sequence design as with a regular DNA chemistry.

The results of the study are shown in **Figure 4.7**. **Figure 4.7 A** shows the fluorescence signal obtained from 2' O methyl MB probe targeting K-Ras mRNA in living cells. The results show a similar distribution of the K-Ras mRNAs in the cytoplasm as obtained earlier with a regular DNA chemistry probes. **Figure 4.7 B** shows the fluorescence signal using the same MB probe in a rapamycin treated sample. The

results clearly shows that the MB signal does not significantly decrease upon treatment with rapamycin, contrary to the results obtained with the DNA chemistry probe. The 2' O methyl probe not only remains bound to its target RNA but also follows the change in K-Ras mRNA localization in the cytoplasm. The results of this study show an aggregated distribution of mRNAs in the cytoplasm upon treatment with rapamycin, which parallels the results obtained with *in situ* hybridization studies using a DNA MB probe (**Figure 4.5**). This indicates that the high affinity 2' O-methyl backbone can prevent the dissociation of MBs from their target RNA upon treatment, therefore following the changes in the localization of mRNAs. This approach, although great for following changes associated with mRNAs, still has several issues related to the functional characteristics of target mRNAs when such high affinity probes are bound to them. High affinity probes such as those used in this experiment could potentially prevent the ribosomes from translating the target mRNAs. It has recently been discovered that ribosome's possess an inherent helicase activity ([3]), which allows them to unwind the local secondary structures with melting temperatures of approximately 70 °C or less.



A



B

**Figure 4.7:** (A) - (B) Detection of K-Ras mRNAs using 2' O Methyl MB probes in untreated and Rapamycin treated cells respectively. The result shows that 2'O Methyl MB probes shows similar localization and signal intensity as obtained with a regular DNA chemistry. Thus result suggests that both chemistries are comparable in detecting signal in living cells. On treatment with Rapamycin, the signal from the MB probes does not diminish as in case of regular DNA chemistry and further the MB probes follows the distribution of mRNAs as they are perturbed by the chemical treatment. Thus 2' O Methyl MB probes does not come-off the bound target and are able to follow the changes in the mRNAs as the translation is repressed by treatment with Rapamycin.

This has implications as these 2' o methyl probes have melting temperatures close to 70 °C or higher ([43]), which may prevent the translocation of ribosomes through the target mRNA. This also has implications that regular chemistry DNA probes bound to the targets with melting points lower than 70 °C will experience on and off rates depending on the speed of translocation of these ribosomes. This observation though cannot be imaged with our present set up for imaging given that the multiple mRNAs localized in a given area will have the probes bound to the target mRNA at any given moment of time. Thus such fluctuations may require us to carry out FCS based measurements to monitor the changes in very small focal volume.

## **Summary**

In summary, we have positively tested a hypothesis that the translational state of mRNAs favors the hybridization of MB probes with its target mRNAs. This study has also provided the evidence that the MB probes are reversibly bound with target mRNAs and the repression of translation processes can cause a removal of the MB probes from its target mRNAs. The study has resulted in an interesting observation that active translational processes in cytoplasm favor the co-localization of K-Ras and GAPDH mRNAs with mitochondria. Further the repression of translation processes induces a significant re-distribution of mRNAs in the cytoplasm of living cells. The study also highlighted the significant differences in the regular DNA chemistry and 2' O methyl backbone chemistry. MB probes with 2' o methyl backbone chemistry were not removed from the target RNAs with the repression of translation in living cells. This backbone was able to follow the changes in the localization of RNAs with the repression of translation.

Future studies will be designed to develop an integrated approach by combining interference based silencing and drug-based knock downs with MB-based imaging to

allow for a comprehensive understanding of various questions in RNA biology and also study basic pathology in a cell culture model systems.

## References

- [1] N. Nitin, P. J. Santangelo, G. Kim, S. Nie, and G. Bao, Peptide-linked molecular beacons for efficient delivery and rapid mRNA detection in living cells, *Nucleic Acids Res* 32 (2004) e58.
- [2] P. J. Santangelo, B. Nix, A. Tsourkas, and G. Bao, Dual FRET molecular beacons for mRNA detection in living cells, *Nucleic Acids Res* 32 (2004) e57.
- [3] S. Takyar, R. P. Hickerson, and H. F. Noller, mRNA helicase activity of the ribosome, *Cell* 120 (2005) 49-58.
- [4] X. Chen, S. T. Cheung, S. So, S. T. Fan, C. Barry, J. Higgins, K. M. Lai, J. Ji, S. Dudoit, I. O. Ng, M. Van De Rijn, D. Botstein, and P. O. Brown, Gene expression patterns in human liver cancers, *Mol Biol Cell* 13 (2002) 1929-1939.
- [5] S. E. DePrimo, M. Diehn, J. B. Nelson, R. E. Reiter, J. Matese, M. Fero, R. Tibshirani, P. O. Brown, and J. D. Brooks, Transcriptional programs activated by exposure of human prostate cancer cells to androgen, *Genome Biol* 3 (2002) RESEARCH0032.
- [6] M. B. Eisen, and P. O. Brown, DNA arrays for analysis of gene expression, *Methods Enzymol* 303 (1999) 179-205.
- [7] J. M. Levisky, and R. H. Singer, Fluorescence in situ hybridization: past, present and future, *J Cell Sci* 116 (2003) 2833-2838.
- [8] A. M. Femino, K. Fogarty, L. M. Lifshitz, W. Carrington, and R. H. Singer, Visualization of single molecules of mRNA in situ, *Methods Enzymol* 361 (2003) 245-304.
- [9] A. M. Femino, F. S. Fay, K. Fogarty, and R. H. Singer, Visualization of single RNA transcripts in situ, *Science* 280 (1998) 585-590.

- [10] Y. Shav-Tal, X. Darzacq, S. M. Shenoy, D. Fusco, S. M. Janicki, D. L. Spector, and R. H. Singer, Dynamics of single mRNPs in nuclei of living cells, *Science* 304 (2004) 1797-1800.
- [11] D. L. Sokol, X. Zhang, P. Lu, and A. M. Gewirtz, Real time detection of DNA:RNA hybridization in living cells, *Proc Natl Acad Sci U S A* 95 (1998) 11538-11543.
- [12] S. Tyagi, and O. Alsmadi, Imaging native beta-actin mRNA in motile fibroblasts, *Biophys J* 87 (2004) 4153-4162.
- [13] J. Perlette, and W. Tan, Real-time monitoring of intracellular mRNA hybridization inside single living cells, *Anal Chem* 73 (2001) 5544-5550.
- [14] G. Dreyfuss, V. N. Kim, and N. Kataoka, Messenger-RNA-binding proteins and the messages they carry, *Nat Rev Mol Cell Biol* 3 (2002) 195-205.
- [15] G. Dreyfuss, Y. D. Choi, and S. A. Adam, The ribonucleoprotein structures along the pathway of mRNA formation, *Endocr Res* 15 (1989) 441-474.
- [16] Y. Oleynikov, and R. H. Singer, RNA localization: different zipcodes, same postman?, *Trends Cell Biol* 8 (1998) 381-383.
- [17] U. Sheth, and R. Parker, Decapping and decay of messenger RNA occur in cytoplasmic processing bodies, *Science* 300 (2003) 805-808.
- [18] Y. Wang, C. L. Liu, J. D. Storey, R. J. Tibshirani, D. Herschlag, and P. O. Brown, Precision and functional specificity in mRNA decay, *Proc Natl Acad Sci U S A* 99 (2002) 5860-5865.
- [19] E. Yang, E. van Nimwegen, M. Zavolan, N. Rajewsky, M. Schroeder, M. Magnasco, and J. E. Darnell, Jr., Decay rates of human mRNAs: correlation with functional characteristics and sequence attributes, *Genome Res* 13 (2003) 1863-1872.
- [20] A. Grolleau, J. Bowman, B. Pradet-Balade, E. Puravs, S. Hanash, J. A. Garcia-Sanz, and L. Beretta, Global and specific translational control by rapamycin in T cells uncovered by microarrays and proteomics, *J Biol Chem* 277 (2002) 22175-22184.

- [21] V. K. Rajasekhar, A. Viale, N. D. Socci, M. Wiedmann, X. Hu, and E. C. Holland, Oncogenic Ras and Akt signaling contribute to glioblastoma formation by differential recruitment of existing mRNAs to polysomes, *Mol Cell* 12 (2003) 889-901.
- [22] V. K. Rajasekhar, and E. C. Holland, Postgenomic global analysis of translational control induced by oncogenic signaling, *Oncogene* 23 (2004) 3248-3264.
- [23] C. G. Proud, Ras, PI3-kinase and mTOR signaling in cardiac hypertrophy, *Cardiovasc Res* 63 (2004) 403-413.
- [24] A. C. Gingras, B. Raught, and N. Sonenberg, mTOR signaling to translation, *Curr Top Microbiol Immunol* 279 (2004) 169-197.
- [25] A. C. Gingras, B. Raught, and N. Sonenberg, Regulation of translation initiation by FRAP/mTOR, *Genes Dev* 15 (2001) 807-826.
- [26] K. Hara, Y. Maruki, X. Long, K. Yoshino, N. Oshiro, S. Hidayat, C. Tokunaga, J. Avruch, and K. Yonezawa, Raptor, a binding partner of target of rapamycin (TOR), mediates TOR action, *Cell* 110 (2002) 177-189.
- [27] D. H. Kim, D. D. Sarbassov, S. M. Ali, J. E. King, R. R. Latek, H. Erdjument-Bromage, P. Tempst, and D. M. Sabatini, mTOR interacts with raptor to form a nutrient-sensitive complex that signals to the cell growth machinery, *Cell* 110 (2002) 163-175.
- [28] C. G. Proud, Role of mTOR signalling in the control of translation initiation and elongation by nutrients, *Curr Top Microbiol Immunol* 279 (2004) 215-244.
- [29] C. G. Proud, mTOR-mediated regulation of translation factors by amino acids, *Biochem Biophys Res Commun* 313 (2004) 429-436.
- [30] D. D. Sarbassov, D. A. Guertin, S. M. Ali, and D. M. Sabatini, Phosphorylation and regulation of Akt/PKB by the rictor-mTOR complex, *Science* 307 (2005) 1098-1101.
- [31] A. Sekulic, C. C. Hudson, J. L. Homme, P. Yin, D. M. Otterness, L. M. Karnitz, and R. T. Abraham, A direct linkage between the phosphoinositide 3-

kinase-AKT signaling pathway and the mammalian target of rapamycin in mitogen-stimulated and transformed cells, *Cancer Res* 60 (2000) 3504-3513.

[32] M. Miron, P. Lasko, and N. Sonenberg, Signaling from Akt to FRAP/TOR targets both 4E-BP and S6K in *Drosophila melanogaster*, *Mol Cell Biol* 23 (2003) 9117-9126.

[33] B. K. Bhandari, D. Feliars, S. Duraisamy, J. L. Stewart, A. C. Gingras, H. E. Abboud, G. G. Choudhury, N. Sonenberg, and B. S. Kasinath, Insulin regulation of protein translation repressor 4E-BP1, an eIF4E-binding protein, in renal epithelial cells, *Kidney Int* 59 (2001) 866-875.

[34] T. Preiss, J. Baron-Benhamou, W. Ansorge, and M. W. Hentze, Homodirectional changes in transcriptome composition and mRNA translation induced by rapamycin and heat shock, *Nat Struct Biol* 10 (2003) 1039-1047.

[35] M. Miron, J. Verdu, P. E. Lachance, M. J. Birnbaum, P. F. Lasko, and N. Sonenberg, The translational inhibitor 4E-BP is an effector of PI(3)K/Akt signalling and cell growth in *Drosophila*, *Nat Cell Biol* 3 (2001) 596-601.

[36] M. Ridderstrale, and H. Tornqvist, PI-3-kinase inhibitor Wortmannin blocks the insulin-like effects of growth hormone in isolated rat adipocytes, *Biochem Biophys Res Commun* 203 (1994) 306-310.

[37] S. A. Barker, K. K. Caldwell, A. Hall, A. M. Martinez, J. R. Pfeiffer, J. M. Oliver, and B. S. Wilson, Wortmannin blocks lipid and protein kinase activities associated with PI 3-kinase and inhibits a subset of responses induced by Fc epsilon R1 cross-linking, *Mol Biol Cell* 6 (1995) 1145-1158.

[38] F. Rozen, I. Edery, K. Meerovitch, T. E. Dever, W. C. Merrick, and N. Sonenberg, Bidirectional RNA helicase activity of eucaryotic translation initiation factors 4A and 4F, *Mol Cell Biol* 10 (1990) 1134-1144.

[39] F. Gebauer, and M. W. Hentze, Molecular mechanisms of translational control, *Nat Rev Mol Cell Biol* 5 (2004) 827-835.

[40] P. De Rijk, E. Robbrecht, S. de Hoog, A. Caers, Y. Van de Peer, and R. De Wachter, Database on the structure of large subunit ribosomal RNA, *Nucleic Acids Res* 27 (1999) 174-178.

[41] W. H. Kalle, M. V. Macville, M. P. van de Corput, B. G. de Grooth, H. J. Tanke, and A. K. Raap, Imaging of RNA in situ hybridization by atomic force microscopy, *J Microsc* 182 ( Pt 3) (1996) 192-199.

[42] J. C. Politz, R. A. Tuft, and T. Pederson, Diffusion-based transport of nascent ribosomes in the nucleus, *Mol Biol Cell* 14 (2003) 4805-4812.

[43] A. Tsourkas, M. A. Behlke, and G. Bao, Hybridization of 2'-O-methyl and 2'-deoxy molecular beacons to RNA and DNA targets, *Nucleic Acids Res* 30 (2003) 5168-5174.

## CHAPTER 5

### Measurement of intracytoplasmic mobility of endogenous messenger RNAs using MB probes in living cells

#### Introduction

There are several important questions related to transport of mRNAs in living cells. It has been proposed that mRNAs after their export from nucleus are directed to specific sites in the cytoplasm of living cells ([1-3]). This process of RNA localization is believed to play a critical role in gene expression and in certain cases the localization of specific proteins ([1, 2, 4, 5]). It has been proposed that internal zip-code sequences within RNA molecules, various RNA binding proteins, cytoskeletal elements and possibly molecular motors ([2, 3, 6]) control the transport rate and localization of RNA molecules in the cytoplasm. It is not clear as to how this complex machinery is organized in the cytoplasm to carryout the transport of RNA molecules and how the specifics of transport process are determined for different RNA molecules. This limited understanding in this fundamental process is partly due to limited direct observation of endogenous mRNAs ([7-10] ) and their transport in the cytoplasm of living cells. In this study, we have developed an approach, which allows for the measurement of intracytoplasmic mobility of endogenous RNAs in living cells. This study combines a modified molecular beacon (MB) probe design with a FRAP (Fluorescence Recovery After Photobleaching) based biophysical tool and biochemical perturbations in a cell culture set-up to quantify the mobility of RNA in the cytoplasm of living cells.

Messenger RNAs begin their journey in the nucleus, after their birth and processing in nucleus (transcription and post-transcription processing (splicing etc.), the

assembly of RNA and its bound proteins), they are transported to the cytoplasm. It was originally proposed ([11]) that the mRNAs are transported vectorially from nucleus to the cytoplasm. Studies by ([12-14]) have shown that mRNAs exhibit a random diffusion in the nucleus rather than a local vectorial transport. This trend has been observed using both FCS (Fluorescence Correlation Spectroscopy) and FRAP based measurement of mRNA transport in the nucleus.

For tagging mRNAs in the nucleus, previous studies ([12-13]) have used fluorescently labeled oligonucleotide probes complementary with Poly A section of mRNAs. One of the major challenges in the above approach for imaging or studying the dynamics of mRNAs is the lack of ability to distinguish the hybridized oligonucleotide from a pool of free unbound oligonucleotides. Various approaches have been used to address this challenge, in one of the approaches used by ([13]), the oligonucleotide were labeled with caged fluorophores. These fluorophores were fluorescent only after photolysis by a UV wavelength in a small focused region. Using the photolysis technique, it may be feasible to study the dynamics of a macromolecule with a high concentration or a generic target (e.g., Poly A sequence can represent the entire pool of mRNAs in the nucleus) in a specific compartment of a cell, but may not be feasible for a low concentration and also a widely dispersed macromolecule. One of the limitations of this technique is that the site of photolysis must be defined or known a priori, without which it may not be possible to study the dynamics of a specific macromolecule. This limitation can be reduced by using a secondary label to define an area of interest. This secondary labeling approach can provide a reference point for the photolysis process. Even with this modification, it is still not possible to study the entire distribution of a particular macromolecule.

The other approach for studying RNA mobility in a nucleus using oligonucleotide probes have been based on using high affinity oligonucleotides chemistries (2' O Methyl)

to allow for stable and faster binding ([12, 15]). This approach in combination with a strict control of the concentration of an exogenous probe can potentially reduce the background levels due to unbound probe molecules. The other advantage of using a high affinity oligonucleotide chemistry especially for targeting a Poly A section of mRNAs can be the higher melting temperature of the hybridized structure as compared to regular DNA chemistry oligonucleotide probe of similar length. This consideration can be important for the design of oligonucleotide probes for live cell studies at 37 °C. Thus to increase the melting point and in turn increase the stability of hybridized probe, longer probe lengths (~43 bp) are required with regular DNA chemistry as compared with 2' O methyl chemistry ([12]). Despite these advantages of high affinity chemistry, still it is challenging to distinguish true signal from the background if the target macromolecule is widely dispersed and further the lack of specificity (SNP etc) of linear oligonucleotide probes can lead to false positives.

The other major limitation in using oligonucleotide probes for live cell studies has been the limited success with non-invasive delivery (transfection agents etc.) of these probes. The studies discussed above have mainly used microinjection based delivery of oligonucleotide probes into cells. Microinjection process is generally limited to few cells, and also the approach is invasive as it creates a micron- sized hole in the plasma membrane and also introduces an exogenous fluid in cells leading to increase in volume of cells. The other disadvantage of this method has been the lack of ability to target mRNAs in the cytoplasm of cells. It has been reported that short oligonucleotide probes delivered using microinjection are imported to the nucleus. ([10, 16, 17]). This limits the targeting of oligonucleotide probes only to mRNAs in the nucleus. To overcome this limitation, recently various moieties (such as streptavidin etc.) have been attached to the oligonucleotide probes to slow down their import into nucleus ([9]).

The above studies have been mainly focused on understanding the dynamics of RNA in the nuclei of living cells. There is no reported study to our knowledge with a quantitative analysis of the mobility of endogenous mRNAs in the cytoplasm of living cells. In part it has been due to the lack of ability to target endogenous mRNAs in the cytoplasm of living cells using microinjection method. Further in the cytoplasm the targeting of Poly A section of mRNAs may not be the best approach as present understanding suggests that mRNAs are segregated and targeted to different sections of cytoplasm. These mRNAs in turn may associate with variety of sub cellular structures including organelle membranes (ER, Mitochondria) and cytoskeleton etc, which may effect their dynamics. These mRNAs can be translated at these sites, maintained in inactive state and also metabolized in the cytoplasm. Thus mRNAs can be at multiple sites and also in multiple states in a cytoplasm. Thus generic targeting using Poly A as a target may not provide a complete understanding of the dynamics. In this direction, this study establishes an experimental approach, which allows for imaging of specific endogenous mRNAs with high specificity, low background noise. This approach in combination with a simple biophysical assays such as FRAP and biochemical/ chemical perturbation of cellular processes allows for a mechanistic and a quantitative understanding of the dynamics of specific mRNAs in living cells.

The oligonucleotide probe used in this study is a dual labeled probe with a stem-loop structure. This stem-loop structure provides the specificity for targeting, while the dye- quencher pair provides a facile method to distinguish the hybridized probe from the unhybridized probe ([18]). Probes used in this study are modified version of classical molecular beacon design. In this design MB probes were modified in the stem domain to conjugate a delivery peptide. The probes used in this study are described in previous **Chapters 2 and 3**, ([7, 8]).

Our objective is to develop an approach, which provides a quantitative understanding of intra- cytoplasmic mobility of RNAs in living cells. To achieve this we have used a fluorescence recovery after photobleaching (FRAP) based approach to study the dynamics in combination with modified MB probes. FRAP has been used by various research groups to measure the mobility of protein molecules in cytoplasm and nucleus of living cells ([19-22]). In this study, we have extended this approach to measure the mobility of specific endogenous RNAs in the cytoplasm. **Figure 5.1** shows the schematic representation of a FRAP process in a cell. The pre-selected region of interest is bleached with a laser pulse, followed by recording of the recovery process (recovery of the fluorescence intensity) in a bleach section due to mobility of fluorophores from surrounding unbleached areas. The schematic view of the process is shown in **Figure 5.1 (A-C)** and the resultant intensity curve is shown in **Figure 5.1 (D)**. Further we have used various chemical perturbations to determine whether the mobility of RNAs in the cytoplasm is mediated by active or passive processes. In this study, we have also directly assessed the contribution of microtubule cytoskeletal elements in the transport of RNA molecules.

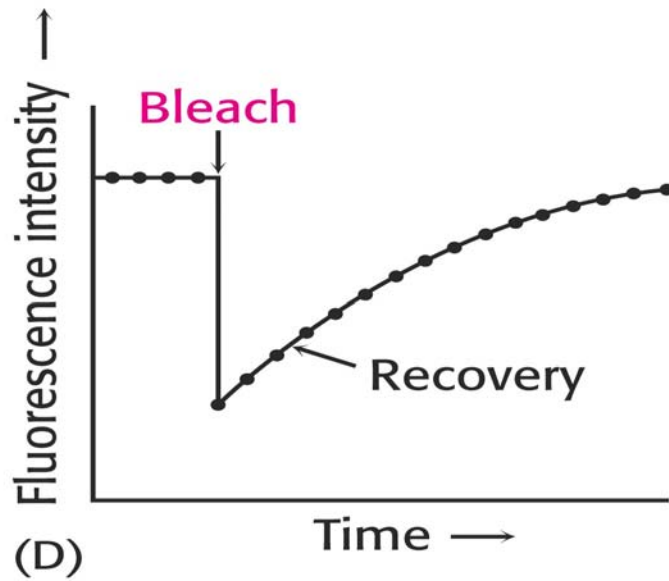
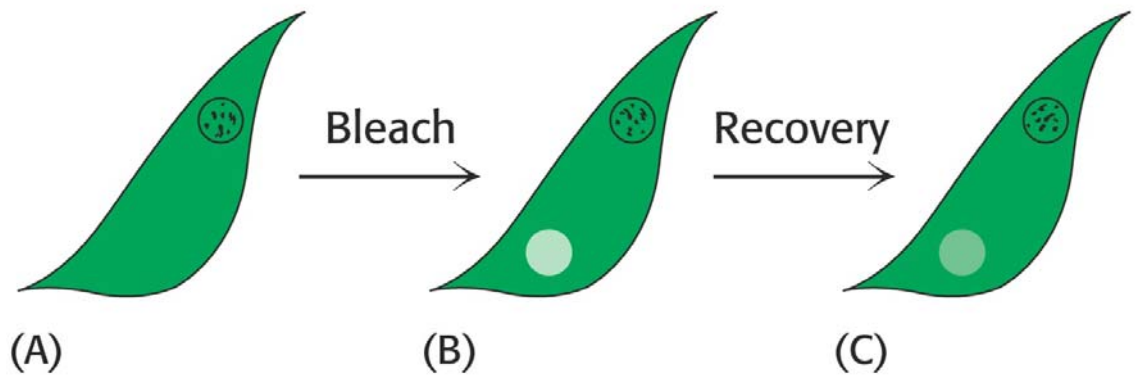


**Figure 5.1:** Schematic representation of a FRAP experiment in a cytoplasm of a cell  
 A-C) Image based representation of a FRAP procedure i.e., pre-bleach, bleach and post bleach recovery  
 D) Normalized fluorescence intensity plot obtained from a FRAP experiment

## **Material and Methods**

### **Chemicals**

Taxol, De-oxyglucose and Nocodazole were obtained from Sigma-Aldrich, Corp and stored as recommended by the supplier.

### **Design of Molecular Beacons**

In this study we have used the same design of MB probes for targeting GAPDH mRNA and 28-s rRNA described in (**Chapter (2 and 3)**).

### **Cell culture**

Normal human dermal fibroblast cells (Cambrex, NJ) were grown in Clonetics fibroblast growth medium supplemented with 2% fetal bovine serum (Cambrex, NJ), insulin, fibroblast growth factor, Gentamicin Sulfate and Amphotericin-B. The cells were cultured on a cover slip glass. The cover slip glass provided by Biotech's Inc. was pre-treated for 2 hours with a cell culture medium to allow for adsorption of serum proteins on the surface. This treatment increased the adhesion of fibroblast cells on the surface. The cells on a surface of a cover slip glass were cultured in a petridish with approximately 2 ml of culture medium and were typically allowed to grow for 3-4 days after every plating. In this study, we have used primary HDF cells with split cycles between 3-9.

### **FRAP Assay**

For FRAP studies, cells cultured on a cover slip glass after all the biochemical treatments and incubation of MBs at 37 °C were transferred to FSC-2 chamber (Biotech's, Inc.) This flow chamber was maintained under static conditions, during the experiment. The culture medium was introduced only during a transfer from a petri dish to a flow chamber. The temperature in the chamber was maintained using a Biotech's closed chamber controller with a heated micro-adduct slide and an objective heater. The

images were acquired with a Zeiss LSM 510 confocal microscope using a 40 X oil objective. The images were zoomed-in using a 2x digital zoom in the Zeiss software. The cells were scanned using a 543 nm laser at 0.5 mW laser power (50% of the maximum power) for imaging. For bleach sequence we used 488 nm and 514 nm lasers each at 40% of the maximum laser power. The bleach sequence was repeated for 100 iterations to ensure irreversible bleaching of the sample. To confirm that the number of iterations has no significant effect on the recovery characteristics of a fluorescent signal, the number of iterations was varied from 50 to 100 during initial experiments. The results indicated no significant differences in the recovery trends evaluated using normalized fluorescence intensity versus time plots. Further the area of a bleached region of interest was varied from  $1 \mu\text{m}^2$  –  $2 \mu\text{m}^2$  to validate if changes in the bleached area have significant effects on the recovery trends. No significant differences were observed in the above case.

Further in this study, we have selected an optical pinhole of 2.4 airy units for imaging and bleach sequence in all the experiments. This slice thickness of the confocal imaging allowed us to model the recovery of fluorescence intensity in a bleached area as a radial diffusion in a cylindrical slice.

### **Molecular beacon delivery via cell permeable peptide**

The molecular beacon targeted to GAPDH and 28-s rRNA (see **Table 5.1**) was linked via a disulfide bridge to the Tat peptide ((N terminus) TyrGlyArgLysLysArgArgGlnArgArgArg (C terminus)-Cys) (as discussed in Chapter 2). For the delivery of molecular beacon, peptide-linked molecular beacons were mixed with the regular media (1 ml) and incubated for 30 minutes at 37°C.

### **Microtubule perturbations**

For these experiments, cells were grown normally on coverslips as described above. After 30 minutes of delivery of MB probes, the cells were treated with 2 $\mu$ M concentration of nocodazole or 10  $\mu$ M concentration of taxol for 30 minutes. After this incubation time, the coverslips were transferred to FSC-2 chamber and analyzed using a FRAP based assay as described above.

### **ATP depletion**

Energy depletion was obtained by addition of 2-deoxy glucose and Na Azide at 5 mM concentration respectively to a regular culture media for 15 minutes at 37 C after regular incubation of celss with MB probes. The cells after this incubation were transferred to FSC-2 chamber and analyzed using a FRAP based assay as described above.

### **Fluorescence *in-situ* hybridization**

Normal human dermal fibroblasts were cultured in a 4-well chambered coverslides for 24 hours in normal growth medium (FGM-2 Cambrex Co.) and then washed with 1x PBS (without Ca or Mg). The slide was fixed in 100% methanol at  $-20^{\circ}\text{C}$  for 10 minutes. After removing the methanol, the slides were allowed to air dry and stored overnight at  $-80^{\circ}\text{C}$ . In-situ hybridization assays were then performed by first washing the slides for 5 minutes in 1x PBS and hybridizing them overnight at  $37^{\circ}\text{C}$  in 1x PBS (no Ca or Mg) containing 200 nM of fluorescently labeled linear probes targeting GAPDH. After hybridization, the cells were analyzed using FRAP assay as outlined above at room temperature. In this study, we did not remove the excess MB probes, thus no washing step was included in the FISH protocol.

## Results and Discussion

### Design of MB probes

The MB probes used in the study are shown in **Table 5.1**. In this study, we have used MB probes for targeting GAPDH mRNAs and 28-s ribosomal RNAs. The sequence design of the MB probe used for targeting the GAPDH mRNAs is same as established in our previous study ([7]), while the sequence of 28-s Ribosomal RNA probe was adapted from ([15, 23]). The discussion on the design criteria for these probes and other details has been presented in ([7]).

**Table 5.1:** Design of molecular beacons

---

***GAPDH molecular beacon***

5'-Cy3-CGACGGAGTCCTTCCACGATACCACG/thiol-dT/CG-BHQ2-3'

---

***28S rRNA molecular beacon***

5'-Cy3-CGACTACCACCAAGATCTGCAGTCG/HQ-2/-3'

---

### **Mobility of GAPDH mRNAs at 37 °C**

After 30 minutes of incubation of peptide linked MBs with cells, the cells were imaged in a FSC-2 chamber maintained at 37 °C. The result of FRAP based intracytoplasmic mobility of GAPDH mRNAs in living cell at 37 °C is shown in **Figure 5.2**. GAPDH mRNAs have a filamentous distribution in the pre-bleach section shown in **Figure 5.2 A**. This is in agreement with our earlier observations ([7]). **Figure 5.2 A** shows a representative time course of the pre- and post bleach distribution of a fluorescent signal from MB probes hybridized with GAPDH mRNAs. The bleach area in these images is highlighted using a white circle. After bleaching the fluorophores in a region of interest, we observed a recovery of the fluorescence signal in the defined region. The result also shows the recovery of the filamentous structure similar to the pre-bleach distribution of GAPDH mRNA. During this experiment, we did not observe any significant changes in the distribution pattern of the fluorescent signal in areas other than the bleached region of interest. Fluorescence intensity data from a bleached region was normalized to changes in the fluorescence intensity in an unbleached control area. This normalization allowed us to account for any variation or overall bleaching of the fluorescence intensity due to repeated exposure of the sample.

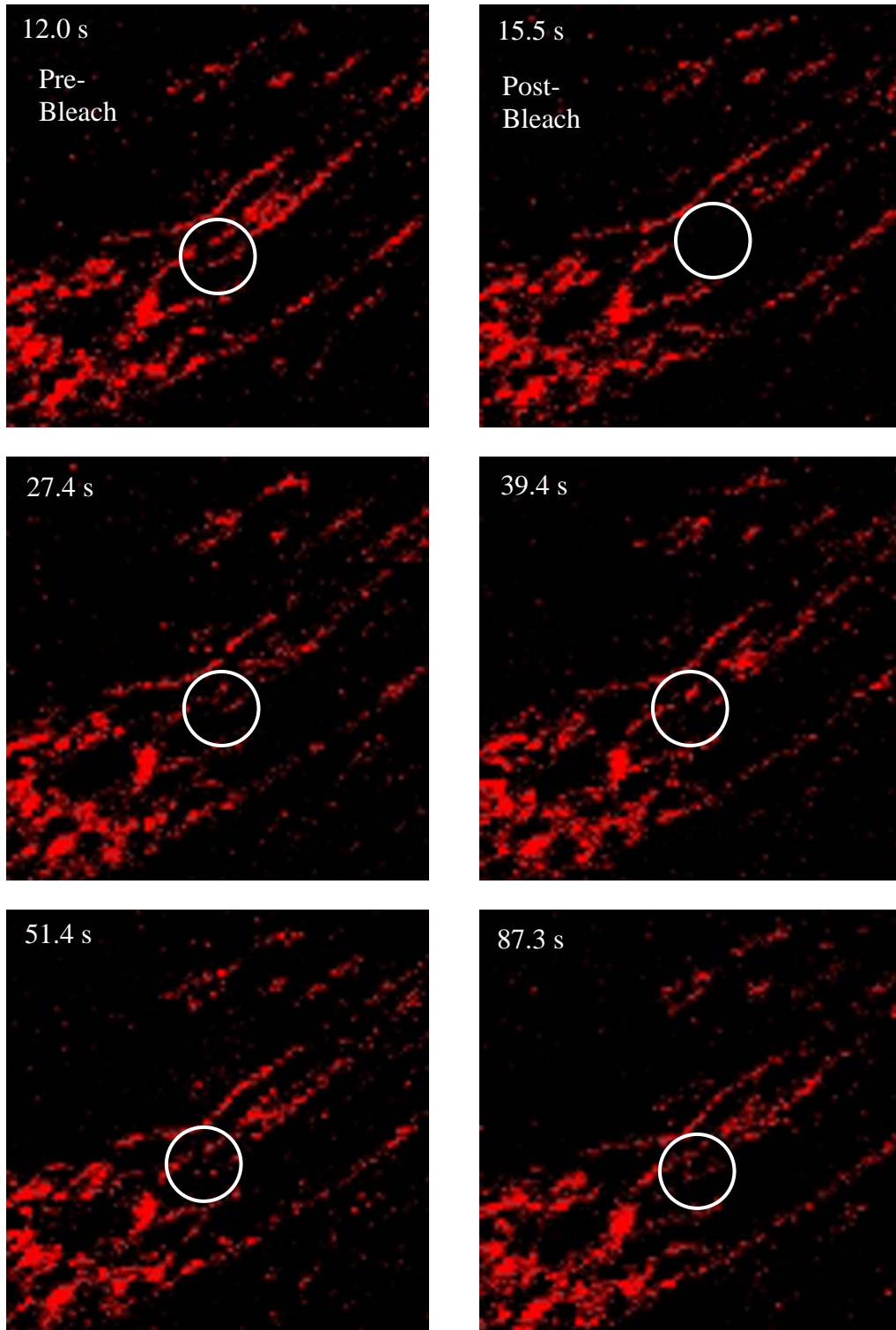


**Figure 5.2 A:** FRAP analysis of the mobility of GAPDH mRNAs at 37°C using MB probes

A. Image based distribution of Fluorescence intensity in a pre-bleach, immediately after bleaching and post bleach recovery for a GAPDH mRNAs in HDF cells.

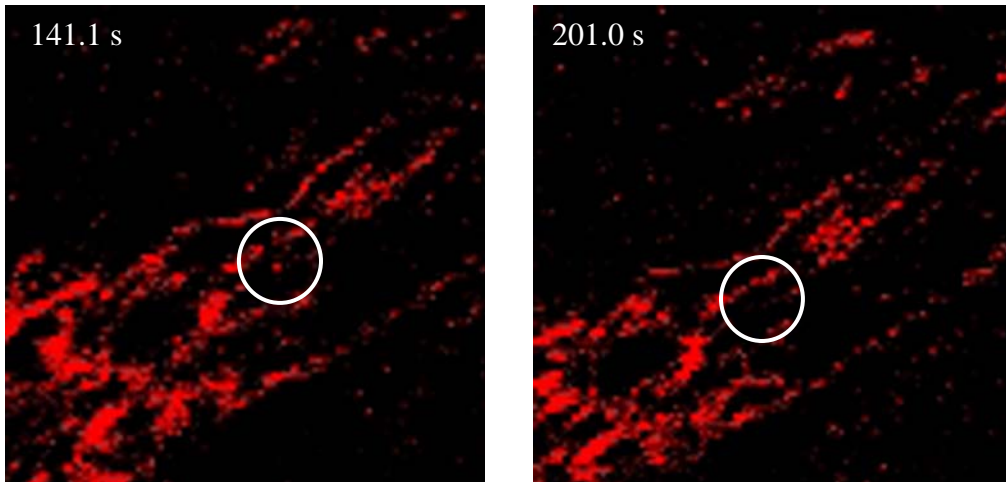


**Figure 5.2 (A) Continued**

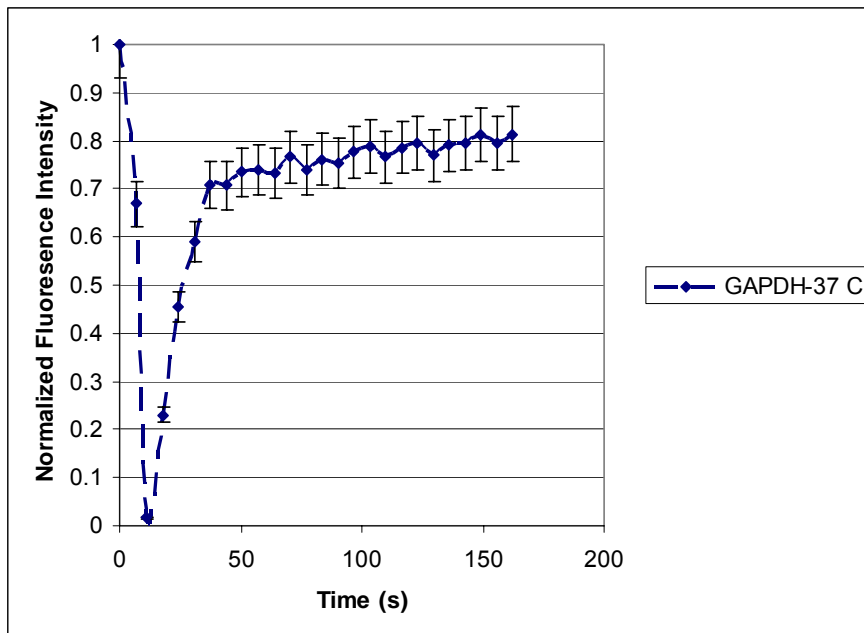


**Figure 5.2 (B)**

**Figure 5.2:** FRAP analysis of the mobility of GAPDH mRNAs at 37°C using MB probes

- A. Image based distribution of Fluorescence intensity in a pre-bleach, immediately after bleaching and post bleach recovery for a GAPDH mRNAs in HDF cells. The results indicate a directed recovery of the fluorescence intensity in a region of interest marked with white circle.
- B. Average normalized fluorescence intensity in a ROI as a function of time. The result shows 80% recovery of the bleached fluorescence signal, indicating significant mobility of the GAPDH mRNAs

The recovery of fluorescence intensity in a bleach area was not a random process but the signal recovered along the same filamentous distribution after photobleaching as in a pre-bleach image. **Figure 5.1 B** shows the variation of fluorescence intensity (normalized average of 9 readings collected over three independent experiments) in a bleach region of interest as a function of time. The results show a rapid bleach of the fluorescence sample followed by the recovery process, which shows increase in fluorescence in a bleached region followed by saturation of recovery at later time points. The plot in **Figure 5.1 B** shows recovery of approximately 80% of the pre-bleach fluorescence intensity after photo bleaching, thus indicating a significant mobility of GAPDH mRNAs under these experimental conditions.

#### **Mobility of GAPDH mRNAs in fixed sample**

To assess the contribution of the dynamics of MB probes (transient hybridization of the probes with RNA target due to inherent “on-off” rates of MB probes) in the observed recovery of GAPDH mRNAs as shown in **Figure 5.2**, we decided to chemically fix the cells without MB probes in methanol. Methanol fixation process precipitates RNA bound proteins and in-turn can enhance the accessibility of MB probe to target mRNAs. We have used this fixation process in our earlier study ([7]) and have observed a similar filamentous distribution of GAPDH mRNAs in the cytoplasm. After fixation, the cells were hybridized overnight with target MB probes. In this study, fixed cells after hybridization were not washed to avoid removal of any unbound probes. These samples were analyzed using a FRAP based assay under same optical imaging conditions as in case of live cells (**Figure 5.2**). These experiments were carried out at room temperature. The results of the study are shown in **Figure 5.3**. **Figure 5.3 A** shows a representative time series of the fluorescence intensity during a FRAP assay. The results show a negligible recovery of the fluorescence intensity in a bleached region. This clearly indicates that we have irreversibly bleached a region of interest with the selected bleach sequence and

other imaging settings (laser power, pinhole, PMT gain etc.). Since we did not observe any significant recovery in the fluorescence after bleaching, it also indicates that the off rate of MB probes does not have significant contribution to the recovery process. **Figure 5.3 B** shows the plot of fluorescence intensity versus time in a region of interest. The result clearly shows no significant recovery of the fluorescence intensity over the same time scale as used in a live cell experiment. It is still a challenge to determine the dynamics (on-off rate) of MB probes in a living cell sample. It is likely that the target mRNA dynamics, cytoplasmic local environment and the inherent probe dynamics contribute to true hybridization and off rates of MB probes in living cells. Using fixed cell samples, we have only studied the inherent probe dynamics in presence of an mRNA target in a cytoplasm, without any contribution from active cellular processes. Further in the discussion section we will highlight some of the approaches, which may allow us to study the true dynamics of MB probes in living cell samples.

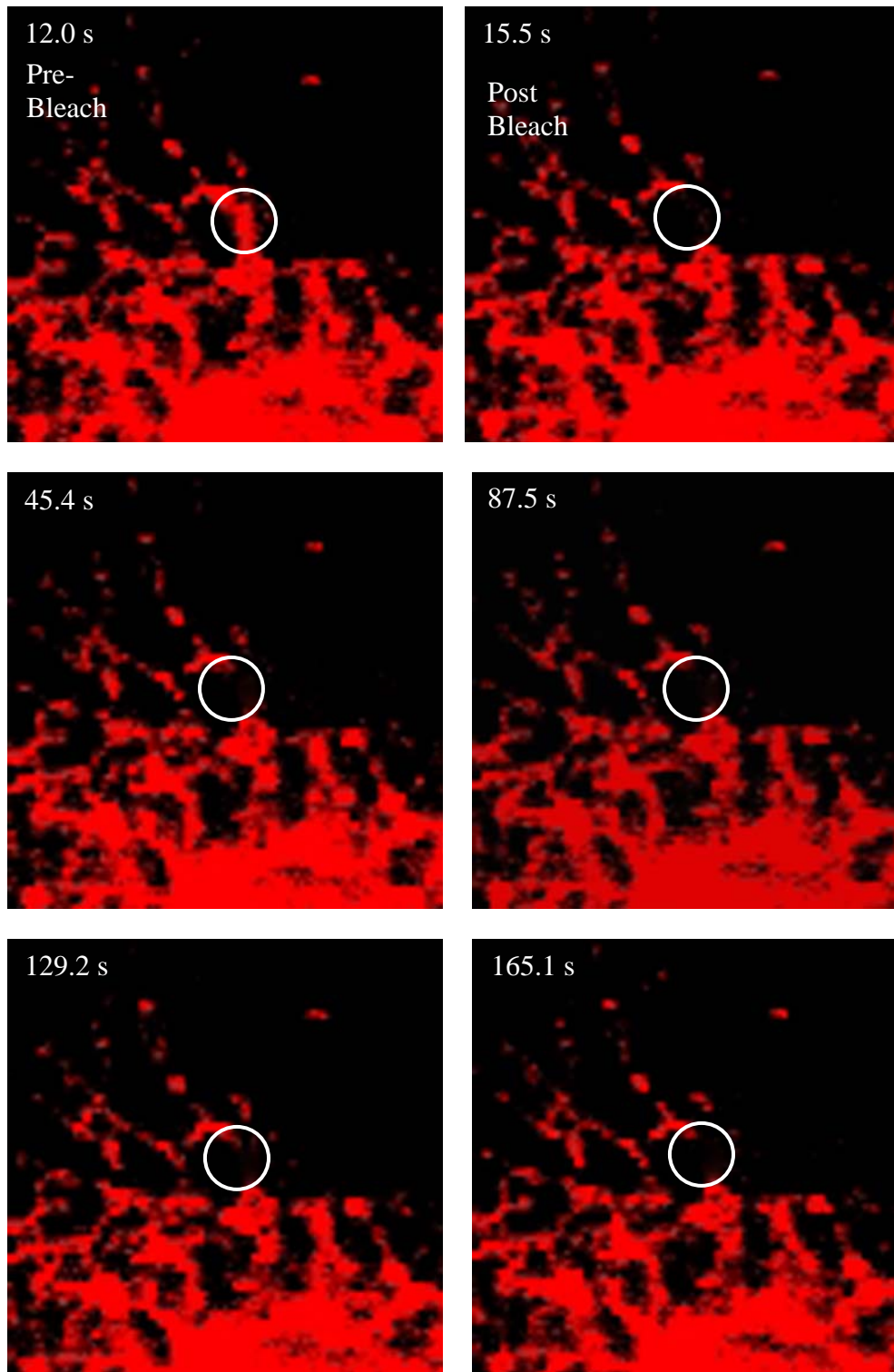


**Figure 5.3 A:** Image based distribution of Fluorescence intensity in a pre-bleach, immediately after bleaching and post bleach recovery for a GAPDH mRNAs in fixed HDF cells.

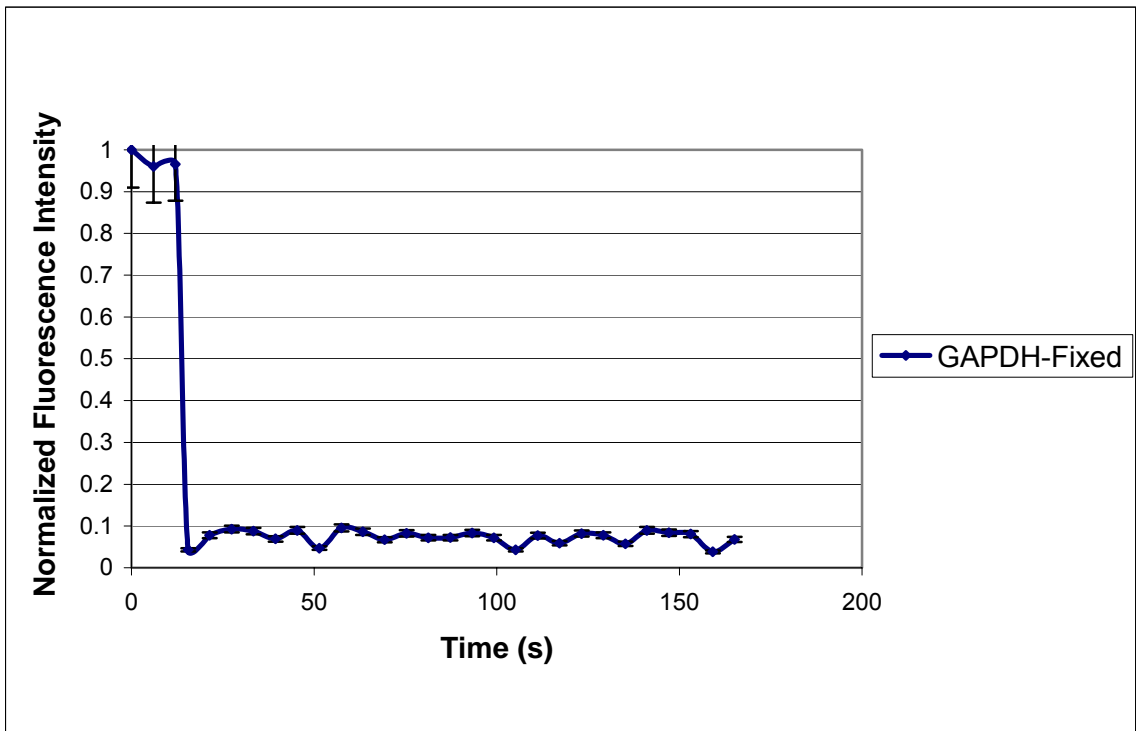


**Figure 5.3 B:** FRAP analysis of the mobility of GAPDH mRNAs in a fixed cell samples using MB probes to estimate the contribution of the off-rate of MB probes in recovery of bleached areas. Average normalized fluorescence intensity in a ROI as a function of time. The result shows very limited recovery of the bleached fluorescence signal, indicating that the inherent-off rate of MB probes does not have significant contributions to the recovery of a fluorescence signal in a bleached section.

### **Effect of Temperature on the mobility of mRNAs in the cytoplasm**

To determine whether temperature conditions have any effect on the mobility of mRNAs in the cytoplasm of living cells, MB probes hybridized with target GAPDH mRNAs for 30 minutes at 37 °C were transferred to the FSC-2 chamber. The chamber was maintained at 25 °C on a confocal microscope stage. FRAP based analysis was carried out under similar confocal settings as in **Figure 5.2**. At 25 °C, the distribution of MB fluorescent signal was not significantly different than observed at 37 °C, indicating there are no major structural changes in cells, and MB probe binding characteristics are similar at both temperature conditions. The results of the fluorescence signal in living cells at different time points of pre and post bleach sequence are shown in **Figure 5.4 A**. Results show that there is a partial recovery of the fluorescence signal in a bleached region of interest. This recovery process was observed to be along a directed direction determined by pre-bleach distribution of fluorescence in the bleached ROI. This is similar to the trend observed at 37 °C even though only a partial recovery of the fluorescence intensity was observed at 25 °C. The result of the fluorescence intensity versus time in a bleached region of interest is shown in **Figure 5.4 B**. Results show that the recovery is slower and partial (approximately 30 % of the original intensity (pre-bleach)) as compared with the results obtained at 37 °C. This result clearly indicates that the mobility of GAPDH mRNA is sensitive to temperature conditions. The temperature dependence of biological processes in general indicates that the mobility of a macromolecule is mediated by active cytoplasmic processes, as there is no significant difference in the true diffusivity of macromolecules at 37 °C and 25 °C conditions. Thus for true diffusion processes we do not expect to observe a significant change in the recovery characteristics at these temperature conditions.

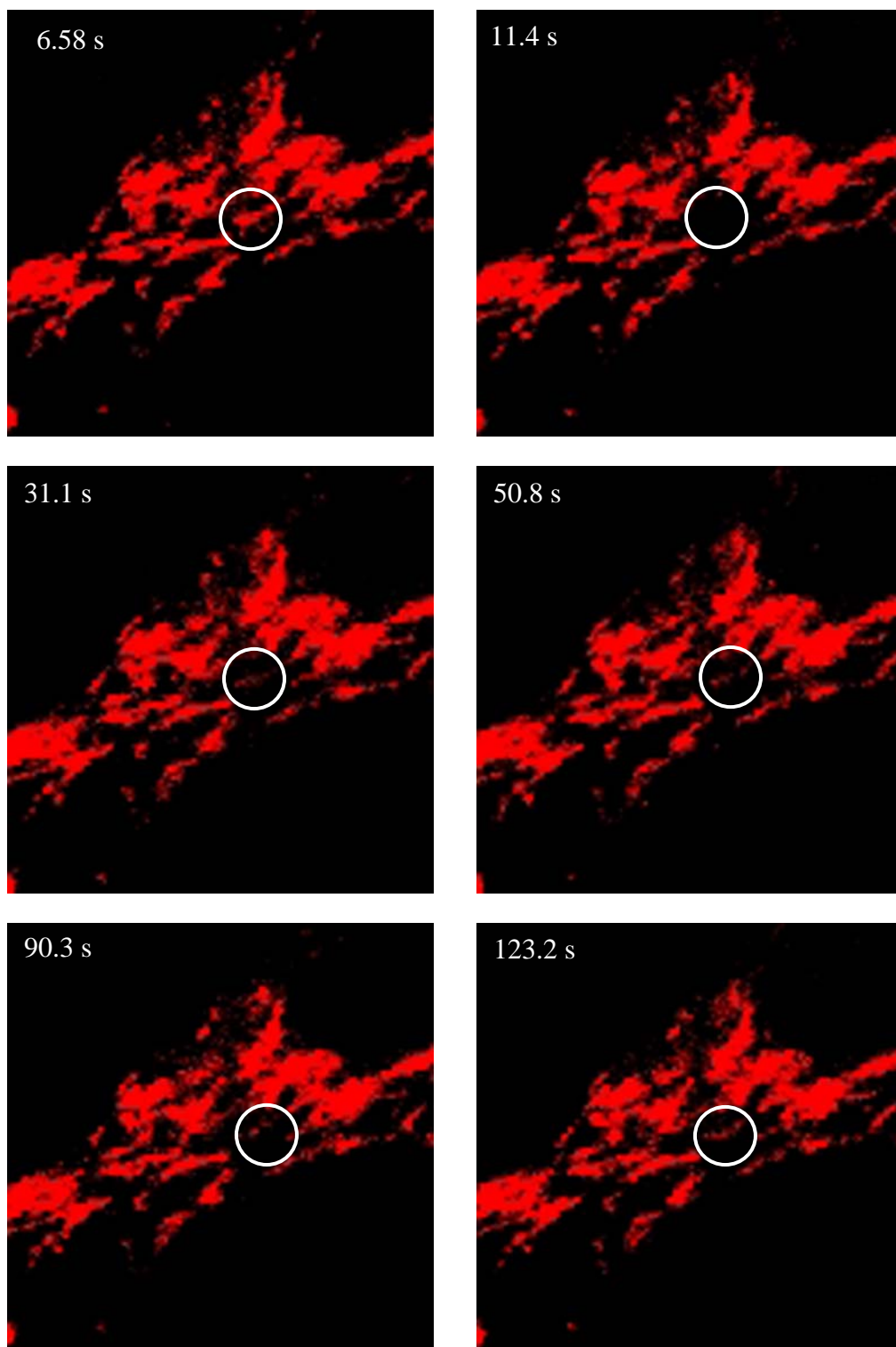


**Figure 5.4 A:** FRAP analysis of the mobility of GAPDH mRNAs at 25 °C using MB probes. Image based distribution of Fluorescence intensity in a pre-bleach, immediately after bleaching and post bleach recovery for a GAPDH mRNAs in HDF cells.

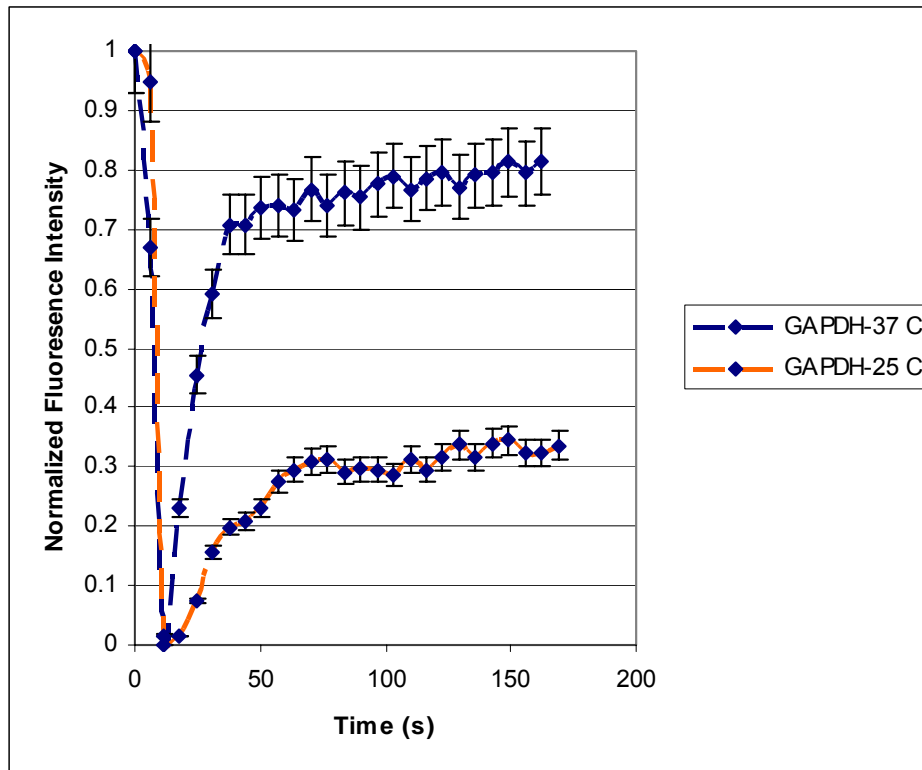


**Figure 5.4 B:** FRAP analysis of the mobility of GAPDH mRNAs at 25 °C using MB probes. Average normalized fluorescence intensity in a ROI as a function of time. The result shows about 30% recovery of the bleached fluorescence signal, indicating significant reduction in mobility of the GAPDH mRNAs at 25 °C as compared to the 80% recovery observed in case of similar experiments at 37 °C. The results also indicate that the recovery process is significantly slower at room temperature as compared to the control experiments at 37°C.

### **Effect of ATP depletion on the mobility of GAPDH mRNAs in the cytoplasm**

To further establish that the mobility of GAPDH mRNAs is mediated by active process, we decided to biochemically deplete the ATP production in living cells. The cells incubated with MB probes were treated with 2-de-oxyglucose and Na Azide at 5 mM concentration respectively for 15 minutes. This concentration of de-oxyglucose has been used in other studies for depletion of ATP ([12, 14]). Depletion of ATP has some effect on the distribution of GAPDH mRNAs in the cytoplasm. These changes are more prominent as compared to the changes in distribution of fluorescent signal, when cells were incubated at room temperature. This is likely as depletion of ATP results in change of mitochondrial distribution, inhibits motor driven transport and effect wide range of other cytoplasmic cellular processes etc. Thus both the concentration of above chemicals and the incubation time were optimized to control significant changes in the distribution of fluorescent signal. The treated cells were studied using FRAP under the same experimental conditions as in **Figure 5.1**. These experiments were carried out at 37 °C. The results of the study are shown in **Figure 5.5**. **Figure 5.5 A** shows a time course of the fluorescence signal in a defined region of interest during a FRAP experiment. The result shows a recovery trend very similar to the trend observed in case of 25 °C (**Figure 5.4**). The bleached area shows a partial recovery of the fluorescence signal, similar to the study at 25 °C. The plot of the average integrated fluorescence intensity in a region of interest versus time is shown in **Figure 5.5 B**. The plot shows a partial recovery of about 25 % after bleaching. The recovery kinetics are slower as compared to 37 °C case and are similar to the trend observed for the FRAP study at 25 °C. Thus the results in **Figure 5.4 and Figure 5.5**, together clearly indicate that active transport processes are responsible for the mobility of GAPDH mRNAs in the cytoplasm of living cells.

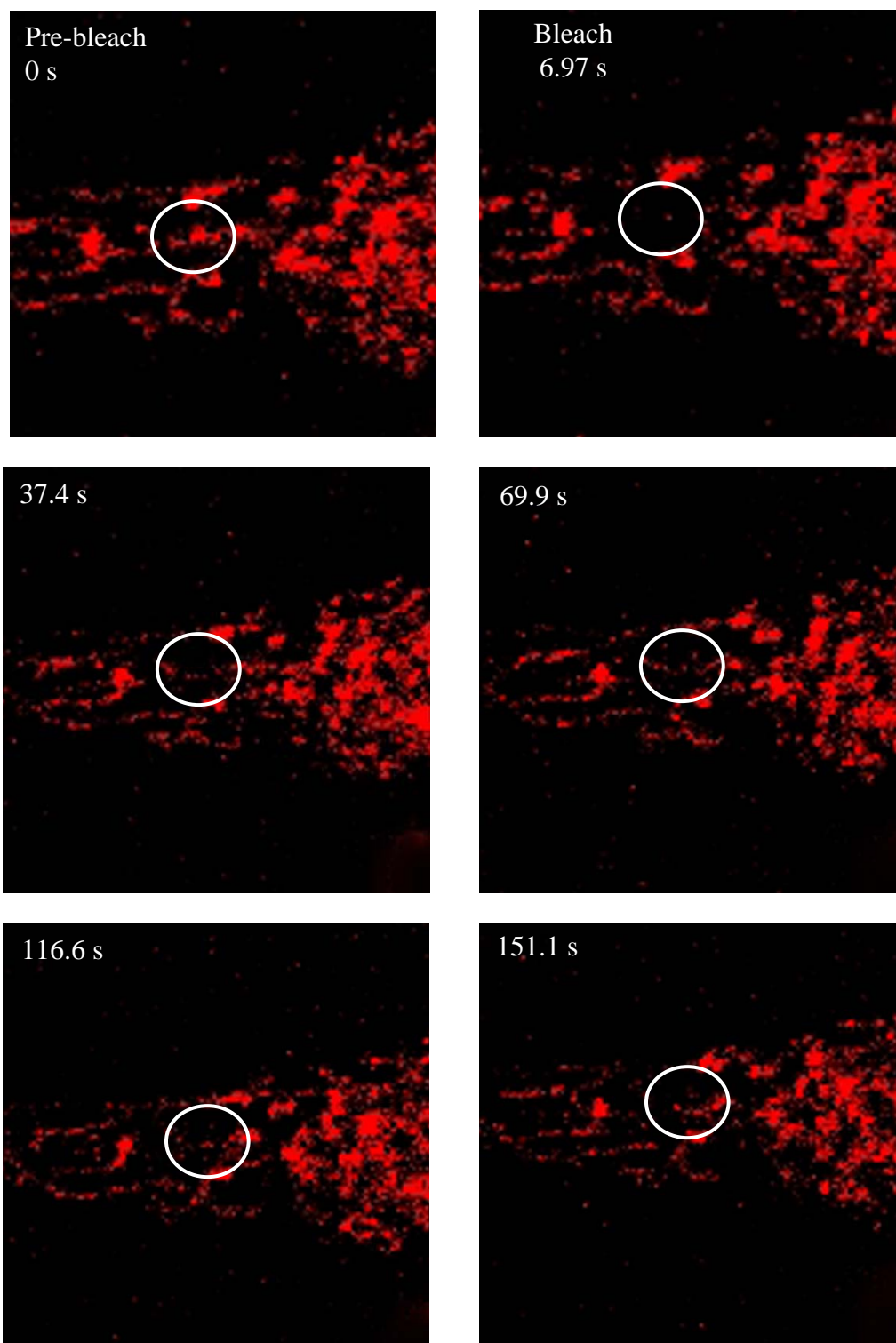


**Figure 5.5 A:** FRAP analysis of the mobility of GAPDH mRNAs at 37 °C with depletion of ATP by treatment with 2-de-oxyglucose and Na Azide for 15 minutes A. Distribution of Fluorescence intensity in a pre-bleach, immediately after bleaching and post bleach recovery for a GAPDH mRNAs in HDF cells with depletion of ATP

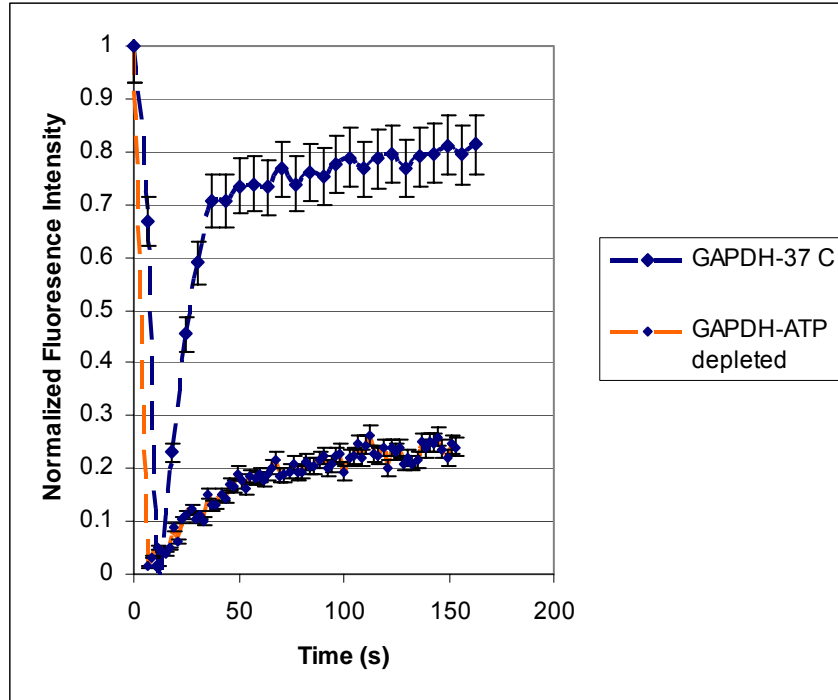


**Figure 5.5 B:** FRAP analysis of the mobility of GAPDH mRNAs at 37 °C with depletion of ATP by treatment with 2-de-oxyglucose and Na Azide at 5 mM concentration for 15 minutes

Average normalized fluorescence intensity in a ROI as a function of time. The result shows about 25% recovery of the bleached fluorescence signal, indicating significant reduction in mobility of the GAPDH mRNAs with ATP depletion as compared with the control experiments at 37 °C. The results also indicates that the recovery process is significantly slower with ATP depletion as compared with the control experiments at 37 °C

### **Effect of Microtubule network on the mobility of GAPDH mRNAs**

To further understand, if these active processes are related to cytoskeleton network, we next studied the role of microtubule in the mobility of GAPDH mRNAs. As a first approach, we have used nocodazole, which is an anti-neoplastic agent and exerts its effect by de-polymerizing microtubules. For initial experiments we used nocodazole at a concentration of 30  $\mu\text{M}$  and incubation time period of 60 minutes. This concentration range was selected based on several studies, which have used this drug to study the role of microtubule network in various cytoplasmic processes ([24, 25]). This concentration of nocodazole resulted in dramatic changes in the distribution of MB probe signal in the cytoplasm of living cells (discussed in **Chapter 3**). The resultant MB signal after treatment was peri-nuclear, thus suggesting that the disruption of a microtubule network has a significant effect on the distribution of GAPDH mRNAs in the cytoplasm. This result indicates the role of microtubule in the localization of mRNAs in the cytoplasm, even though this treatment was too invasive to study the effect of microtubules on the mobility of mRNAs.

To reduce the invasiveness of nocodazole treatment, we lowered the concentration of nocodazole to 2  $\mu\text{M}$  for an incubation time of 30 minutes. The cells after treatment were studied using FRAP to measure the mobility of GAPDH mRNAs. The results of this study are shown in **Figure 5.6**. **Figure 5.6 A** shows the time series of a fluorescence signal in pre and post bleach sequence. The results indicate that the recovery process after bleaching is more random as compared to the directed recovery (i.e., without significant changes in the shape of a fluorescent signal after bleaching and recovery in a region of interest) observed in earlier FRAP conditions (**Figure 5.2-5.5**). Thus microtubule appears to play a role in a directed recovery process. The result of the integrated average fluorescence intensity in a region of interest versus time is shown in **Figure 5.6 B**. This result is also directly compared with a control result (**Figure 5.2 B**)

obtained under same experimental conditions without nocodazole. The plot clearly indicates a partial recovery (about 45 %) of the fluorescence intensity in a bleach area with a slower kinetics as compared with a control case at 37 °C. This result provides a direct observation of changes in the mobility of GAPDH mRNAs in the cytoplasm upon treatment with a microtubule-depolymerizing drug.

Further to study the role of microtubules in the mobility of GAPDH mRNAs, we decided to perturb the microtubule network with taxol. Taxol causes a significant re-organization of microtubule network by catalyzing the assembly of microtubules from the sites other than microtubule organization center. This assembly leads to stabilization of microtubule network. It has been reported ([26]) that taxol reduces the transport frequency as well as the speed of transport of cargo along the microtubules. To test the effect of taxol on the mobility of GAPDH mRNAs, HDF cells with MBs were treated with 10  $\mu$ m of taxol for a time interval of 30 minutes.

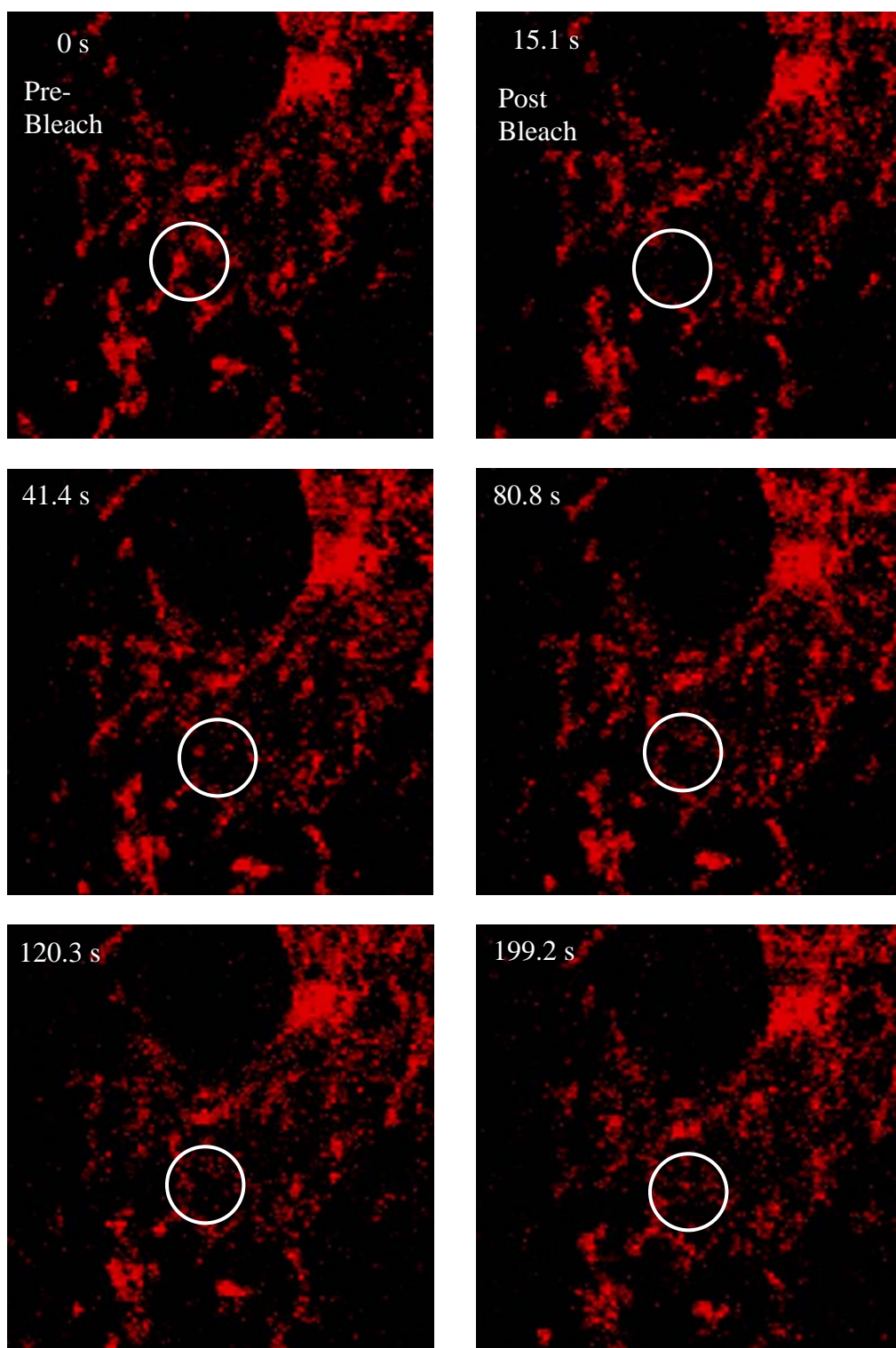


**Figure 5.6 A:** FRAP analysis of the mobility of GAPDH mRNAs at 37 °C with perturbation of microtubule network by treatment with Nocodazole

Distribution of Fluorescence intensity in a pre-bleach, immediately after bleaching and post bleach recovery for a GAPDH mRNAs in HDF cells with depolymerization of microtubules.

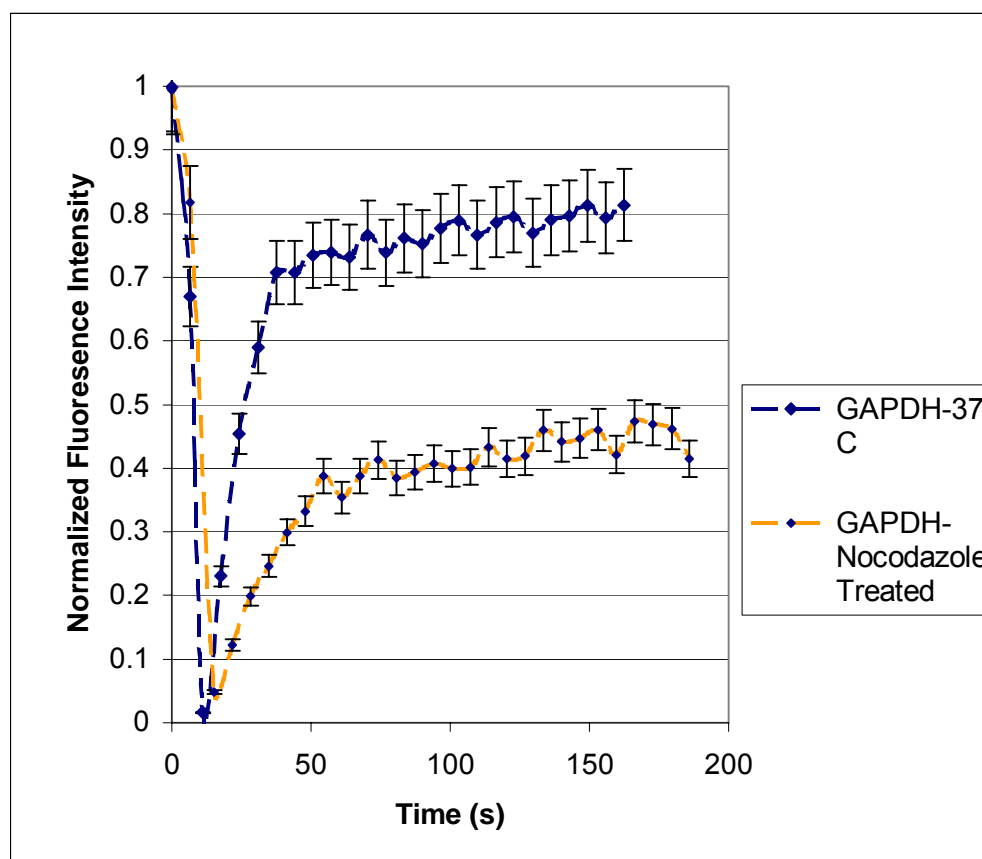


**Figure 5.6 B**

**Figure 5.6 B:** FRAP analysis of the mobility of GAPDH mRNAs at 37 °C with perturbation of microtubule network by treatment with 2  $\mu$ M concentration of Nocodazole for 30 minutes

Average normalized fluorescence intensity in a ROI as a function of time. The result shows about 25% recovery of the bleached fluorescence signal, indicating significant reduction in mobility of the GAPDH mRNAs with nocodazole treatment as compared with the control experiments at 37 °C. The results also indicates that the recovery process is significantly slower with nocodazole treatment as compared with the control experiments at 37 °C

The representative result of a FRAP analysis for the mobility of GAPDH mRNAs in taxol treated cells is shown in **Figure 5.7**. **Figure 5.7 A** shows the time course of the fluorescence signal in pre and post bleach images. The results show a partial recovery of the fluorescent signal in a bleach region of interest as compared with the pre-bleach signal. This trend is similar to the trend observed with nocodazole. Unlike nocodazole, the signal recovery is still along a directed path (reference with pre-bleach signal morphology) as compared to more diffuse recovery with nocodazole. This clearly suggests that by stabilizing microtubules, we have reduced the randomness in the recovery of a fluorescent signal in a region of interest, although only partial recovery was observed, similar to the case of a nocodazole treatment. The plot of the integrated fluorescence signal in a region of interest versus time is shown in **Figure 5.7 B**. The results indicate that in comparison with control cells, the taxol treatment reduces the rate and extent of recovery (~45% recovery of the initial level of fluorescence intensity) of the fluorescent intensity in a bleached area of interest. These results taken together clearly illustrate the role of microtubules in the mobility of GAPDH mRNAs in living cells.

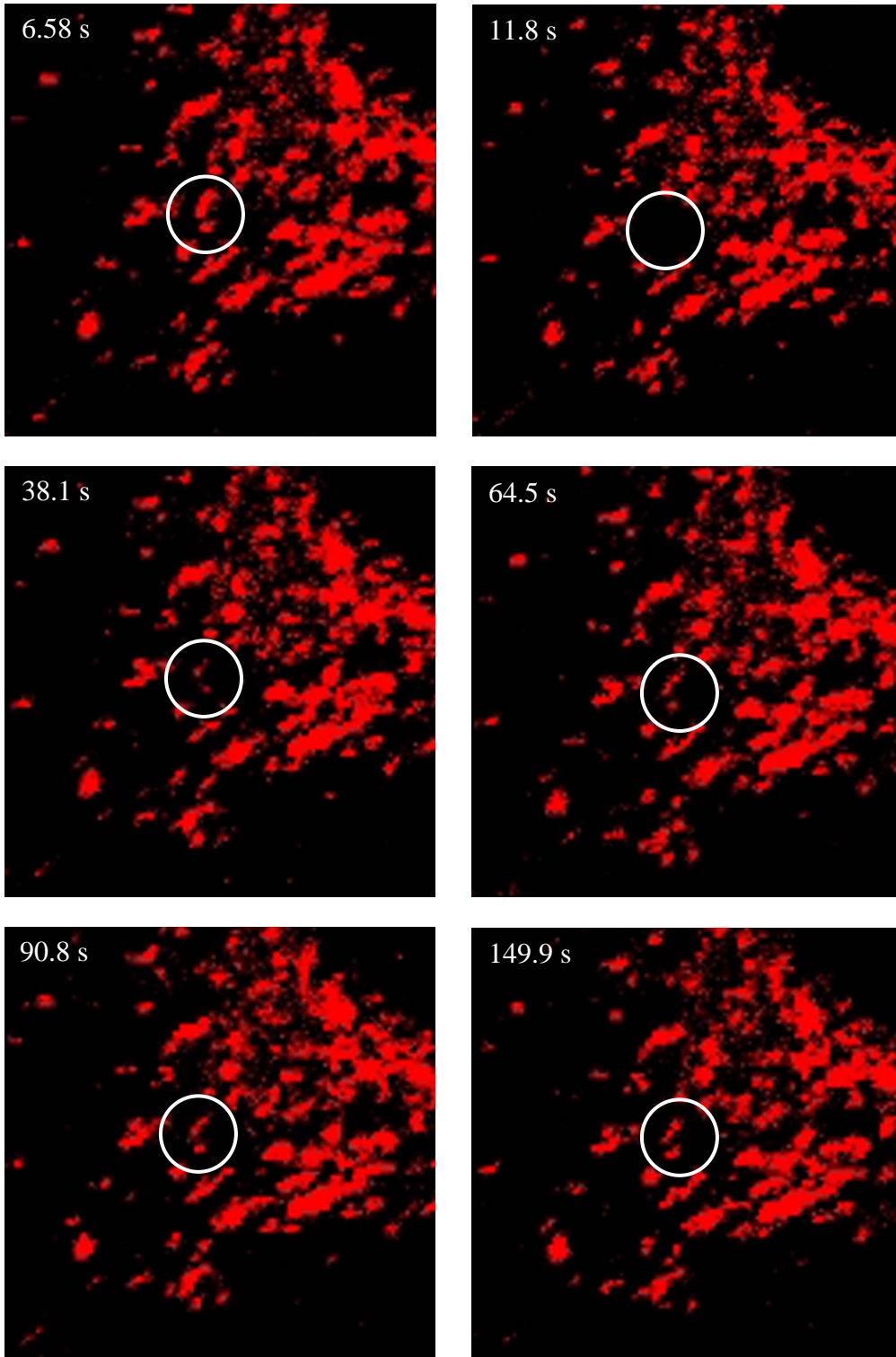
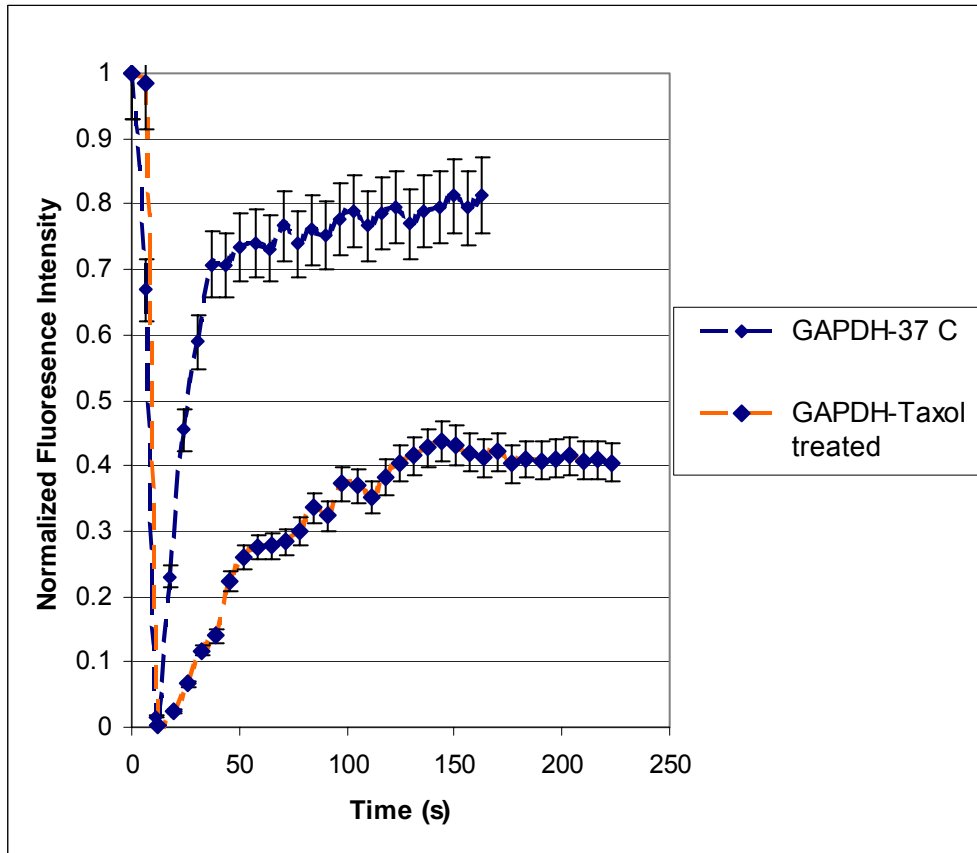


Figure 5.7 A



**Figure 5.7 B**

**Figure 5.7:** FRAP analysis of the mobility of GAPDH mRNAs at 37 °C with perturbation of microtubule network by treatment with 10  $\mu$ M concentration of Taxol for 30 minutes

- A) Image based distribution of Fluorescence intensity in a pre-bleach, immediately after bleaching and post bleach recovery for a GAPDH mRNAs in HDF cells with taxol treatment. The results indicate a partial directed recovery of the fluorescence intensity in a region of interest marked with a white circle.
- B) Average normalized fluorescence intensity in a ROI as a function of time. The result shows about 25% recovery of the bleached fluorescence signal, indicating significant reduction in mobility of the GAPDH mRNAs with taxol treatment as compared with the control experiments at 37 °C. The results also indicates that the recovery process is significantly slower with taxol treatment as compared with the control experiments at 37 °C

### **Mobility of 28-s rRNA in the cytoplasm of living cells**

Further a question remains, if what we have observed for the case of GAPDH mRNAs is representative of various RNA molecules in the cytoplasm of living cells. To make the study more generic to various class of RNAs, we selected to study the mobility of 28-s rRNA. 28-s rRNA was selected as a candidate RNA for this study, as it has a known localization (associated with ER membrane) in the cytoplasm of living cells and is a part of most abundant class of RNAs (ribosomal RNAs) in the cytoplasm. Transport of ribosomal complex in the nucleus has been studied using oligonucleotide probes targeted to 28-s rRNA in combination with a FRAP based assay ([23]). In this study, we have targeted the 28-s rRNA in the cytoplasm of cells. The study was carried out to study the effect of temperature and ATP depletion on the mobility of 28-s rRNA in the cytoplasm. The MB probe signal for 28-s rRNA has a peri-nuclear distribution, co-localized with the ER membrane in the cytoplasm (**Chapter 3**).

The results of the FRAP study to measure the mobility of 28-s rRNA in a cytoplasm are shown in **Figure 5.8**. **Figure 5.8 A** shows a representative time series of a fluorescent signal in a bleached region of interest (pre and post bleach) in the cytoplasm of living cells at 37 °C. The results show a significantly limited recovery of the fluorescence intensity in a bleached region of interest. This trend is significantly different from the recovery trend observed for GAPDH mRNAs. To further understand the differences in the mobility of 28-s rRNA, we decided to compare the recovery trend at 25 °C with that observed at 37 °C. **Figure 5.8 B** shows the time series of the pre and post bleach fluorescent signal intensity in a region of interest. The results indicate only a partial recovery as observed at 37 °C in **Figure 5.8 A**. The normalized integrated fluorescence intensity for the 28-s rRNA at 37 °C and 25 °C are shown in **Figure 5.8 C**. The results show only a partial recovery (approximately 25 %) of the fluorescence intensity. The lack of effect of temperature on the mobility of 28-s rRNA suggests that

passive processes in living cells mediate the movement of 28-s rRNA. The extent and rate of recovery observed in this case are significantly different from the trend observed for GAPDH mRNAs. These results in **Figure 5.8** and **Figure 5.2**, strongly suggests that different RNA molecules in the cytoplasm can have large differences in their mobility. These differences could be due to differences in associations in the cytoplasm of living cells. It is likely that mRNAs associated with cytoskeleton elements/ motors through different zip code domains may be more mobile than the RNAs associated with the ER membrane.

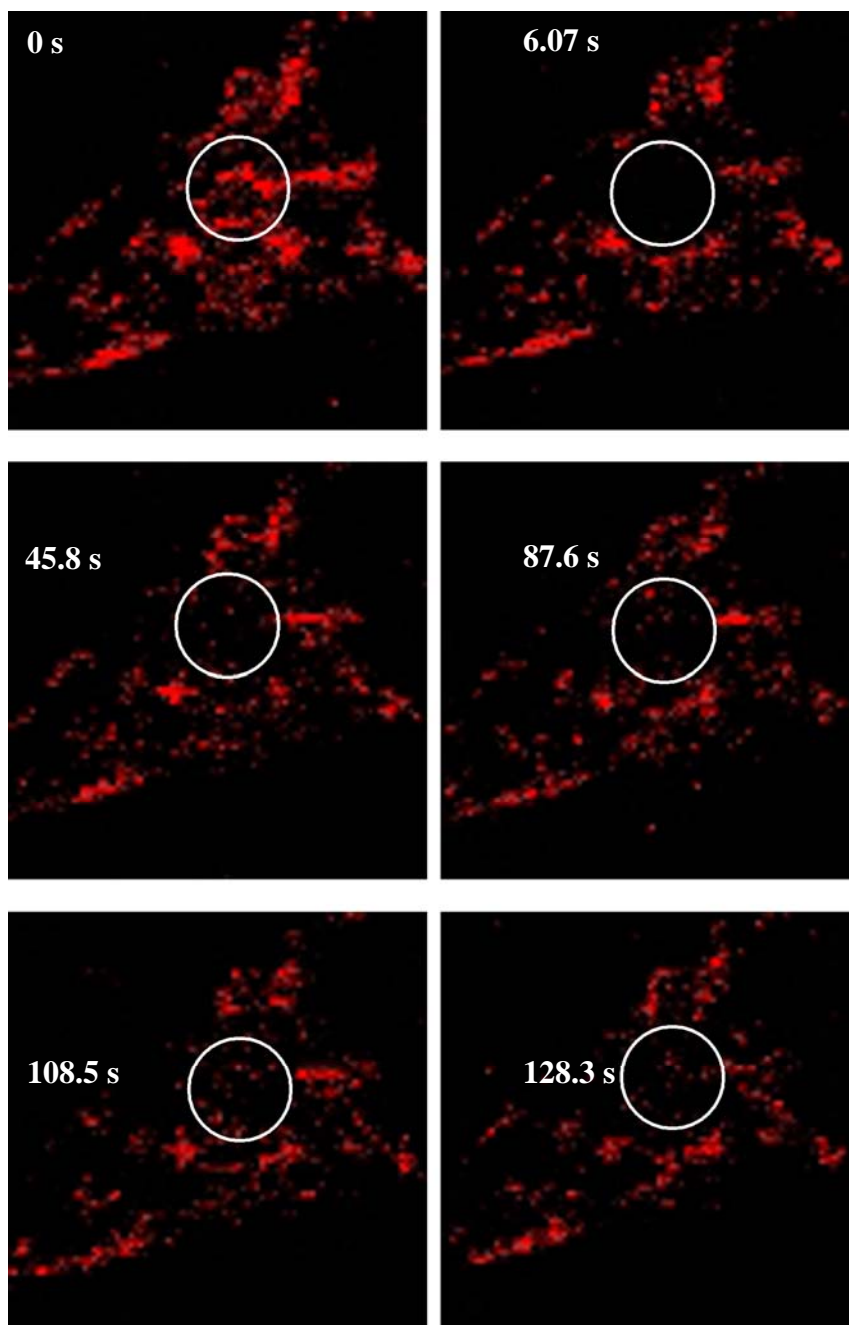


**Figure 5.8 A:** FRAP analysis of the mobility of 28-s rRNA at 37°C using MB probes. Image based distribution of Fluorescence intensity in a pre-bleach, immediately after bleaching and post bleach recovery for a 28-s rRNA in HDF cells at 37°C

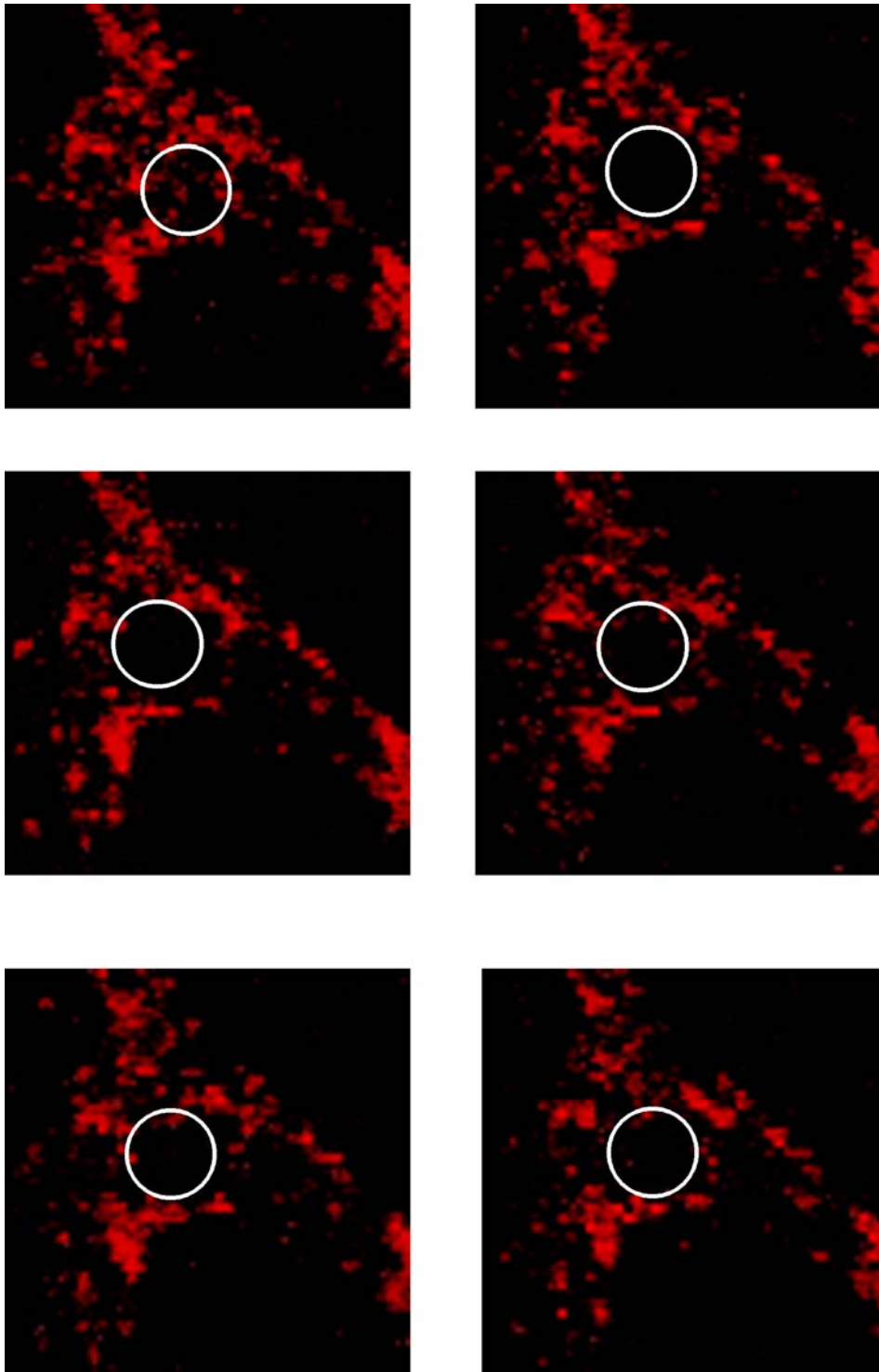


**Figure 5.8 B:** FRAP analysis of the mobility of 28-s rRNA at 25°C using MB probes  
Image based distribution of Fluorescence intensity in a pre-bleach, immediately after bleaching and post bleach recovery for a 28-s rRNA in HDF cells at 25°C

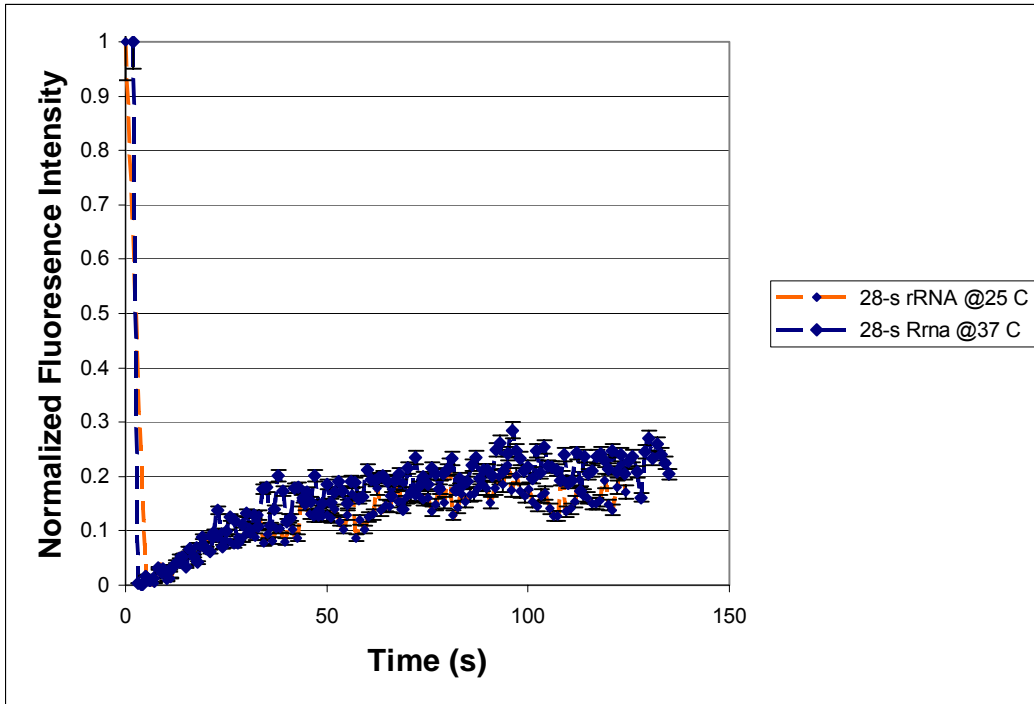


**Figure 5.8 C:** FRAP analysis of the mobility of 28-s rRNA at 37°C and 25 °C using MB probes.

C. Average normalized fluorescence intensity in a ROI as a function of time. The result shows about 20% recovery of the bleached fluorescence signal at 37 and 25 °C, indicating a reduced mobility of 28-s rRNA in living cells.

### Calculation of apparent diffusion coefficients

To quantitatively compare the above results, we calculated the apparent diffusion coefficients. These coefficients can provide us a quantitative measure of the differences in the mobility of mRNAs under different experimental conditions. The average data obtained under each experimental condition was fitted to the analytical solution of a 2-d diffusion equation in a radial geometry ([27]) using Curvefit toolbox in Matlab.

Equation:

$$F(t) = A * \exp^{-2T/t} * (I_0(2T/t) + I_1(2T/t)) + B$$

Here  $I_0$ ,  $I_1$  are modified Bessel functions,  $B$  sets the fluorescence directly after the photobleaching and summation of  $A+B$  determines the saturation value of the recovery. From this equation we obtained the value of  $T$ , which is a characteristic recovery time for the diffusion equation. This characteristic time is analogous to half-life ( $T_{1/2}$ ) time constant of a first order kinetics. The aim of this analysis is to provide a quantitative measure of the mobility of RNAs in living cells. We realize that there are multiple moieties (binding to multiple proteins, membranes, transport etc.) involved in the regulation of this process and this analysis is a first order approximation of this complex process. Thus the overall aim is not to model the process but to simulate the dynamics using a simplified analysis as outlined above.

From the fits, we obtained a characteristic time, which was further used to calculate the diffusion coefficients for each experimental condition.

Equation:

$$D_{\text{exp}} = r^2 / 4T$$

The calculated apparent diffusion coefficients are shown in **Table 5.2**. We also calculated the ratio of the diffusion coefficients with various treatments as discussed in above sections. The results indicate that the diffusion coefficient for GAPDH mRNAs

ranged from 0.052-0.03  $\mu\text{m}^2/\text{s}$ . This range is in agreement with the range of diffusivity values obtained by ([12, 14]) in the nucleus by targeting poly A mRNAs or by studying an engineered RNA molecules with multiple fluorescent proteins attached to it. Further these results are in agreement with the single particle diffusion measurements for RNAs in the cytoplasm by ([28]). Ratio of the diffusion coefficients under different treatment is in the range of 1.6-1.8, indicating a significant role played by ATP and microtubule network in the mobility of GAPDH mRNAs. Further the ratios of change in the apparent diffusivity in the cytoplasm with a change in temperature or depletion of ATP are in agreement with the results obtained by ([12, 14]).

**Table 5.2:** Apparent diffusivity of GAPDH mRNAs

Sample	Characteristic Time (s)	Apparent Diffusion Coefficient ( $\mu\text{m}^2/\text{s}$ )	Ratio of Diffusion Coefficient
GAPDH-37 °C	10.69	0.0512	
GAPDH-25 °C	18.1	0.0309	1.68
GAPDH-ATP Depleted	18.43	0.0302	1.72
GAPDH-Taxol	20.1	0.0278	1.87
GAPDH-Nocodazole	17.3	0.0327	1.59

## Summary

In this chapter, we have studied the mobility of RNA molecules in the cytoplasm of living cells. We have extended our MB based detection and imaging approaches to fundamental biophysical studies to address questions related to dynamics of RNAs in living cells. The results of this study highlighted that different RNAs can have significantly different dynamics in the cytoplasm. Using FRAP based method, we established that the mobility of GAPDH is mediated by active cellular processes which requires ATP and microtubule cytoskeleton. The recovery process after bleaching was along a directed path, which provided a further evidence to support our claims for active transport process in a cytoplasm. Using a nocodazole-based depolymerization of microtubule network, we reduced the directed recovery process in the bleached area. On the contrary using Taxol, we only observed a reduction in the extent of recovery but no significant changes in the overall shape of recovered signal compared with pre-bleach distribution. This trend clearly suggests significant role of the microtubules in mediating the mobility of RNAs.

In contrast with GAPDH studies, 28-s rRNAs have a significantly different dynamics. These ribosomal RNAs are not highly mobile in the cytoplasm of living cells. These differences could be inherently due to different localization in the cytoplasm. We need to still resolve the relationship between these differences in dynamics and the functional aspects of RNAs in the cytoplasm. To achieve this we clearly need to develop and combine multiple strategies to understand these processes. We believe that this study will provide an initial step in this direction.

## References

- [1] K. Ainger, D. Avossa, A. S. Diana, C. Barry, E. Barbarese, and J. H. Carson, Transport and localization elements in myelin basic protein mRNA, *J Cell Biol* 138 (1997) 1077-1087.
- [2] G. J. Bassell, K. L. Taneja, E. H. Kislauskis, C. L. Sundell, C. M. Powers, A. Ross, and R. H. Singer, Actin filaments and the spatial positioning of mRNAs, *Adv Exp Med Biol* 358 (1994) 183-189.
- [3] K. L. Taneja, L. M. Lifshitz, F. S. Fay, and R. H. Singer, Poly(A) RNA codistribution with microfilaments: evaluation by in situ hybridization and quantitative digital imaging microscopy, *J Cell Biol* 119 (1992) 1245-1260.
- [4] G. Aakalu, W. B. Smith, N. Nguyen, C. Jiang, and E. M. Schuman, Dynamic visualization of local protein synthesis in hippocampal neurons, *Neuron* 30 (2001) 489-502.
- [5] B. Zhou, and M. Rabinovitch, Microtubule involvement in translational regulation of fibronectin expression by light chain 3 of microtubule-associated protein 1 in vascular smooth muscle cells, *Circ Res* 83 (1998) 481-489.
- [6] A. F. Ross, Y. Oleynikov, E. H. Kislauskis, K. L. Taneja, and R. H. Singer, Characterization of a beta-actin mRNA zipcode-binding protein, *Mol Cell Biol* 17 (1997) 2158-2165.
- [7] N. Nitin, P. J. Santangelo, G. Kim, S. Nie, and G. Bao, Peptide-linked molecular beacons for efficient delivery and rapid mRNA detection in living cells, *Nucleic Acids Res* 32 (2004) e58.
- [8] P. J. Santangelo, B. Nix, A. Tsourkas, and G. Bao, Dual FRET molecular beacons for mRNA detection in living cells, *Nucleic Acids Res* 32 (2004) e57.
- [9] A. Tsuji, Y. Sato, M. Hirano, T. Suga, H. Koshimoto, T. Taguchi, and S. Ohsuka, Development of a time-resolved fluorometric method for observing hybridization in living cells using fluorescence resonance energy transfer, *Biophys J* 81 (2001) 501-515.
- [10] S. Tyagi, and O. Alsmadi, Imaging native beta-actin mRNA in motile fibroblasts, *Biophys J* 87 (2004) 4153-4162.

- [11] G. Blobel, Gene gating: a hypothesis, *Proc Natl Acad Sci U S A* 82 (1985) 8527-8529.
- [12] C. Molenaar, A. Abdulle, A. Gena, H. J. Tanke, and R. W. Dirks, Poly(A)<sup>+</sup> RNAs roam the cell nucleus and pass through speckle domains in transcriptionally active and inactive cells, *J Cell Biol* 165 (2004) 191-202.
- [13] J. C. Politz, R. A. Tuft, T. Pederson, and R. H. Singer, Movement of nuclear poly(A) RNA throughout the interchromatin space in living cells, *Curr Biol* 9 (1999) 285-291.
- [14] Y. Shav-Tal, X. Darzacq, S. M. Shenoy, D. Fusco, S. M. Janicki, D. L. Spector, and R. H. Singer, Dynamics of single mRNPs in nuclei of living cells, *Science* 304 (2004) 1797-1800.
- [15] C. Molenaar, S. A. Marras, J. C. Slats, J. C. Truffert, M. Lemaitre, A. K. Raap, R. W. Dirks, and H. J. Tanke, Linear 2' O-Methyl RNA probes for the visualization of RNA in living cells, *Nucleic Acids Res* 29 (2001) E89-89.
- [16] D. P. Bratu, B. J. Cha, M. M. Mhlanga, F. R. Kramer, and S. Tyagi, Visualizing the distribution and transport of mRNAs in living cells, *Proc Natl Acad Sci U S A* 100 (2003) 13308-13313.
- [17] M. M. Mhlanga, D. Y. Vargas, C. W. Fung, F. R. Kramer, and S. Tyagi, tRNA-linked molecular beacons for imaging mRNAs in the cytoplasm of living cells, *Nucleic Acids Res* 33 (2005) 1902-1912.
- [18] S. Tyagi, and F. R. Kramer, Molecular beacons: probes that fluoresce upon hybridization, *Nat Biotechnol* 14 (1996) 303-308.
- [19] A. Calapez, H. M. Pereira, A. Calado, J. Braga, J. Rino, C. Carvalho, J. P. Tavanez, E. Wahle, A. C. Rosa, and M. Carmo-Fonseca, The intranuclear mobility of messenger RNA binding proteins is ATP dependent and temperature sensitive, *J Cell Biol* 159 (2002) 795-805.
- [20] G. Carrero, D. McDonald, E. Crawford, G. de Vries, and M. J. Hendzel, Using FRAP and mathematical modeling to determine the in vivo kinetics of nuclear proteins, *Methods* 29 (2003) 14-28.
- [21] R. D. Phair, S. A. Gorski, and T. Misteli, Measurement of dynamic protein binding to chromatin in vivo, using photobleaching microscopy, *Methods Enzymol* 375 (2004) 393-414.

- [22] R. D. Phair, and T. Misteli, Kinetic modelling approaches to in vivo imaging, *Nat Rev Mol Cell Biol* 2 (2001) 898-907.
- [23] J. C. Politz, R. A. Tuft, and T. Pederson, Diffusion-based transport of nascent ribosomes in the nucleus, *Mol Biol Cell* 14 (2003) 4805-4812.
- [24] N. Bayer, D. Schober, E. Prchla, R. F. Murphy, D. Blaas, and R. Fuchs, Effect of bafilomycin A1 and nocodazole on endocytic transport in HeLa cells: implications for viral uncoating and infection, *J Virol* 72 (1998) 9645-9655.
- [25] J. C. Molero, J. P. Whitehead, T. Meerloo, and D. E. James, Nocodazole inhibits insulin-stimulated glucose transport in 3T3-L1 adipocytes via a microtubule-independent mechanism, *J Biol Chem* 276 (2001) 43829-43835.
- [26] S. F. Hamm-Alvarez, B. E. Alayof, H. M. Himmel, P. Y. Kim, A. L. Crews, H. C. Strauss, and M. P. Sheetz, Coordinate depression of bradykinin receptor recycling and microtubule-dependent transport by taxol, *Proc Natl Acad Sci U S A* 91 (1994) 7812-7816.
- [27] M. Weiss, Challenges and artifacts in quantitative photobleaching experiments, *Traffic* 5 (2004) 662-671.
- [28] D. Fusco, N. Accornero, B. Lavoie, S. M. Shenoy, J. M. Blanchard, R. H. Singer, and E. Bertrand, Single mRNA molecules demonstrate probabilistic movement in living mammalian cells, *Curr Biol* 13 (2003) 161-167.

## CHAPTER 6

### Peptide linked MBs for imaging of endogenous RNAs in nuclei of living cells

#### Introduction

In this study, we were interested in developing an imaging approach, which can allow for highly specific detection of RNA molecules and simultaneously imaging of multiple RNAs in nuclei of living cells. In order to achieve this goal, we have developed a bi-functional oligonucleotide probe that combines peptide-based delivery to nuclear compartment with molecular beacon based detection of RNA in nuclei of living cells. Imaging of RNAs in the nuclei can provide essential information regarding their organization, dynamics and can address basic questions related to transcription, processing of pre-mRNA, splicing and transport of RNPs from the nucleus to the cytoplasm.

Approaches to image RNA in living cells have provided new insights into localization and dynamics of RNA in context with sub-cellular organization of these macromolecules ([1],[2, 3],[4],[5]). These developments have transformed the world of static FISH based studies, and enabled the study of RNA dynamics and function in living cells. In this area of live cell imaging of RNA, there are two recently developed complementary technologies, which have advanced this area significantly.

One of these technologies is based on using a transgenic system where the fusion protein, GFP-MS2, is used to track the localization and the dynamics of RNA in living cells ([1, 6]). For this approach, two engineered plasmids are transfected, one containing a cassette expressing GFP-MS2 (MS2 is a Phage protein) and a second plasmid with a cassette expressing a RNA with MS2 binding sequences, engineered to

bind multiple MS2-GFP proteins (i.e. 20-25 MS2-GFP proteins on single RNA). This technique though very powerful in tracking RNA molecules with single molecule sensitivity, still lacks the ability to image endogenous RNAs. Further this approach may not be optimal for imaging small RNAs as linking multiple MS2-GFP fusion sites may perturb the structure and hence the function of these RNA molecules.

The other complementary approach is aimed at imaging endogenous RNA in live cells. This approach has a clear advantage as it can allow for the study of basic RNA biology in living cells. In this approach, exogenous probes with sequences complementary to RNA targets are introduced into living cells. Among this class of probes, molecular beacons (MB) are among the most promising probe technology. These probes are described in **Chapter 1 and 2**.

In our previous studies [2, 3] we have shown that using these probes we can image and detect endogenous RNA in the cytoplasm of living cells. Similarly, studies by [4, 7], have used MB probes for imaging of RNA localization in embryos during development and in living cells. In addition to MB approach, studies have been done by introducing labeled RNA in living cells ([8]) or by using linear probes to study RNA in the nuclei and the cytoplasm of living cells respectively ([8-10]). One of the major challenges in using linear probes is distinguishing a background signal from a true signal. By controlling probe affinity, concentration, and by utilizing FRET between two linear probes targeted to the same RNA, and studying highly localized RNAs, some of those challenges may be resolved. Further, in using exogenous probes, one of the major challenges is in the delivery of probes to the specific compartments of living cells. In previous studies ([7, 9-12]) probes are introduced into living cells by microinjection. Following microinjection of oligonucleotide probes into cytoplasm, it has been reported that most probes (including molecular beacons) are sequestered in the nucleus of living cells and often results in non-specific signal ([7]). Further, microinjection process is a

highly invasive and is typically limited to few cells. In this study we have developed an alternative approach, in which we utilize the active transport of MB probes from the cytoplasm to the nucleus. To achieve this, we have developed a peptide-linked molecular beacon approach in which, a single NLS (Nuclear Localization Sequence) peptide is chemically linked to the molecular beacon to form a bifunctional nanoprobe. Since NLS sequence does not have a membrane translocation function, the probes are introduced into cytoplasm by using a reversible membrane permeabilizing agent SLO (Streptolysin O). SLO makes approximately 20-25 nm reversible pores in the cholesterol rich regions of plasma membrane. Using the combined approaches of NLS and SLO mediated delivery we have demonstrated that probes delivered to the nucleus retain high signal-to-noise ratio and specificity. The major motivation for this study is to develop a multifunctional MB based toolbox to study RNA biology in the nuclear compartment of cell, to allow for detection and study of viral replication in the nucleus and in combination with our previous work ([2]), this method can provide an integrated picture of RNA distribution in both nucleus and cytoplasm of living cells.

In this study, we have chosen to study small nuclear RNP's (U1 and U2 snRNPs) and small nucleolar RNP (U3 snoRNP) as target RNAs for imaging using this bifunctional MB probes. U1 and U2 snRNPs are the key members of the splicing complex called spliceosome, a complex composed of multiple small RNAs and proteins. This complex is responsible for the splicing of nuclear pre-mRNA [13, 14]. Most of the information regarding function and organization of the splicing complexes has been developed using biochemical studies based on *in vitro* assembly of proteins and snRNPs in nuclear extracts and using *in situ* hybridization in fixed cells. To understand the function of this splicing process *in vivo*, there is a clear need to detect and image these small RNAs in living cells. U3 snoRNP is one of the best characterized small nucleolar RNP involved in biogenesis of ribosomes [15, 16]. This RNP is involved in

endonucleolytic cleave events of various pre-rRNA that leads to generation of 18-s pre-RNA. Since these small nuclear RNAs have been previously studied ([13, 14, 16-21]) using *in situ* hybridization technique in fixed cells, the results in our study are directly compared with the fixed cell studies to validate our observations in living cells.

For delivery of MBs in nuclei of living cells, we have used a combination of SLO based passive delivery of probes to cytoplasm along with NLS mediated transport of probes from the cytoplasm to the nucleus of cells. NLS sequence selected in this study is based on the SV40 NLS domain [22, 23]. The sequence and design of peptide-linked MB are shown in **Figure 6.1**. After SLO based delivery of probes to the cytoplasm, the single NLS peptide-linked with MB probe was effective in delivering the probes to nuclei of living cells.

## **Material and Methods**

**Molecular beacon** probes (as shown in **Table 6.1**) with modification in the stem region (dT- NH<sub>2</sub> on the quencher side) were synthesized by MWG Biotech, NC and Biosearch Corp, CA. Molecular beacons were designed with regular DNA chemistry (De-oxy ribonucleotide backbone). The probes were purified using double HPLC. Probes for U1, U2 snRNPs and U3 snoRNPs were designed with Cy3 fluorophore and BHQ-II quencher pair. U1 snRNP probe was also designed with Cy5 fluorophore and BHQ-III quencher. In all MB designs, quencher end was the 3' end, while a fluorescent dye was conjugated to the 5- end of MB.

### **Peptides**

SynPep Inc synthesized the NLS peptide (99% purity) as shown in **Table 6.1**. The peptide sequence was modified at its carboxy terminus to introduce cysteine residue. The spacer (Ahx) equivalent to length of 1 amino acid was introduced between the carboxy terminus residue of NLS sequence and cysteine residue.

## **Cell Line**

All experiments in this study were carried out using HeLa cells. This cell line has been used in several nuclear transport studies ([22]) and also in study of various snRNPs in fixed cells [13, 14]. HeLa cells were cultured using Dulbecco's modified Eagle's medium + fetal calf serum (10%) + horse serum (2.5 %). HeLa cells were plated in T-25 (cell culture flask) using 1:10 dilution after each splitting cycle. A batch of HeLa cells was cultured only for about 10 splitting cycles. For imaging experiments, cells were plated on 4 well or 8 well Nalgene-Nunc chamber cover slides 24 hours prior to the experiment.

## **Chemicals**

All chemicals (1X and 10 X PBS, TCEP, Streptolysin O (SLO), DMSO) except bio-conjugation reagents (bi-functional crosslinker) used in this study were bought from Sigma Aldrich Corp. The bio-conjugation reagent sulfo-SMCC was purchased from Pierce Biotech Corp.

## **Peptide Conjugation**

In the direct linkage approach shown in **Figures 6.1**, a molecular beacon was modified at the same nucleotide position on the quencher-arm using modified nucleotide dT-amine group with a 6-carbon spacer. To generate stable linkages using a chemical bridge between a peptide and a molecular beacon, the NLS peptide was modified with a cysteine group at its C terminus. Amine modified molecular beacon on the beacon was reacted with a heterofunctional crosslinker sulfo-SMCC (Pierce Biotech) for a period of 3 hours at room temperature with intermediate shaking. The reaction was carried out with 1x (2  $\mu$ m) molecular beacon and 20x (40  $\mu$ m) sulfo-SMCC in PBS buffer. After 3 hours, the excess of sulfo-SMCC was removed from the reaction mixture using centrifugal filter (YM-10) with a cut off of 10 kDa. The resultant solution was brought to same initial

volume by adding PBS and reacted with 2x (4  $\mu$ m) concentration of Cys modified NLS peptide for overnight at room temperature. Following this reaction, peptide linked molecular beacon complex was dialyzed overnight using Slide-A-Lyzer Dialysis Unit, 10K MWCO (Pierce Biotech Inc., Rockford, IL) to remove unconjugated peptide. To significantly reduce the probability of forming beacon-beacon conjugates, a higher (2x) concentration of peptides was used compared with that of beacons. Further, the positive charged peptides helped prevent the formation of a disulfide bridge between two peptides.

### **Solution assay to measure the signal-to-background ratio of modified and unmodified Molecular Beacons**

Measurement of signal-to-background ratio of peptide linked molecular beacons and unmodified beacons were carried out using a SAFIRE microplate monochromator reader (TECAN, Austria). To determine the signal-to-background ratios, 200 nM conventional and peptide-linked molecular beacons were mixed with 200 nM of complementary target respectively in the microplate reader, and the fluorescence intensity at equilibrium (10 minute incubation time) was recorded. The fluorescence signal of each molecular beacon type (conventional and peptide-linked) in the absence of target was recorded as background signal.

### **Cellular delivery of peptide-linked Molecular Beacons**

For cellular delivery of peptide-linked molecular beacons, experiments were carried out using HeLa cells (ATCC, VA). For imaging experiments cells were cultured in a 4 or 8-well Nalge Nunc culture plate with a glass coverslip bottom in their respective cell culture media (as described above) for 24 hours before the experiment. For

delivery, cells were treated with activated streptolysin O (SLO) for a period of 10 minutes as described in [3], peptide-linked molecular beacons were mixed (1  $\mu$ m concentration) with activated solution of streptolysin O in serum free media and incubated with the specific cells at 37°C for 10 minute period. After this incubation period, the medium was changed to regular serum rich media. The cells were incubated for a period of 1 hour following this change in medium. Following 1 hour of incubation, cells were imaged live using confocal microscope (Axiovert LSM-100, Zeiss). For detection and imaging of localization of U1, U2 snRNPs and U3 snoRNP we used laser excitation at 543 nm with emission detection using a band pass filter from 560-610 nm. For imaging co-localization of U1 and U2 snRNPs we used both 543 nm and 640 nm laser excitation. The signal was detected using band pass filter from 560-610 nm for Cy3 signal detection and long pass filter from 660 nm for Cy5 signal detection.

### **Fixed cell studies**

HeLa cells were cultured in 8-well chambered coverslides for 24 hours in normal growth medium (FGM-2 Cambrex Co.) and then washed with 1x PBS (without Ca or Mg). The slide was fixed in 4% paraformaldehyde buffer with 10% acetic acid for 10 minutes. After removing the fixative, the slides were incubated overnight with 70% ethanol at 4 °C to improve the permeability of fixed cells. In-situ hybridization assays were then performed by first washing the slides for 5 minutes in 1x PBS and hybridizing them overnight at 37°C in 1x PBS (no Ca or Mg) containing 100 nM of MB probes targeting U1, U2 snRNAs and U3 snoRNAs along with RNase free BSA as recommended in protocol by Singer lab. After removing the hybridization solution with washing and adding 1x PBS, the cells were imaged.

## Results and Discussion

### Design of peptide linked MB

In this study we have designed and synthesized the peptide-linked molecular beacons for targeting U1, U2 snRNPs and U3 snoRNPs, as well as a molecular beacon with a 'random' probe sequence. The specific oligonucleotide sequences of these MBs and the sequence of NLS peptide are shown in **Table 6.1**. The design of these probes to target the segments of RNPs in nuclei of living cells are based on previous in-situ studies in fixed cells with linear oligonucleotide targets [13, 14, 17, 19]. Since linear oligonucleotide probes used in previous FISH studies were able to access the target in fixed cells, the same target sequences were used to generate loop domains for design of MBs. To achieve a stable hairpin structure (MBs structure) and appropriate melting temperature (based on Mfold predictions), the stem domains (complementary base paired regions at 3' and 5' ends of the probe) were added to the linear oligonucleotide sequences. These regions are underlined in **Table 6.1**. The 'random' beacon was designed as a negative control, with a 17-base probe sequence that does not have any match in the mammalian genome [2]. The probes used in this study are of DNA chemistry (Deoxy-nucleotide backbone). The dye and quencher pairs (Cy3-BHQ-II and Cy5-BHQ-III) were selected to ensure effective quenching of the probes in their unhybridized state (hairpin shape).

The conjugation approach was developed to link MBs with an NLS sequence as shown in **Figure 6.1**. The MBs were modified in the stem domain on the quencher arm, to introduce a functional group, a dT-(c6)-NH<sub>2</sub>. The details of the conjugation chemistry and the purification are discussed in the material and methods section. This design is similar to the approach developed in our previous study ([2]).

**Table 6.1:** The design of NLS peptide-linked molecular beacons

---

*U3 snoRNA Molecular Beacon (5'-3')*

Cy3-CGACCGGCTTCACGCTCAGGGG(dT-C6-NH<sub>2</sub>)CG-BHQ2

---

*U1 snRNA Molecular Beacon (5'-3')*

Cy3-GCAGCCTGCCAGGTAAGTATGC(dT-C6-NH<sub>2</sub>)GC-BHQ2

---

*U2 snRNA Molecular Beacon (5'-3')*

Cy3-CGAGCACAGATACTACACTTGGC(dT-C6-NH<sub>2</sub>)CG-BHQ2

---

*Negative Control Molecular Beacon (5'-3')*

Cy3-CGACGCGACAAGCGCACCGATACG(dT-C6-NH<sub>2</sub>)CG-BHQ2

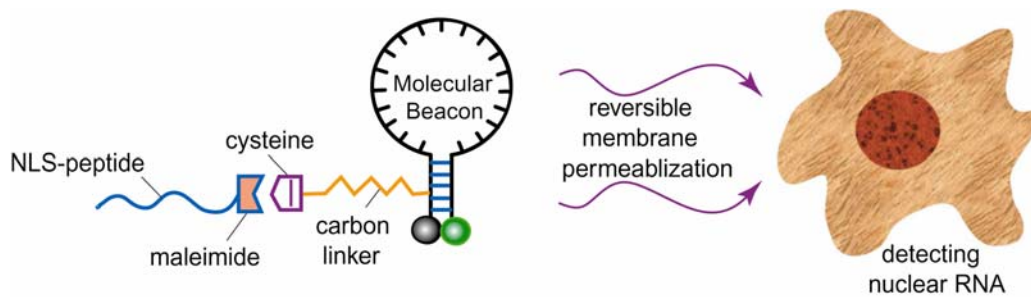


**Figure 6.1:** Shows a schematic design of a peptide linked Molecular beacon and its delivery into the nucleus of living cells. The NLS peptide is covalently linked to the MB using a modified (dT- C6-NH<sub>2</sub>) at the third base from the 3' end on its quencher arm. The NLS linked MBs are delivered into cytoplasm of living cells using a reversible membrane permeabilization agent Streptolysin O (SLO). Following the delivery of probe into the cytoplasm, the NLS peptide actively transport the MB-peptide complex to the nucleus of living cells.

### **Signal-to-Noise ratio of peptide-linked molecular beacons**

To determine the possible effect of peptide conjugation on the function of MB probes, in-solution hybridization assays were carried out to compare the S/N ratio (signal-noise ratio) of the peptide-linked molecular beacons with unmodified beacons. When the positively-charged NLS peptide is conjugated to a molecular beacon, the electrostatic interactions of the peptide with the negatively-charged hairpin, oligonucleotide backbone may interfere with the probe-target (RNA) binding. As shown in **(Figure 6.2)** there is no significant change in the S/N ratio for each MB probe design after modification with an NLS peptide. This result is in agreement with our earlier results with Tat peptide-linked MBs for cytoplasmic delivery ([2].)

### **Imaging of U3 snoRNP, U1 and U2 snRNPs in the nucleus of living cells using multifunctional probes**

To demonstrate the delivery of peptide linked MBs, specific detection and imaging of an endogenous RNA in the nuclei of living cells, we have targeted the small nucleolar RNA (U3 snoRNA) and small nuclear RNAs (U1 and U2 snRNAs) in nucleus of living cells. NLS- linked MB probes targeted to respective RNAs were introduced into cytoplasm by using Streptolysin O (SLO) based reversible permeabilization. The result for the detection of U3 snoRNP in the nucleus of a living cell is shown in **Figure 6.3 A**. The result shows a very discrete localization of signal in the nucleus of living cell with no detectable signal in the cytoplasm. The localized signal was detected in the nucleolus and discrete peri-nucleolar foci. The results obtained for U3 snoRNA imaging are in agreement with the results obtained in previous studies ([9, 13, 15, 18, 24]).

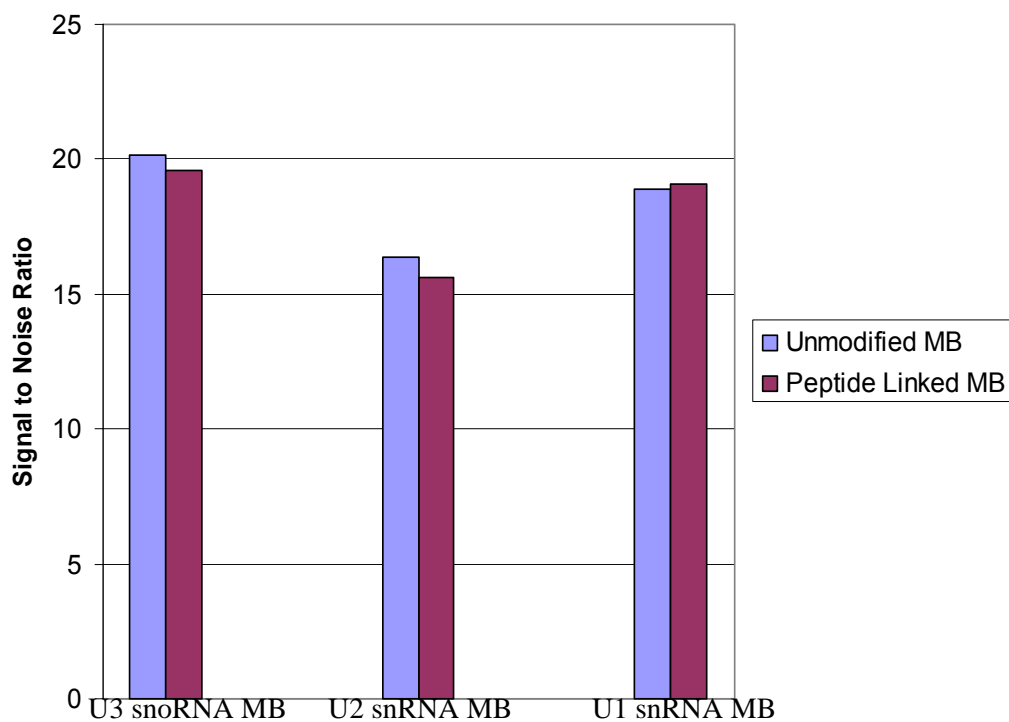


**Figure 6.2:** Signal to-noise ratio of the NLS linked Molecular Beacons and the unmodified molecular beacons. The NLS linked MBs and the unmodified MBs were hybridized with complementary oligonucleotide targets (2 x concentration) at room temperature for 5 minutes. In addition the control wells had MB probes without any oligonucleotide target. MBs hybridized with the complementary target provided the numerical value of the signal intensity and the MBs without any target provided the background noise from these probes. The ratio of the signal to noise for the three MB probes with and without modification are shown in the plot. The plot shows no significant difference in the signal to noise ratio of MB probes with and without peptide attachment.

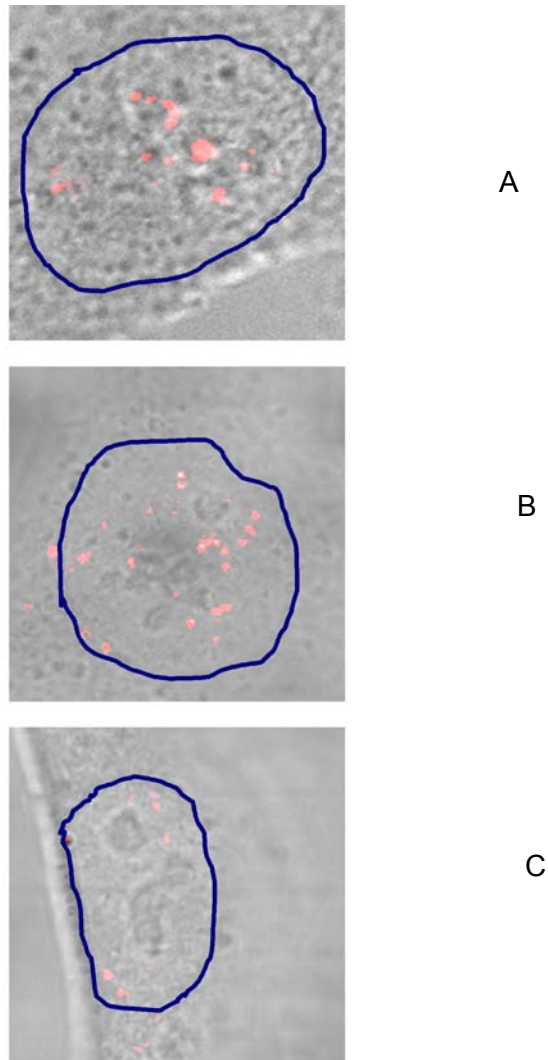


**Figure 6.3:** Imaging of U3 snoRNA, U1 and U2 snRNAs in the nucleus of living cells using NLS linked MB probes respectively.

(A): Imaging of U3 snoRNA in the nucleus of a living cell using the NLS –linked MB’s. Most of the MB signal was obtained in the nucleolar and discrete peri-nucleolar region in the nucleus, with no signal in the cytoplasm.

(B): Imaging of U1 snRNAs in the nucleus of a living cell using NLS-linked MB’s. The result shows MB signal in the nucleoplasm of a living cell excluding the nucleolus. The localized foci of U1 snRNPs are widely distributed in the nucleoplasm, with few foci at discrete peri-nucleolar regions.

(C): Imaging of U2 snRNAs in the nucleus of a living cell using NLS-linked MB’s. The result shows MB signal at discrete foci in the nucleoplasm of living cells. The overall signal of U2 snRNAs is significantly lower than the signal obtained from U1 snRNAs. In addition few discrete foci were also observed in the peri-nuclear region of the cytoplasm, similar to the U1 snRNAs.

These studies have shown U3 snoRNA to be localized in the nucleolus and in certain cases associated with cajal bodies. U3 snoRNA is processed in cajal bodies prior to its transport and localization to nucleolus. Furthermore, we have observed a heterogeneous localization (punctate pattern) of U3 snoRNA in some nucleoli and a uniform fluorescence pattern in others. This observation is in agreement with the results obtained by ([18]).

The result of detection and imaging of U1 snRNPs using NLS peptide-linked MBs is shown in **Figure 6.3 B**. The result shows a discrete localization of U1 snRNPs in the nucleoplasm of HeLa cells clearly excluding the nucleolus. The localized foci of U1 snRNPs are widely distributed in the nucleoplasm, with few foci at discrete peri-nucleolar regions. This widespread localization of U1 snRNPs in the nucleoplasm is in agreement with previous studies. ([13, 14, 17, 20]). These studies have shown U1 snRNPs to be associated with both cajal bodies (processing of U1 snRNP after its import from cytoplasm) and speckles (site of assembly of splicing complex) sites in fixed cells. In addition to widespread nucleoplasmic localization, we also observed a localized signal at discrete spots in the cytoplasmic, peri-nuclear region. This signal indicates the fraction of U1 snRNPs in the cytoplasm. In the case of U1 and other snRNPs (excluding U6), they are exported from nucleus to the cytoplasm for assembly of snRNP complexes and processing of their 5' cap. After which, they are imported back into the nucleus, and are believed to be further processed in cajal bodies before being transported to speckle sites ([25]). Detection of both populations (nuclear and cytoplasmic) of U1 snRNPs suggests high sensitivity of this approach.

The result of detection and imaging of U2 snRNPs is shown in **Figure 6.3C**. The result shows localization at discrete foci in the nucleoplasm, excluding the nucleoli. In contrast to widespread localization of U1 snRNP's in the nucleoplasm, U2 snRNP has a few discrete foci in the nucleus. This observation validates the result that the U2 snRNAs

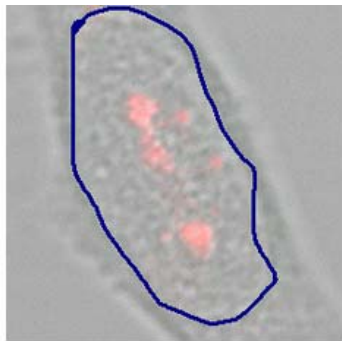
are less abundant than the U1 snRNAs (Dreyfus et al, 2002). Further the localization pattern in this result is in agreement with previous studies ([13, 14, 19, 21]). In addition, a discrete signal was also observed in the peri-nuclear region of the cytoplasm. The U2 snRNPs, similar to the U1 snRNPs, are also exported to the cytoplasm for processing.

These results demonstrate that single NLS peptide-linked MB probes are transported from cytoplasm to the nucleus. To highlight high specificity of these probes in nuclei of living cells, we have shown the detection of snoRNAs and snRNAs with different distributions (nucleoplasm vs nucleolus) in the nucleus and the difference in transcription levels (U1 snRNA > U2 snRNA) of these RNPs. Furthermore, based on single-probe based approach, we cannot absolutely conclude whether U2 snRNP/ U1 snRNPs are restricted to cajal bodies, or the pattern observed represents both cajal bodies and speckle sites. In live cell imaging studies, this will require us to simultaneously label some of the proteins in the speckle domains such as SF2/ASF ([26]). The combination of fusion proteins with an exogenous probe can provide valuable insight into dynamics and function of RNAs in living cells. Future studies will be designed to address some of the issues in this direction.

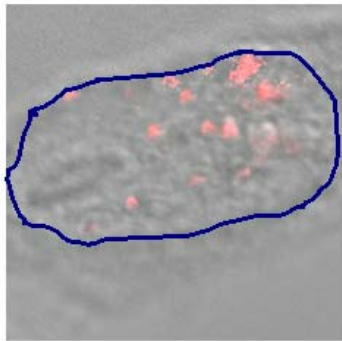
#### ***In-situ hybridization in fixed cells***

To validate observations in live cell studies (**Figure 6.3**), we carried out *in-situ* hybridization in fixed cells. The cells were fixed and permeablized according to the protocol described in the Material and Methods section. The results for the detection of the U3 snoRNAs in fixed samples are shown in **Figure 6.4 A**. The results clearly show localization of U3 snoRNAs in the nucleoli, similar to the results in live cells. The results for the detection of U1 snRNAs and U2 snRNAs are shown in **Figure 6.4 B** and **6.4 C** respectively. The results clearly show localization of both these snRNAs in the nucleoplasm excluding the nucleolus. Further U1 snRNAs are more wide spread in the nucleoplasm as compared to few discrete foci in the case of U2 snRNAs. These

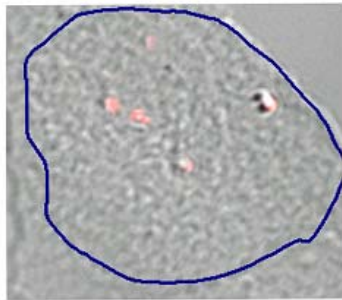
observations are in agreement with the results obtained in live cell studies. Further in fixed cells, we could not detect any localized signal of these snRNAs in the cytoplasm as was observed for live cells studies. This could be due to loss of RNAs during fixation and washing processes or due to lack of accessibility of target sequences. In conclusion, the results obtained by *in situ* studies are in agreement with the ones obtained from live cell assays.



A



B



C

**Figure 6.4:** Fluorescent *in situ* hybridization (FISH) to image the U3 snoRNA, U1 and U2 snRNAs in the nucleus of fixed cells. Cells were fixed using the protocol from Singer's lab for a detection of RNAs in the nucleus.

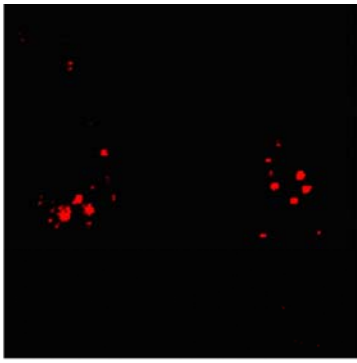
(A) *In situ* hybridization for U3 snoRNA

(B) *In situ* hybridization for U1 snRNA

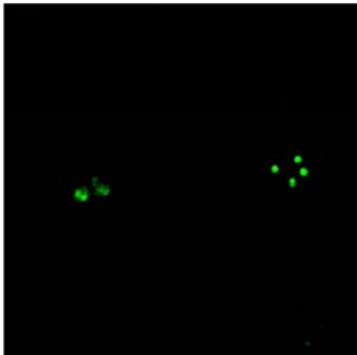
(C) *In situ* hybridization for U2 snRNA

### **Co-localization of U1 and U2 snRNAs in living cells**

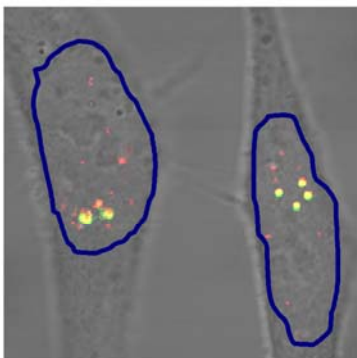
U1, U2 and other family members of snRNP family and other non-snRNP proteins form a splicing complex responsible for trans-splicing of pre-mRNA transcripts [17]. The assembly of this complex requires various snRNPs to come together and form a complex with defined structure and composition. The assembly and working of this complex is till date only characterized by *in vitro* assembly of snRNPs and proteins [17, 20]. There are several unknown steps involved in the assembly and working of spliceosome complex, e.g., it is not clear at what stage U1 and U2 snRNPs form a complex in living cells? To address this issue we will need a probe, which can non-invasively detect complex formation in living cells, have an ability to multiplex, provide high S/N ratio and specificity in detection. As an initial step in this direction, we have studied the co-localization of U1-U2 snRNAs in living cells to demonstrate the ability to simultaneously detect multiple RNAs in the nuclei of living cells. The results of this study are shown in **Figure 6.5 A-C**. The results show clear co-localization of snRNAs at discrete foci in the nucleoplasm of living cells. Further the results also show a more widespread distribution of U1 snRNP in addition to the co-localized foci of U1-U2 snRNAs. This result is in agreement with the earlier results (**Figure 6.3 B-C**). As mentioned earlier, we could not absolutely conclude whether the detected co-localization of U1-U2 snRNAs is in cajal bodies or speckles exclusively. This co-localized pattern may be a initial step towards the formation of U1-U2 complex required for spliceosomal assembly.



A



B



C

**Figure 6.5:** Imaging of Co-localized U1 and U2 snRNAs in the nucleoplasm of living cells using peptide linked Molecular Beacons.

(A): Image shows the fluorescent signal from the U1 snRNA targeted by NLS linked MB in living cells.

(B): Image shows the fluorescent signal from the U2 snRNAs targeted by NLS linked MB in living cells

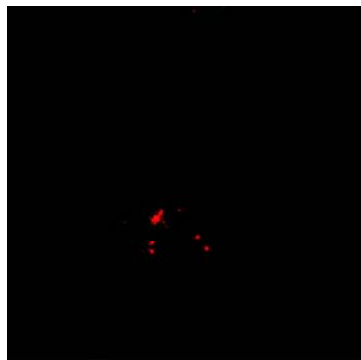
(C): The image shows the overlay of the two channels to show the co-localization of U1 and U2 snRNAs in the nucleus of living cells. The result shows co-localization of U1 and U2 snRNAs at discrete foci in nucleoplasm. In addition to co-localized foci, U1 snRNAs can also be observed at other foci in the nucleoplasm.

To our knowledge this is the first observation of co-localization of U1-U2 snRNAs in living cells. The results shown in this study are in agreement with the *in-situ* results obtained in fixed cells (17).

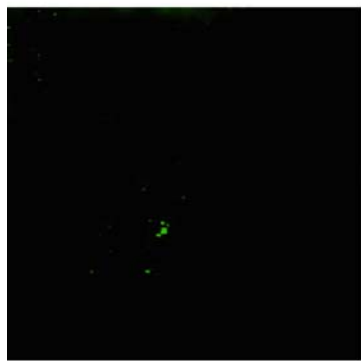
The question that remains to be resolved with regard to use of probes is what percentage of RNA population is detected with this method? This limitation can be due to limited accessibility of our probe to a given target in certain states, and an increased off-rate in certain conditions, such as when the probe is targeted to a protein-binding site. In this study we have observed widespread localization of U1 snRNPs and restricted localization of U2 snRNP in the nucleoplasm. This can potentially be true localization of these snRNPs or it may reflect only a fraction, which is accessible with the given probe. Given that we have seen similar patterns of localization in fixed and live cells, it is likely that we are able to access a large proportion of the population. This issue is a crucial factor in developing a comprehensive understanding of their organization and function.

#### ***In-situ* Hybridization of co-localization in fixed cells**

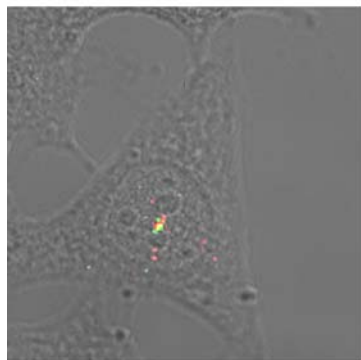
To validate our observations of co-localization of U1-U2 snRNAs in living cells, we have performed *in situ* hybridization in fixed cells using probes targeted to U1 and U2 snRNAs. The results of *in situ* hybridization are shown in **Figure 6.6 A-C**. The results clearly show discrete foci of co-localized U1 and U2 snRNAs. In addition to this, we also observed more widespread localization of U1 snRNAs in the nucleoplasm of fixed cells. The results obtained by *in situ* hybridization in fixed cells are in agreement with the results obtained from live cell studies.



A



B



C

**Figure 6.6:** Fluorescent in situ hybridization to validate the co-localization of U1 and U2 snRNAs in fixed cells. The cells were fixed using the same protocol as in Figure 4.

(A): Detection of U1 snRNAs in fixed cells using the same MB probes as in Figure 6.5(A) using the same imaging conditions as in Figure 6.5(A)

(B): Detection of U2 snRNAs in fixed cells using the same MB probe as in Figure 6.5(B) using the same imaging conditions as in Figure 6.5(B)

(C): Overlay of two channels to show the co-localization of U1 and U2 snRNAs in the nucleoplasm of fixed cells.

### Control Studies in living cells

In order to determine the level of non-specific interactions of MB probes in living cells, we designed control studies with 'random' molecular beacons. These molecular beacons have sequences with no target in the human genome. **Figures 6.7 A**, shows a result of non-specific signal from the delivery of NLS peptide-linked 'random' beacon. The results show no detectable signal under the same imaging conditions as in case of **Figure 6.3**. This result clearly indicates that these probes delivered to cells using the combination of SLO and NLS peptide maintain their specificity and are stable during the timeframe of these studies.

Further to prove that active transport from cytoplasm to the nucleus is necessary to transport significant amount of probes to the nuclei of living cells, we did a control study in which the probes targeted to U1 snRNAs and U3 snoRNA were delivered into cytoplasm using SLO without any NLS peptide conjugated to them. These snRNAs were selected for the control study as their expression level is higher as compared with U2 snRNAs. **Figure 6.7 B** shows the result of U1 snRNAs detection using SLO delivered MB probe. The result shows discrete foci in the peri-nuclear region of the cytoplasm without any detectable signal in the nucleus. Similarly **Figure 6.7 C** shows the results of U3 snoRNAs using the same approach as above. In this case we were not able to detect any significant signal either in the cytoplasm or in the nucleus of cells. This clearly indicates that without an NLS sequence attached to the MB probes, they are not actively transported to the nuclei of living cells. Since U1 snRNAs are exported from nucleus for their processing before being re-imported back to the nucleus, their detection in cytoplasm is in agreement with our earlier results, which also showed discrete foci in the peri-nuclear region. In case of U3 snoRNAs, which are only present in the nucleus, we are not able to detect any signal without attaching NLS sequence to the MB probe.



**Figure 6.7:** Negative Controls to validate the measurements made in this study. (A) The background signal from the delivery of a 'random' sequenced probe to the nucleus of living cells. This was designed to test the possibility of non-specific opening of MB beacons during the delivery to the nucleus. Result shows no significant background with the 'random' probe, which has no target in the mammalian genome. (B-C) The signal obtained from the delivery of the MBs with SLO without an NLS peptide for its active transport to the nucleus. This study was designed to demonstrate that the active transport is essential for delivery of MB probes to the nucleus and detection of target RNAs. (B): Shows the signal obtained by delivery of the MB probe without NLS peptide targeting U3 snoRNA in living cells. (C): Shows the signal obtained by delivery of the MB probe without NLS peptide targeting U1 snRNA in living cells.

## **Summary**

In this study, we have developed a method, which allows for direct imaging of endogenous RNAs in the nuclei of living cells. This approach combines a molecular beacon with NLS peptide, for efficient delivery of oligonucleotide probes to the nucleus. Using this approach, we have imaged with high specificity and sensitivity the distribution of small nuclear and small nucleolar RNAs. This method in combination with our previous study to detect RNA in the cytoplasm of living cells, allows for direct imaging of distribution and organization of RNA from the birth site in nucleus to its journey in the cytoplasm. In combination, with biophysical approaches such as FRAP/ FCS, this approach can allow for study of transport of RNAs from the nucleus to the cytoplasm. Further, in combination with labeled proteins, this approach can be used to study the dynamics and function of RNP complexes in the nuclei of living cells.

## References

- [1] Y. Shav-Tal, X. Darzacq, S. M. Shenoy, D. Fusco, S. M. Janicki, D. L. Spector, and R. H. Singer, Dynamics of single mRNPs in nuclei of living cells, *Science* 304 (2004) 1797-1800.
- [2] N. Nitin, P. J. Santangelo, G. Kim, S. Nie, and G. Bao, Peptide-linked molecular beacons for efficient delivery and rapid mRNA detection in living cells, *Nucleic Acids Res* 32 (2004) e58.
- [3] P. J. Santangelo, B. Nix, A. Tsourkas, and G. Bao, Dual FRET molecular beacons for mRNA detection in living cells, *Nucleic Acids Res* 32 (2004) e57.
- [4] D. P. Bratu, B. J. Cha, M. M. Mhlanga, F. R. Kramer, and S. Tyagi, Visualizing the distribution and transport of mRNAs in living cells, *Proc Natl Acad Sci U S A* 100 (2003) 13308-13313.
- [5] C. Molenaar, A. Abdulle, A. Gena, H. J. Tanke, and R. W. Dirks, Poly(A)<sup>+</sup> RNAs roam the cell nucleus and pass through speckle domains in transcriptionally active and inactive cells, *J Cell Biol* 165 (2004) 191-202.
- [6] Y. Shav-Tal, R. H. Singer, and X. Darzacq, Imaging gene expression in single living cells, *Nat Rev Mol Cell Biol* 5 (2004) 855-861.
- [7] S. Tyagi, and O. Alsmadi, Imaging Native  $\beta$ -Actin mRNA in Motile Fibroblasts, *Biophys J* 87 (2004) 4153-4162.
- [8] J. Wang, L. G. Cao, Y. L. Wang, and T. Pederson, Localization of pre-messenger RNA at discrete nuclear sites, *Proc Natl Acad Sci U S A* 88 (1991) 7391-7395.
- [9] C. Molenaar, S. A. Marras, J. C. Slats, J. C. Truffert, M. Lemaitre, A. K. Raap, R. W. Dirks, and H. J. Tanke, Linear 2' O-Methyl RNA probes for the visualization of RNA in living cells, *Nucleic Acids Res* 29 (2001) E89-89.

- [10] A. Tsuji, H. Koshimoto, Y. Sato, M. Hirano, Y. Sei-Iida, S. Kondo, and K. Ishibashi, Direct observation of specific messenger RNA in a single living cell under a fluorescence microscope, *Biophys J* 78 (2000) 3260-3274.
- [11] J. Perlette, and W. Tan, Real-time monitoring of intracellular mRNA hybridization inside single living cells, *Anal Chem* 73 (2001) 5544-5550.
- [12] J. C. Politz, R. A. Tuft, T. Pederson, and R. H. Singer, Movement of nuclear poly(A) RNA throughout the interchromatin space in living cells, *Curr Biol* 9 (1999) 285-291.
- [13] M. Carmo-Fonseca, R. Pepperkok, B. S. Sproat, W. Ansorge, M. S. Swanson, and A. I. Lamond, In vivo detection of snRNP-rich organelles in the nuclei of mammalian cells, *Embo J* 10 (1991) 1863-1873.
- [14] S. Huang, and D. L. Spector, U1 and U2 small nuclear RNAs are present in nuclear speckles, *Proc Natl Acad Sci U S A* 89 (1992) 305-308.
- [15] A. Narayanan, J. Eifert, K. A. Marfatia, I. G. Macara, A. H. Corbett, R. M. Terns, and M. P. Terns, Nuclear RanGTP is not required for targeting small nucleolar RNAs to the nucleolus, *J Cell Sci* 116 (2003) 177-186.
- [16] W. Speckmann, A. Narayanan, R. Terns, and M. P. Terns, Nuclear retention elements of U3 small nucleolar RNA, *Mol Cell Biol* 19 (1999) 8412-8421.
- [17] M. Carmo-Fonseca, R. Pepperkok, M. T. Carvalho, and A. I. Lamond, Transcription-dependent colocalization of the U1, U2, U4/U6, and U5 snRNPs in coiled bodies, *J Cell Biol* 117 (1992) 1-14.
- [18] A. G. Matera, K. T. Tycowski, J. A. Steitz, and D. C. Ward, Organization of small nucleolar ribonucleoproteins (snoRNPs) by fluorescence in situ hybridization and immunocytochemistry, *Mol Biol Cell* 5 (1994) 1289-1299.
- [19] A. G. Matera, and D. C. Ward, Nucleoplasmic organization of small nuclear ribonucleoproteins in cultured human cells, *J Cell Biol* 121 (1993) 715-727.
- [20] D. L. Spector, G. Lark, and S. Huang, Differences in snRNP localization between transformed and nontransformed cells, *Mol Biol Cell* 3 (1992) 555-569.
- [21] K. P. Smith, and J. B. Lawrence, Interactions of U2 gene loci and their nuclear transcripts with Cajal (coiled) bodies: evidence for PreU2 within Cajal bodies, *Mol Biol Cell* 11 (2000) 2987-2998.

[22] C. M. Feldherr, R. E. Lanford, and D. Akin, Signal-mediated nuclear transport in simian virus 40-transformed cells is regulated by large tumor antigen, *Proc Natl Acad Sci U S A* 89 (1992) 11002-11005.

[23] C. M. Feldherr, and D. Akin, Signal-mediated nuclear transport in proliferating and growth-arrested BALB/c 3T3 cells, *J Cell Biol* 115 (1991) 933-939.

[24] M. P. Terns, and R. M. Terns, Small nucleolar RNAs: versatile trans-acting molecules of ancient evolutionary origin, *Gene Expr* 10 (2002) 17-39.

[25] S. C. Ogg, and A. I. Lamond, Cajal bodies and coilin--moving towards function, *J Cell Biol* 159 (2002) 17-21.

[26] T. Misteli, J. F. Caceres, and D. L. Spector, The dynamics of a pre-mRNA splicing factor in living cells, *Nature* 387 (1997) 523-527.

## CHAPTER 7

### Development of magnetic nanoparticles based MR contrast agents

#### Introduction

The integration of nanotechnology and biology is expected to produce major breakthroughs in medical diagnostics, therapeutics, molecular biology, and bioengineering ([1]; [87]). Recent advances include the development of functional nanoparticles (electronic, optical, or magnetic) that are covalently linked to biological molecules such as peptides, proteins, and nucleic acids ([88]; [89]; [90]). Due to their size-dependent properties and dimensional similarities to biomolecules ([91]) these bioconjugates are well suited as contrast agents for in-vivo magnetic resonance imaging (MRI) ([92]; [93]) , as luminescent dyes for cellular imaging, and as molecular beacons for ultrasensitive optical imaging and detection ([12];[94]; [40]).

In this study, we plan to develop a probe with a potential for deep tissue imaging. For detection in deep tissue, optical/ luminescence probes have limited applications. The limit is due to the inability for us to detect signal non-invasively from deep tissue sections using optical/ luminescence detectors. This provides a fundamental limitation of optical probes for studying biological processes non-invasively in deep tissue. For deep tissue imaging, PET, CT and MRI are leading technologies, which have been used both for research and clinical diagnosis.

With the aim, to develop a probe for imaging in deep tissue, we decided to develop a contrast agent for MRI application. Although contrast agents are often used in MRI to enhance lesion detection, typically they are not specifically targeted. For clinical diagnostic imaging, the most widely used contrast agent is that derived from chelates of

Gadolinium, a paramagnetic substance. In the presence of a paramagnetic substance, the relaxation properties, namely  $T_1$ ,  $T_2$  and  $T_2^*$  ( $1/T_2^* = 1/T_2 + 1/T_2'$ , with  $T_2'$  being a time constant arising from magnetic field inhomogeneity) of proton nuclear spins are shortened to some extent. In clinical practice, the shortening of  $T_1$  is usually used as a basis for diagnosing disease. Another type of contrast agent is based on superparamagnetic iron oxides (SPIO) or superparamagnetic nanoparticles, which affect the relaxation times in a more significant way. Shortening of  $T_2$  relaxation times using magnetic nanoparticles is used as a basis of clinical diagnostics. The currently approved SPIO particles for diagnostic are bulkier (larger than 50 nm), with limited ability to target intracellular targets. With a long term goal of developing an intracellular contrast agent, which can allow not only cell labeling in tissues etc but also provide disease specific contrast in deep tissue, we decided to develop this approach.

To meet the above requirement for intracellular targeting of biomolecules, for potential disease detection, our first major challenge was to develop functionalized magnetic nanoparticles with smaller coatings such that the entire complex could be of 10-15 nm or smaller than that. After successful development of this construct our next goal was to achieve high efficiency intracellular delivery of these functionalized nanoparticles and its validation. Following the success of this, the next step has focused on optimization of coating design to enhance the contrast developed by this magnetic contrast agent.

### **Specific Aims**

- Development of water soluble magnetic nanoparticles with functionalized surface
- Delivery of functionalized nanoparticles in living cells
- Optimization of the coatings design for contrast enhancement and stability

Super-paramagnetic iron oxide nanoparticles have a wide range of applications including high-density magnetic storage, catalytic and separation processes [1], magnetic resonance imaging [2], in vivo tracking of stem cells and tumor progression [3, 4], cell and DNA sorting [5], drug delivery [6], and cell mechanics studies [7]. Most of these applications require the magnetic nanoparticles to be water-soluble, stable, and monodispersed. Recently, there has been a growing interest in developing multifunctional magnetic nanoparticle probes for intracellular molecular imaging. One challenge of this application is to develop magnetic nanoparticle probes with sizes highly uniform and comparable to the target proteins and nucleic acids (~2-15 nm). To facilitate cellular delivery and specific intracellular targeting, a probe domain and delivery/targeting ligands must be conjugated to the nanoparticle surface. These sophisticated nanoparticle probes can be multifunctional, including self-delivery into deep tissue, targeting specific cell types, and generating contrast based on target-specific clustering or other molecular switch mechanisms [8]. A critical step in developing such molecular probes for intracellular gene detection is to functionalize the nanoparticles with a biocompatible coating.

A variety of *in situ* and post-synthesis coating strategies have been developed for stabilization and functionalization of magnetic nanoparticles. Post-synthesis coating processes include the use of monolayer ligands [9, 10], polymers [11, 12] and silica coatings [13-15]. The monolayer ligand coatings rely on effective adsorption or chemisorption of the ligand on the surface of the nanoparticle. These coatings tend to have low colloidal stability, limited flexibility for functionalization, and the tendency to form incomplete coatings due to residual surfactant on the surface. The polymer- and silica-based coating processes are difficult to control, often resulting in multilayered

coatings and multiple nanoparticles in the same encapsulation [14]. *In situ* coating approaches such as that with dextran [16] often lead to multilayered coatings which can result in a heterogeneous size distribution. *In situ* synthesis conditions also limit the variety of functionalization that can be achieved.

Here we report the development of functionalized magnetic nanoparticles for intracellular delivery that are water-soluble, monodispersed, biocompatible, and easily adaptable for multifunctional bioconjugation of probes and ligands. This is a part of our effort to develop an MRI contrast agent for intracellular measurements of gene expression in deep tissue. In this approach, superparamagnetic iron oxide nanoparticles (MIONs) are encapsulated in a PEG-modified phospholipid micelle structure [17-19] (**Figure 7.1**). A similar encapsulation strategy has been used for various hydrophobic drug molecules [18, 20] and more recently, quantum dots [21]. This approach exploits the hydrophobic nature of the nanoparticle surface by utilizing an amphiphilic PEG-phospholipid, whose hydrophobic portion interacts with the nanoparticle surface to create micelles, resulting in a self-assembled monolayer coating. The PEG portion of the coating confers solubility and biocompatibility while the use of modified PEG allows for bioconjugation [22] of proteins, multiple ligands, and nucleic acid probes.

## **Materials and Methods**

### **Coating of Magnetic Nanoparticles**

The magnetic iron oxide ( $\text{Fe}_3\text{O}_4$ ) nanoparticles (MIONs) (kindly provided by Dr. Charles O'Connor, University of New Orleans) were dispersed in toluene and insoluble in water prior to modification. Mixtures of 1,2-distearoyl-*sn*-glycero-3-phosphoethanolamine polyethylene glycol 2000 (DSPE-PEG 2000) and 1,2-distearoyl-

*sn*-glycero-3-phosphoethanolamine-N-[amino(polyethylene glycol) 2000] (DSPE-PEG 2000 amine) were dissolved in chloroform (1:8 ratio of DSPE-PEG 2000:DSPE-PEG 2000 amine), and iron oxide nanoparticles was added to the solution at a concentration of 0.33 mg/ml. This mixture was then dried under argon gas and left in a vacuum dessicator for 48 hours to remove all traces of organic solvents. The dried film was easily resuspended in deionized water with agitation. The solution obtained was filtered using 0.2  $\mu\text{m}$  Anotop inorganic membrane syringe filters (Whatman International Ltd., England).

### **Size Determination**

To determine the size of the micelle-coated MIONs, we employed dynamic light scattering (DLS) using a DynaPro-LSR instrument (Protein Solutions, England), which allows specific measurement of the hydrodynamic radius of macromolecules in the size range of 1 nm-1  $\mu\text{m}$ . Micelle-coated MIONs were filtered first using Anotop 0.2  $\mu\text{m}$  inorganic membrane syringe filters (Whatman International); dynamic light scattering experiments were then conducted at room temperature. The size of the micelle-coated MIONs was calculated by fitting the data to a polydispersed model [23] using the Dynamics software (version 5.26) provided with the instrument.

To further determine the size of the coated nanoparticles, transmission electron microscopy (TEM) was performed on micelle-coated MIONs. MIONs were spun in a microfuge at 14000 rpm for 6 minutes to obtain a concentrated solution. The supernatant was decanted and 5  $\mu\text{L}$  of this concentrate was placed on a carbon grid. 5  $\mu\text{L}$  of 1% phosphotungstic acid was added and allowed to sit for 30 seconds for negative staining. Liquid was then removed from carbon grid, and the grid was imaged on a Hitachi H-7500 transmission electron microscope (TEM).

## Bioconjugation and Functionalization

To functionalize magnetic nanoparticles for bioconjugation and subsequent delivery and imaging studies, we incorporated phospholipid-PEG molecules with primary amines (DSPE-PEG-amine) into the micelle structure. For fluorescence imaging of the nanoparticles delivered into cells, we used Texas Red STP ester (1  $\mu\text{M}$ ) and the heterobifunctional cross-linking reagent, *N*-succinimidyl 3-(2-pyridyldithio)propionate (SPDP) (10  $\mu\text{M}$ ) to react with amine groups on the micelle-coated MIONs (mMIONs). These were allowed to react for 2 hours in 1X Dulbecco's phosphate buffered saline without Ca or Mg (PBS; from ICN, Ohio). To reduce the thiol group on SPDP, 20 mM of the reductant tris(2-carboxyethyl) phosphine hydrochloride (TCEP) was added and the mixture was incubated for 1 hour. A Microcon YM10 filter unit was used to remove unreacted Texas Red and TCEP. For cellular delivery, we used the cell penetrating peptide (CCP) Tat. The Tat peptide-6-aminohexonic acid-Cys construct was reacted overnight with the fluorescently labeled mMIONs via the SPDP crosslinker at a concentration of 1  $\mu\text{M}$ . Unreacted peptide was removed by dialysis into 2L of PBS buffer using a Slide-A-Lyzer Dialysis Cassette with a molecular weight cutoff of 10000 Da (Pierce Biotechnology, Rockford, IL) for 24 hours.

## Iron Concentration Determination

Iron concentration of the mMION solution was determined colorimetrically using o-phenanthroline with a procedure modified from [24]. Iron solutions for a standard curve with concentrations ranging from 0.5 mg/L to 5 mg/L were diluted from a stock solution of  $\text{FeSO}_4$  (with 1:1000 dilution of concentrated  $\text{H}_2\text{SO}_4$ ) with a  $\text{Fe}^{2+}$  concentration of 40 mg/L. Samples and standards both contained 0.2% hydroxylamine HCl to maintain iron in the  $2^+$  state and sodium citrate (150  $\mu\text{l}$  per mL of iron solution) to maintain an acidic pH for Fe-phenanthroline complex formation. To dissolve the iron

oxide nanoparticles and release  $\text{Fe}^{2+}$  for analysis, 0.15% v/v mercaptoacetic acid was added to each mMION solution and incubated overnight prior to analysis. O-phenanthroline was added from a 0.25% w/v stock in water to a final concentration of 0.0075% w/v for each of the standards and samples. Absorbance was read at 510 nm.

### **Cell Culture**

Primary human dermal fibroblast (HDF) cells (Cambrex, NJ) and kidney-derived MDBK cells (ATCC, VA) were used in this study. Primary HDF cells were cultured using FGM-2® Fibroblast Growth Medium 2 with 2% serum (Clonetics® Media Systems, NJ), while MDBK cells were cultured using Dulbecco's-modified Eagle's medium with fetal calf serum (10%) and horse serum (2.5%). Primary HDF and MDBK cells were plated in T-25 cell culture flask using 1:10 dilution after each splitting cycle. A batch of primary HDF cells was cultured for no more than 12 splitting cycles, while the MDBK cell line was cultured for 15-18 splitting cycles.

### **Fluorescent Imaging**

For fluorescence imaging studies, both HDF and MDBK cells were plated on 8-well Nalgene Nunc cell culture plates and allowed to grow for 48 hours. The cells were incubated for an hour with TxRed-Tat peptide conjugated mMIONs (final Fe concentration of 42  $\mu\text{g}/\text{mL}$ ) in suitable cell culture medium (FGM-2 for HDF's and DMEM+FCS (10%) + HS (2.5%) for MDBKs). After incubation, cells were washed in PBS twice to remove unbound and extracellular mMIONs. Fresh media was added to cells after washing, and the cells were imaged using a Zeiss confocal microscope (40 X magnification, using a 543 nm laser).

## Magnetic Contrast Measurements

A 0.47 T Bruker Minispec Analyzer MQ20 was used for  $T_2$  measurements. MDBK cells were grown in a T25 culture plate (approximately  $10^6$  cells) and then incubated with a 1:4 dilution of mMIONS and media as in fluorescent imaging preparation. After 1 hour of incubation, cells were washed twice with PBS to remove extracellular and unbound mMIONS. Following washing, cells were trypsinized, removed from the culture plate, and resuspended in a final volume of 1.5 mL of media. 500  $\mu$ L of this cell suspension were placed in a 10 mm sample tube to determine the  $T_2$  value, using the CPMG pulse sequence. The same cell samples were collected in media in 200  $\mu$ l microfuge tubes and imaged by a 3T Siemens TRIO MRI system using a  $T_2$ -weighted Turbo Spin Echo sequence.

## Results and Discussion

The magnetic nanoparticles were successfully coated with a PEG-phospholipid micelle coating using the process described in the **Materials and Methods** section. The magnetic iron oxide ( $\text{Fe}_3\text{O}_4$ ) nanoparticles (MIONS) used in our studies had an average size of 6.6 nm with size variation of 11%, as determined by transmission electron microscopy (Charles O'Connor, personal communication). These nanoparticles were synthesized using the reverse micelle technique, which allows efficient control of the size of nanoparticles [25, 26]. Due to the synthesis process, the nanoparticles had a residual capping of surfactant molecules such as cetyltrimethylammonium bromide (CTAB) that rendered them soluble only in organic solvents. To make the particles water-soluble and biocompatible, we employed a phospholipid-PEG micelle coating approach, which takes the advantage of the interaction between the residual hydrophobic capping ligands on the magnetic nanoparticles and the amphiphilic PEG-phospholipids. The surface-

exposed hydrophilic PEG chains provide high solubility of the coated magnetic nanoparticles.

Using the coating process schematically represented in **Figure 7.1**, we found that the nanoparticles were water-soluble (free from cloudiness) and stable in water or 1X PBS for a period of weeks when kept at 4°C. As described in the **Materials and Methods** section, we characterized the mMIONs by measuring the size and Fe concentration. Using dynamic light scattering (DLS) measurements, the average hydrodynamic radius of the mMIONs was 7.34 nm ± 0.71 nm (93.9% of mass). The size distribution as a function of percent mass is shown in **Figure 7.2 A**. The size range of the coated MIONs obtained with DLS is similar to that reported by [21] for micelle-encapsulated quantum dots. The DLS results also indicated a very narrow range of polydispersity in mMIONs, which may provide a crucial advantage for molecular imaging applications based on clustering of magnetic nanoparticles, as discussed later.

Electron microscopy was also performed to verify the presence of coating and to determine the coating thickness. As shown in **Figure 7.2 B**, negative staining allowed a contrast between the background and the dark iron core, revealing an unstained micelle coating around the MIONs. The size of mMIONs as determined by the TEM image is between 12 to 14 nm, similar to the results obtained by DLS. This indicates that the coating thickness is around 3 nm. Note that a fraction of micelles without iron cores were also observed in the TEM image shown in **Figure 7.2 B**. Ultracentrifugation may be used in the future to separate empty micelles from mMIONs. The Fe concentration of the coated magnetic nanoparticles (mMIONs) was colorimetrically determined to be 168 µg/mL using o-phenanthroline.

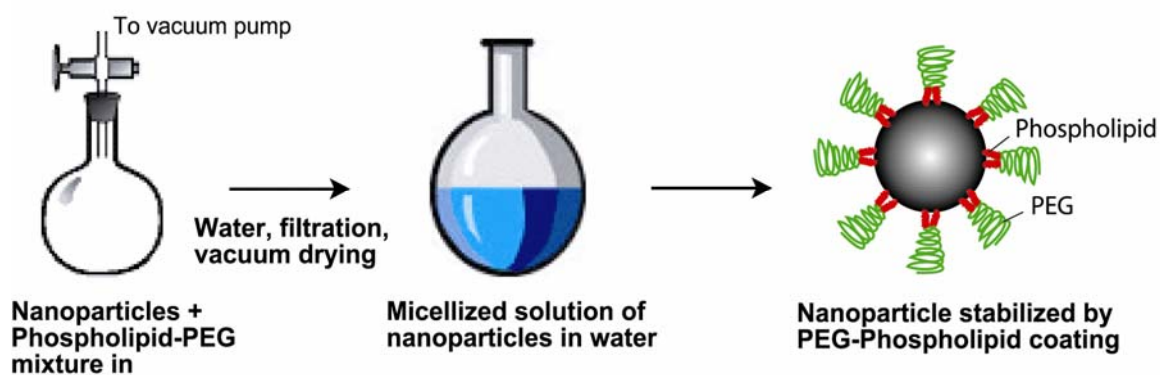


**Figure 7.1:** The scheme for the development of micelle-encapsulated superparamagnetic iron oxide magnetic nanoparticles (mMIONS). In the first step, a mixture of phospholipid-PEG and phospholipid-PEG-amine (1:10) is dissolved in chloroform and then MIONS are added (final concentration of 0.33 mg/mL iron oxide). The mixture is dried under argon and left in vacuum desiccator for 48 hours. Particles are dissolved deionized water with agitation. The final solution is filtered using a 0.2  $\mu\text{m}$  syringe filter.

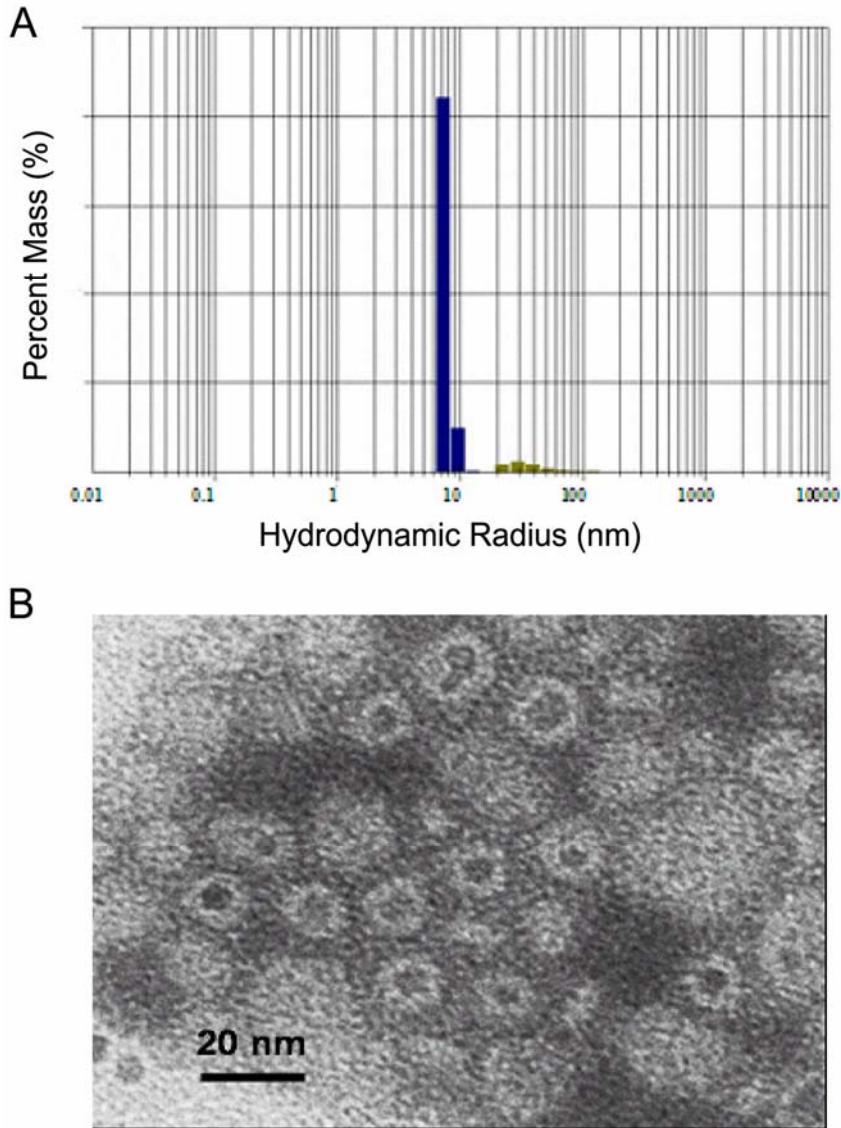


**Figure 7.2:** The size of mMIONS.

A. Particle size distribution [% mass vs. hydrodynamic radius,  $R_h$ , (nm) of particles] of mMIONS measured using dynamic light scattering. 93.9% of the sample mass has a hydrodynamic radius of 7.34 nm.

B. Electron micrograph of negatively stained mMIONS at a magnification of 60 kx. Dark iron cores can be seen encircled by unstained micellar coating against the stained carbon grid background, indicating a coating thickness of ~ 3-4 nm.

The use of phospholipids-PEG to coat MIONS provides a flexible framework for nanoparticle functionalization since PEGs modified with a variety of functional groups, including amines and sulfhydryls, are commercially available and can be easily incorporated into micelles. Therefore, various moieties including proteins, nucleic acids and delivery/targeting ligands can be readily conjugated to the mMIONS. In this study, to demonstrate the ability of mMIONS to generate intracellular contrast, we used Tat peptide for nanoparticle delivery into living cells. Specifically, fluorescent dye molecules and delivery peptides were simultaneously attached to the surface of the mMIONS through a reactive amine group. As a member of the cell penetrating peptide (CPPs) family, Tat peptide has been shown to deliver proteins, macromolecules, nanoparticles, and liposomes of sizes 2 nm to 200 nm across the cell membrane both in cell culture and *in vivo* applications [27, 28], making them very attractive for various intracellular delivery applications. To validate the intracellular delivery of mMIONS, we used two reporting modalities: fluorescence imaging and magnetic contrast. To obtain fluorescence imaging capability, the mMIONS were conjugated with TxRed dye (**Figure 7. 3**). The iron oxide nanoparticles provided the magnetic contrast, as described below.

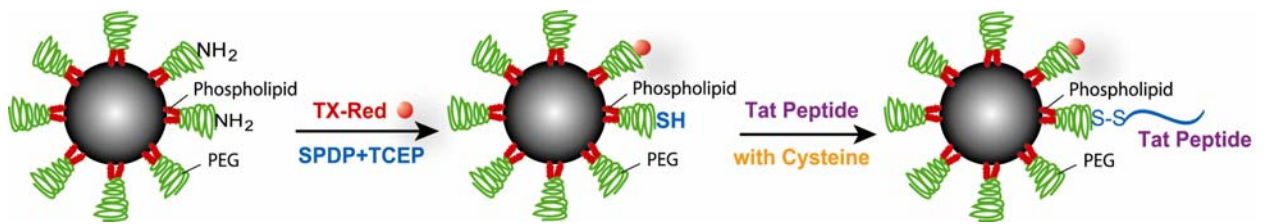
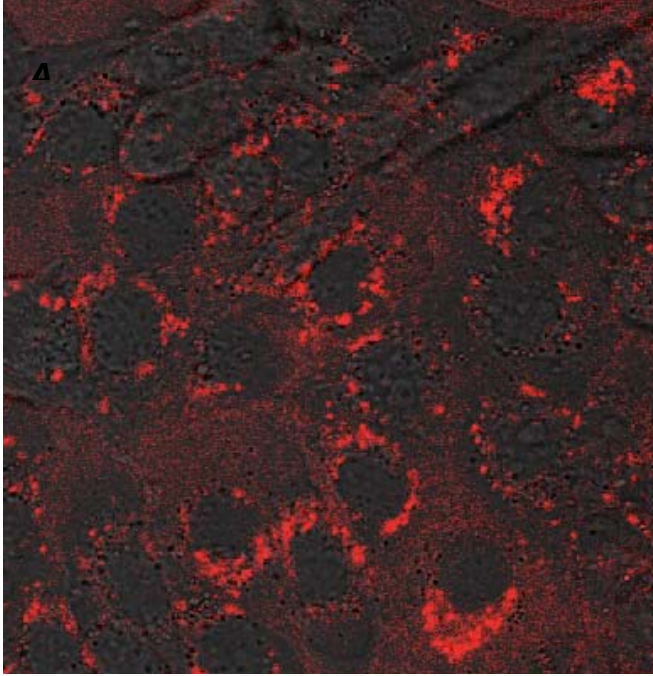


**Figure 7.3:** Steps for conjugating Tat peptide and fluorescent label (TxRed) to mMIONS for cellular delivery and imaging (microscopy, MRI). The first step involves the simultaneous reaction of TxRed STP-ester and crosslinker SPDP with amines on the surface of mMIONS. TCEP is added after the reaction to generate free thiols on surface-bound SPDP. The second step is the reaction of the Cys-modified Tat peptide with the free thiols of SPDP.

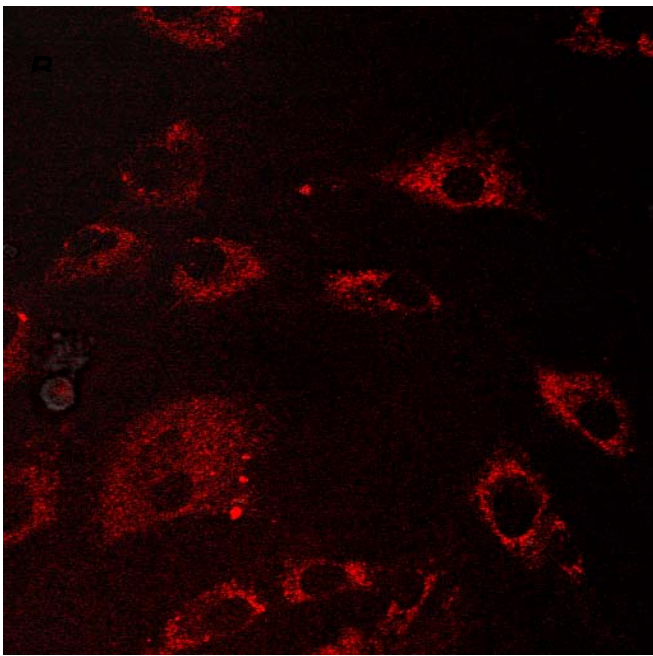
For fluorescence imaging studies, both HDF and MDBK cells were incubated with TxRed-Tat conjugated mMIONS for an hour. Cells were washed to remove unbound and extracellular mMIONS. Following washing, cells were incubated with fresh media and were imaged using a confocal microscope. **Figures 7.4 A and 7.4 B** show the fluorescence images as a result of intracellular delivery of mMIONS in both cell lines. Note that in images of MDBK cells (**Figure 7.4 A**), the background signal is slightly higher than that in HDF cells. We believe that this is due to the close clustering of MDBK cells in culture, which may contribute to signal increase due to out-of-focus cells. HDF cells have a more extended structure and are less densely packed.

To further validate the delivery of the mMIONS into live MDBK cells, we measured  $T_2$  (transverse) relaxation times and obtained MRI contrast images. These measurements are based on the induced changes in water relaxation caused by magnetic nanoparticles. In the presence of a paramagnetic substance such as mMIONS, water relaxation properties, namely  $T_1$ ,  $T_2$  and  $T_2^*$  ( $1/T_2^* = 1/T_2 + 1/T_2'$ , with  $T_2'$  being a time constant arising from magnetic field inhomogeneity) of proton nuclear spins are shortened [29]. For  $T_2$  measurements, a Bruker Minispec Analyzer MQ20 was used. MDBK cells were incubated with TxRed-Tat mMIONS for 1 hour and then washed to remove extracellular and unbound mMIONS. A suspension of this preparation was then used for  $T_2$  measurements. The  $T_2$  relaxation time determined for cells with mMIONS was  $623 \pm 2$  ms. In contrast, for control cells without mMIONS, the  $T_2$  time was  $1503 \pm 20$  ms (see **Figure 7.5 A**). Therefore, in the mMION-treated cells, the  $T_2$  time is at least a factor of two shorter than control cells, indicating significant internalization of magnetic nanoparticles. We further performed MR imaging using a 3T Siemens TRIO MRI system, and a shortened  $T_2$  time resulted in a darker image. As can be seen in **Figure 7.5 B**, when the same cell sample as used for  $T_2$  measurements was imaged

using an MRI system, cells containing incubated with mMIONS gave a darker image than control cells, once again indicating the presence of the relaxation agent inside cells.

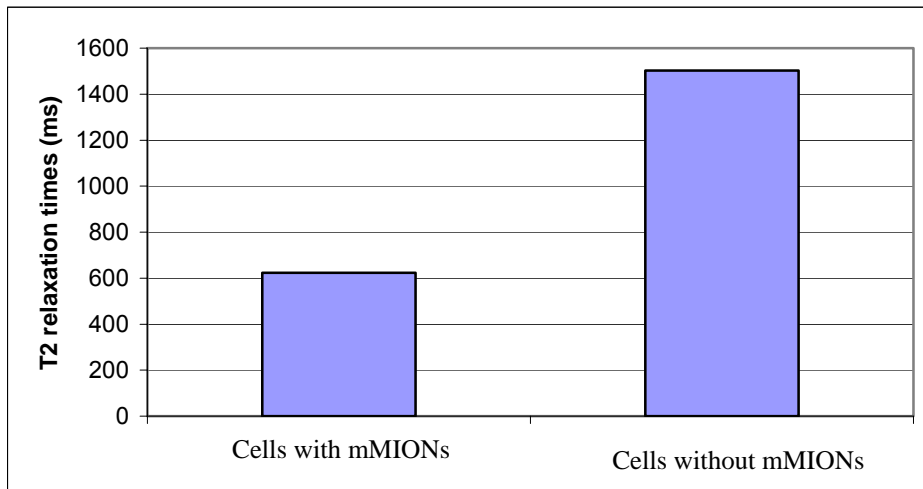


A



B

**Figure 7. 4:** Fluorescent images of Tat-linked, TxRd-labeled mMIONs in living cells.  
(A) Images of TxRd-labeled mMIONs in MDBK cells.  
(B) Images of TxRd-labeled mMIONs in HDF cells. Images were obtained using a Zeiss confocal microscope with excitation at 543 nm and emission detection at 560 nm.



**B**

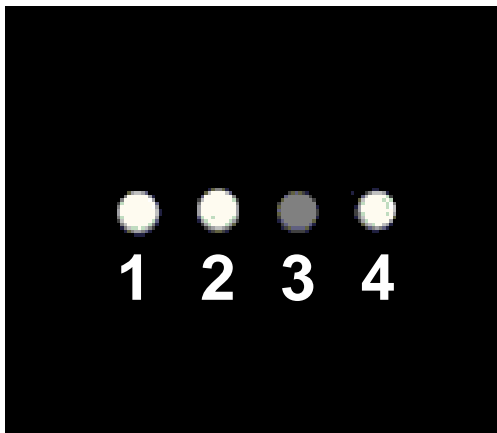


**Figure 7.5:** The effect of mMIONs on water relaxation inside living cells.

- A. T<sub>2</sub> relaxation time (ms) measurements obtained using Bruker mq20 Minispec. MDBK cells with mMIONs gave a T<sub>2</sub> relaxation time of 623 ms while cells without mMIONs had a T<sub>2</sub> time of 1503 ms.
- B. MRI images of four different samples: (1) culture media only, (2) cells without mMION, (3) cells with mMION, (4) culture media only. Images were obtained using a 3T Siemens TRIO, turbo spin echo, TR 4000, TE 310, in-plane voxel size 0.5 x 0.5 mm.

## Summary

In this work we have developed a micelle-based coating strategy for functionalizing superparamagnetic iron oxide nanoparticles. The coating of small, uniformly-sized iron oxide nanoparticles resulted in an MRI contrast agent with a narrow size distribution that is biocompatible, water soluble, stable, and has a functionalized surface to which multiple ligands can be attached. Using the Tat peptide, we have demonstrated rapid (within 1 hour) delivery of mMIONS into living cells. Intracellular delivery was validated using both fluorescence imaging and MRI contrast measurement. The surface of these mMIONS provides a flexible platform to which proteins, nucleic acid probes and a variety of ligands for cell delivery and targeting can be attached. Because of the small sizes (10-15 nm), functionalized mMIONS are well suited as a contrast agent for probing intracellular events with less perturbation than other currently used iron oxide-based molecular probes. The small and uniform size may also confer an advantage in clustering-based molecular switching techniques for specific detection of gene expression in deep tissue using MRI. Therefore, the development of functionalized mMIONS in this study is a crucial step towards developing novel intracellular molecular probes for MRI-based deep tissue imaging.

## References

1. Dyal A, Loos K, Noto M, Chang SW, Spagnoli C, et al. (2003) *J Am Chem Soc* 125: 1684-5
2. Zhao M, Kircher MF, Josephson L, Weissleder R. (2002) *Bioconjug Chem* 13:840-4
3. Bulte JWM, Douglas T, Witwer B, Zhang S-C, Strable E, et al. (2001) *Nat Biotechnol* 19:1141-7
4. Lewin M, Carlesso N, Tung CH, Tang XW, Cory D, et al. (2000) *Nat Biotechnol*. 18:410-4
5. Dressman D, Yan H, Traverso G, Kinzler KW, Vogelstein B. (2003) *Proc Natl Acad Sci USA* 100:8817-22
6. Lanza GM, Abendschein DR, Yu X, Winter PM, Karukstis KK, et al. (2002) *Acad Radiol* 9 Suppl 2:S330-1
7. Butler JP, Kelly SM. (1998) *Biorheology* 35:193-209
8. Perez JM, O'Loughin T, Simeone FJ, Weissleder R, Josephson L. (2002) *J Am Chem Soc* 124:2856-7
9. Liu Q, Xu Z. (1995) *Langmuir* 12:4617-22
10. Yee C, Kataby G, Ulman A, Prozorov T, White H, et al. (1999) *Langmuir* 15:7111-5
11. Harris LA, Goff JD, Carmichael AY, Riffle JS, Harburn JJ, et al. (2003) *Chem Mater* 15:1367-77
12. Burke NAD, Stover HDH, Dawson FP. (2002) *Chem Mater* 14:4752-61
13. Santra S, Tapeç R, Theodoropoulou N, Dobson J, Hebard A, Tan W. (2001) *Langmuir* 17:2900-6

14. Lu Y, Yin Y, Mayers BT, Xia Y. (2002) Nano Letters 2:183-6
15. Butterworth MD, Illum L, Davis SS. (2001) Colloids and Surfaces A: Physicochemical and Engineering Aspects 179:93-102
16. Kim DK, Mikhaylova M, Zhang Y, Muhammed M. (2003) Chem Mater 15:1617-27
17. Jones M, Leroux J. (1999) Eur J Pharm Biopharm 48:101-11
18. Perkins WR, Ahmad I, Li X, Hirsh DJ, Masters GR, et al. (2000) Int J Pharm 200:27-39
19. Torchilin VP. (2002) Adv Drug Deliv Rev. 54:235-52
20. Torchilin VP, Lukyanov AN, Gao Z, Papahadjopoulos-Sternberg B. (2003) Proc Natl Acad Sci U S A 100:6039-44
21. Dubertret B, Skourides P, Norris DJ, Noireaux V, Brivanlou AH, Libchaber A. (2002) Science 298:1759-62
22. Gref R, Couvreur P, Barratt G, Mysiakine E. (2003) Biomaterials 24:4529-37
23. Braginskaya, Dobitchin, Ivanova, Klyubin, Lomakin, et al. (1983) Physica Scripta 28:73-9
24. Atkins RC. (1975) J Chem Educ 52:550
25. Feltin N, Pileni MP. (1997) Langmuir 13:3927-33
26. Seip CT, O'Connor CJ. (1999) NanoStructured Materials 12:183-6
27. Torchilin VP, Levchenko TS, Rammohan R, Volodina N, Papahadjopoulos-Sternberg B, D'Souza GG. (2003) Proc Natl Acad Sci U S A 100:1972-7
28. Torchilin VP, Rammohan R, Weissig V, Levchenko TS. (2001) Proc Natl Acad Sci U S A 98:8786-91

29. Haacke EM, Brown RW, Thompson MR, Venkatesan R. (1999) Magnetic Resonance Imaging: Physical Principles and Sequence Design. John Wiley and Sons. New York

## CHAPTER 8

### Effect of coating thickness on magnetic relaxation characteristics of iron-oxide nanoparticles

#### Introduction

First introduced as MRI contrast agents in the mid-1980s ([1-3]), iron oxide nanoparticles display a property defined as superparamagnetism. They are most often magnetite ( $\text{Fe}_2\text{O}_3/\text{Fe}_3\text{O}_4$ ), and have crystal-containing regions of unpaired spins (**Figure 8.1**), ([4]). These magnetic domains are disordered in the absence of a magnetic field, but when a field is applied, the magnetic domains align to create a magnetic moment much greater than the sum of the individual unpaired electrons. This does not, however, result in residual magnetization of the particles.

Compared with micrometer-sized magnetic particles and chelates of paramagnetic ions such as gadolinium diethylenetriaminopentaacetic acid (Gd-DTPA), magnetic nanoparticles are much more efficient as relaxation promoters and their effect on the relaxivities of water is measurable even at nanomolar concentrations, as demonstrated theoretically [5] and experimentally [6-9]. Specifically, the use of ferromagnetic and superparamagnetic nanoparticles as contrast agents can induce a more than 10-fold increase in proton relaxivities [10]. In the presence of a paramagnetic or superparamagnetic substance, the relaxation properties, namely  $T_1$ ,  $T_2$  and  $T_2^*$  ( $1/T_2^* = 1/T_2 + 1/T_2'$ , with  $T_2'$  being a time constant arising from magnetic field inhomogeneity) of proton nuclear spins are shortened to some extent. Superparamagnetic iron oxides (SPIO) or superparamagnetic nanoparticles affect the  $T_2$  relaxation time more significantly than  $T_1$ , whereas gadolinium chelates predominantly affect  $T_1$ .

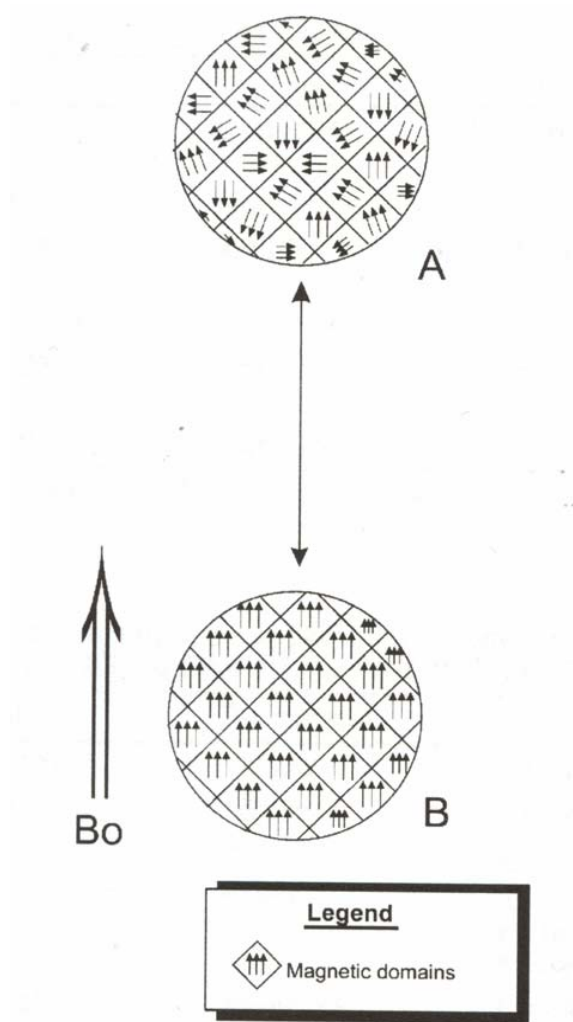


**Figure 8.1:** (A) SPIO crystal in the absence of an external magnetic field ( $B_0$ ); the orientation of the magnetic domains is random.

(B) Application of an external magnetic field aligns the magnetic domains with  $B_0$ . (adapted from Wang et al, 2001[4])

This shortening of  $T_2$  results in a darkening of the image where the SPIOs are located referred to as negative contrast. Due to better relaxation characteristics of the SPIO's, these superparamagnetic particles are used in various applications. For several medical applications, the size of the SPIO's and their coating are adjusted to target them to specific organs of the body ([4]). Particles ranging in size from 60 nm to 150 nm are quickly sequestered by the body's reticuloendothelial system (RES) upon injection, rapidly appearing in the liver and spleen. Even smaller particles under clinical investigation (referred to as ultrasmall SPIOs) are typically between 10 and 40 nm; these particles circulate in the blood stream much longer than the larger particles, can cross capillary walls and often are taken up extensively by lymph nodes and bone marrow. Even without specific targeting ligands conjugated on the surface of particles, a variety of different organ systems can be specifically imaged. Further, differential cell uptake in cancerous tissue leads to contrast enhancement between normal and tumor tissues, which can be used clinically for cancer detection. There are a number of SPIO compounds already FDA-approved for use in the clinic (see **Table 8.1**), as well as others undergoing clinical trials. In this study, our focus is on ultrasmall SPIOs as described in previous Chapter (7).

Although magnetic nanoparticles or SPIO's have been extensively studied and used for various applications related to MR imaging in clinical and research settings, the processes which contribute to the relaxation characteristics of MIONs have not been well characterized ([11-13]).

**Table 8.1:** Properties and applications of some SPIO agents (modified from Wang et al[4])

<b>Agent</b>	<b>Particle Size</b>	<b>Target Organs</b>	<b>FDA Approval</b>
AMI-121[14]	300 nm	GI lumen	Approved
OMP[15]	3.5 $\mu$ m	GI lumen	Approved
AMI-25[16, 17]	80-150 nm	Liver/spleen	Approved
SHU 555A[16, 18, 19]	62 nm	Liver/spleen, blood pool	Phase III
AMI-277[20-22]	20-40 nm	Lymph nodes, blood pool	Undergoing review
NC100150[23, 24]	20 nm	Blood pool	Under development
Code 7228[25]	30 nm	Blood pool	Phase II

It is not clear whether the relaxation processes are mediated by the diffusion of protons or chemical exchange of protons. It is likely that the processes involved in magnetic relaxation events not only depend on the magnetic core but also on the coating layer, which usually renders these nanosize particles water-soluble and stable in physiological buffers. Thus to fully understand the relaxation characteristic of MIONs, we have to understand not only the behavior of protons in the vicinity of iron oxide core but also their interactions with the coating material. Depending on their thickness and chemical characteristics, coating materials can influence the diffusion of protons and chemical exchange processes.

In most of the studies involving magnetic nanoparticles ([8, 26-29]), it is typically not possible to independently change the coating size without a significant change in the chemistry of a surface coating. With a number of existing coating methods, it is very difficult to obtain a narrow size distribution of coated particles ([26-30]). This size variation can limit an independent analysis of the role of size and chemistry of coatings on relaxivity characteristics of MIONs. These factors have limited the experimental approaches needed to gain a fundamental understanding of the magnetic relaxation processes. To provide an insight into the role of coating thickness in magnetic relaxation processes, we have varied the size of the surface coatings in this study, with constant magnetic core and fixed chemical composition of the coating material. This approach will allow us to independently probe the contributions from coating thickness in determining the effective magnetic relaxivities of mMIONs.

In Chapter 7, we developed a coating approach, which allows for modular coating of magnetic nanoparticles using amphiphilic phospholipid-PEG micelles. One of the advantages of the micelle-based coating was the monodispersity in the size of the coated magnetic nanoparticles in contrast with the other coatings such as silanes or dextran coating. The results were shown in **Figure 7.2** of **Chapter 7**. The other

significant advantage was the ability to tailor the surface of the coated particles with variety of ligands using mixture of modified phospholipids-PEG molecules. Using this approach we have conjugated multiple biomolecules on the surface of the coated MIONS (**Figure 7.4** in **Chapter 7**). In this study, we exploit another significant advantage in which we can change the coating size by changing the size of the PEG chain, while keeping the same core size and the chemistry of the coating. By employing a series of phospholipid-PEG conjugates with increasing molecular weights (PEG 550, PEG 750, PEG 1000, PEG 2000, and PEG 5000) and demonstrating a corresponding increase in coating layer thickness with dynamic light scattering (DLS), we have studied the impact that coating layer thickness has on both T1 and T2 relaxation properties. To gain a more complete understanding of these effects on relaxation, we have done computer simulations (in collaboration with Dr Hu's lab) to predict how changes in coating thickness will affect relaxivity, using a model that assumes that water is excluded by the coating. Thus a thicker coating will have a larger exclusion volume for water protons.

## **Material and Methods**

### **Coating of Magnetic Nanoparticles**

The magnetic iron oxide ( $\text{Fe}_3\text{O}_4$ ) nanoparticles (MIONS) (kindly provided by Dr. Charles O'Connor, University of New Orleans) were dispersed in toluene and insoluble in water prior to modification. These nanoparticles were coated with different size of DSPE-PEG polymers similar to the approach developed in **Chapter 7**. The chemistry of the lipid chain and the PEG backbone was maintained constant in this study. In a typical coating procedure, we added an excess of DSPE-PEG at a concentration of 1 mg/ml (e.g. we added 100  $\mu\text{l}$  of DSPE-PEG 2000, 1,2-distearoyl-*sn*-glycero-3-phosphoethanolamine polyethylene glycol 2000 at 10 mg/ml concentration) to a iron

solution at 0.33 mg/ml dissolved in chloroform. This mixture was then dried using a rotary evaporator at water bath temperature of 60°C. This step was a slight modification to the procedure described in **Chapter 7**. The use of the rotary evaporator with a vacuum pump allowed us to better remove the toluene and chloroform from the mixture as compared with argon evaporation and vacuum dessicator used in previous chapter. The dried film was easily resuspended in deionized water with agitation. The solution obtained was filtered using 0.2 µm Anotop inorganic membrane syringe filters (Whatman International Ltd., England).

### **Size Determination**

To determine the size of the micelle-coated MIONs, we employed dynamic light scattering (DLS) using a PSS-Nicomp ZLS 380 (PSS, Corp.), which allows specific measurement of the hydrodynamic radius of macromolecules in the size range of 1 nm-1 µm. Micelle-coated MIONs were filtered first using Anotop 0.2 µm inorganic membrane syringe filters (Whatman International); dynamic light scattering experiments were then conducted at room temperature. The size of the micelle-coated MIONs was calculated by fitting the data to a NICOMP algorithm provided by PSS Corp. The number weighted average of three readings was used as representative size measurements of these particles.

### **Iron Concentration Determination**

Iron concentration of the mMION solution was determined colorimetrically using o-phenanthroline with a procedure modified from [31]. Iron solutions for a standard curve with concentrations ranging from 0.5 mg/L to 5 mg/L were diluted from a stock solution of FeSO<sub>4</sub> (with 1:1000 dilution of concentrated H<sub>2</sub>SO<sub>4</sub>) with a Fe<sup>2+</sup> concentration of 40 mg/L. Samples and standards both contained 0.2% hydroxylamine HCl to maintain iron in the 2<sup>+</sup> state and sodium citrate (150 µl per mL of iron solution) to

maintain an acidic pH for Fe-phenanthroline complex formation. To dissolve the iron oxide nanoparticles and release  $\text{Fe}^{2+}$  for analysis, 0.15% v/v mercaptoacetic acid was added to each mMION solution and incubated overnight prior to analysis. O-phenanthroline was added from a 0.25% w/v stock in water to a final concentration of 0.0075% w/v for each of the standards and samples. Absorbance was read at 510 nm. For each O-phenanthroline reading, we made three independent samples at two different dilutions. Three repeats of this process were carried out for each of the DSPE-PEG coated particles.

### **Magnetic Contrast Measurements**

A 0.47 T Bruker Minispec Analyzer MQ20 was used for  $T_2$  and  $T_1$  measurements. The samples for the  $T_2$  and  $T_1$  were prepared by 1:10 dilutions of the coated stock solutions in 1X PBS. 500  $\mu\text{L}$  of this sample was placed in a 10 mm sample tube to determine the  $T_2$  and  $T_1$  measurement, using the CPMG and the inversion recovery pulse sequences respectively. All the measurements were made at 20°C using a temperature-controlled probe cavity with an external water bath. Each measurement was repeated three times to measure variations within the readings, and each coating thickness was repeated with at least three independent preparations of MIONs.

## Results and Discussion

The mMIONS coated with DSPE-PEG (550, 750, 1000, 2000, and 5000) were prepared as described in the Materials and Methods section. To measure a change in the size of mMIONS coated with different sized polymers, the coated particles were analyzed using dynamic light scattering (DLS). Results of the size variation of mMIONS coated with PEG chains of different lengths using amphiphilic polymers of the type DSPE-PEG (DSPE-PEG 550, 750, 1000, 2000 and 5000) are shown in **Table 8.2**. The result shows an increase in the particle diameter with an increase in polymer coating size. The DLS results show no significant difference in the size of DSPE-PEG 550 and 750. The DSPE-PEG 5000 particles had a diameter of 17 nm. This data is in agreement with the size of the micelles reported with these coatings ([32]).

**Table 8.2:** Variation of diameter of coated mMIONS with changes in coating size

<b>Serial Number</b>	<b>Coating Type</b>	<b>Size (Diameter (nm))</b>
1	DSPE-PEG-550	8.0 nm
2	DSPE-PEG-750	9.1±1.7 nm
3	DSPE-PEG-1000	11.9±1.7 nm
4	DSPE-PEG-2000	14.2±1.4 nm
5	DSPE-PEG-5000	16.8±3 nm

For the measurement of  $T_2$  and  $T_1$  relaxation times, the sample was prepared by dilution (1:10 in 1x PBS) of the stock solution of coated magnetic nanoparticles. The measured  $T_2$  and  $T_1$  relaxation times (ms) were converted to  $R_2$  and  $R_1$  values ( $1/\text{mM}\cdot\text{s}$ ) by normalizing the relaxation times with the concentration of samples. The concentration of the samples was measured using the o-phenanthroline method as outlined in the Methods section. The results for  $R_2$  as a function of DSPE-PEG size (PEG 550, 750, 1000, 2000 and 5000) are shown in **Figure 8.2**. The results show that the  $R_2$  value increases as the size of the DSPE-PEG polymer is reduced. The relaxivity curve as a function of DSPE-PEG size indicates a sharp drop (nearly exponential) in the relaxivity as the polymer size is increased from PEG 550 to PEG 2000. The curve also indicates that there is a significant (ratio of about 2.5 fold) increase in the magnetic relaxivity with the decrease in coating size from DSPE-PEG 550 to DSPE-PEG 5000. Upon increasing polymer size from PEG 2000 to PEG 5000, we did not observe any significant changes in the relaxivity value, suggesting an asymptotic trend in the  $R_2$  values. These results clearly indicate the role of coating size in determining the net magnetic relaxivity of MIONs. The highest  $R_2$  value is obtained for the MIONs coated with DSPE-PEG 550. This indicates that by reducing the coating size, we can increase the contrast produced by MIONs. This is important for medical applications, as higher contrast translates into a reduced amount of MIONs required for imaging.

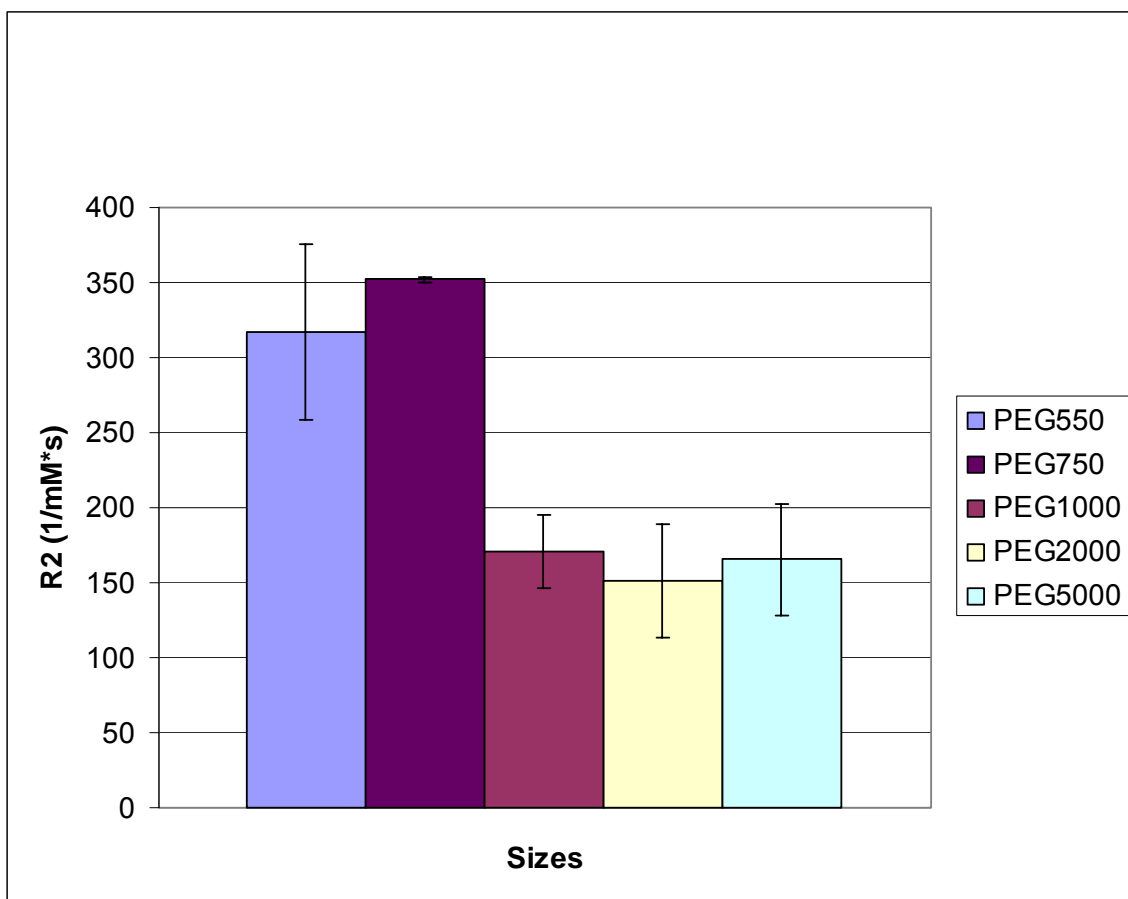


**Figure 8.2:** Variation of  $R_2$  for mMIONS coated with micelle coating of various sized phospholipid-PEG chains (DSPE-PEG 550, 750, 1000, 2000 and 5000)

The results for the variation of  $R_1$  as a function of polymer size is shown in **Figure 8.3**. The results show that the  $R_1$  values change with the changes in polymer coatings. The mMIONs coated with DSPE-PEG 550 and 750 had a lower value of  $R_1$  as compared with rest of the mMION samples. This result shows that the size variation of the DSPE-PEG coatings does have significant effect on the  $R_1$  relaxivity values of the mMIONs. The magnetic nanoparticles have been predominantly used as negative contrast agent ( $R_2$  relaxivity) for most clinical applications, but there has been recent interest in decreasing the  $R_2/R_1$  ratio, which may allow these particles to be used as blood pool agents ([12, 33]). Typically  $Gd^{3+}$ ,  $Gd^{3+}$ -linked albumin and other such  $R_1$  contrast agents have dominated the blood pool agent field. Due to the need for higher concentrations, shorter circulation times, and toxic side effects associated with  $Gd^{3+}$  and its conjugates, there has been increasing interest in exploring the use of magnetic nanoparticles as alternative blood pool agents ([12, 33]). In this study we were interested in determining how polymer coating size can play a role in affecting the  $R_2/R_1$  ratio ([12, 33]). The results of **Figure 8.2** and **8.3** taken together suggest that by decreasing the polymer coating size, we can increase the ratio of  $R_2/R_1$ . Thus for this coating chemistry, the use of larger polymer coatings may be desirable to achieve a decreased  $R_2/R_1$  ratio, thus making these particles more suitable for blood pool applications. Using modified chemistries, we may be able to further affect the ratio of  $R_2/R_1$  to optimize the properties of magnetic nanoparticles for use as blood pool agents in MR imaging.

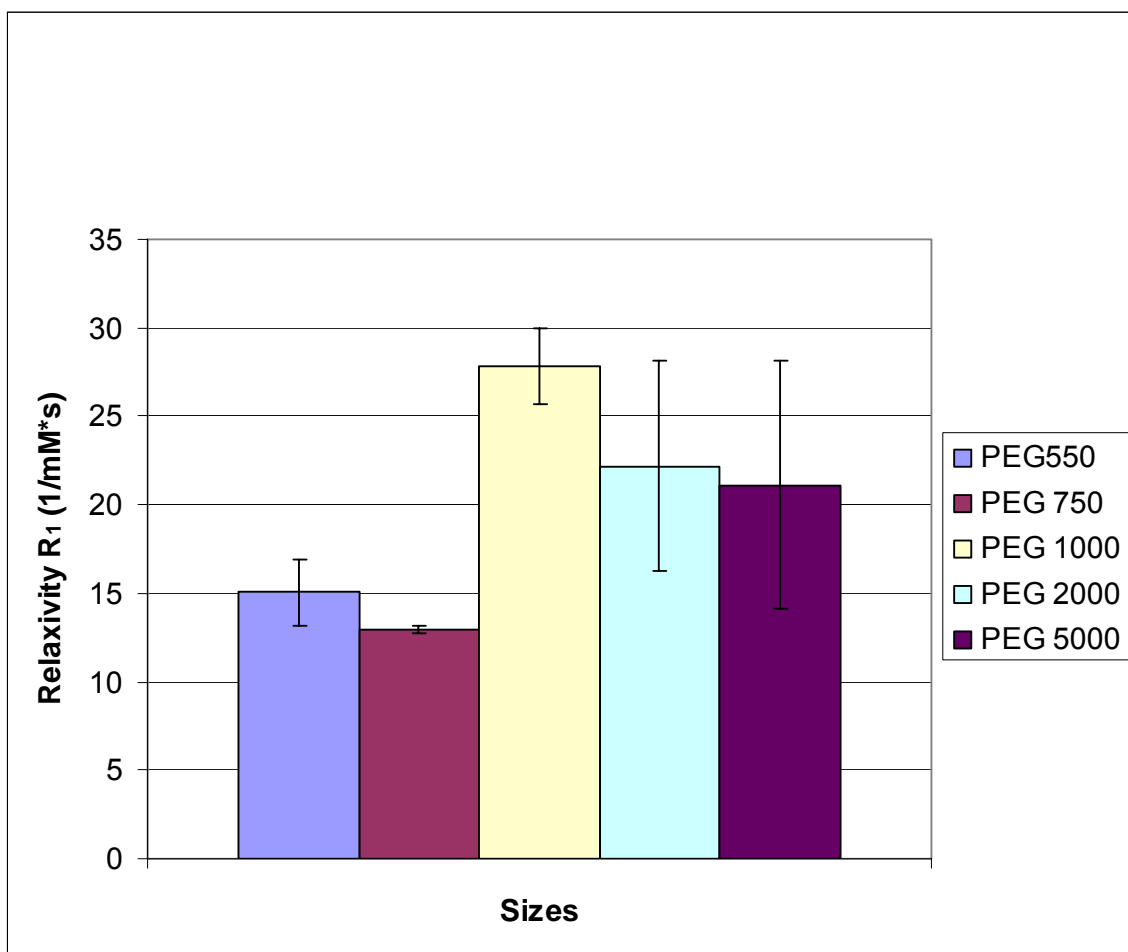


**Figure 8.3:** Variation of  $R_1$  for mMIONS coated with micelle coating of various sized phospholipid-PEG chains (DSPE-PEG 550, 750, 1000, 2000 and 5000)

Results in **Figure 8.2** and **Table 8.2** taken together indicate that with size changes of magnetic nanoparticles from an average diameter of 9 nm to 17 nm, there is a considerable decrease in the  $R_2$  relaxivity of magnetic nanoparticles (factor of 3). This is important for various biological applications, especially when using bimolecular conjugates such as antibodies (antibodies with average diameter around 10 nm). It is likely that the attachment of these biomolecules can have a considerable effect on the  $R_2$  characteristics of these MIONs by changing the overall apparent thickness of the coating. Attachment of multiple moieties on a single nanoparticle's surface can cause a considerable increase in the overall size of nanoparticles, potentially resulting in a decrease in the relaxivity of a contrast agent.

To further gain a mechanistic understanding of the change in magnetic relaxivity with changes in the size of a polymer coating, our collaborators (Omar Zurkiya, Dr Hu's lab) have developed a numerical approach using a Monte- Carlo simulation to understand the proton movement in a sample with magnetic nanoparticles. The approach uses a first-order approximation in which coatings are considered as an exclusion layer for protons, thus effectively controlling the minimal distance of approach for protons in solution (**Figure 8.4 A**).

Using the above assumptions, Monte Carlo simulations were performed as previously described [11, 34] to model movement of protons in a field with nanosize magnetic inhomogeneities. Briefly, protons take random walks through the particle fields. At each time step, the sum of  $B_z$  due to the particle dipolar fields is computed and the proton accumulates a phase according to  $\Phi = \gamma \cdot B_z \cdot \Delta t$  (where  $\gamma$  is the gyromagnetic ratio and  $\Delta t$ , time step, 0.5 $\mu$ s). Simulations were performed using 2000 protons, and magnetic parameters used were representative of nanoparticles with a 6.6 nm core diameter (6070 Fe atoms per particle). Phase changes were accumulated in 10  $\mu$ s

intervals and  $R_2$  and  $R_2^*$  were calculated as previously described [3]. An additional parameter, exclusion radius, was introduced as a spherically-shaped, excluded space into which protons were not allowed to diffuse. Simulations were performed varying exclusion radius to mimic variation in the size of polymer coatings.

The results of the simulation are shown in **Figure 8.4 B**. The trend observed in the numerical simulation is in agreement with the results of the experimental studies shown in **Figure 8.2**. The simulation data (**Figure 8.4 B**) show  $R_2$  decreasing with increasing exclusion volume. This drop indicates that changes in the size, on the scale of nanometers, can have a significant effect on  $R_2$ . In solution, it is likely that many processes occur at the interface of the particle coating and the surrounding water, making it difficult to directly compare coating size to excluded volume. However, the similarity of the results indicates that at least some of the decrease in  $R_2$  observed with increasing coating thickness in the PEG-modified nanoparticles is due to physical exclusion of protons from the immediate neighborhood of the magnetic core. In all simulations, values for  $R_2$  and  $R_2^*$  were the same as expected for the motion averaging regime for superparamagnetic particles of small radius.

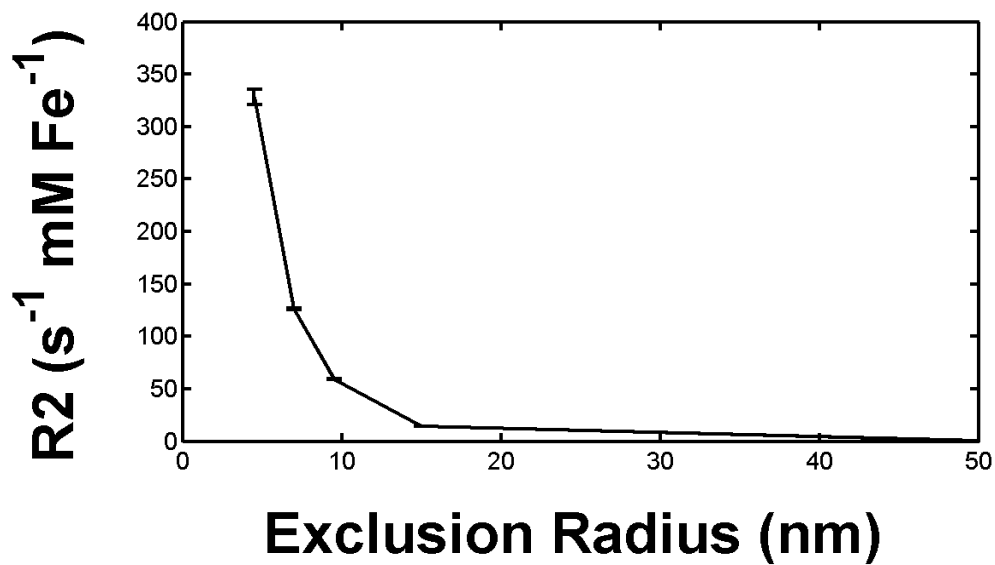
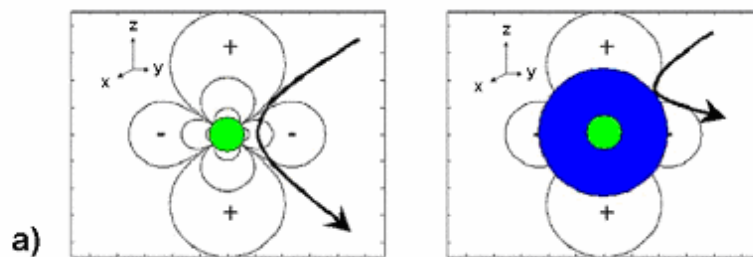


**Figure 8.4:** (A) Schematic picture of the exclusion volume concept used for monte-carlo simulation for calculation of relaxivity values for coated magnetic nanoparticles

B) Predicted variation of  $R_2$  values as a function coating thickness obtained from numerical simulation. (Courtesy: Omar Zurkiya, Dr Hu's Lab)

## Summary

In this study, we have demonstrated that the coating thickness of magnetic nanoparticles can play a significant role in the relaxivity characteristics of these nanoscale particles. The coating size has a significant effect on the  $R_2$  value of the MIONs, with little influence on the  $R_1$  relaxivity values. The results of this study have considerable impact on the design of magnetic nanoparticles-based contrast agents and their applications in medical diagnostics. The numerical simulation results indicate that we can mimic the effect of the coating size on magnetic relaxivity values with a very basic model, which relies solely on physical exclusion of protons from the coated shell of MIONs. Future studies will be designed to vary the chemistry of the coatings and environmental factors such as pH and solvent to gain a more comprehensive mechanistic understanding of the processes determining the proton relaxation characteristics of MIONs.

## References

- [1] M. B. E. Olsson, B. R. B. Persson, L. G. Salford, and U. Schröder, Ferromagnetic particles as contrast agents in T2 NMR imaging., *Magn Reson Imaging* 4 (1986) 437-440.
- [2] M. H. Mendonca Dias, and P. C. Lauterbur, Ferromagnetic particles as contrast agents for magnetic resonance imaging of liver and spleen, *Magn Reson Med* 3 (1986) 328-330.
- [3] P. F. Renshaw, C. S. Owen, A. C. McLaughlin, T. G. Frey, and J. S. Leigh, Jr., Ferromagnetic contrast agents: a new approach, *Magn Reson Med* 3 (1986) 217-225.
- [4] Y. X. Wang, S. M. Hussain, and G. P. Krestin, Superparamagnetic iron oxide contrast agents: physicochemical characteristics and applications in MR imaging, *Eur Radiol* 11 (2001) 2319-2331.
- [5] S. H. Koenig, and K. E. Kellar, Theory of  $1/T_1$  and  $1/T_2$  NMRD profiles of solutions of magnetic nanoparticles, *Magn Reson Med* 34 (1995) 227-233.
- [6] J. W. Bulte, Y. Hoekstra, R. L. Kamman, R. L. Magin, A. G. Webb, R. W. Briggs, K. G. Go, C. E. Hulstaert, S. Miltenyi, T. H. The, and et al., Specific MR imaging of human lymphocytes by monoclonal antibody-guided dextran-magnetite particles, *Magn Reson Med* 25 (1992) 148-157.
- [7] G. Le Duc, L. Vander Elst, J. M. Colet, A. Roch, P. Gillis, J. F. Le Bas, and R. N. Muller, Ultrasmall particulate iron oxides as contrast agents for magnetic resonance spectroscopy: a dose-effect study, *J Magn Reson Imaging* 13 (2001) 619-626.
- [8] L. Josephson, C. H. Tung, A. Moore, and R. Weissleder, High-efficiency intracellular magnetic labeling with novel superparamagnetic-Tat peptide conjugates, *Bioconjug Chem* 10 (1999) 186-191.
- [9] J. M. Perez, T. O'Loughin, F. J. Simeone, R. Weissleder, and L. Josephson, DNA-based magnetic nanoparticle assembly acts as a magnetic relaxation nanoswitch allowing screening of DNA-cleaving agents, *Journal of the American Chemical Society* 124 (2002) 2856-2857.

- [10] I. Coroiu, Relaxivities of different superparamagnetic particles for application in NMR tomography, *J Magn Magn Mater* 201 (1999) 449-452.
- [11] P. Gillis, F. Moiny, and R. A. Brooks, On T(2)-shortening by strongly magnetized spheres: a partial refocusing model, *Magn Reson Med* 47 (2002) 257-263.
- [12] K. E. Kellar, D. K. Fujii, W. H. Gunther, K. Briley-Saebo, A. Bjornerud, M. Spiller, and S. H. Koenig, NC100150 Injection, a preparation of optimized iron oxide nanoparticles for positive-contrast MR angiography, *J Magn Reson Imaging* 11 (2000) 488-494.
- [13] Y. Gossuin, A. Roch, R. N. Muller, and P. Gillis, An evaluation of the contributions of diffusion and exchange in relaxation enhancement by MRI contrast agents, *J Magn Reson* 158 (2002) 36-42.
- [14] P. F. Hahn, D. D. Stark, J. M. Lewis, S. Saini, G. Elizondo, R. Weissleder, C. J. Fretz, and J. T. Ferrucci, First clinical trial of a new superparamagnetic iron oxide for use as an oral gastrointestinal contrast agent in MR imaging, *Radiology* 175 (1990) 695-700.
- [15] T. Bach-Gansmo, Ferrimagnetic susceptibility contrast agents, *Acta Radiol Suppl* 387 (1993) 1-30.
- [16] P. Reimer, and B. Tombach, Hepatic MRI with SPIO: detection and characterization of focal liver lesions, *Eur Radiol* 8 (1998) 1198-1204.
- [17] R. Weissleder, D. D. Stark, B. L. Engelstad, B. R. Bacon, C. C. Compton, D. L. White, P. Jacobs, and J. Lewis, Superparamagnetic iron oxide: pharmacokinetics and toxicity, *AJR Am J Roentgenol* 152 (1989) 167-173.
- [18] P. Reimer, E. J. Rummeny, H. E. Daldrup, T. Balzer, B. Tombach, T. Berns, and P. E. Peters, Clinical results with Resovist: a phase 2 clinical trial, *Radiology* 195 (1995) 489-496.
- [19] T. Ichikawa, A. S. Arbab, T. Araki, K. Touyama, H. Haradome, J. Hachiya, M. Yamaguchi, H. Kumagai, and S. Aoki, Perfusion MR imaging with a superparamagnetic iron oxide using T2-weighted and susceptibility-sensitive echoplanar sequences: evaluation of tumor vascularity in hepatocellular carcinoma, *AJR Am J Roentgenol* 173 (1999) 207-213.
- [20] A. E. Stillman, N. Wilke, D. Li, M. Haacke, and S. McLachlan, Ultrasmall superparamagnetic iron oxide to enhance MRA of the renal and coronary arteries: studies in human patients, *J Comput Assist Tomogr* 20 (1996) 51-55.

[21] Y. Anzai, M. R. Prince, T. L. Chenevert, J. H. Maki, F. Londy, M. London, and S. J. McLachlan, MR angiography with an ultrasmall superparamagnetic iron oxide blood pool agent, *J Magn Reson Imaging* 7 (1997) 209-214.

[22] W. W. Mayo-Smith, S. Saini, G. Slater, J. A. Kaufman, P. Sharma, and P. F. Hahn, MR contrast material for vascular enhancement: value of superparamagnetic iron oxide, *AJR Am J Roentgenol* 166 (1996) 73-77.

[23] C. Z. Simonsen, L. Ostergaard, P. Vestergaard-Poulsen, L. Rohl, A. Bjornerud, and C. Gyldensted, CBF and CBV measurements by USPIO bolus tracking: reproducibility and comparison with Gd-based values, *J Magn Reson Imaging* 9 (1999) 342-347.

[24] L. Rohl, L. Ostergaard, C. Z. Simonsen, P. Vestergaard-Poulsen, L. Sorensen, A. Bjornerud, K. B. Saebo, and C. Gyldensted, NC100150-enhanced 3D-SPGR MR angiography of the common carotid artery in a pig vascular stenosis model. Quantification of stenosis and dose optimization, *Acta Radiol* 40 (1999) 282-290.

[25] W. Li, S. Tutton, A. T. Vu, L. Pierchala, B. S. Li, J. M. Lewis, P. V. Prasad, and R. R. Edelman, First-pass contrast-enhanced magnetic resonance angiography in humans using ferumoxytol, a novel ultrasmall superparamagnetic iron oxide (USPIO)-based blood pool agent, *J Magn Reson Imaging* 21 (2005) 46-52.

[26] M. D. Butterworth, L. Illum, and S. S. Davis, Preparation of ultrafine silica- and PEG-coated magnetite particles, *Colloids and Surfaces A: Physicochemical and Engineering Aspects* 179 (2001) 93-102.

[27] S. Santra, R. Tapeç, N. Theodoropoulou, J. Dobson, A. Hebard, and W. Tan, Synthesis and characterization of silica-coated iron oxide nanoparticles in microemulsion: the effect of nonionic surfactants., *Langmuir* 17 (2001) 2900-2906.

[28] Q. Liu, and Z. Xu, Self-assembled monolayer coatings on nanosized magnetic particles using 16-mercaptohexadecanoic acid, *Langmuir* 11 (1995) 4617-.

[29] D. K. Kim, M. Mikhaylova, Y. Zhang, and M. Muhammed, Protective coating of superparamagnetic iron oxide nanoparticles, *Chem Mater* 15 (2003) 1617-1627.

[30] L. Josephson, C. H. Tung, A. Moore, and R. Weissleder, High-efficiency intracellular magnetic labeling with novel superparamagnetic-Tat peptide conjugates., *Bioconjug. Chem.* 10 (1999) 186-191.

[31] R. C. Atkins, Colorimetric determination of iron in vitamin supplement tablets. A general chemistry experiment, *J Chem Educ* 52 (1975) 550.

[32] M. Johnsson, and K. Edwards, Phase behavior and aggregate structure in mixtures of dioleoylphosphatidylethanolamine and poly(ethylene glycol)-lipids, *Biophys J* 80 (2001) 313-323.

[33] K. E. Kellar, D. K. Fujii, W. H. Gunther, K. Briley-Saebo, A. Bjornerod, M. Spiller, and S. H. Koenig, Important considerations in the design of iron oxide nanoparticles as contrast agents for T1-weighted MRI and MRA, *Acad Radiol* 9 Suppl 1 (2002) S34-37.

[34] R. M. Weisskoff, C. S. Zuo, J. L. Boxerman, and B. R. Rosen, Microscopic susceptibility variation and transverse relaxation: theory and experiment, *Magn Reson Med* 31 (1994) 601-610.

## CHAPTER 9

### Summary and Future Work

#### Summary

In the first part of this dissertation, we have focused on the development of a technology platform which can allow for optical imaging of endogenous RNAs in living cells. To achieve this aim, we have developed a bi-functional probe, which allows for imaging of endogenous RNA in living cells by simple addition of the probes to a regular cell culture media. This bi-functional probe design combines a specific optical switch (molecular beacon) for detection of RNA with the peptide-based delivery approach for the transport of probes across plasma membrane of living cells. This study has adapted existing molecular beacon probes from conventional homogeneous assays typically in a PCR setting to intracellular measurement/imaging of RNA expression in living cells. The early stage studies have focused on the development of bio-conjugation approaches to allow for specific conjugation of peptides to molecular beacons. The major challenge in this process was the non-specific (electrostatic mediated) coupling of peptides with nucleic acid probes. To overcome this challenge we have altered the salt conditions in the reaction buffer used for conjugation to reduced non-specific interactions.

Using peptide linked molecular beacons, we have developed an approach to image endogenous RNAs in living cells (**Chapter 2**). To prove that our delivery approach is highly efficient and effective in delivering MBs into the cytoplasm and also maintaining their specificity, we have carried out a comparison of the TAT-peptide linked MBs with both dendrimer and liposome based approaches for delivering oligonucleotide probes into living cells. The results of these studies demonstrate that the traditional delivery methods (using liposomes/dendrimers) are significantly slower as compared to the

peptide-linked delivery of MBs and these traditional delivery approaches also lead to non-specific opening of MB probes. Further for various transfection agents, cells have to be maintained in a serum-free media or a reduced-serum media, which can potentially change the gene expression profiles of cells due to major roles played by serum proteins and other ligands in various intracellular signaling events related to both transcription and translation processes. Thus using traditional transfection methods, we not only have a higher probability of imaging false positive events due to probe degradation but also more likely change the RNA levels and functional state that we aim to observe. To validate the specificity of targeting mRNAs with peptide linked MB probes, we have carried out various positive and negative control experiments (random sequenced probes, organic dyes, *In-situ* hybridization, other target RNAs with known localization patterns) to validate our observations. In this study, we have chosen GAPDH and K-Ras mRNAs as target RNAs for demonstration of the ability to image endogenous gene expression in living cells using MBs. To further demonstrate the ability of this technology to detect differential levels of gene expression which is crucial for its applications in disease diagnostics, we have selected survivin as a target RNA for this purpose and shown successfully such an ability of molecular beacons. Survivin expression levels have been shown to be higher in pancreatic cancer cells and other forms of cancers including breast cancer.

After successful demonstration of the technology, we have applied these tools to study basic biological questions related to localization and co-localization of mRNAs in living cells. This is an area that has not been extensively explored due to the lack of tools to image endogenous RNAs in living cells. At present, we have a relatively good understanding of the localization patterns of proteins, but there has not been much success in mapping of RNA localization and its related processes in living cells. With this tool, we have made initial attempts to address various aspects of RNA localization in

living cells. In this direction, our first study (**Chapter 3**) provided key information regarding the co-localization of GAPDH and K-Ras mRNAs with mitochondria in living cells. This localization pattern was significantly different from the RNA localization pattern observed with MB probes targeting 28-s RNA (a positive control in this study). This to our knowledge was one of the first successful studies aimed at imaging endogenous RNAs in living cells with high specificity and sensitivity. Experiments were also designed to study the role of cytoskeleton structure in the organization of mRNAs in the cytoplasm of living cells. The results of these studies clearly indicate microtubules are essential in the localization of GAPDH mRNAs in living cells.

Further in this thesis work, we were interested in developing a connection between the functional state of mRNAs and the fluorescent signal observed in our imaging experiments. To achieve this goal, we treated cells with Rapamycin and Wortmannin which alters the translational state of mRNAs in living cells. The results of these studies (**Chapter 4**) indicate that the translational state of mRNAs favors the hybridization of MB with its target sequence. This study has also provided the evidence that MB probes are reversibly bound with target mRNAs and the repression of the translation process can prevent MBs from binding to its target RNAs once coming off. The study has also provided an interesting observation that the active translational processes in cytoplasm favor the co-localization of K-Ras and GAPDH mRNAs with mitochondria. Further, we found that the repression of translation induces a significant re-distribution of mRNAs in the cytoplasm of living cells. The study also revealed the significant differences in the regular DNA backbone chemistry and 2'-O-methyl backbone chemistry of MBs. Specifically, MB probes with 2'-O-methyl backbone were not removed from the target RNAs with the repression of translation in living cells. This backbone was able to follow the changes in the localization of RNAs with the repression of translation.

To expand the static studies, we were interested in understanding the dynamics of RNA molecules in the cytoplasm of living cells and their relationship with cytoskeleton and other biochemical processes in living cells. In this effort (**Chapter 5**), we have studied the mobility of RNA molecules in the cytoplasm of living cells. The results of this study highlighted that different RNAs can have significantly different dynamics in the cytoplasm. Using a FRAP based method, we established that the mobility of GAPDH mRNAs is mediated by an active cellular process which requires ATP and intact microtubule cytoskeleton. The recovery process after bleaching was always along a directed path, which provided a further evidence to support our claims for active transport processes in the cytoplasm. Using a nocodazole-based depolymerization of microtubule network, we reduced the directed recovery process in the bleached area. In contrast, using Taxol, we only observed a reduction in the extent of recovery but there was no significant change in the overall shape of recovered signal compared with the pre-bleach distribution. This trend clearly suggests a significant role of the microtubules in mediating the mobility of mRNAs.

In contrast with GAPDH mRNA studies, the 28-S rRNAs have a significantly different dynamics. These ribosomal RNAs are not highly mobile in the cytoplasm of living cells. These differences could be inherently due to different localization in the cytoplasm. We still need to resolve the relationship between these differences in dynamics and the functional aspects of RNAs in the cytoplasm. To achieve this we clearly need to develop and combine multiple strategies. We believe that the present study provides an initial step in this direction.

So far we have focused our efforts on studying RNA molecules in the cytoplasm of living cells. However, most RNA molecules begin their journey from the nucleus of a cell. After being synthesized and processed by macromolecular machineries in cell nucleus mRNAs are exported to the cytoplasm for various functions. To expand our

technology we have developed a method (**Chapter 6**), which allows for direct imaging of endogenous RNAs in the nucleus of living cells. This approach combines a molecular beacon with a NLS peptide, for efficient delivery of oligonucleotide probes to the nucleus. Using this approach, we have imaged with high specificity and sensitivity the distribution of small nuclear and small nucleolar RNAs. This method in combination with our previous study to detect RNA in the cytoplasm of living cells, allows for direct imaging of distribution and organization of RNA from its birth site in the nucleus to its journey in the cytoplasm. In combination with biophysical approaches such as FRAP/FCS, this approach can allow for the studies of transport of RNAs from the nucleus to the cytoplasm. Further, in combination with labeled proteins, this approach can be used to study the dynamics and function of RNP complexes in the nuclei of living cells.

### **Future Work**

There are several areas where we need to extend this thesis work to realize the full potential of this technology.

### **Future work in technology development**

#### Development of design rules for MBs to target various RNAs

A significant challenge to the future success of the molecular beacons technology for living cell gene detection is to establish design rules that can provide a better accessibility for MBs to bind with the target RNA molecules in different stages of the RNA life. Meeting this challenge requires not only an extensive study of the behavior of MB probes but also a detailed understanding of RNA biology in living cells. This challenge is similar to that faced by antisense and RNAi research. To make design rules,

we can either take an empirical approach in which we study each target RNA as a unique problem and optimize the design for each target by iterative efforts, or a fundamental approach in which we classify the target RNAs in various groups and develop approaches to predict the secondary structure of RNP's as well as the sequences that are occupied by RNA-binding proteins, and then design MBs based on those classifications. Although we have been using only the first approach, in the future, studies should be designed to bridge the gap between an empirical approach and a fundamental RNA biology approach. Along this direction, we may perform initial experiments using an *in-vitro* reconstituted system and develop a fundamental understanding of various issues with well controlled experimental conditions.

#### Detection of point mutations

To detect point mutations of RNA with high specificity, we need to optimize the design of MBs by developing a better understanding of the thermodynamics and kinetics of probes in the intracellular environment. This will require a better design of probes with the optimal melting temperature under physiological (intracellular) conditions. This ability will extend this technique to the diagnosis of several diseases including cancers.

#### Delivery in tissue samples

Using a peptide based delivery approach, we have developed a method to allow for effective delivery of molecular beacons in to living cells. This method was selected as it has the potential for delivery *in vivo*, including tissue samples, animal models or even human studies. Establishing this capability, in combination with near-IR dyes will allow us to image the molecular processes including disease markers in intact tissues and animal models in the near future.

### Development of biophysical tools to understand probe and RNA dynamics

In this study, we have made initial attempts to combine molecular beacon based detection of RNA with biophysical approaches such as FRAP to understand the dynamics of RNA molecules in living cells. As a future direction, FRAP studies may be complemented with FCS based molecular analysis of the dynamics of probe and RNA molecules. Further, we may expand the biophysical studies with advanced optical imaging to improve the optical resolution (STED microscopy) which can allow for better understanding of the organization and dynamics of RNA. These techniques may also be combined with biophysical approaches of single molecule imaging to have highly sensitive imaging of RNA molecules in living cells. For example, the use of quantum dots could lead to single molecule sensitivity in detecting RNA molecules in living cells.

### **Future Work in areas of fundamental biological studies**

We have several unresolved questions related to the biology of RNA, for which novel probes and related imaging methods can provide cutting edge tools to address those questions.

### Interactions of RNA with RNA-binding proteins in living cells

Proteins are the essential partners of various RNA molecules and they play a critical role in the functions and life of RNA. There are various crucial protein-RNA interactions at different stages of the RNA life cycle, which can be of potential interest for future studies. Some of these interactions can be related to the export and transport of RNPs from cell nucleus to the cytoplasm of living cells. There are other interactions, which control the metabolism of RNAs. Future studies can be potentially designed to address various fundamental biological questions related to different aspects of RNA journey in living cells. In this area, we need to combine molecular beacons with various

approaches to label partner proteins using fluorescent labels such as GFP, FIAsH etc. These approaches may provide a functional understanding of RNA-protein interactions. Development of these tools will not only address the fundamental biological issues but also provide a crucial tool set to address questions related to molecular processes leading to disease states. It has been suggested that certain RNA-protein interactions can stabilize the RNA molecules associated with oncogenes in cancer cells.